CATALYTIC CONVERSION OF BIOMASS TOWARDS VALUABLE CHEMICALS

Alisa Doroshenko

PhD

UNIVERSITY OF YORK

GREEN CHEMISTRY CENTRE OF EXCELLENCE

September 2020

Abstract

Lignocellulosic bio-waste is generated in billions of tons annually. Failure to offer a sustainable solution of their valorization leads to large economic loss and environmental damage. The lignocellulosic biomass and bio-wastes, consisting mainly of cellulose, lignin and hemicellulose, potentially represent a great source of multifunctional oxygen-containing molecules. However, the currently existing thermochemical methods (pyrolysis) are not sufficiently selective in the production of these valuable chemicals, while expensive separation makes the biorefinery commercially unattractive. Application of catalysts is one of the most popular ways to drive thermochemical processing of bio-wastes towards multifunctional chemicals. The other methods to improve the selectivity of pyrolysis is the use of alternative types of heating, such as microwave (MW).

This PhD is dedicated to the catalytic thermochemical valorization of cellulose, one of the major constituents of lignocellulosic resources, aiming a selective production of valuable chemicals. Another aim is to investigate an opportunity of co-application of MW together with the catalytic approach to get a better control under biomass pyrolysis process. The results of the research are given in terms of the yields and the selectivity of valuable chemicals, such as levoglucosenone, 5-hydroxymethylfurfural and levoglucosan.

A mechanism of cellulose thermal decomposition was developed based on the real-time kinetic analysis of the volatiles produced and a kinetic constants were estimated. It was found that rearrangements of polymer structure and presence of internal water are critical parameters, controlling cellulose pyrolysis process.

The crucial impact of water on the way of cellulose decomposition was further proved by the analysis of the influence of natural clays during the MW-assisted pyrolysis process. The developed experimental approach was expanded to study valorization of Ni-hyperaccumulators and acid-doped starch.

A catalytic effect of bentonite and ZSM-5 on the products of cellulose decomposition was systematically investigated. An optimal conditions for the production of levoglucosenone were proposed.

Table of Contents

INTRODUCTION

CHAPTER 1: LITERATURE OVERVIEW

CHAPTER 5. CONVENTIONAL PYROLYSIS OF STARCH IN THE PRESENCE OF ACID
CATALYST

CHAPTER 6. REAL-BIOMASS: MW-ASSISTED PYROLYSIS OF NI-
HYPERACCUMULATORS

CHAPTER 7. MATERIALS AND METHODS

CHAPTER 8. CONCLUSIONS AND PERSPECTIVES

List of Tables

List of Figures

9

List of Accompanying Material

Acknowledgements

In the first turn, I appreciate all my family members for their support through my life, wherever I go. Particularly to my parents: Alla and Sergey Doroshenko.

I appreciate the University of York for giving me a chance to do my PhD thesis on the basis of the Overseas Research Scholarship. A special gratitude I would like to express to my both supervisors: Prof James Clark and Dr Vitaliy Budarin, who were continuously supporting and guiding through an intricate world of science. I will keep a memory of our monthly catchups during all my life. I warmly appreciate the support and valuable advice of Circa Group, particularly its director – Tony Duncan. I received a very valuable experience during our presentations and discussions. I really appreciate Dr Avtar Matharu and Dr Francois Jerome for the acceptance of being the internal and external examiners respectively.

A special gratitude I would like to give to the technical team of the Green Chemistry Centre of Excellence, who are extremely generous, helpful and reliable experts: Paul Elliot, Dr Tabitha Petchey, Dr Richard Gammons and Dr Hannah Briers. Without them, it would be impossible to complete my PhD successfully. I appreciate Dr Duncan Macquarrie, Dr Rob McElroy, Dr Florent Bouxin and Dr Mario De Bruyn for the comprehensive scientific discussions and great advice.

I would like to express my gratitude to many people at the University of York, who were continuously helping, guiding and supporting me: Karl Heaton for the valuable experience with mass spectrometry and chromatography; Heather Fish for the great guidance with NMR techniques; Dr Stephen Cowling for the help with X-Rays methods; Rachel Crooks and Sharon Stewart for their support, understanding and kind reminders on the organization matter; Alison Edmonds, Dr Hannah Briers, Sophie Palmer and Katy Brook for the administration and organization help; Mike Keogh and Stephen Hau for their support at the chemical store; Dr Simon Sweeney for the support, various discussions and valuable advice; Dr Peter Karadakov, Dr Seishi Shimizu, Dr Elizabeth Wheeldon and Dr Meghan Halse for their guidance in math demonstrating and teaching experience; and many others.

I appreciate many people from Ukraine, who inspired me to do PhD thesis, including Prof Nikolai Plemyannikov, Dr Ihor Pylypenko, Prof Ihor Astrelin, Ihor Renskiy and Dr Aleksanrd Vasilkevich. I would like to express special gratitude to Prof Boris Kornilovich for sharing his scientific vision and valuable advice.

Last but not least, I appreciate my real friends around the world, including Andy Maneffa, Alexandra Dudkosvkaia, Anna Zhenova, Olga Semenova, Artem Semenov, Nataliia Avadaniy, Ihor Pylypenko, Maria Muchkina, Anastasia Kotolevets, Anita Brusentseva and many others.

Declaration

I declare that this thesis is a presentation of original work and I am the sole author. This work has not previously been presented for an award at this, or any other, University. All sources are acknowledged as References.

INTRODUCTION

1. Topic and context

The rapid development of scientific and technological progress in the twentieth century was based primarily on non-renewable resources. However, at the beginning of this century, there has been a global shift towards using biomass as a source of fuels and chemicals necessitated by decreasing fossil reserves, increasing oil prices, the security of supply and environmental issues. Notably, fossil fuels availability has declined, and the world's population and standard of living have grown substantially, requiring increasingly significant energy resources. Moreover, the increased consumption of fossil fuels leads to greenhouse gas emissions and global warming. As such, it is fundamental to have a novel, green and efficient technologies that provide sustainable and efficient routes to manufacturing essential products from biomass and biomass waste and reduce humanity's dependence on fossil feedstocks and environmental impact.

A new concept based on sustainable biomass processing into a spectrum of marketable products (food, feed, materials, chemicals) and energy (fuels, power, heat) was named a biorefinery concept. The biorefinery concept is based on two major approaches: biochemical and thermochemical. Biochemical conversion of biomass involves use of bacteria, microorganisms and enzymes. Thermochemical route involves the application of high-temperatures for biomass transformations. Both of these approaches have some advantages and disadvantages. High speed and relatively small physical space footprint of the process are significant advantages of thermal treatment. Thermochemical conversion of biomass can be performed via several primary pathways, such as hydrothermal liquefaction, combustion (reaction between biomass and oxygen), gasification (the thermal biomass treatment with steam or air to produce gas without combustion), and pyrolysis.

Pyrolysis is the thermal decomposition of materials at elevated temperatures in an inert atmosphere. The biomass pyrolysis allows converting nearly 100% biomass producing biochar (charcoal), bio-oil (tar) and gas. The market for products made from biomass is volatile. The price of fuel fluctuates sharply even during the year. If the price of petroleum products is low, the production of biofuels becomes unprofitable. Therefore, modern pyrolytic methods of biomass processing should control the distribution between biochar and bio-oil. It is one of the most critical challenges of biomass chemistry. For industrial production of charcoal and activated carbon, the most important is to increase biochar yield. The high yield of bio-oil is critical for the production of bio-diesel and chemicals.

2. Focus and scope

The ability to produce chemicals in a pure form will make a biorefinery robust and profitable even when the fuel price is low. Considering that biomass waste is produced in large quantities, the substances obtained should have large markets, such as solvents and polymers. Such production of a variety of valuable products makes it possible to maintain the efficiency of biowaste pyrolysis of biowaste, regardless of market changes.

This dissertation focuses on developing novel approaches and technologies to increase the bio-oil yield and better control its composition. There are many methods to get control of bio-oil production. In the eighties, it was shown that a fast heating rate leads to an increase in the tar yield. Organic materials rapidly heated to 450 - 600 °C in the absence of air typically produce around 60-75 wt.% of bio-oil. However, the industry could not achieve large scale production of tar using this technology due to the necessity of reaching a high temperature (above 500°C) on the biomass particles' surface. Furthermore, the fast pyrolysis cannot selectively produce individual relatively pure chemical compounds. The thesis focuses on increasing yield of bio-oil and selectivity of chemical production based on a deep understanding of pyrolysis mechanism and using advanced, green approaches such as catalysis and microwave heating.

3. Relevance

The development of novel pyrolysis technology of biomass for controllable chemicals production is a significant part of sustainable chemistry. Currently, almost one billion tonnes of biowaste is produced per year, and its controllable conversion will make tens and hundreds of tonnes of polymers and solvents improve world sustainability. The production of biofuels is crucial for the development of a carbon-free power system. For example, according to the Renewable Energy Association report, increasing renewable bioenergy sources by 10% would enable the UK to meet future carbon budgets affordably. Therefore, research in pyrolysis is at the forefront of biorefinery science with more than 2000 publication in peer reviewed journals per year.

4. Aims and objectives.

The main aim of this PhD thesis is to develop selective pyrolysis of biomass towards valuable chemicals based on advanced, green technologies.

Achieving this goal requires a realization of the following objectives:

- developing a continuous method of the pyrolysis;
- investigation of the kinetics of cellulose pyrolysis;
- elaboration of a molecular level of understanding of cellulose pyrolysis based on measured kinetics data;
- identification of parameters that control biomass thermal decomposition
- identification of high-value chemicals which could be produced during pyrolysis;

- the extension of this approach to study other polysaccharides.
  - Application of novel green technologies such as microwave and catalysis and understanding their influence on the biomass pyrolysis process is another primary goal of the thesis

The proposed approach assumes that the complexity of bio-oils result in secondary reactions of primary pyrolysis products. Therefore, in this thesis, much attention has been paid to developing methods for suppressing all secondary processes, except for obtaining a specific chemical that is valuable on the market. A deep understanding of the biomass thermal decomposition mechanism helps us to choose the best catalyst for the selective transformation of primary product to an easily separated valuable chemical. Microwave radiation application was suggested as a heating method due to its volumetric character to ensure there is no surface overheating.

5. Overview of the structure.

- The first chapter (the literature overview) covers the biorefinery concepts, thermal degradation of biomass, application of various catalysts during biomass pyrolysis as well as mechanistic models for cellulose (one of the major constituents of lignocellulosic biomass) pyrolysis. The chapter discusses in depth the potential primary pyrolysis products and their transformation, focusing on identifying possible useful products. The applications of microwave technology and catalysts are also discussed in this chapter.

- The second chapter represents quantitative thermogravimetric method coupled with Fourier-Transformed Inftrated analysis (TG-FTIR) explicitly developed for continuous monitoring off-gases produced during pyrolysis. The established FTIR kinetic analysis confirms water and levoglucosan (LGA) as primary products of this process. Based on the obtained kinetic data, an improved cellulose pyrolysis mechanism has been proposed showing the optimum condition to maximize the LGA yield. An efficient and selective LGA-centred biorefinery was proposed.

- The third chapter summarises conventional cellulose pyrolysis data obtained in the presence of both liquid acids and heterogeneous catalysts. Sulfuric acid was used as a liquid catalyst while bentonite and ZSM-5 were tested as heterogeneous catalysts. Systematic investigation of the influence of the aluminosilicates loading indicates sharp stepwise changes of volatiles composition, creating five different behaviour zones with a consistent composition of chemicals within each zone. In the presence of acid catalysts, the platform molecule levoglucosenone (LGO) could be obtained in a significant yield and an acceptable purity.

- The fourth chapter deals with microwave-assisted (MW) cellulose pyrolysis in the presence of both liquid acids and heterogeneous catalysts. Sulfuric and phosphoric acids were applied as liquid catalysts. 19% bio-oil was obtained with significantly improved (up to 30-35%) LGO content. A few clays and zeolite were applied as heterogeneous catalysts. Microwave activity of

the catalyst was investigated before the pyrolysis experiments. It was found that clay hydrophobicity plays a substantial role in their MW activity. Even a low quantity of hydrophilic bentonite intensively interacts with microwave radiation while more hydrophobic kaolinite microwave activity is much lower.

- The fifth chapter offers a methodology on the sustainable and efficient valorization of starch-related wastes towards simultaneous production of multifunctional mesoporous materials (Starbon) and valuable chemicals. Starbon preparation consists of many stages, including MW-assisted expansion of starch followed by by doping with *p*-toluenesulfuric acid. The production of volatile chemicals during the carbonization step was studied using TG-FTIR methodology and the developed algorithm of spectra processing. It was found that levoglucosenone is a value-added product during the Starbon preparation process.

- The sixth chapter reports studies on the effects of naturally accumulated nickel on the pyrolysis behaviour of the host plants. Ni-rich biomass offers very different product distributions with unusually high bio-char yields and different cellulose-derived chemical products. Thus the phenomenon was applied for maximising the energy value of biomass (by co-firing with coal) as well as the more selective production of cellulose-derived platform chemical products. The use of hyperaccumulator plants to make chemicals and energy can significantly add to the economic and environmental attractiveness of using these species to remediate nickel contaminated land or the alternative land use of metalliferous soil that is poorly suited to food crop production. The research opens the door to further application of metal-doped plants to control thermochemical biomass valorization.

- The seventh chapter represents materials and methods applied in the thesis.
- The eighties chapter discusses conclusions, future work and perspectives.

CHAPTER 1. LITERATURE OVERVIEW

1.1. Introduction: biorefinery concepts

The nineteenth century is associated with the industrial revolution and the development of petroleum, coal and natural gas-based fuels, targeting to exploit cheap, readily available fossil feedstocks. These are used to produce a variety of essential products such as chemicals, pharmaceuticals, detergents, plastics, pesticides, asphalt and fuels.

However, this progress generated many issues such as an energy source crisis, global warming, as well as the concerns of air pollution, ozone depletion, acid deposition and forest damaging.[1] Limited petroleum reserves in conjunction with economic, ecological and environmental factors enable to conclude that fossil resources are no longer regarded as sustainable[1, 2].

The terms biorefinery means "*the sustainable processing of biomass into a spectrum of marketable products (food, feed, materials, chemicals) and energy (fuels, power, heat)*" stated by IEA Bioenergy Task 42.[3] Following the EU definition, the chemical products that are wholly or partly derived from materials of biological origin are bio-based chemicals.[4] The modern biorefinery concept involves the conversion of biomass residues to power, high-value chemicals and fuels using a combination of thermochemical and/or biochemical approaches.[5]

Nevertheless, significant limitations in the replacement of crude oil with biomass are yet to be overcome with the issues arising from geographical distribution, high moisture content and low bulk density of biomass resources, resulting in expensive transportation and processing costs.[6] These can be overcome through pre-treatment and densification of biomass as a source or through the development of localised processing and energy production facilities,[7] which require investments, government backing[8] and the development of the biology and chemistry of biomass processing.[5] Scientists are playing a leading role in the generation of future industries, and new synergies of biological, physical, chemical and technical sciences must be developed.[9]

Furthermore, attempts to substitute and augment fossil liquid transport fuel with liquids derived from lignocellulosic biomass have been made economically unattractive by overproduction of crude oil, resulting in significant reductions in its market price since 2014.[10] These economic trends run counter to global initiatives aimed at reducing total greenhouse gas emissions. The resulting low oil price is currently well below the viability threshold of bio-ethanol set at 1.34 \$ (6th July 2020) [11] and 1.39 \$ per gallon (6th July 2020),[12] illustrating how the volatility of oil prices can negatively influence the future of the fuel-based bioeconomy. Therefore, taking into account current market prices for the platform molecules and ethanol, the production

of biofuels from biomass could be profitable only if they are produced simultaneously with high-value chemicals.(*10*)

The most important chemicals and platform molecules which could be produced from biomass are glucose, levoglucosan (LGA), levoglucosenone (LGO), phenols, 5-hydroxymethylfurfural (5- HMF) and other furans (e.g. benzofuran) with market opportunities for the antioxidant, pharmaceutical and polymer industries as well as for solvents production. LGO, for example, has multiple applications, among them a precursor of 1,6-hexanediol and 1,2,6-hexanetriol. These compounds are key intermediates in the industrial synthesis of 1,6-hexanediamine, caprolactone and caprolactam, which are used for the manufacturing of polyester, polyamide and polyurethanes, representing multi-million tonne per year operations.(*10*, *13*) LGO can also be isomerized into 5-HMF, a valuable precursor for both fuels and pharmaceuticals. The chiral nature of LGO also lends itself to the synthesis of a wide variety of natural products.(*14*) LGO can also be reduced to the aprotic organic solvent Cyrene^{TM}.(*10*) The production of similar platform chemicals needs a technology which could specifically produce these target molecules in high yield and purity.

Therefore, the processing of renewable resources to selectively produce valuable chemicals is one of the most intensive areas of research.

1.2. Biomass And its Structural Components

By the one definition, *biomass* is contemporaneous (non-fossil) and complex biogenic organic-inorganic solid product generated by natural and anthropogenic processes and comprises(*15*):

1. Natural constituents originated from growing land- and water-based vegetation via photosynthesis or generated via animal and human food digestion;

2. Technogenic products derived via processing of the above natural constituents.

There exists different classifications of biomass varieties(*16*), but the most general is present in Table 1.

Table 1. A general classification of biomass varieties resources according to their biological diversity, source and origin

Biomass groups	Biomass subgroups, varieties and species
Wood and woody biomass	Coniferous or deciduous; angiospermous or gymnospermous; soft or hard; stems, branches, foliage, sawdust and others from various wood species
Hebaceous and agricultural biomass	Annual or perennial and field-based or processed-based such as: Grasses and flowers Straws Other residues (fruits, shells, husks…)

Aquatic biomass	Marine or freshwater algae, macroalgae
Animal and human biomass wastes	e.g. bones, meat-bone meal, litter
Contaminated biomass and industrial biomass waste (semi-biomass)	Municipal solid waste, demolition wood, refuse-derived fuel, sewage sluge, hospital waste
Biomass mixtures	Blends from the above varieties

The primary biomass structural components include starch, cellulose, hemicellulose and lignin.

1.2.1. Starch

Most starches are composed of two kinds of polysaccharides – amylose and amylopectin. A non-branched helical polymer of glucose molecules connected in an α-(1,4) configuration is amylose (Figure 1).(*17*) Amylopectin consists of α-(1,4) linked glucan with 4.2-5.9% α-(1,6) branch linkages (Figure 2).(*17*) The ratio between amylose and amylopectin depends on the source of the starch. Usually, amylopectin is a significant constituent at the typical ratio of 3:1 to amylose.(*18*) However, there are mutants such as waxy maize, waxy corn and others, consisting of 100% amylopectin.(*17*, *19*)
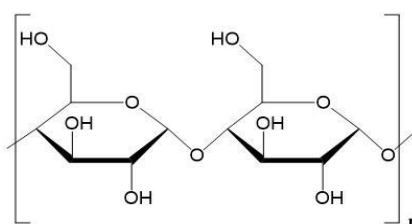
Figure 1. Chemical structure of amylose
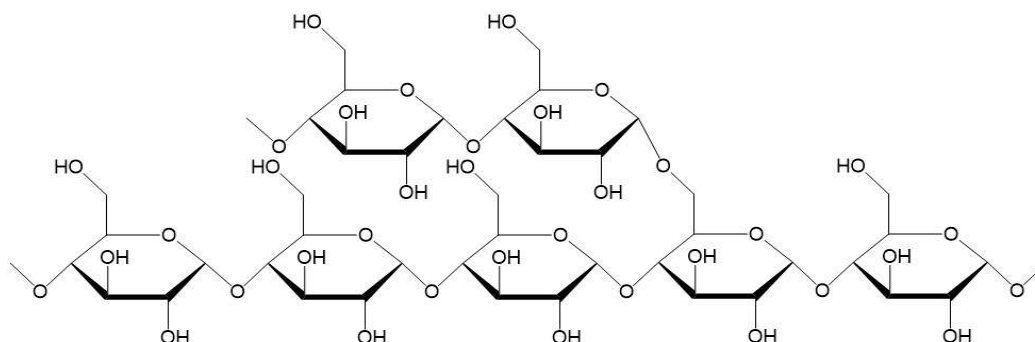
Figure 2. Chemical structure of amylopectin

1.2.2. Hemicellulose

Hemicelluloses are polysaccharides, having β-(1,4) linked backbones with an equatorial configuration (Figure 3).(*20*) In contrast to starch, hemicelluloses consist of a variety of sugars monomers. They are represented by both the five-carbon sugars such as xylose and arabinose and the six-carbon sugars mannose and galactose.(*20*) Hemicelluloses vary in amount and structure

depending on the plant type, and generally, they constitute around 20–30% of cell walls.(*21*) This inconsistency of the composition leads to the variety of structures of hemicellulose depending on the plant type.
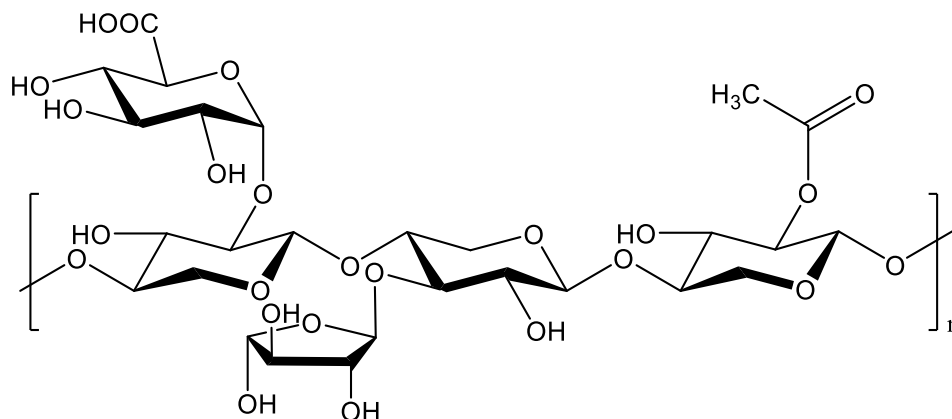
Figure 3. Visualization of approximate hemicellulose structure

1.2.3. Lignin

Lignin is a three-dimensional amorphous polymer with a highly branched molecule composed of prop-2-enylbenzene units with strong intramolecular bonding.(*22*) The main structural units are *trans-p*-coumaryl alcohol (H, Figure 4), *trans*-coniferyl alcohol (G, Figure 4), *trans*-sinapyl alcohol (S, Figure 4).(*23*) It is not possible to define the precise structure of lignin because it shows an individual variation in their chemical composition.(*24*) However, it is well-accepted that it consists of a dendritic network polymer of *phenyl*propene units.(*25*) Original lignin is hydrophobic, and therefore it is insoluble in the water.(*26*) However, there are different types of processed lignin, like lignosulfonates (world annual production of 500,000 tons) and Kraft lignins (under 100,000 tons p.a.). These both types incorporate sulfur within the structure. It was reported Kraft lignin can be dissolved in water under certain conditions(*27*) and lignosulfonates are water-soluble if containing a large amount of sulfur-containing groups.(*28, 29*)
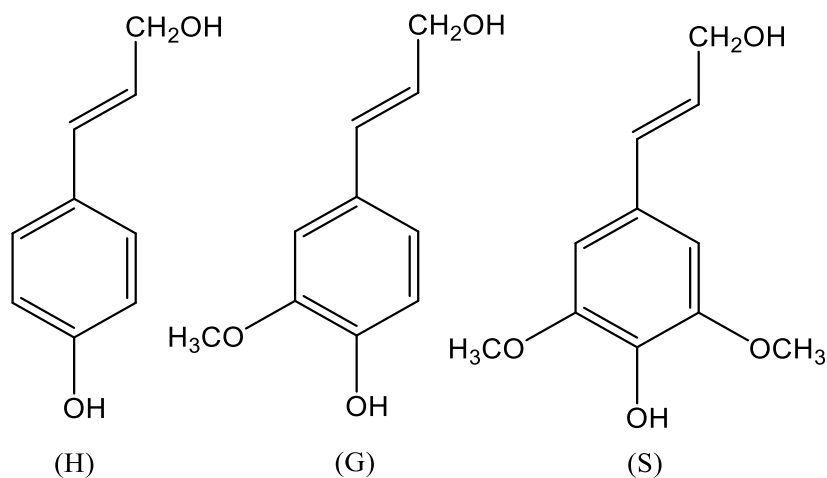
Figure 4. Visualization of approximate lignin structure

1.2.4. Cellulose

Cellulose is a polymer of repeating D-glucose ($C_6H_{10}O_5$) units connected in a β-(1,4) configuration. (Figure 5) The chains are consisting of hundreds to tens of thousands of D-glucose molecules.(*30*)

The long un-branched structure of cellulose contains inter- and intra- H-bonds, that makes it thermally and mechanically stable. Cellulose has varies crystal forms: cellulose I, II, III and IV.(*31*) Cellulose I is the most abundant and it exists in two crystal phases Iα and Iβ. The source of cellulose determines the relative ratio of these phases. Cellulose II is more stable ctystalline form than cellulose I. Cellulose II can be found as a result of alkali-treated cotton. Cellulose III is a result of native cellulose treatment with anhydrous ethylamine or liquid ammonia. Cellulose IV is produced with certain high-temperature treatment.

The crystalline cellulose face is hydrophobic that makes it resistant to acids forming a layer of water at the interface.(*32*)
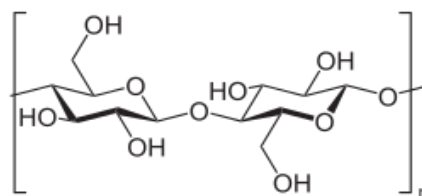
Figure 5. Cellulose polymer chain, represented by a general formula of *($C_6H_{10}O_5$)$_n$*

1.2.5. Importance of cellulose and woody-related biomass

Cellulose has many industrial applications such as fabric production from cotton as well as the manufacturing of cardboard and paper and has a long history. The paper production is based on the processing of wood, making it well-known and developed process. This, together with a well-defined crystalline structure, simplifies the scientific research based on this material. The Food and Agricultural Organization estimated the wood volume and reported that the global volume of forests was 386 billion cubic metres, and the worldwide aboveground woody biomass was about 422 billion tonnes.(*33*) Wood waste is non-food based biomass and, therefore, represent a promising feedstock for renewable and alternative fuels and materials.

1.3. Main Biorefinery Approaches

1.3.1 Biochemical Approach

Biochemical route for the lignocellulosic wastes processing is mainly focused on the production of added-value bioproducts.(*34*) iochemical processing of biomass towards alcohols, biogas and sugars is widely discussed in the literature.(*35–41*) There are three major ways of

biomass processing: fungal, bacterial and enzymatic. The major advantages and disadvantages of mentioned biochemicals methods are summarized in Table 2.(*34*)

Table 2. Advantages and disadvantages of the biochemical approach following Liguori and Faraco (*34*)

Biological approach	Advantages	Disadvantages
Fungal	Low cost	Long time (3-5 months)
Bacterial	Eco-friendly	Feedstock loss
	Low T and P	Low conversion efficiency
	Low water	No-byproduct tolerant strains
	Low waste generation	
	Low energy demand	
Enzymatic	Eco-friendly	High enzyme cost
	Low T and P	Moderate enzymatic performance
	Wide range of pH	Enzymes recycling
	Not long time (hours)	Enzymes immobilization
	High efficiency (selectivity)	

As it is seen from Table 2, the biochemical route can be selective but needs a lot of space and time.

1.3.2 Thermochemical approach of biorefinery

Thermochemical methods are based on the thermal activation of biomass. Such approach involves the application of high temperature, making it faster than biochemical processes. There are different types of thermochemical processing depending on the environment, including thermal hydrolysis, combustion, gasification and pyrolysis.

Hydrolysis is a biomass thermal treatment in the presence of water.(*42*) It is mainly used for the production of sugars and side by-products such as furans, their derivatives and other degradation products.(*43*)

Combustion is thermal processing of biomass directly to heat.(*44*) This process happens at high temperatures in the presence of oxygen and widely used for local utilization of wastes.

Gasification means converting biomass at relatively high temperature (>700 °C) with low oxygen levels to produce syngas, a mixture of H_2 and CO.(*45*, *46*) Syngas can be used directly as a biofuel or can be a chemical intermediate for the production of fuels or chemicals.

Pyrolysis happens at relatively moderate temperatures between 100 and 500 °C in the absence of oxygen.(*47*) This process is used to produce charcoal, bio-gas and bio-oil.(*48*, *49*)

1.4. Pyrolysis
1.4.1 History of Pyrolysis technology

Pyrolysis method on the production of biochar and bio-oil (tar) was established several thousand years ago and until the beginning of technological revolution remaining a major large-scale technology for global industries such as metallurgy, shipbuilding, and domestic fuels.(*50*)

At the end of the 19th century, the amounts of charcoal and tar produced were comparable to those of nowadays. For example, nearly 1 million tonnes of biochar had been generated annually only in the USA, while Finland was exporting around 29 million liters of tar.(*51*) In the pre-industrial period, the charcoal was produced in the Earth pits (Figure 6A). A shield of the earth was used as a protection against oxygen as well as thermal insulation. Usually, pits for charcoal are large (at least 9.4–11 m in diameter), and burning takes place progressively from the one end to the another (Figure 6B).(*51*, *52*)
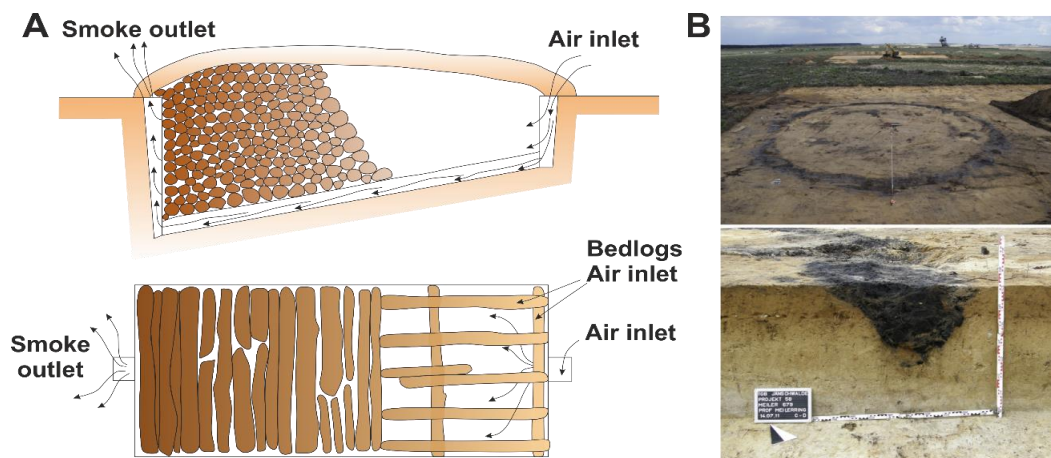
Figure 6. A) Scheme of the charcoal pit and B)Photographs from charcoal kiln excavations: top - view on the planum of a charcoal kiln , bottom - view on a profile in the ditch of charcoal kiln.(*52*)

The pyrolysis has a classification based on the source of heating.

1.4.2 Conventional pyrolysis

Biomass pyrolysis takes place at a temperature range between 100 and 500 °C.(*47*) At temperatures below 180 °C the biomass is drying. Above this temperature, the actual carbonisation process is divided into three main steps. Two of them are endothermic and associated with water production.(*47*) At the temperature range between 180<T<250 °C the formation of water makes the most critical impact in cellulose weight-loss. At temperature between 250 and 290°C the water production is accomplished with CO_2 and CO generation.(*47*) During the exothermic stage (T> 290 °C), the organic volatiles such as alkyl furans, aromatics, anhydrosugars and condensed aromatics are dominated. There is also considerable elimination of gases such as CO, CO_2, H_2, CH_4 and condensable water. At this point, the thermal decomposition process accelerates and releases a significant amount of heat, and therefore the pyrolysis process is self-sustained and does not need external heat after it is started. Furthermore, the produced heat could be used by running

other chemical processes. The final residue of this exothermic step is charcoal, which, when heated to near 500 °C, has a low volatile content and a high fixed carbon content.

The modern process of biomass carbonisation takes place in a special continuous kilns (Figure 7). Crushed (10-40 mm) and pre-dried raw material (with the moisture level of <15%) is loaded into the "feed material" section. Afterwards, it enters the loading hopper that is located in the upper part of the kiln. The active area of the kiln consists of vertical downhole shafts-channels that end with dampers for unloading the finished product. Raw material descends the channels during the processes of preheating, pyrolysis, calcination and stabilization of charcoal. Gases released from the kiln enter the channel for flue gases and then move on to the afterburner, where they are combusted.
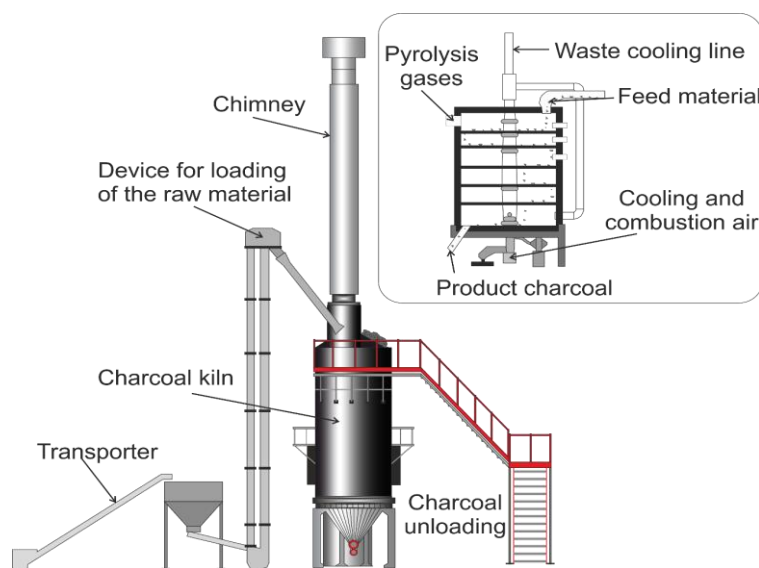
Figure 7. Continuous charcoal kiln BIO-KILN according to the "GreenPower" company.(53)

The main disadvantage is a lack of selectivity towards individual valuable chemicals. The producing a renewable liquid (bio-oil or tar) contains a complicated organic mixture of oxygenated chemicals such as anhydrosugars, furans, phenols and acids.(54)

1.4.3. Microwave-assisted pyrolysis

Microwave heating is a process in which electromagnetic wave with a frequency from one MHz to 300 GHz energy penetrates the material and then converted to heat due to interaction with ions or dipolar molecules within the materials. Microwave heating is a process that involves direct energy conversion within the treated material since microwave can take couple of seconds.

Microwave energy is delivered directly to the material through molecular interaction with the electromagnetic field. Since microwaves can penetrate the material and supply energy, heat can be generated throughout the volume of the material resulting in volumetric heating.(55) Microwaves lie in the electromagnetic spectrum between infrared waves and radio waves. The

wavelengths 12.2 cm (2.45 GHz) or 33.3 cm (900 MHz) only are allowed to be used by international agreement for dielectric heating (unless thorough shielding precautions are taken) as the other frequencies are used for radar and telecommunications. The majority of domestic and commercially available microwave applications operate at 2.45 GHz as this frequency has the right penetration depth for heating food and also chemical reactions. Besides, the energy in a microwave photon (c.a. 1 kJmol^{-1}) is very low, relative to the typical energy required to break not only a covalent bond (300 - 500 kJmol^{-1})[55] but even a hydrogen bond in water (c.a. 20 kJmol^{-1}).[56]

Presently, microwave heating is well established in many industrial and commercial applications (e.g. food industry, pharmacy, polymer industry). It was shown that full-scale ceramic products could be processed with microwave energy faster, more cost-effectively, and with equal or superior performance.[57]

In general, microwave heating for specific applications is more efficient than conventional heating and should be considered as an alternative and potentially faster, greener methodology (Table 3).

Table 3. Comparisons of microwave and conventional technologies of a biomass heating

Heating technology		Comments
Conventional	Microwave	
Slow and Superficial	Rapid and Volumetric	Microwave irradiation is rapid and volumetric, with the whole material heated simultaneously. In contrast, conventional heating is slow due to poor thermal conductors such of biomass[57]
Slow control	Instant control	Microwave heating can be controlled instantly, due to direct transformation of microwave power to the heat.[55]
Non-selective	Selective heating	The microwave power will selectively concentrate on the component which has the highest dielectric loss factor[58]
Time-consuming	Fast, Energy efficient	Microwave-assisted chemical transformations usually take less time and therefore, energy than conventional processes.[59]
Stationary	Mobile	The advantage of microwave technology in terms of mobility have been highlighted by Ruan.[60]

A number of scientific articles discussed the application of microwaves for the production of higher quality bio-oils from biomass pyrolysis.[61] In the majority of cases, the optimisation involved operational conditions (*e.g.* microwave power, temperature, residence time or concentration of different microwave susceptor additives).[61] At the same time, special attention in MW-chemistry should be given to the scaling-up issues, which have to be solved for further development.[62, 63]

1.4.4. Future industrial application of pyrolysis

The production of relatively cheap charcoal and energy from biomass is already a well-established process. However, these manufactures are not commercially attractive. A potentially profitable direction of pyrolysis is the conversion of available biomass into high-value chemicals.

The main disadvantage of pyrolysis is its low selectivity. It produces bio-oil (tar), containing a wide range of oxygenated chemicals such as anhydrosugars, furans, phenols and acids.(*64*)

The oxygen-containing complex individual molecules of the bio-oil are more valuable than main components of crude oil because their transformations to the building blocks require a lower number of upgrading steps. However, separation of bio-oil constituents is a real challenge. The application of chromatography columns results in high costs and commercial unprofitability. The well-established distillation technology cannot be directly applied for bio-oil separation due to high boiling points of naturally low thermal and chemical stabilities of the bio-oil substituents.(*64*)

The Huber group reported one of the solutions for the bio-oil fractionation through catalytic hydrogenation.(*64*) Another solution for large-scale biorefinery is an initially selective catalytic feedstock transformation to the chemicals which can be easily distilled out.

There are a few chemicals of particular interest for large-scale biorefinery those can be stable at the distillation, including 5-hydroxymethylfurflral and levoglucosenone.

1.4.4.1. 5-hydroxymethylfurfural

5-Hydroxymethylfurfural is a multifunctional chemical reagent (Figure 8) and considered one of the essential platform chemicals produced from plant biomass.(*65*) 5-hydroxymethylfurfural is furan substituted at positions 2 and 5 by formyl and hydroxymethyl substituents, respectively (Figure 8A). The 5-HMF melting point is around 32 °C and at room temperature it is a white solid. It is crucial for 5-HMF purification that due to reasonably low

boiling point (~115 °C at 1 mbar) this compound could be distilled out from reaction mixture (Figure 8B).
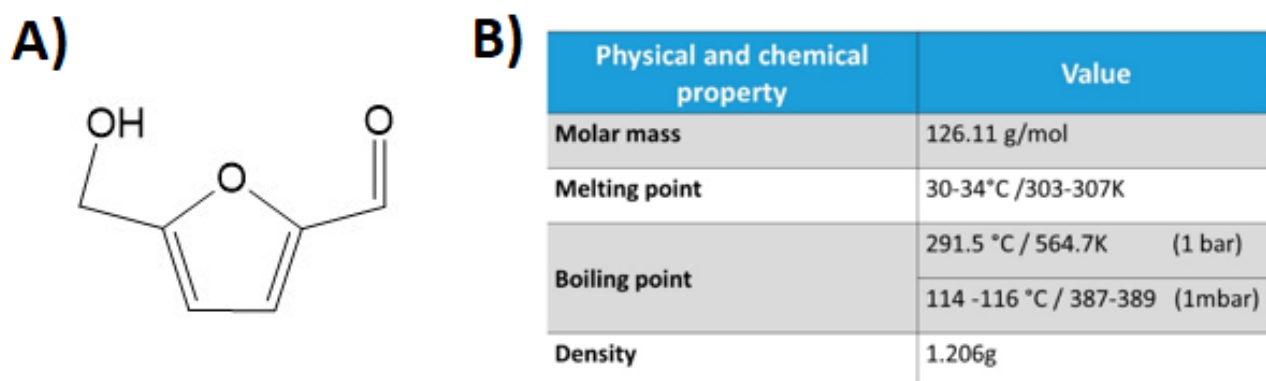
Figure 8. A) Chemical structure of 5-HMF; B) basic properties of 5-HMF

5-HMF is called "a sleeping giant" because its high potential versatility in the chemical manufacturing industry includes enormous application fields in chemical manufacturing sectors such as the production of monomers for polymers, motor fuels and solvents, medicines, pesticides and chemical reagents.(*66*)

The main synthetic pathways to 5-HMF are based on the acid or metal-catalysed dehydration of hexoses. Monosaccharides (mainly fructose and glucose), disaccharides (saccharose) and polysaccharides (starch and cellulose) are used as the hexose feedstock. It is widely accepted, that conversion of polysaccharides to the 5-HMF synthesis starts with their hydrolysis to hexose,(*66*) which then loses three water molecules to give 5-HMF (Figure 9).(*67*)
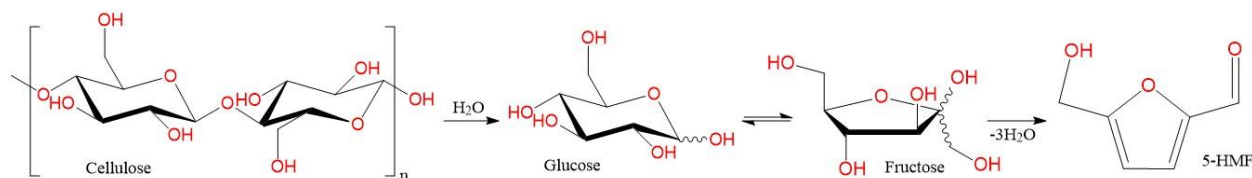
Figure 9. The pathway of the cellulose transformation to 5-HMF

Two general groups of mechanisms for the direct formation of 5-HMF by acid-catalysed dehydration of a hexose by eliminating three water molecules have been suggested in the literature. The mechanistic pathways can be divided into two general groups. One group assumes the reaction to proceed via acyclic intermediates and the other group assumes cyclic intermediates (Figure 10). The body of experimental evidence to support either of the mechanistic routes is still very small, and a consensus on the actual mechanism has not been reached.(*68*)

The acyclic pathways (Figure 10A) assume as the rate-limiting step the formation of a linear 1,2-enediol. The first dehydration step from a cyclic D-fructofuranose would yield the enol form of 2,5-anhydro-D-mannose, a 2,5- anhydro sugar. The cyclic pathway (Figure 10B) presumes

that the conversion process of simple aldose sugar substrates (different from fructose, such as glucose) into fructose is an essential reaction pathway in the synthesis of 5-HMF.
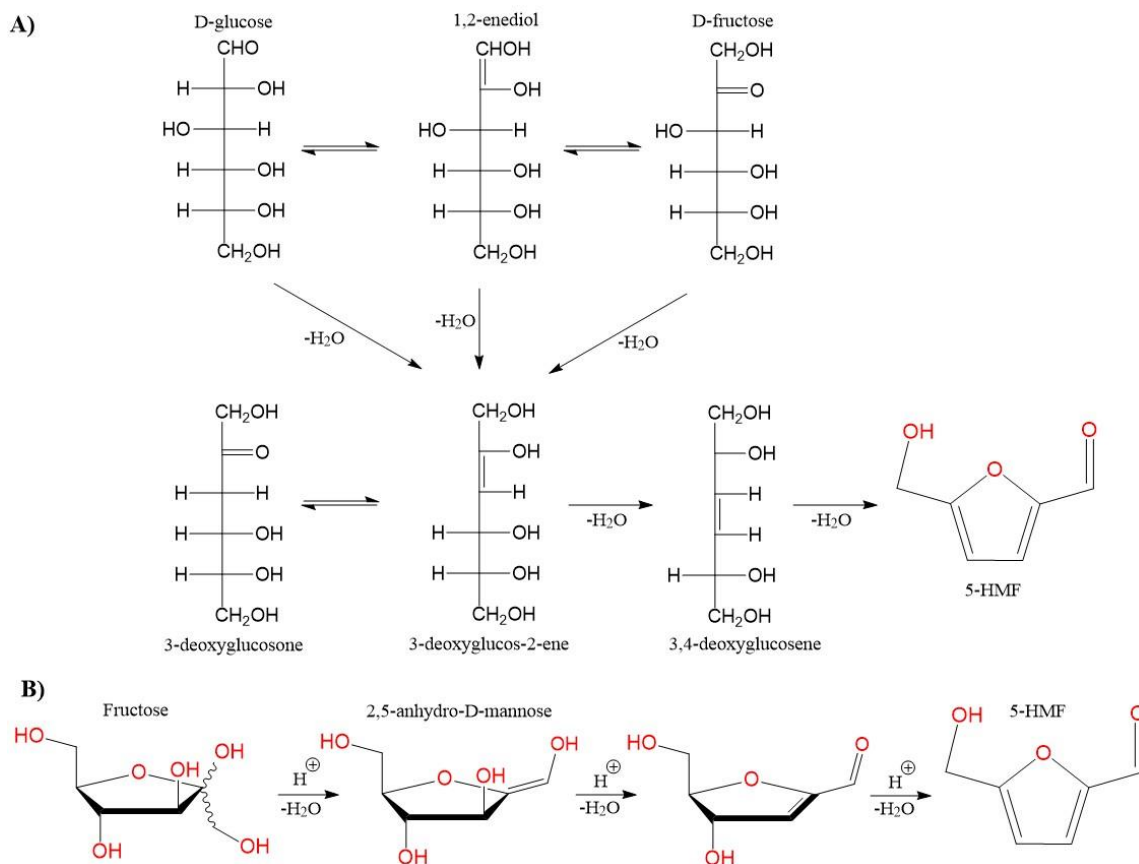
Figure 10. Pathway in the dehydration of hexoses to 5-HMF: A) linear mechanism; B) cyclic mechanis
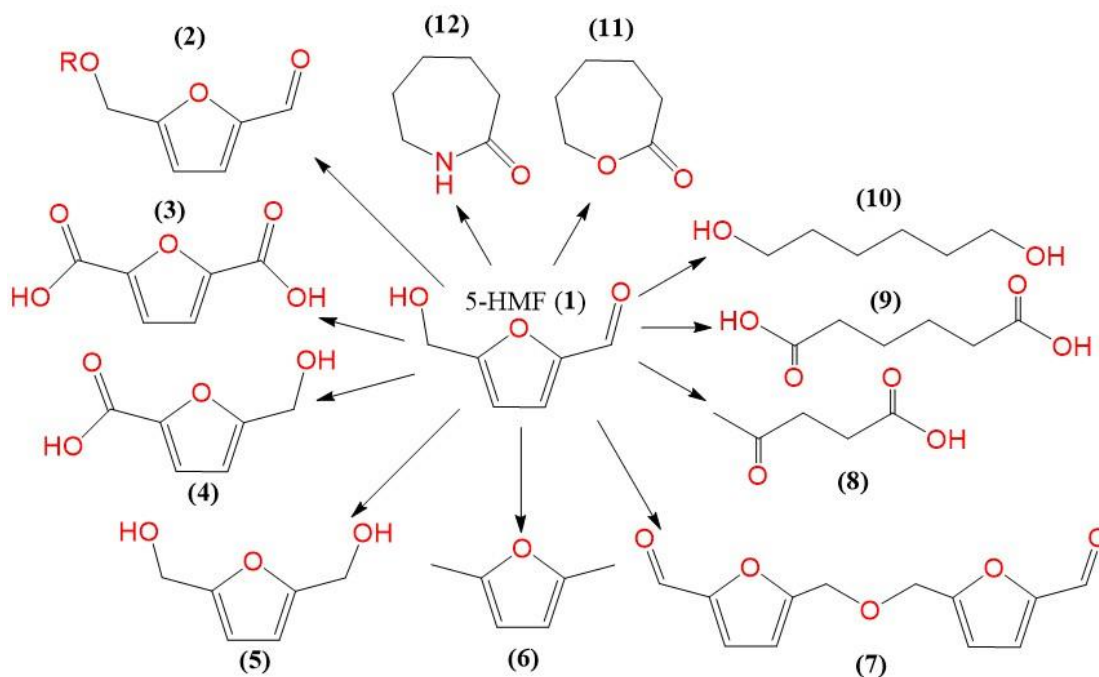
Figure 11. 5-HMF as a chemical platform and an intermediate for other chemicals

As can be seen in Figure 11 there are many important C-6 compounds can be formed through 5-HMF (1). Alkoxymethylfurfurals (2), 2,5-furandicarboxylic acid (3), 5-hydroxymethylfuroic acid (4),bishydroxymethylfuran (5), 2,5-dimethylfuran (6), and the diether of 5-HMF (7) are furan derivatives with a high potential in fuel or polymer applications. Some important non-furanic compounds can also be produced from 5-HMF, namely, levulinic acid (8), adipic acid (9), 1,6-hexanediol (10), caprolactam (11), and caprolactone (12). The difficulty of achieving a highly selective process with a high isolated yield has thus far resulted in a relatively high-cost price of 5-HMF, restricting its potential as a key platform chemical.

The synthesis of 5-HMF by the dehydration of carbohydrates is usually accompanied by the formation of by-products. Typical by-products are levulinic and formic acids, which are formed upon the rehydration of 5-HMF; 2-hydroxypropanoic acid; furfural; 2-hydroxyacetylfuran; polymeric compounds of a complex structure and variable composition (humins) and some other products. In aqueous systems losses due to humin formation amount to 35% 1M fructose going down to 20% for 0.25M. In particular for non-aqueous system, fewer problems occur with polymerisation. Before the 1980s, most 5-HMF synthesis methods were based on the homogeneous acid-catalysed dehydration of sugars in aqueous solution. The modern methods for 5-HMF preparation from carbohydrates are often classified depending on the solvent system used.(*67, 69*)

It was shown recently that during pyrolysis, there is an opportunity for the transformation of the pyranose ring of glucose to its furanose form though an intermittent open structure.(*70*) This finding stimulates cellulose pyrolysis research to produce lower molecular weight products, including 5-5-HMF.(*71*)

5-HMF, as a versatile intermediate, can be exploited for the production of industrially useful chemicals and biofuels using raw plant feedstocks such as starch-rich plant and lignocellulosic plant sources. It can be a target of biorefinery technology. At the moment, the primary attention has been paid to methods of production 5-HMF using acid catalysed hydrolysis. However, there is a potential to produce 5-HMF as a co-product of biomass pyrolysis.

1.4.4.2. Levoglucosenone

The correct structure of LGO given by Helpern, Riffer and Broido.(*72*) They reported that phosphate salts catalysed pyrolysis of the cellulose, collected volatiles and separated them by preparative gas chromatography. CHN, GC-MS, IR Spectroscopy, ^{13}C and ^{1}H NMR methods were used to identify the structure assigned to 1,6-anhydro-3,4-dideoxy-β-D-pyranosen-2-one (Figure 12) that is currently named as levoglucosenone.
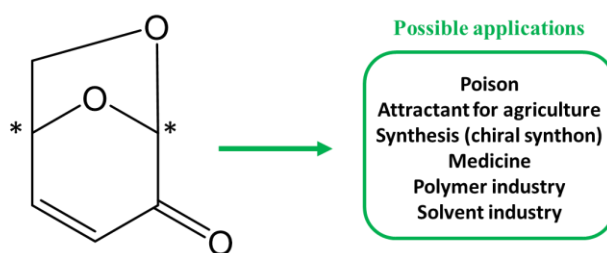
Figure 12. Structure of levoglucosenone and its possible applications

One of the examples of the use of levoglucosenone as a starting material is the efficient total synthesis of optically active (-)-tetrodotoxin done by Isobe's group.(*73*) The final compound has complex molecular architecture being a toxic component of fugu fish poison with potent toxicity around 25 times stronger than potassium cyanide. (Figure 13).
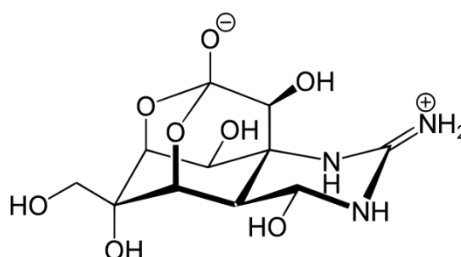
Figure 13. Chemical structure of tetrodotoxin

Another exciting use of levoglucosenone in natural product synthesis is the production of (+)-γ-pelargonolactone that is used as a flavouring agent and an attractant of rice and corn weevils *Sitophiltus zaemais (*Figure 14*).(*74*)
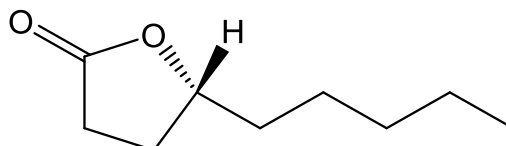
Figure 14. Chemical structure of (+)-γ-pelargonolactone

Synthesis and medicinal application

The chiral nature of levoglucosenone (Figure 12) lends itself to the synthesis of natural and synthetic products. Some of the applications are reported in Table 4. More examples are available in the papers (*75–78*) and reviews.(*14*, *79*, *80*)

Table 4. Levoglucosenone application in synthesis and medicine

Final product	Yield, %	Ref
C-linked disaccharide derivative	~19	(*81–84*)
Thiodisaccharides	~20	(*85, 86*)
Cyclopentane derivatives	~30-40	(*87–89*)
d-ribose	~25	(*90*)
d-xylose		

31

Intermediate for the polymer industry

Levoglucosenone has multiple applications as a precursor of 1,6-hexanediol and 1,2,6-hexanetriol. These are key intermediates in the industrial synthesis of 1,6-hexanediamine, caprolactone and caprolactam, which are used for the manufacturing of polyester, polyamide and polyurethanes, representing multimillion tons operations (Figure 15).(*10*, *91*, *92*)

Figure 15. Application of the levoglucosenone as an intermediate for polymers

Intermediate for solvent industry

One of the examples of the used of levoglucosenone as a precursor is a work done by Clark group reporting dihydrolevoglucosenone (Cyrene™) as a bio-based alternative for dipolar aprotic solvents.(*93*) Dihydrolevoglucosenone has been reported as a safe replacement for the reprotoxic solvents NMP and DMF, and its production (managed by Circa Group) is now at pilot plant scale reflecting strong industrial interest.

The Circa Group process produces levoglucosenone from the acid-catalysed *conventional* pyrolysis of pine sawdust (Furacell™ technology). This process has been upscaled to a 6.5 $ million prototype plant in collaboration with Norske Skog demonstrating that pyrolysis can be a realistic and viable large-scale process for the making of levoglucosenone.(*94*)

Typical methods on the production of LGO are displayed in Table 5.

Table 5. Typical methods on the production of LGO

Feedstock	Conditions	Levoglucosenone yield, %	Reference
Cellulose	Sulfolane, H_2SO_4, at 215°C, inert atmosphere	43.1	(*95*)
Glucose		43.1	
Levoglucosan		53.6	
Cellulose	3wt% of phosphoric acid	9	(*96*)
Cellulose	Sulfuric acid in 1,4-dioxane at 210 °C under 51716.2 Torr for 47 h.	33.7	(*97*)

Glucose	Heteropolyacid-Based Ionic Hybrid, NaCl in tetrahydrofuran and water at 180 °C; 2 h	7	(98)
Cellulose	Sulfated zirconia at 335 °C	8.45	(99)

A potential improvement of this technology can be based on the use of selective alternative heating. Sarotti group reported the microwave-assisted pyrolysis of cellulose for the production of levoglucosenone, giving the product yield of 7.53wt%.(100)

This shows that the application of selective MW-assisted technology seems to be very promising for the efficient conversion of biomass into valuable chemicals, such as LGO. At the same time, this effect can be even more improved with the application of catalysts.

1.5. Catalytic pyrolysis of biomass

Catalytic pyrolysis involves the degradation of the polymeric materials by heating them in the absence of oxygen and the presence of a catalyst. There are two main ways for catalytic upgrading of biomass pyrolysis products. The first one, which is referred to as "*in-situ*", involves the upgrading of vapours passing via a catalytic bed. The other method involves a direct mixture between a catalyst and a feedstock.(116)

It is a well-known that catalysts influence the pyrolysis pathway.(117–127) An analysis of the catalytic influence of acids, alkali, metals and silica-based porous materials is given in the section below.

1.5.1. Acids and Alkalis

1.5.1.1. Influence of acids

The addition of strong acid substantially influences the pyrolysis of cellulose. For example, the addition of 5.4wt% of phosphoric acid causes almost 80 °C decreased decomposition point for cellulose (Table 6 and Figure *16*. Temperature of the maximum rate of volatiles evolution depending on the loading of H_3PO_4Figure *16*).(101)

Table 6. A shift of the cellulose pyrolysis temperature depending on the amount of added acid

Amount of H_3PO_4 in cellulose, wt%	Temperature for maximum rate of volatiles evolution, °C
Blank	325
1.5	280
2.8	270
5.4	260
10.2	245
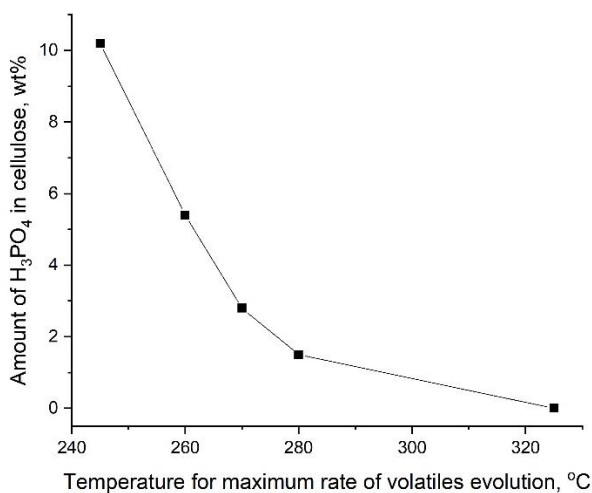
Figure 16. Temperature of the maximum rate of volatiles evolution depending on the loading of H_3PO_4

One of the possible explanations of such temperature shift caused by acid is due to weakening of the hydrogen bonding in cellulose. Some authors suggested that this reduction of H-bond strength promotes the formation of glucose oligomers as reaction intermediates, which are subsequently dehydrated to low molecular weight compounds at increased temperatures.(*102*) The sugars are dehydrated, resulting in a low levoglucosan (LGA) yield during acid-catalysed pyrolysis of cellulose.(*102*)

Indeed, it is logical to assume that impregnation with acid influences the H-bonds in cellulose, because acids bring free protons H^+ to the system. Also, a partial reduction of the H-bonding network can explain the lowering of pyrolysis temperature of acid-doped cellulose.

The observed reduction of the LGA yield can be explained by its transformation to other chemicals, including industrially important LGO. Many studies confirm the formation of LGO during acid-doped cellulose pyrolysis.(*72*, *97*, *101*, *103*, *104*) The Huber group reported 31wt% of LGO from cellulose pyrolysis in water mixture with polar aprotic solvents under 68 atm using sulfuric acid and a special high-pressure reactor.(*97*) Alternatively, Dobele and co-workers reported 22.3wt% yield of LGO in the absence of solvent and high pressure. The authors were soaking cellulose in aqueous solutions of phosphoric acid with different concentration: 1.5, 2.8, 5.4 and 10.2wt% of H_3PO_4, giving 18.2, 20.8, 22.3 and 16.5wt% LGO respectively. The yield of LGA was not exceeded by 2wt% for any of the acid-doped cellulose pyrolysis experiment. Dobele and co-workers claimed that dehydration is a rate-limiting step in the production of LGO.(*101*)

The pathway of acid-doped cellulose decomposition was studied depending on various parameters. The effects of pyrolysis temperature and ball milling were summarised.(*105*) Interestingly, the yield of LGO is apprently independent on the way of acid impregnation. For

example, the cellulose was mixed with acid diluted in water, and different evaporation methods have been tested, such as vacuum, and under air at different temperatures. However, there is no crucial dependency was identified.(*103*)

The studies on cellulose pyrolysis in the presence of other acids, such as formic and acetic, did not attract the attention of researches for a long time because of their low boiling points. Only recently, in 2020, it was discussed the impacts of the co-feeding of formic acid or acetic acid on the pyrolysis behaviour of cellulose at 400 and 600 °C, respectively. The results showed that the co-feeding of the acids significantly affected properties of both the resulting bio-oil and biochar. Co-feeding of acetic acid remarkably promoted the formation of heavier organics with π-conjugated structures. Furthermore, the co-feeding of formic acid or acetic acid also affected the elemental composition, the defective structure, the crystallinity and the thermal stabilities of the resulting biochar at varied pyrolysis temperature in distinct ways. It was suggested that the carboxylic acids or their derivatives interfered with the formation of the volatiles or reacted directly with the organic components on the surface of biochar, which substantially modified the physiochemical properties of the biochar.(*106*)

1.5.1.2. Influence of alkalis

Alkaline and alkaline earth metals exhibit a strong catalytic effect on altering the decomposition rate and chemical pathways during cellulose pyrolysis.(*107*) Even trace levels of alkaline and alkaline earth metals can cause a dramatic reduction in levoglucosan yield. Alkaline and alkaline earth metals can restrain the primary depolymerization pathways leading to levoglucosan formation and favour the fragmentation reaction . Neat cellulose is mainly depolymerized to levoglucosan, while in the presence of alkaline and alkaline earth metals, small molecular species (e.g. glycoaldehyde) are formed as the major products.

The Dauenhaouer group showed a comparison of cellulose pyrolysis products under thin-film and powder conditions revealed that alkaline earth metals act primarily on secondary (diffusion-limited) reactions of volatile species within molten cellulose. Calcium ions were more active than magnesium ions, and they were able to promote the primary formation of char from cellulose, the conversion of levoglucosan to light oxygenates and furans, and the consumption of furans to secondary char and permanent gases. The addition of either calcium or magnesium ions to cellulose increased the C/O ratio of the bio-oil, which suggests that there is some benefit (i.e., deoxygenation) of the presence of these metal ions despite the decrease of the bio-oil yield and increase in the yield of low-molecular-weight species.(*107*)

1.5.2. Transition metals

Transition metals are well known as another efficient group of catalysts for biomass transformation.

Recently the catalytic effect of different transition metals and lanthanides were studied to control the pathway of biomass thermal conversion to valuable chemicals.(143-145) (*108–110*) Nickel is considered to be one of the most promising metals among others because of its wide range of oxidation states (Ni(0) /Ni(I) /Ni(II) /Ni (III)) and facile activation of unsaturated molecules. (*111*, *112*) Moreover, Kumagai and Alvarez investigated Ni–Mg–Al impregnated catalysts for the pyrolysis-gasification of a biomass/plastic mixture and found that adding of Ni-based catalyst could significantly reduce the coke deposition on the catalyst surface.(*113*)

Comparison between nickel and iron as catalysts in isothermal pyrolysis of rice husk was provided by Liu et al.(*114*) The results indicated that the addition of iron and nickel salts led to a high catalytic efficiency on the formation of hydrogen while displaying a negative effect on CH_4 release. Furthermore, nickel showed a better catalytic effect on H_2 compared with iron.

Influence of nickel concentration on the yield of bio-oil was investigated by Yu et al.(*115*) With the increase in nickel loading, the tar production and the yield of syngas were increased. The temperature had an influence on the quality and yield of the bio-oil.

The influence of the ratio between biomass and nickel catalysts was also investigated.(*116*) The presence of nickel improved the overall aromatic hydrocarbon yield and conversion of pyrolysis vapour oxygenates over a biomass/catalyst ratio of 1:1. Results indicated that, relative to ZSM-5, increasing NiO loading resulted in an increase in aromatic hydrocarbon production. Other benefits received from nickel presence on ZSM-5 have increased catalyst stability and reduced oxygenate breakthrough.(*116*)

The naturally incorporated Ni could be used for *in-situ* the pyrolytic pathway control. Taking into account the nature of Ni-hyperaccumulator plants, the suggested approach could be considered double-green.

The fact is Ni-hyperaccumulator plants are used in the phytoextraction processes to extract the metal from Ni contaminated land. The further use of these Ni containing plants is mainly their pyrolysis aiming to obtain carbonaceous Ni-containing catalyst. An attractive opportunity to receive value-added products in the pyrolysis of the Ni-containing plant led the GCCE to the project calls PhytoCat.(*117*)

One of the PhytoCat project consortium member supplied a set of Ni-containing plants for the investigation of any value-added products in the result of their pyrolysis. This study is described in the relevant part.

1.5.3. Silica-based solid catalysts in thermal processes

The silica-based catalysts are very well known and widely available.

Clays are worldwide known green and readily available catalysts for petroleum cracking.(*118–120*) However, in the 1970-1980 clays have been substituted by zeolites because of their improved efficiency.(*121–124*) In the 1985-1990, it was reported that pillared clay is a potential alternate for zeolites in the petroleum cracking process. However, difficulties in the large-scale production of pillared clays made zeolites the number one catalysts in petroleum cracking and green chemistry.(*125–127*)

The summarisation of research interest in the applications of clays, pillared clays and zeolites for petroleum and renewable resources is shown in Figure 17.
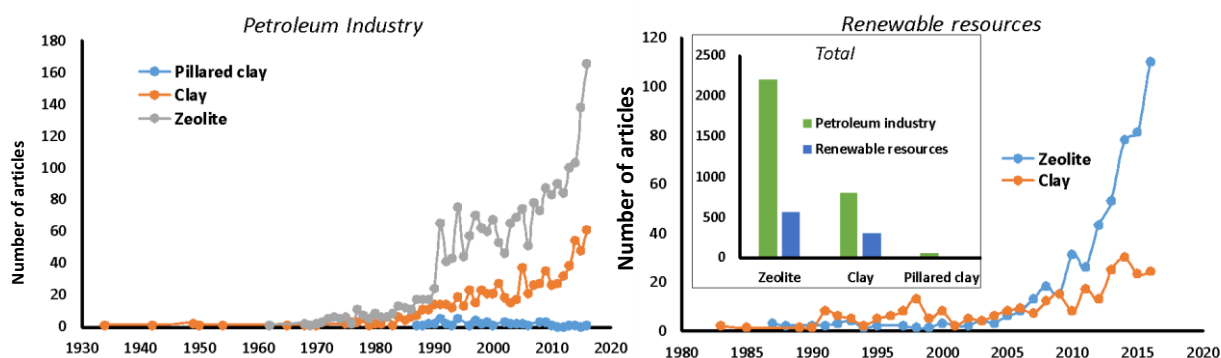
Figure 17. Analysis of the literature published about zeolite, clay and PILC clay catalysts (based on Web of Knowledge)

The majority of zeolite- and clay-based researches on the biomass processing (around 80%) are dedicated to the bio-oil upgrading (*128–130*) and gas-phase oxidation, (*131–134*) while pyrolysis processes were almost unnoticed before 2008-2012. It this period, the Huber group has achieved a significant breakthrough for fast conventional zeolite-catalysed pyrolysis.(*64, 135–138*) They reported that aromatic-rich products are formed in the amount of 30wt% as a result of zeolite/biomass (~20:1) pyrolysis at 1000 °C/s heating rate.(*135*)

Various applications of different silica-based solid catalysts are given in Table 7.

Table 7. Summary of the literature related to the catalytic effect of zeolites and clays on the renewable resources chemistry

Compound	Product	Catalyst	Conversion of the compound to the product, %	Selectivity, %	Refer ence
Fuels and chemicals					
Canola Oils	Fuels and chemicals	Al-PILC montmorillonite	Up to 98	-	(*139*)

Heavy liquid fuels	More valuable lower-boiling products (hydrocracking)	Cr/SnO$_2$-PILC montmorillonite	Up to 45	-	(*140*)
Palm Oil	Gasoline	Ni-Cu/Zr-bentonite	53.6	-	(*141*)
Cumene Cracking	To lower molecular weight of hydrocarbons	Al-grafting-Si-PILC MMT	65.0	-	(*142*)
Vegetable Oil	Bio-diesel Bio-lubricant	TPA-modified-K10	86	67 to fatty acid ME	(*143*)
Switchgrass	Gas, bio-oil and biochar	Mechanical mixture of K$_3$PO$_4$ and bentonite (1/2)	Yield: Biochar – 38% Yield: Bio-oil – 33%		(*144*)
Cellulose	Water-soluble oligosaccharides	Treated kaolinite	81	-	(*145*)
Heavy oil	Gasoline	AlGa-PILC bentonite	70	27	(*146*)
Glycerol	Glycerol steam reforming (H$_2$, CO$_2$, CO, C$_2$, CH$_4$)	Ni-load-MMT	85	76 to H$_2$	(*147*)
Plant asphalt	Gas/gasoline	Ni/Si-PILC MMT	81.1-90.2	Gas – 14.7-31.1 Gasoline – 45.9-32.5	(*148*)
	Kerosine		10.1	69.1	
Free fatty acids	Methyl oleate	H-treated Si-PILC bentonite	100	100	(*149*)
Waste cooking oil	Fatty acid methyl esters	Ba/K10 MMT	83.38 yield to FAME		(*150*)
Soybean	Biodiesel	KF treated smectite	99.7 to methyl esters		(*151*)
Waxes	Hydrocracking to high quality diesel	Pt/Al$_{13}$ – PILC MMT Pt/Zr$_4$ – PILC MMT	77.2 78.3	C$_{11}$-C$_{20}$ = 84.2 C$_{11}$-C$_{20}$ = 81.9	(*152*)
Glucose	Aromatics/olefins	ZSM-5	14.3/12.32		(*136*)
Sorbitol			24.45/8.19		
Oak wood bio-oil			11.18/9.81		
Pine wood bio-oil			18.47/8.19		
Low-temperature hydrogenated			18.46/14.74		

oak wood bio-oil				
Low temperature hydrogenated water-soluble pine bio-oil			32.70/23.36	
High temperature hydrogenated water-soluble bio-oil			50.77/21.47	
Bio-oil derived from wood	Toluene/xylene	H-ZSM-5	28 % - yield for C6-C9	(153)
Bio-oil derived from wood (ENEL)	Aromatics	H-ZSM-5	13 % - yield	(130)
Pyrolytic lignin	Coke	H-ZSM-5	83 % - yield	(154)
Pyrolytic lignin	Acetic acid	H-ZSM-5	15.33 % - yield	(154)
	1-Hydroxy-2-propanone		15 % - yield	
	Methanol		10.6 % - yield	
Lignocellulosic biomass	Aromatic/olefins	Ru/H_2 + Pt/H_2 + ZSM-5	Benzene – 27% (C selectivity) Toluene – 49.3%(C selectivity) Xylene – 19.1%(C selectivity) EtBenzene – 2.3%(C selectivity) Ethylene – 32% (C selectivity) Propylene – 55.4% (C selectiv.) Butylene – 12.8% (C selectivity)	(64)
Lignocellulosic biomass	Aromatic/olefins	Ru/H_2 + ZSM-5	Benzene – 17.6% (C selectivity) Toluene – 45.5%(C selectivity) Xylene – 31.3%(C selectivity) EtBenzene – 2.6%(C selectivity) Ethylene – 31.8% (C selectivity) Propylene – 55.4% (C selectiv.)	(64)

Feedstock	Product	Catalyst	Yield	Ref
			Butylene – 12.8% (C selectivity)	
Lignocellulosic biomass	Aromatics	ZSM-5	30 % - yield	(*138*)
		Silicate	7 % - yield	
		Beta – zeolite	3 % - yield	
		Silica-alumina	0 % - yield	
		Y - zeolite	0.5 % - yield	
Xylitol	Aromatics	ZSM - 5	47 % - yield	(*135*)
Glucose			29 % - yield	
Cellubiose			26 % - yield	
Cellulose			29 % - yield	
Cellulose	Benzene + toluene + xylene	ZSM - 5	30 % -yield	(*155*)
Hemicellulose			20 % - yield	
Lignin			7 % - yield	
Glucose	Aldehydes Furans Ketones	Ce – ZSM-5	80 % (liquid carbon selectivity to furans)	(*156*)
Rice husk	Light Olefins	La – ZSM-5	10.5% - yield	(*157*)
Sawdust			7.9% - yield	
Sugarcane Bagasse			12.1% - yield	
Cellulose			16.2% - yield	
Hemicellulose			14.7% - yield	
Lignin			5.3% - yield	
Straw stalk bio-oil	Light olefins	Mg – ZSM-5 with ethanol	96% - yield	(*158*)
Cellulose	Light olefins	Fe-ZSM-5	34.99% - yield	(*159*)

As it is shown in Table 7, many studies have been done on the transformation of biomass into valuable chemicals. At the same time, the efficiency of this research development could be much higher if a clear molecular-level understanding of pyrolysis processes would be achieved. Pyrolysis is an extremely complicated process and produce many chemicals species. The investigation of such complicated processes is better to start on the material with reproducible formula, and crystal structure. Following the previous literature overview, cellulose, one of the major constituents of biomass, fits the abovementioned criteria.

1.6. Mechanistic study on thermal degradation of cellulose

Historically, the debates on the nature of cellulose pyrolysis are still ongoing (Figure 18). In the 1950-1960, the visions of the researches on the mechanism of cellulose pyrolysis were basically divided by the type of the mechanism: homo- or hetero-lytic. Later in 1960-1970, a new significant uncertainty was appeared – what is an "active cellulose" species. Then, in 1980-1990, the actual existence of "active cellulose" step was critically questioned. And finally, since the start

of 2000th, the researches were presenting the data achieved, in many cases, on the basis of modelling study.
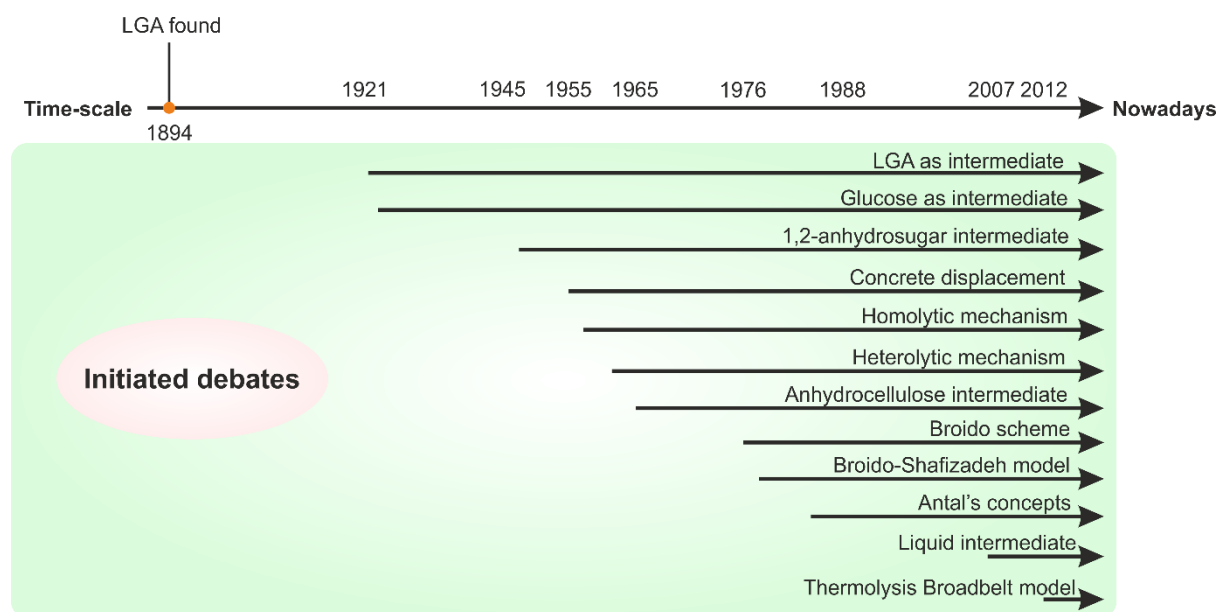
Figure 18. Historical overview of some debates rising around cellulose pyrolysis mechanism

As it is seen from Figure 14, the debates are happening on both the nature of the intermediate compounds and nature of the cellulose pyrolysis mechanism (homo- and hetero-lytic).

It is impossible to highlight all the developments in cellulose thermal degradation done during all time, but it is possible to point at a few crucial turns, which significantly influenced the development of the field. In such a way, the works of A. Pictet, P. Karrer, G. Coleman, W. Parks, S. Madorsky, O. Golova, W. Reeves, D. Gardiner, A. Broido, F. Shafizadeh, M. J. Antal, V. Mamleev and L. Broadbelt can be particularly representative to do research in the cellulose pyrolysis field.(*70*, *160–170*)

1.6.1. Mechanisms proposed between 1920th and 1960th

Pictet, and Sarasin probably did the first work aiming some mechanistic understandings of cellulose pyrolysis.(*171*) They reported the formation of levoglucosan (Figure 19), in the yield of 30wt% in pyrolysis of cotton cellulose.
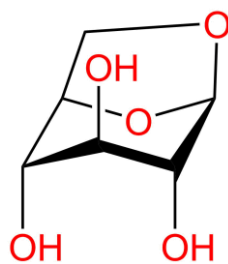
Figure 19. Chemical structure of levoglucosan

However, the first mention of levoglucosan is dated in 1894 by C. Tarnet, who was treating picein, salicin and coniferin (Figure 20) in baryte-containing water at 100 °C. He named a new compound "levoglucosan" because of the *levorotation* properties to distinguish it from the potential *dextrorotation* isomer - the glucosan, published earlier by A. Gelis.(*171*) The glucosan is a result of α-glucose transformations,(*172*) while in 1920, P. Karrer found levoglucosan to be a by-product of β-glucose vacuum distillation.(*161*) Therefore the first mechanism of cellulose pyrolysis was based on the dehydration of the formed β-glucose towards levoglucosan (Figure 21).(*173*) In such a way, the historically first active centre in cellulose pyrolysis is β-glucose.
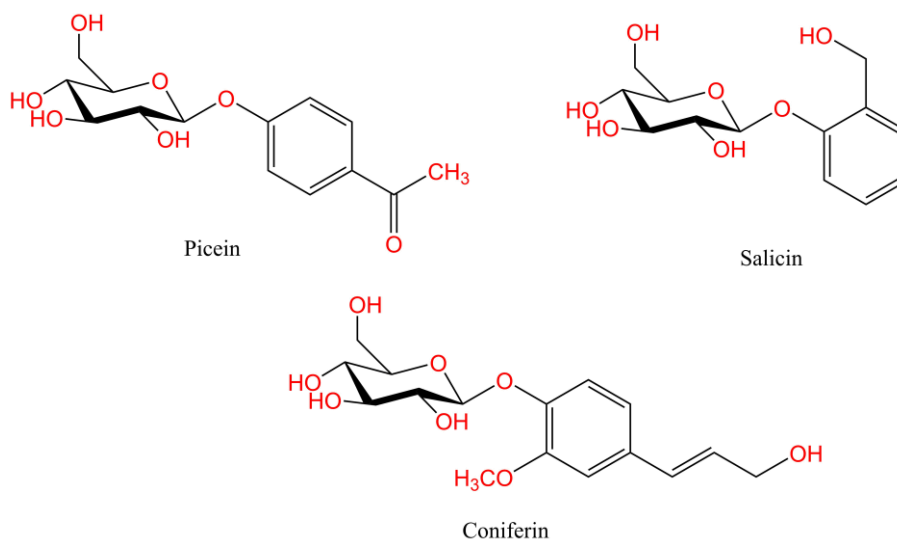
Figure 20. Chemical structures of picein, salicin and coniferin used to produce LGA
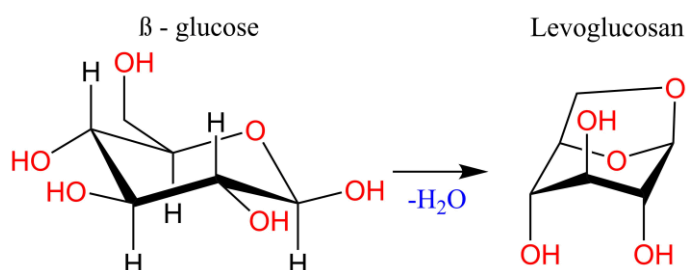
Figure 21. Glucose dehydration towards levoglucosan

High yield of LGA indicates a vital role of this molecule in pyrolysis processes. Parks and co-workers made a clear statement of levoglucosan playing a crucial role in cellulose pyrolysis in 1955.(*163*) Unfortunately, many details on the work conducted by Parks in 1955 are not available due to it was presented a long time ago at the conference, the proceedings of which include only a short synopsis overview. Nevertheless, it is known that Parks and co-workers applied kinetics' analysis, determining the production of LGA as a rate-determining step as well as suggested direct conversion of cellulose into levoglucosan by concerted displacements without a pre-intermediate, indicating of OH-group at C-6 atom being the active centre in cellulose pyrolysis (Figure 22).(*174*)
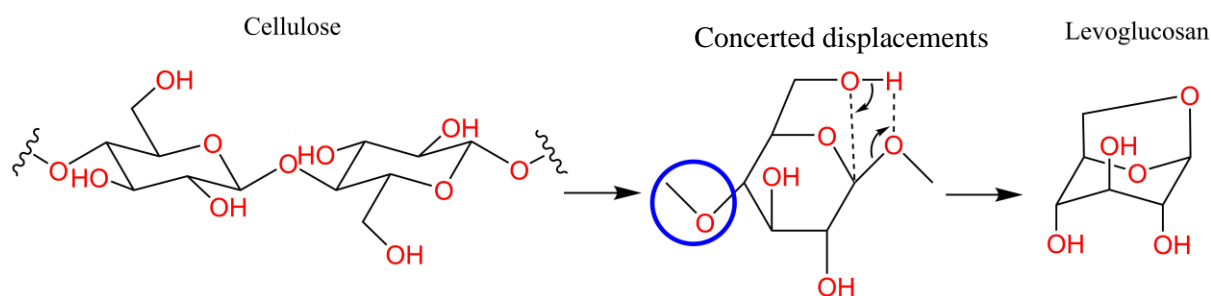
Figure 22. A reaction scheme suggested by Parks and co-workers on LGA production during cellulose pyrolysis as a result of concerted displacements

This mechanism is, probably, the most popular among others. The reaction looks relatively simple. However, there is uncertainty regarding the mechanism of opening the in the blue circle the C-O (Figure 22). The transformation of the intermediate to LGA (Figure 22) requires a presence of internal water, which looks problematic at a temperature above 100 $^{\circ}$C. An alternative possibility is that the formation of LGA due to continuous unzipping of the cellulose polymer. Then it would yield a near-quantitate value of LGA, that is not in line with the experimental works.(*175–180*)

The mechanism assumed by Parks initiated a series of important papers published in the next three years highlighting the mechanism of thermal degradation of cellulose and a role of levoglucosan in this process.(*164*, *177*, *181*)

In 1956, S. Madorsky and co-workers published their work on pyrolysis of cotton, cotton hydrocellulose, and viscose rayon. Both the neat and impregnated cellulose were investigated. The materials were impregnated with sodium carbonate or sodium chloride.(*117*) The pyrolysis was done at 250 °C and 397 °C under high vacuum. The analysed volatile fraction contained mainly CO, CO_2, water and levoglucosan. They found that impregnation of the samples with salts increase the yield of gas and char of the expense of bio-oil amount. Plotting the rate of reaction over its mass-loss let them conclude that activation energies of pyrolysis of pure samples are much higher than those of the impregnated samples.

They assume a thermal degradation process consists of two stages happening simultaneously: dehydration (randomly along the chain) and thermal scissions of the polymer chain. Referring to their previous works with polyethylene oxide, they concluded that the C-O bonds were less thermally stanle than the C-C. The breakdown of a, b, c and d bonds leads to the break of the part of the chain yielding H_2O, CO_2, CO and C (char) (Figure 19).(*117*) The scissions of C-O (Figure 19, c-bond) bond may result in the formation of 1-6 oxygen linkage by a process similar offered by McCloskey and Coleman, giving 1,2-anhydrosugar intermediate (Figure 19).(*182*) In the current mechanism, the whole elemental unit of cellulose (two glucans) is considered to be the active centre.
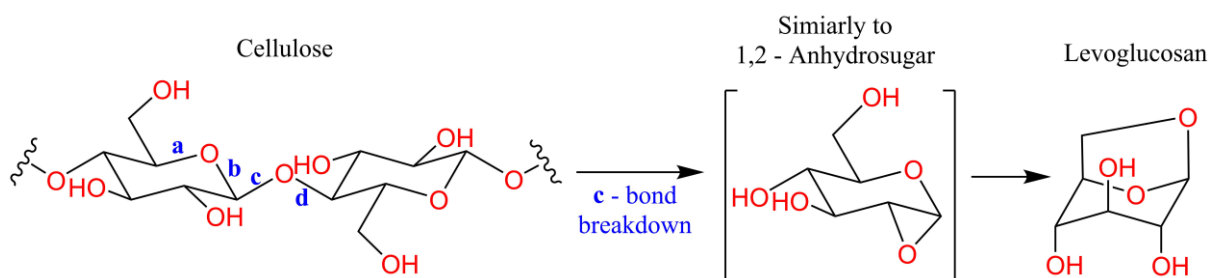
Figure 23. The mechanism suggested by S. Madorsky and co-workers

D. Gardiner was working on the same 1,2-anhydrosugar intermediate pathway, studying the thermal degradation of hexoses, and di-, tri-, and poly-saccharides.(*167*)

However, the suggested pathway has a few issues. First of all, in the reaction suggested by S. Madorsky, the formation of the 1,2-anhydrosugar intermediate (in square brackets, Figure 23) requires a molecule of water for hydrolysis of C-4. Secondly, such intermediate is identified only in alkali conditions as was shown in the original work by McCloskey and Coleman; and therefore it cannot be directly applied for pyrolysis of neat cellulose.(*182*)
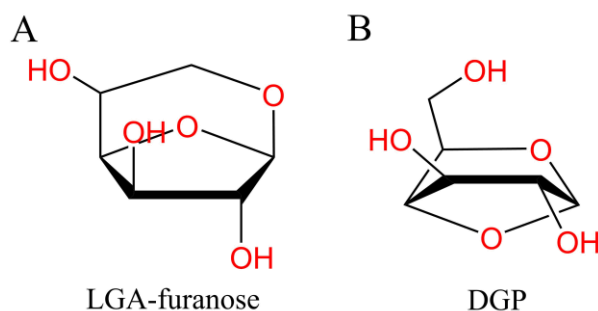
Figure 24. Chemical structures of other cellulose pyrolysis by-products: A-1,6-anhydro-β-D-glucofuranose (LGA-furanose) and B - 1,4:3,6-dianhydro-α-D-glucopyranose (DGP)

Also, D. Gardiner was working on 1,4-anhydrosugar intermediate, trying to explain the formation of other by-products such as 1,6-anhydro-β-D-glucofuranose (levoglucosan isomer,

LGA-furanose, Figure 24-A) and 1,4:3,6-dianhydro-α-D-glucopyranose (DGP, Figure 24-B). He has proposed that rearrangement of the D-glucopyranose residues at the nonreducing end (LGA-end) of the polysaccharide chain provides 1,4-anhydro-a-D-glucopyranose, which is subsequently converted into 1,6-anhydro-β-D-glucofuranose or 1,4:3,6-dianhydro-a-D-glucopyranose (Figure 25). The formation of 1,4-anhydrosugar intermediate at the C-6 blockage was shown previously by the Golova.(*167, 174*)
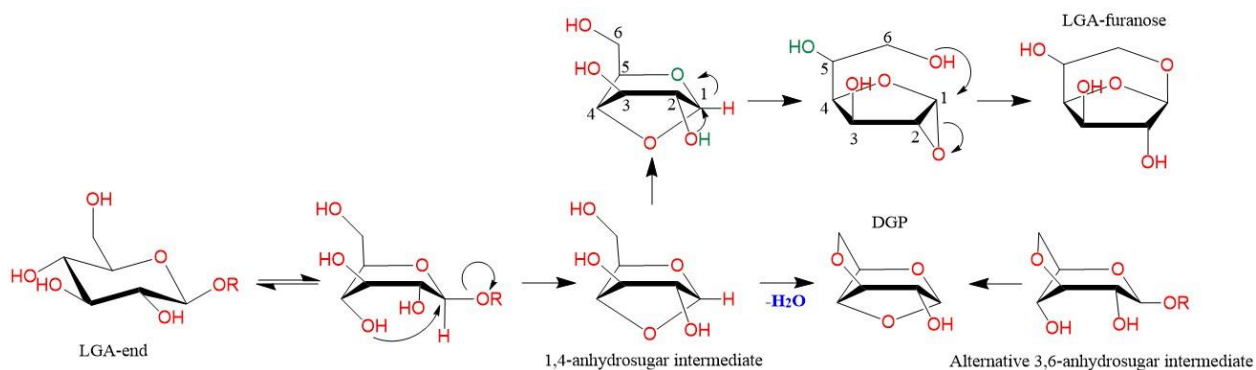
Figure 25. The mechanism of LGA-furanose and DGP formation from the LGA-end via 1,4-anhydrosugar intermediate based on Gardiner concepts

At the same time, there was no pathway suggested on the conversion of 1,4-anhydrosugar into the principal intermediate (LGA).

In 1957, Golova and co-workers published a research paper highlighting the influence of degree of polymerization on the yield of levoglucosan.(*177*) The data (Table 8) indicate there is no direct influence of the initial length of the polymer chain on the yield of levoglucosan. At the same time, the pyrolysis of cellobiose resulted in only 4wt% LGA yield. Also, in this work, Golova challenged the production of LGA from glucose as Irvine and Oldham assumed it in 1921.(*173*) Golova conducted pyrolysis of pure β-D-glucose as well as its mixture with cellulose. The results are displayed in Figure 26.

A significant outcome of this work was experimental evidence that formation of LGA requires the presence of the supramolecular structure, specifically, at least more than 2 molecules in the chain (Table 8).(*177*) Furthermore, it indicates that the cellulose pyrolysis is not happening at the end of the polymer chain.

Table 8. Results of pyrolysis of cellulose with different polymerization degree*(177)*

Polymerization degree	Number of COOH-groups in 100 glucans	Yield, wt% from cellulose		Yield of levoglucosan, wt% from cellulose
		Solid distillate	Liquid distillate and the dry residue	
1000		78	19	60
450		72	23	56
200	0.144	76	22	54
190		74	25	53
150		75	20	54
Cellobiose	—	25	—	3-4
β-D-glucose	—	41.5	57	5-6

As it is seen from Figure 26, the adding of glucose, even at small amounts, decreases the yield o LGA to 30wt%. Therefore, the mechanism of cellulose pyrolysis passing via hydrolysis of the polymer to glucose and its further dehydration towards LGA was not confirmed.(*177*) Instead, it was offered a cellulose decomposition model involving radicals, indicating that cellulose pyrolysis active centre is radicals. According to their vision, at the first stage, an amorphous region of cellulose is decomposed. This statement was supported by the experiments showing increased packing density and lowering the molecular weight to about 200 units.(*174*)
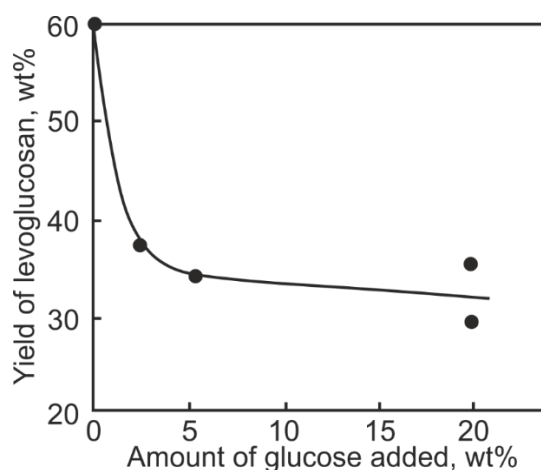
Figure 26. Results on the LGA yield depending on the glucose additive in cellulose pyrolysis

The second stage includes a conversion of tightly packed cellulose fragments into levoglucosan at very high yield via unzipping reaction, involving radicals (Figure 27). It was suggested that the radical I from Figure 27 is decomposed, giving 50wt% maximum yield of LGA.(*165*) However Golova assumed, that radical I negatively affects the stability of 1,4-glycosidic bond on the neighbouring glucan, leading to its cleavage. Then a hydrogen atom at the C-6 moves to the C-4, giving 1,6-anhysugar formation (Figure 27).
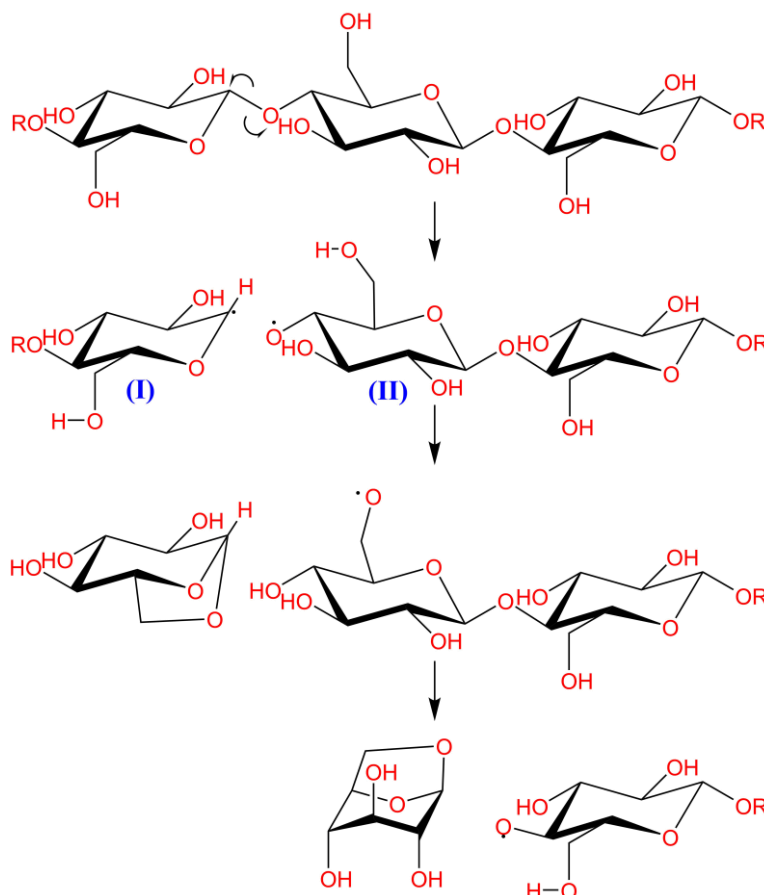
Figure 27. Homolytic mechanism of cellulose pyrolysis suggested by Golova

The proposed radical mechanism initiated an intense scientific discussion, creating two groups of scientists, depending on their preference to homolytic (radical) or heterolytic cellulose pyrolysis mechanisms.
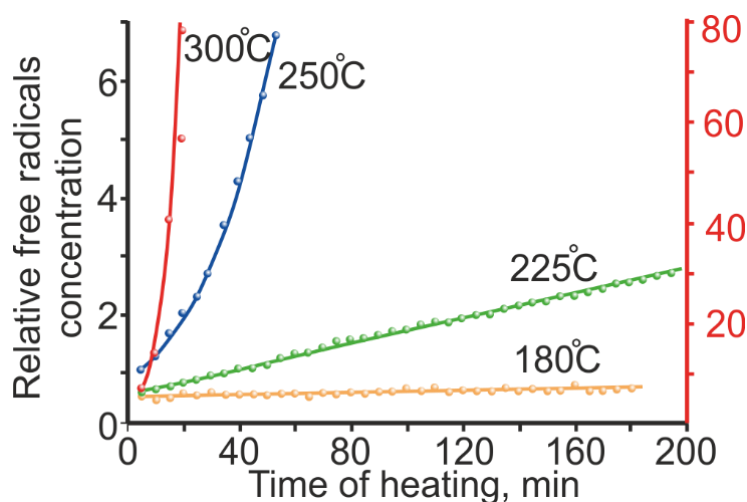
Figure 28. The relative concentration of free radicals detected by ESR during cellulose isothermal pyrolysis(183)

The scientists supported the homolytic pathway(165, 184) based their arguments on the ESR (electron spin resonance) experiments about the thermal initiation of free radicals (Figure 28).(183) At the same time, following to the opinion of other researchers (185) asserts the formation of radicals and the related reactions are occurring in char and showed that char, formed at some conditions, can be highly reactive.(186)

Byrne, Gardiner and Holmes were supporting the formation of LGA as a result of concrete displacement (offered earlier by Parks).(163) They developed the idea of concrete displacement mechanism and suggested that any intramolecular rearrangements are controlled by the conformation of the pyranose ring.(187)

1.6.2. Mechanisms proposed between 1960th and 2010th

1.6.2.1. Broido-Shafizadeh model

Broido

The first publication of Broido made on cellulose pyrolysis mechanism was done in 1965.(168) He exploited DTA, TGA and chromatography methods to investigate the thermal breakdown of cellulose gained from a variety of sources.

Broido offered a scheme of cellulose thermal decomposition displayed in Figure 29.
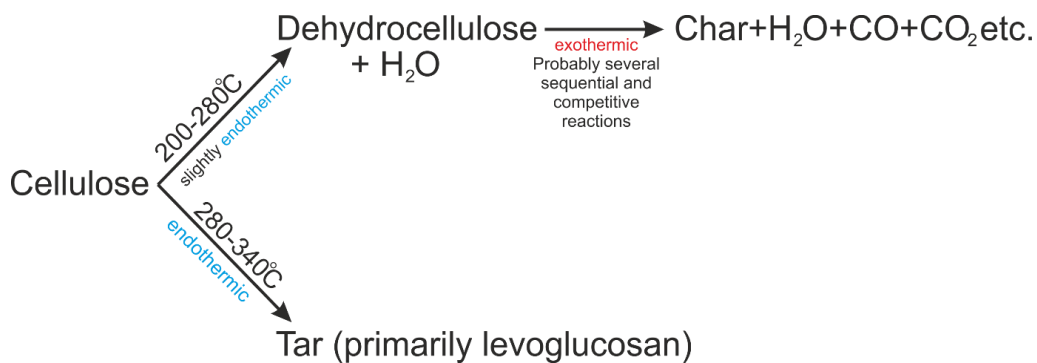
Figure 29. Formation of dehydrocellulose as the active centre in solid residue transformations*(168)*

The dehydrocellulose can be potentially classified as depending on the centre for water removal. The formation of dehydroellulose following the Broido vision involves the scheme displayed in Figure 30.
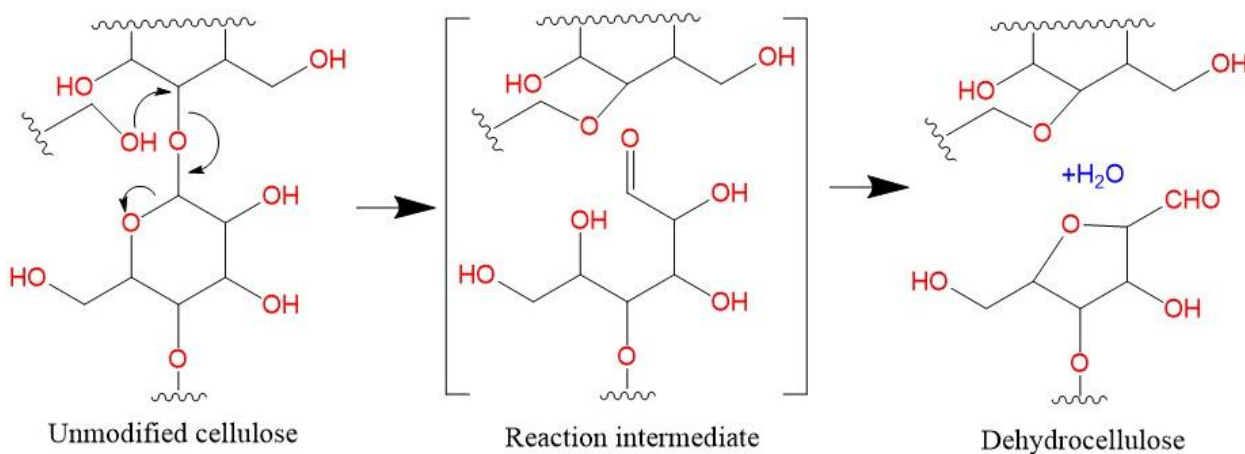
Figure 30. The formation of dehydrocellulose during pyrolysis process*(168)*

Notably, in 1970 the study done by D. Arseneau stated the absence of the "anhydrocellulose" stage.(*188*) He proposed a scheme consisting of two competitive reactions and determined their activation energies: Ec = 152 kJmol^{-1} (char) and Ev = 190 kJmol^{-1} (volatiles).
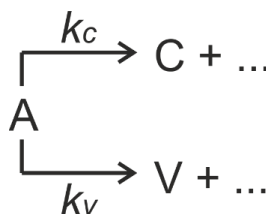
Figure 31. The cellulose pyrolysis scheme suggested by D. Arseneau without "anhydrocellulose"

In 1975 Broido published results on char yield during cellulose pyrolysis at different conditions (using the simplified scheme published in 1965), calculating some kinetic parameters.

Notably, he determined a ratio between kinetic constants responsible for the formation of volatiles and solid productions and their temperature dependence.(*189*)

However, in 1976 Broido published another work based on the data collected at isothermal pyrolysis of cellulose in a temperature range of 226-259 °C. As a result, a few extra steps were added to his previous model (Figure 32).(*190*) These changes caused an updating of active centre meaning.

$$\text{Cellulose} \xrightarrow{K_1} \text{Active cellulose} \xrightarrow{K_B} \text{Volatiles}$$

$$\text{Cellulose} \xrightarrow{K_1} \text{Active cellulose} \xrightarrow{K_2} \text{Solid residue} \xrightarrow{K_3} \text{Solid residue}'' \xrightarrow{K_4} \text{Solid residue}'''...$$
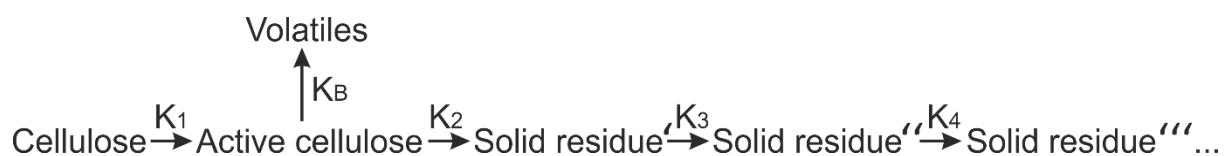
Figure 32. Broido scheme for cellulose pyrolysis

Following the updated Broido's concept, cellulose pyrolysis passes via a transformation of cellulose to "active cellulose" in the initial "incubation period". Importantly, this step proceeds without mass-loss, which can be observed from the S-curve of mass-loss (Figure 30).(*230*)
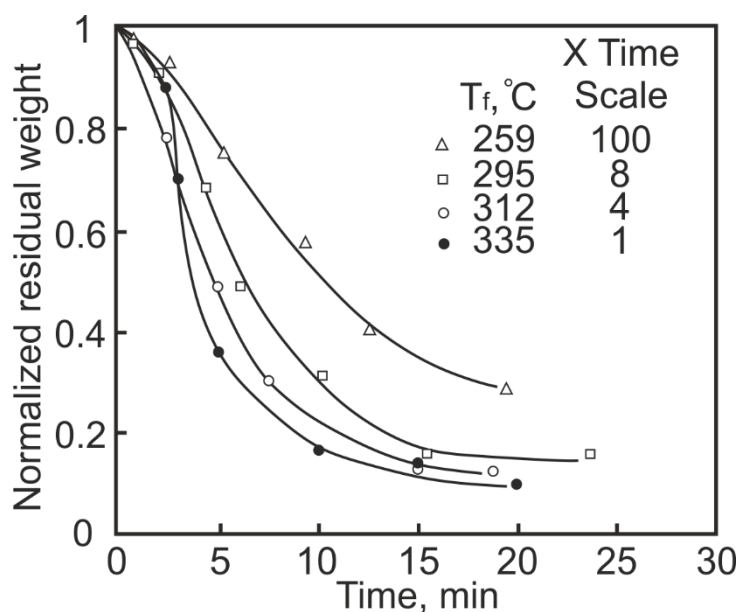
Figure 33. Isothermal mass-loss curves of cellulose pyrolysis at different temperatures(*169*)

Shafizadeh

If Broido used more likely physical and physical-chemical methods in the investigation of cellulose pyrolysis, Shafizadeh used approaches of organic chemistry.

In 1968, Shafizadeh already established his vision, that levoglucosan is considered to be a principle (not primary) intermediate for cellulose pyrolysis.(*174*) He suggested a pathway on the production of ^{14}C labelled cellulose and converted it to LGA selectively labelled in C-1, C-2 and

C-6 positions.(*191*) The pyrolysis of these labelled LGA molecules was done in neat, $ZnCl_2$ and NaOH conditions. The yields of the detected chemicals are displayed in Table 9.

Table 9. The products detected in the pyrolysis of ^{14}C-labelled LGA

Product	Yields, wt%		
	Neat	+ZnCl$_2$	+NaOH
Acetaldehyde	1.1	0.3	7.3
Furan	1.0	1.3	1.6
Acrolein	1.7	<0.1	2.6
Methanol	0.3	0.4	0.7
2,3-Butanedione	0.5	0.8	1.6
2-Butenal	0.7	0.2	2.2
1-Hydroxy-2-propanone	0.8	<0.1	1.1
Glyoxal	1.4	<0.1	4.9
Acetic acid	1.7	0.7	1.5
2-Furaldehyde	0.9	3.0	0.4
5-Methyl-2-furaldehyde	0.1	0.3	-
CO$_2$	2.9	6.8	5.7
Water	8.7	20.1	14.1
Char	3.9	29.0	16.0
Balance (tar)	74.3	36.8	40.3

The distribution of the labelled species is portrayed in Table 10.

Table 10. Percentage of ^{14}C traces of the labelled carbons in the resulted products

Compound	Percentage of ^{14}C labelled carbons, %								
	Neat			5wt% NaOH			5wt% ZnCl$_2$		
	1-^{14}C	2-^{14}C	6-^{14}C	1-^{14}C	2-^{14}C	6-^{14}C	1-^{14}C	2-^{14}C	6-^{14}C
2-Furaldehyde	60.8	103.4	35.8	30.2	100.7	73.0	86.0	95.8	16.6
2,3-Butanedione	24.8	54.6	31.3	16.5	31.0	56.5	64.8	57.7	26.9
Methyl-glyoxal	27.3	26.3	19.1	23.3	42.0	30.7	49.7	46.7	29.6
Acetaldehyde	10.1	30.5	36.0	6.3	29.2	55.1	4.4	7.3	29.8
Glyoxal	15.4	19.2	6.9	25.5	48.3	36.0	29.5	28.2	29.2
CO$_2$	34.3	24.5	6.3	31.2	17.7	8.9	43.7	33.3	9.5

| CO | 21.1 | 18.9 | 16.8 | 38.4 | 18.0 | 13.7 | 36.7 | 27.6 | 11.1 |

Shafizadeh suggested the possible pathways of formation of 2-furaldehyde, 2,3-butanedione, pyruvaldehyde, acetaldehyde, glyoxal, carbon dioxide and carbon monoxide.(*191*) Also, he was working on the mechanisms of LGO formation production of LGA and glucose during cellulose and biomass pyrolysis. (*192–195*),(*196*, *197*)

In 1979, F. Shafizadeh simplified the model of Broido, conducting a series of isothermal cellulose pyrolysis reactions at a temperature range between 259-341 °C (higher than that one of Broido's) under reduced pressure. These conditions were reported to be used in the preparation of levoglucosan and related products during cellulose pyrolysis. The scheme that is now known as Broido-Shafizadeh model is represented in Figure 34.
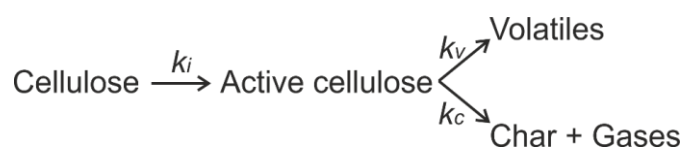
Figure 34. The Broido-Shafizadeh model

Various investigations of cellulose pyrolysis have been carried out, giving a large number of kinetic models and mechanisms.(*174*, *198–200*) For example, Broido used thermogravimetry to study the pyrolysis of filter paper and obtained residual weight-time curves. In the temperature range, 226-259 °C he found that the reaction order was close to first in cellulose mass throughout. The other authors suggested alternative kinetic schemes involving a variety of activation energies to describe cellulose pyrolysis data. (*199*, *200*)

Shafizadeh has found that small sample size (as shown by thermogravimetry on 2 mg samples) leads to smaller char fractions whereas higher pressure (using the procedure in this study with a nitrogen flow at atmospheric pressure) leads to more significant char fractions. This indicates that the residence time of the volatiles in the cellulose during the pyrolysis reaction largely influences the extent of char formation. Pyrolysis of levoglucosan is known to give some residual char, and it has even been suggested that char formation is not a primary step but is a result of repolymerisation of volatile compounds.(*169*)

1.6.2.2. Michael Jerry Antal model

M. J. Antal and co-workers criticized the Broido-Shafizadeh model, in the first turn, for its oversimplicity of a complicated process. The model of Broido was based on the changes in char yield depending on heating rates. Antal considers these differences as small and even negligible.

He argued that both Broido and Shafizadeh worked together with a comparatively large samples mass: 90 mg and 250 mg, respectively. Therefore, there is a possibility that diffusion of the pyrolytic vapours through these relatively large samples led to secondary reactions which could obscure the underlying decomposition chemistry.(*201*)

In contrast to Broido and Shafizadeh, Antal's experimental set up involves the mass of the sample 2-3 mg and applied the kinetic analysis of isothermal curves achieved at a set of temperatures, which allowed him to minimize the physical effects.

Antal and co-workers have described the Broido-Shafizadeh model (Figure 35), using the system of ordinary differential equations (Figure 36).

$$A \xrightarrow{k_B} B \begin{cases} \xrightarrow{k_C} C + \ldots \xrightarrow{k_D} D + \ldots \xrightarrow{k_E} E + \ldots \\ \xrightarrow{k_V} \text{Volatile tar} \end{cases}$$
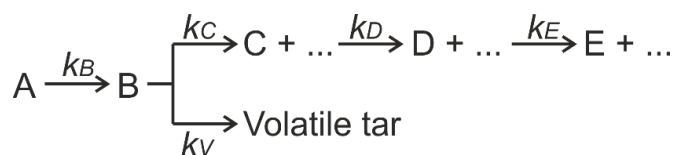
Figure 35. The Boido-Shafizadeh model, represented by Antal, which was used in the calculation of kinetic constants

$$\begin{cases} \dfrac{dA}{dt} = -k_b A \\[4pt] \dfrac{dB}{dt} = y_b k_b A - k_c B - k_v B \\[4pt] \dfrac{dC}{dt} = y_c k_c B - k_d C \\[4pt] \dfrac{dD}{dt} = y_d k_d C - k_e D \\[4pt] \dfrac{dE}{dt} = y_e k_e D \\[4pt] \dfrac{dV}{dt} = y_v k_v B \end{cases}$$

Figure 36. The system of differential equations used to derive the kinetic parameters from the Broido-Shafizadeh model

They found the reaction cellulose → activated cellulose is either very fast or does not take place at all, completely changing the meaning of an active centre initiating pyrolysis. Therefore, Antal has simplified the scheme drawn in Figure 37, receiving the model very similar proposed by D. Arseneau.(*188*)

$$A \begin{cases} \xrightarrow{k_C} C + \ldots \xrightarrow{k_D} D + \ldots \xrightarrow{k_E} E + \ldots \\ \xrightarrow{k_V} \text{Volatile tar} \end{cases}$$
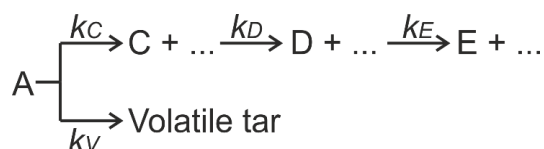
Figure 37. The modified model of Arseneau following to the Antal's vision

The calculated kinetic parameters for the suggested model are present in Table 11.

Table 11. The kinetic parameters, calculated by Antal for the modified model of Arseneau

Reaction	E_{act}, kJmol^{-1}	Rate constants (ks^{-1}) at			
		250 °C	290 °C	330 °C	370 °C
c	147	$8 \cdot 10^{-6}$	$8 \cdot 10^{-5}$	$7 \cdot 10^{-4}$	$4 \cdot 10^{-3}$
d	174	$3 \cdot 10^{-5}$	$5 \cdot 10^{-4}$	$6 \cdot 10^{-3}$	$5 \cdot 10^{-2}$
e	250	$6 \cdot 10^{-8}$	$3 \cdot 10^{-6}$	$1 \cdot 10^{-4}$	$3 \cdot 10^{-3}$
v	238	$(2 \pm .9) \cdot 10^{-8}$	$(1 \pm .4) \cdot 10^{-4}$	$(3 \pm 1) \cdot 10^{-3}$	$(6 \pm 2) \cdot 10^{-2}$

Antal and co-workers showed that the parameters of reaction C (char formation) are very well defined, and their determination is not sensitive to the experimental techniques or the mathematical methods employed. Note that at low temperatures the decomposition is so slow that heat transfer limitations do not impact on results.

In 2001 Banyasz offered an updated kinetic scheme, separating anhydrocellulose and activated cellulose, partially connecting Antal's and Broido-Shafizadeh schemes. The suggested pathway is displayed in Figure 38.(*202*)
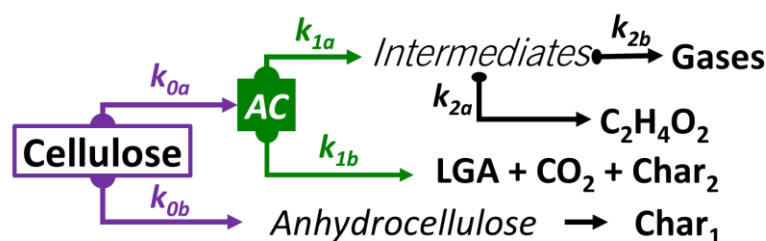
Figure 38. Cellulose decomposition offered by Banyasz

Notable, that $k_{1b} \neq k_{2b} \neq k_{2a}$, making depolymerising (active) cellulose involved in three independent decomposition pathways. Char$_1$ is unrealistically produced without gases. At the same time, there is no apparent difference between depolymerising and anhydro-celluloses.

1.6.2.3. Linda Broadbelt model

Probably, the most comprehensive kinetic model was proposed by Broadbelt and co-workers who reported a detailed mechanistic model for fast pyrolysis of neat glucose-based carbohydrates. A set of the investigated compounds includes glucose, cellobiose, maltohexaose, and cellulose. The kinetic model was obtained through both experiments and theoretical calculations.(*203*, *204*) Over 300 reactions of 103 species were investigated in the mechanistic model to describe the decomposition of cellulosic polymer chains, intermediates decomposition, and formation of over 60 low molecular weight compounds. Each elementary reaction step was specified in terms of Arrhenius parameters. An introduction of thermohydrolysis reaction (hydrolysis happening during pyrolysis) is a novel feature of the work.

The suggested mechanisms of formation of levoglucosan and glucose through chain reactions involving glycosidic bond cleavage and hydrolysis are displayed in Figure 39.
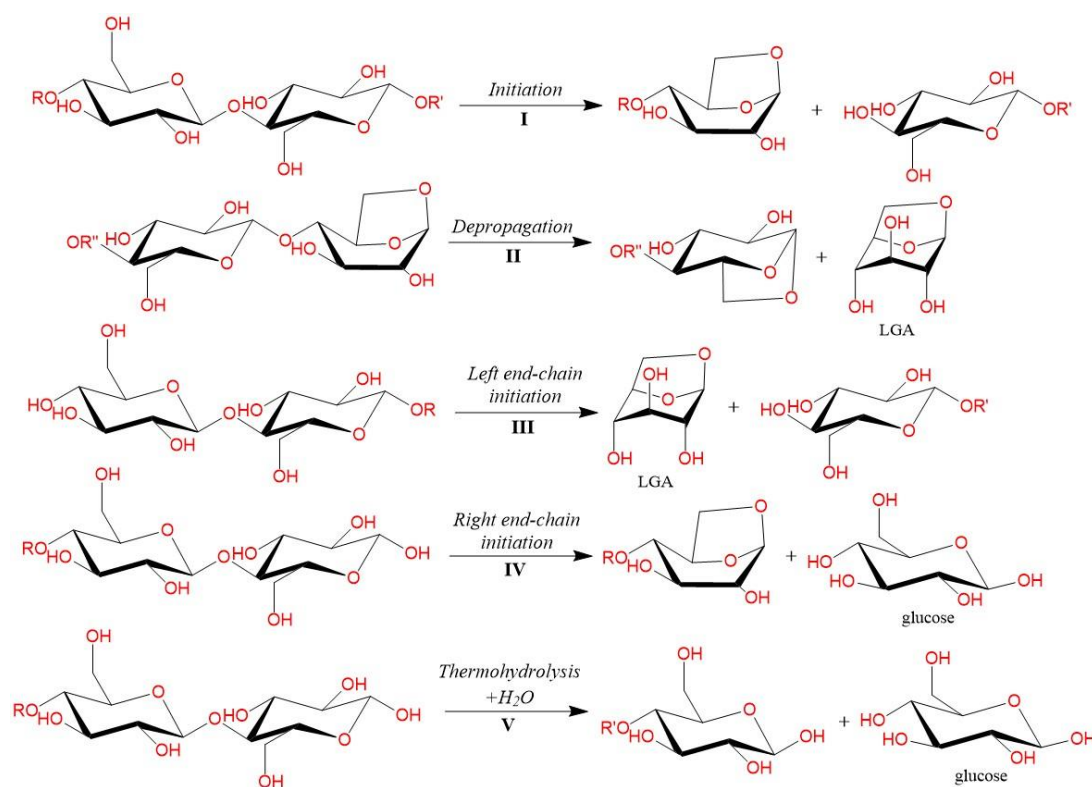
Figure 39. Broadbelt scheme on the formation of LGA and glucose

The steps I-IV (Figure 39) are based on the concerted displacements mechanism offered by Parks, while the reaction of thermohydrolysis was suggested for the first time. The attention on the role of water for facilitating cellulose depolymerization was emphasized earlier in the works of Antal and Mamleev.(*170*, *205*, *206*)

Interesting that there is a minimal number of publications highlighting real-time kinetics of volatiles. At the same time, it is known that precisely kinetic analysis is associated with the development of mechanistic understanding. This challenge is associated with complexity on the real-time monitoring of the volatiles. Any GC-related methods are not suitable for real-time kinetics analysis because the separation of each fraction is required. Other methods like TG-MS are not very suitable for the investigation of such a complex system, especially in terms of quantitative analysis. An invention of such a procedure can substantially facilitate the development of a clear molecular level of understanding of cellulose pyrolysis.

Summary

The literature overview has covered the biorefinery concepts, thermal degradation of biomass, application of various catalysts during biomass pyrolysis as well as mechanistic models for cellulose (one of the major constituents of lignocellulosic biomass) pyrolysis.

Limited petroleum reserves in conjunction with economic, ecological and environmental factors enable to conclude that fossil resources are no longer regarded as sustainable. Biomass offers the most readily implemented and low-cost solution for sustainable advanced transportation fuels, and the only non-petroleum route to organic molecules for the manufacture of bulk, fine and speciality chemicals and polymers.

There are two approaches to the processing of biomass: biological and thermochemical. Alternatively to the biological route, the thermochemical method (pyrolysis) is fast but not sufficiently selective in the production of valuable chemicals. The resulted liquid (bio-oil) is a complicated mixture of oxygen-containing chemicals. The value of these individual chemicals is higher than those of crude oil chemicals because they are readily multifunctional. However, the separation of the complicated mixture to individual compounds is one of the significant challenges for profitable biorefinery. The application of well-established distillation equipment is impossible due to high-oxygen content and chemical instability of the bio-oil. The application of chromatography columns is an expensive decision of large-scale industry.

In such a way, selective thermochemical activation of biomass targeting production of oxygen-containing chemicals suitable for distillation (levoglucosenone, 5-HMF, furfural) is currently under intensive research.

One of the possible ways to improve the selectivity of pyrolysis is conducting it at lower temperatures. It was shown that microwave-assisting pyrolysis activates biomass at ~100 °C lower than conventional. This effect can facilitate a selective production of valuable chemicals during the thermal decomposition of biomass. Application of catalysts is another well-known method to drive the catalytic decomposition of biomass. It is demonstrated that aluminosilicates are promising, cost-efficient, available and green catalysts. However, the development of a clear mechanistic understanding of the influence of heterogeneous catalysts during biomass pyrolysis could substantially facilitate the improvement of biomass (e.g. cellulose) conversion efficiency.

The mechanistic models for cellulose pyrolysis have changed substantially over time. In the middle of 1950s, the visions of the research on the mechanism of cellulose pyrolysis were basically divided by the type of the mechanism: homo- or hetero-lytic. Later in 1960-1970s, a new significant uncertainty has raised – what is an "active cellulose" species? Then, in 1980-1990s, the actual existence of "active cellulose" step was critically questioned. Finally, since the start of 2000s, the researchers' conclusions were made based on mathematical and programming study.

Regardless of a substantial success achieved in this field, there is not a clear vision on the pathway of cellulose thermal decomposition which is supported with an unprecedented amount of experimental data.

All in all, there is a challenge on the selective conversion of biomass (including cellulose) towards valuable chemicals.

In such a way, the PhD thesis **main aim** is to develop selective pyrolysis of biomass towards valuable chemicals based on advanced, green technologies.

A following gaps should be covered to achieve this goal:

- developing a continuous method of the pyrolysis process investigation;
- investigation of the kinetics of cellulose pyrolysis;
- elaboration of a molecular level of understanding of cellulose pyrolysis based on obtained kinetics data;
- identification of parameters control biomass thermal decomposition and high-value chemicals that could be produced during pyrolysis in a pure form;
- the testing developed approaches using other polysaccharides.

Application of novel green technologies such as microwave and catalysis and understanding their influence on the biomass pyrolysis process is another primary goal of the thesis. The application of microwave radiation was suggested as a heating method due to its volumetric character, which ensures that there is no surface overheating.

The proposed approach assumes that the complexity of bio-oil results from secondary reactions of primary pyrolysis products. A special attention should be given to developing methods for suppressing all secondary processes, except for obtaining a specific chemical that is valuable on the market.

A development of a deep understanding of the biomass thermal decomposition mechanism can substantially facilitate the large-scale biorefinery, particularly in choosing a catalyst for the selective transformation of primary product to an easily separated valuable chemical.

CHAPTER 2. MECHANISTIC STUDY OF CELLULOSE PYROLYSIS

2.1 Introduction

There are two main approaches to the activation and utilization of biomass: biochemical and thermochemical (biomass pyrolysis). The scalability of the thermochemical approach has been proven by hundreds of years of production of biochar and bio-oil. Until the 19th century, the scale of charcoal production satisfied all the needs of metallurgy while tar production covered all the demands of shipbuilding. In the 20th century, cheap coking coal and crude oil steadily replaced charcoal and tar. In the 21st century, we are increasingly concerned about crude oil availability, global warming and ecological problems leading to a resurgence in interest in biomass and bio-waste valorisation.(*207–209*) Well established industries produce substantial amounts of lignocellulosic waste (biomass). The pulp and paper industries alone produce 40–50 kg of dry sludge per 1 tonne of paper. In the USA, more than 21 million tonnes of paper and paperboard waste go to landfill every year. The success of future biorefineries will heavily depend on our ability to convert the highly oxygenated building blocks of biomass into many of the chemicals used today.(*210*)

The separation of the bio-oil components produced in pyrolysis of biomass is a major challenge.(*211*) The oils contain high-boiling and thermally unstable compounds making conventional distillation methods problematic. The in-situ control of selectivity to more valuable will be essential if we are to fully exploit this technological route to more sustainable chemical industry.(*49*, *91*, *212*) To do this will require a detailed understanding of the pyrolysis mechanism. Widely accepted mechanisms for cellulose pyrolysis are based only on mass-loss analysis.(*168*, *169*, *213*, *214*) While the systematic analysis of the kinetic behaviour of volatiles produced during pyrolysis has not yet been done.

Information about the kinetic behaviour of all volatile products and intermediates could fundamentally improve the mechanistic understanding of cellulose pyrolysis. This will require a detailed analysis of the compounds produced in the pyrolysis process in real-time. One of the most robust and straightforward methods for online quantitative monitoring of volatile compounds is the Fourier-transform infrared (FTIR) analysis. The pioneering work of Wojtovich has already shown the potential of a thermogravimetry (TG) coupled with FTIR (TG-FTIR) for the study of biomass pyrolysis enabling the quantification of some products.(*215*)

The systematic use of TG-FTIR to thoroughly analysis the volatile compounds produced during cellulose pyrolysis has allowed achieving an unprecedented understanding of the process. Such an approach, in turn, could open the door to more controlled pyrolysis processes maximising the yield of target products. Thus, this chapter proposed an advanced mechanism of cellulose

pyrolysis. This model predicts the maximum 70% yield of levoglucosan at a heating rate around 70Kmin^{-1}. This conclusion is crucial for the development of an efficient and selective LGA-centred biorefinery focusing on levoglusenone, 5-hydroxymethylfurfural and others.

2.2. Details of TG-FTIR experiment

The schematic representation of the TG-FTIR equipment is displayed on Figure *40*.

The sample in the amount of 50±2 mg was placed into the thermostable and chemically inert ceramic crucible. The crucible was located on the sample carrier (stand) connected to balances. When the sample is placed into the oven, the vacuum pump was making the pressure about 5 mbar in the system. In the current experiment, it was used nitrogen as a carrier gas. The oven is filled with nitrogen gas to get atmospheric pressure. The vacuum procedure is repeated three times to remove all oxygen from the system. At the last run, the oven filled with nitrogen gas was opened by means of adapter switcher. The flux of nitrogen at 300 mlmin^{-1} rate was passed via the transfer-pipe and FTIR cell for 40 mins to remove oxygen molecules from the system. Meanwhile, the FTIR detector is cooled with liquid nitrogen. Then the nitrogen gas flow was established at 100 mlmin^{-1}, and the background is recorded. The background was collected on 128 scans at a 4 cm^{-1} resolution for a 550-4000 cm^{-1} range. The cellulose samples were heated up at different heating rates (5, 10, 15, 20, 30, 35, 40, 45 and 50 Kmin^{-1}) from T_{start}=23 °C to T_{final}= 500 °C. The FTIR detector was recording the evolved pyro-gas spectra in time (temperature of pyrolysis) at 32 scans (for heating rates below 35 Kmin^{-1}) or 16 scans (for heating rates above 35 Kmin^{-1}) at the resolution of 4 cm^{-1} and 550-4000 cm^{-1} range of wavenumbers. Each spectrum was automatically associated with the spectra collection starting and finishing times. These times are matching to the thermal regime to understand what an average sample temperature should be assigned with the relevant spectrum.

The initial set of experiments includes the collection of bio-oil into a liquid nitrogen trap. The FT-FTIR oven was slightly modified, and the adapter has been changed to a special glass adapter leading to liquid nitrogen trap. The trap represents a dewar with a cold-finger filled with liquid nitrogen (Figure 41).
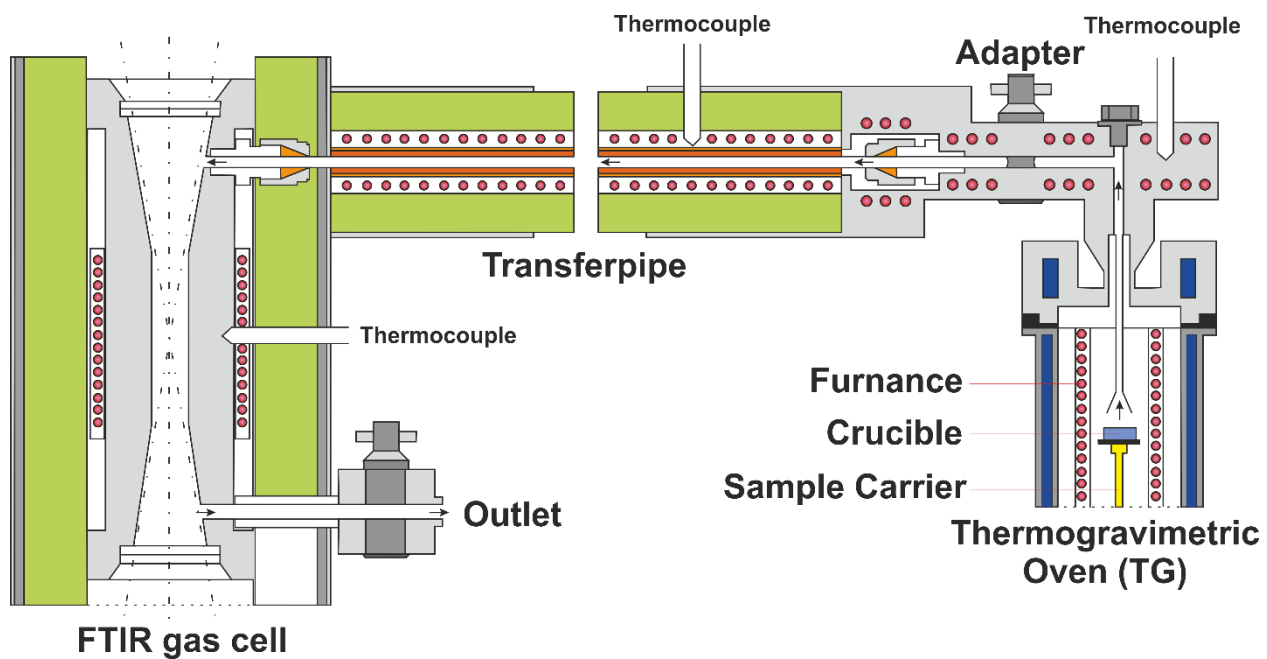
Figure 40. Schematic representation of TG-FTIR set-up
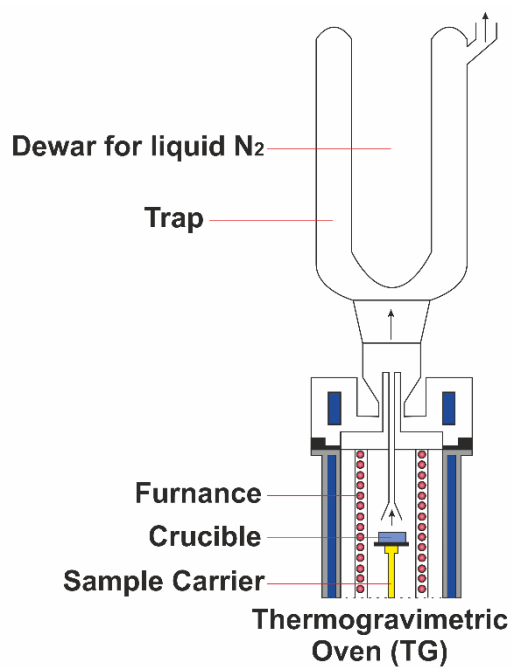
Figure 41. Cold-trap experimental set up
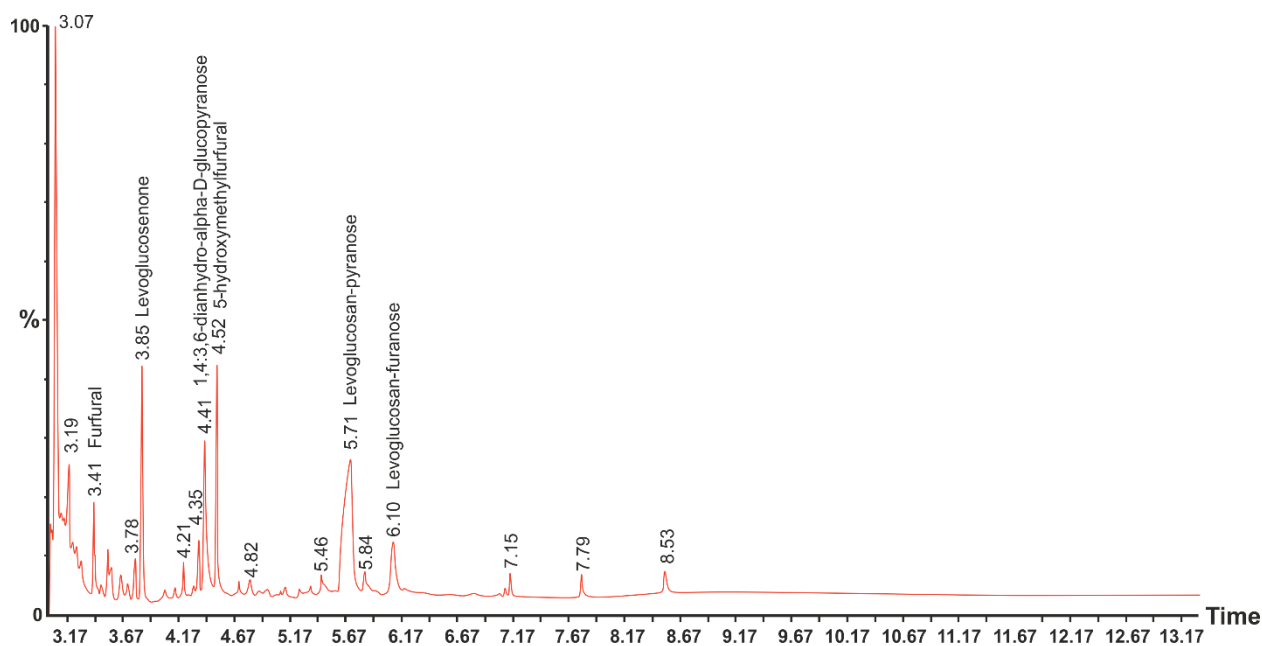
Figure 42. GC-MS spectra of the bio-oil collected at 10Kmin^{-1}

The obtained bio-oil in acetone was submitted for GC-MS analysis, the details of which is described at the relevant part. The obtained GC-MS spectrum is portrayed in Figure 42.

2.3. TGA data processing and char yield

Mass-loss curves were used to find the dTG dependence from time. This curve indicating the amount of mass loss per second (a minute or any other time unit).

It was found that the maximum of cellulose decomposition is shifting towards higher temperatures at faster heating rates (Figure 43). Notably, this shift is observed only at a heating rate below 35 Kmin^{-1}. Above this value, both the temperature of maximum decomposition and the maximum rate of pyrolysis does not change (Figure 43).
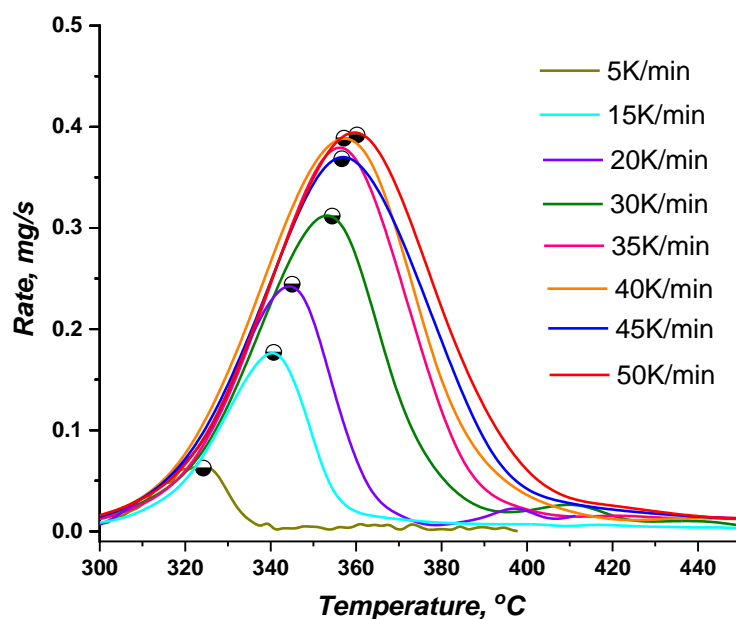
Figure 43. Rate of cellulose decomposition

TG analysis also shows that the amount of char is decreasing with increasing the heating rate (Figure 44), that is in line with the literature.(*216*) The formation of second dTG signal at ~400 °C (20 Kmin^{-1} and 30 Kmin^{-1}, Figure 44) is related to the formation of a chemical compound with high decomposition temperature.
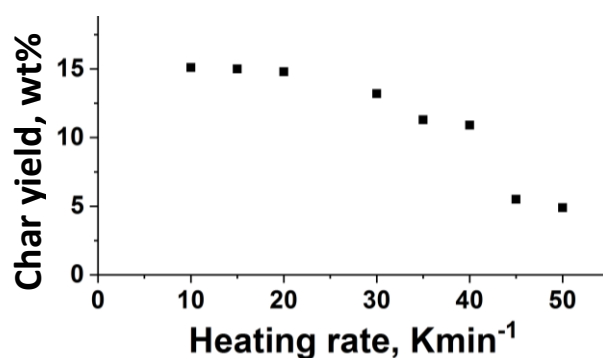
Figure 44. The amount of char depending on the heating rate

2.4. TG-FTIR data processing
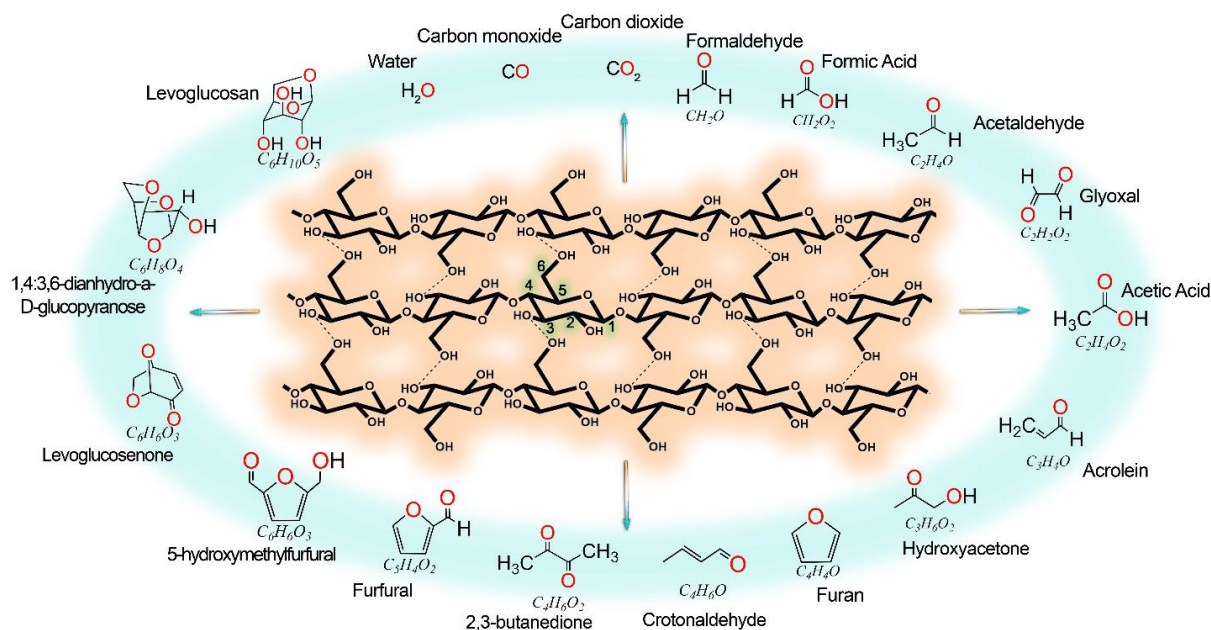
Figure 45. A set of chemicals chosen to describe the cellulose pyrolysis gas mixture

The initial set of standard compounds for the accurate description of experimental FTIR spectra were carefully chosen based on preliminary experiments of the bio-oil collection (Figure 42) and the literature.(*214*, *217*, *218*) It was found that a minimum set of 18 compounds (Figure 45) is representative enough to describe cellulose pyrolysis quantitatively. To estimate the molar absorptivity of the standard compounds, their individual TG-FTIR were obtained. By systematically monitoring the gas-phase FTIR spectra of each standard compound as it is vaporised from the TG furnace, we can measure extinction coefficients of all of 18 compounds (Figure 46A-B). By using linear regression procedure altogether with the extinction coefficients, it is possible to measure the composition of the pyrolysis gases quantitatively and therefore their rate of production. By adding these rates together, it is possible to obtain a total rate of decomposition of cellulose estimated by FTIR. This total rate was then compared to the decomposition rate measured by thermal analysis, with a 98% correlation (Figure 46C). This good correlation evidences the validity of FTIR data processing.

As a further check of the validity of this approach, the $C_xH_yO_z$ contents of the 18 components were added together to identify the composition of the residual char at five different times in the pyrolysis process (Figure 46D). The difference between this total elemental composition and that of cellulose never exceeded 5%.

A

Experimental spectrum
Combination of 18 references

H_2O bands
CO_2 bands
CO bands
H_2O bands
CO_2 bands

Intensity, a.u.
Wavenumbers, cm^{-1}

B

4P 8P 12P 16P
5P 9P 13P 17P
6P 10P 14P 18P
7P 11P 15P

Intensity, a.u.
Wavenumbers, cm^{-1}

C

Time, min
26 28 30 32 34 36 38 40 42

Experimental rate (DTG)
FTIR detected rate

98% correlation fit

Rate, mgs^{-1}
Temperature, °C

D

$$C_{gas} = \sum_{volatiles} mol\%^{volatile} \, i^{volatile}$$

$$C_{system} = wt\%^{char} C_i^{char} + wt\%^{volatiles} C_i^{gas}$$

Carbon   Hydrogen   Oxygen

Temperature, °C	Carbon	Hydrogen	Oxygen
500	C_6	$H_{9.5}$	O_5
352	C_6	$H_{9.64}$	$O_{4.55}$
334	C_6	$H_{9.10}$	$O_{4.6}$
324	C_6	$H_{9.11}$	$O_{4.84}$
305	C_6	$H_{9.93}$	O_5
20	C_6	H_{10}	O_5

wt% from $(C_6H_{10}O_5)_n$

E

Compound name	Yield, wt%
H_2O	30.67
CO	5.94
CO_2	6.00
Formaldehyde (4P)	4.14
Formic Acid (5P)	1.55
Acetaldehyde (6P)	8.07
Glyoxal (7P)	4.22
Acetic Acid (8P)	3.35
Acrolein (9P)	0.06
Hydroxyacetone (10P)	8.33
Furan (11P)	0.02
Crotonaldehyde (12P)	0.01
2,3-butanedione (13P)	0.03
Furfural (14P)	0.77
5-Hydroxymethylfurural (15P)	5.52
Levoglucosenone (16P)	2.03
1,4:3,6-dianhydro-a-D-glucopuranose (17P)	0.50
Levoglucosan (18P)	1.01
Char	15.10
Unidentified	2.53
Total	100.00

Figure 46. TG-FTIR verification procedures and yields: A – comparison between modelling and experimental IR-spectra; B – FTIR-spectra of the standard references; C – comparison between exterimental and FTIR detected rates; D – evaluation of $C_xH_yO_z$ composition of the solid residue based on the TG-FTIR gas composition; E – yields of the chemicals resulted in conventional pyrolysis of cellulose (10 Kmin^{-1})

Such processing and verification procedures make the TG-FTIR method efficient in the quantitative processing of pyrolysis kinetics and chemical distribution of the volatiles (Figure 46E). The developed TG-FTIR processing methodology was then applied to investigate the influence of heating rates (5-50 Kmin^{-1}) on the cellulose pyrolysis products.

2.5. Yields of chemicals resulted from cellulose pyrolysis at different heating rates

The yields of the compounds for the measured heating rates are presented in

Table 12 and Table 13.

Table 12. The yields of the products from the total mass

References	Heating rates, Kmin^{-1}								
	5	10	15	20	30	35	40	45	50
H_2O	31.5	30.7	27.1	25.5	20.1	19.3	17.6	16.5	14.6
CO	5.7	5.9	6.1	5.7	4.9	5.3	5.4	6.4	5.4
LGO	1.4	2.0	2.7	2.8	1.6	1.4	1.1	1.1	0.3
HMF	3.4	5.5	5.8	5.3	4.4	3.8	2.6	2.9	1.6
Furan	0.0	0.0	0.0	0.0	0.0	0.3	1.2	1.8	1.1
Formic acid	1.6	1.6	1.0	1.0	0.3	0.2	0.1	0.1	0.0
Furfurul Alcohol	0.0	0.1	0.0	0.7	3.8	2.9	2.4	1.3	0.6
Furfural	0.0	0.8	2.1	3.0	0.1	0.0	0.0	0.0	0.1
Acetic Acid	2.6	3.4	3.2	2.1	2.0	2.7	1.6	2.5	0.6
CO_2	5.6	6.0	6.7	6.9	9.9	9.1	9.3	8.6	7.9
Formaldehyde	3.4	4.1	4.2	5.4	4.7	5.5	4.9	5.7	5.8
Hydroxyacetone	8.2	8.3	7.8	8.1	9.9	9.0	6.8	5.1	3.2
Acrolein	0.1	0.1	0.1	0.1	0.1	0.0	0.0	0.1	0.0
2,3-butanedione	0.4	0.0	0.0	0.0	0.1	0.0	0.0	0.0	0.0
Acetaldehyde	7.3	8.1	7.7	7.3	9.7	9.9	9.6	11.7	9.8
Crotonaldehyde	0.0	0.0	0.1	0.4	0.8	1.3	1.9	2.1	2.8
Glyoxal	3.3	4.2	4.9	4.4	3.9	3.2	2.5	2.2	0.6
LGA	0.3	1.0	1.2	1.8	5.2	11.0	15.7	21.9	33.2
DGP	0.2	0.5	0.7	1.0	3.0	3.1	3.4	3.8	5.1
TOTAL	**75.2**	**82.4**	**81.5**	**81.7**	**84.6**	**88.0**	**86.1**	**93.7**	**92.8**

Table 13. The yields of the products from the mass loss

References	Heating rates, Kmin^{-1}								
	5	10	15	20	30	35	40	45	50
H$_2$O	40.6	36.1	32.2	31.2	23.3	21.2	19.9	17.4	15.6
CO	7.4	7.0	7.3	7.0	5.5	5.8	6.0	6.8	5.8
LGO	1.8	2.4	3.3	3.4	1.8	1.5	1.2	1.2	0.3
HMF	4.4	6.5	6.9	6.5	4.9	4.2	2.8	3.1	1.7
Furan	0.0	0.0	0.0	0.0	0.0	0.3	1.4	1.9	1.2
Formic acid	2.1	1.8	1.2	1.2	0.4	0.2	0.1	0.1	0.0
Furfurul Alcohol	0.0	0.2	0.0	3.6	0.1	0.0	0.0	0.1	0.1
Furfural	0.0	0.9	2.5	0.8	4.2	3.2	2.6	1.4	0.7
Acetic Acid	3.3	3.9	3.9	2.6	2.3	3.0	1.8	2.6	0.6
CO$_2$	7.3	7.1	8.0	8.4	11.0	10.0	10.2	9.1	8.4
Formaldehyde	4.4	4.9	5.0	6.6	5.2	6.0	5.3	6.0	6.2
Hydroxyacetone	10.6	9.8	9.2	9.9	11.0	9.8	7.4	5.4	3.4
Acrolein	0.1	0.1	0.1	0.1	0.1	0.0	0.0	0.1	0.0
2,3-butanedione	0.5	0.0	0.0	0.0	0.1	0.0	0.0	0.0	0.0
Acetaldehyde	9.4	9.5	9.1	8.9	10.8	10.9	10.5	12.4	10.5
Crotonaldehyde	0.0	0.0	0.2	0.5	0.9	1.5	2.0	2.2	3.0
Glyoxal	4.3	5.0	5.8	5.4	4.4	3.5	2.7	2.3	0.7
LGA	0.4	1.2	1.4	2.3	5.8	12.1	17.2	23.2	35.5
DGP	0.2	0.6	0.9	1.3	3.3	3.4	3.7	4.1	5.5
TOTAL	**96.8**	**97.0**	**96.8**	**99.7**	**95.0**	**96.6**	**95.0**	**99.3**	**99.2**

2.6. Data discussion

It was found that the first pyrolysis product is water, whose kinetics indicates two types of behaviour (Figure 47A). The peak below 150 °C is associated with the evaporation of physisorbed water. The shoulder above 238 °C occurs at temperatures lower than the production of organic compounds (T< 280 °C) and could be associated with the first stage of cellulose pyrolysis. This observation is in good agreement with Broido's hypothesis of dehydrocellulose (DHC) formation as a result of inter-molecular condensation, supported by recent studies on glycosidic bond cleavage.(*70*, *168*)

This water release could cause a point defect in the cellulose polymer structure, forcing disturbance of nearby hydrogen bonds and provoking further decomposition. Increasing the heating rate simplifies significantly the composition of the volatile mixture produced at >280 °C (Table 12 and Table 13). The total volatile mixture can be divided into two groups. The first group comprises CO_2, CO, formaldehyde, and acetaldehyde. The hydroxyacetone was not included to the list because its yield is depending on the heating rates (Table 13). The molar yield of the chosen compounds is substantially higher than that of other products for all heating rates (Figure 47B), and their total yield corresponds to 1/3 (33wt%) of the cellulose mass loss (Figure 47C). As the char yield is small at fast heating rates (5wt%), we can assume that rest of the mass (up to 66%) will comprise the second group of compounds and consistently corresponds to the remaining 2/3 (67wt%) of the total mass.(*170*)
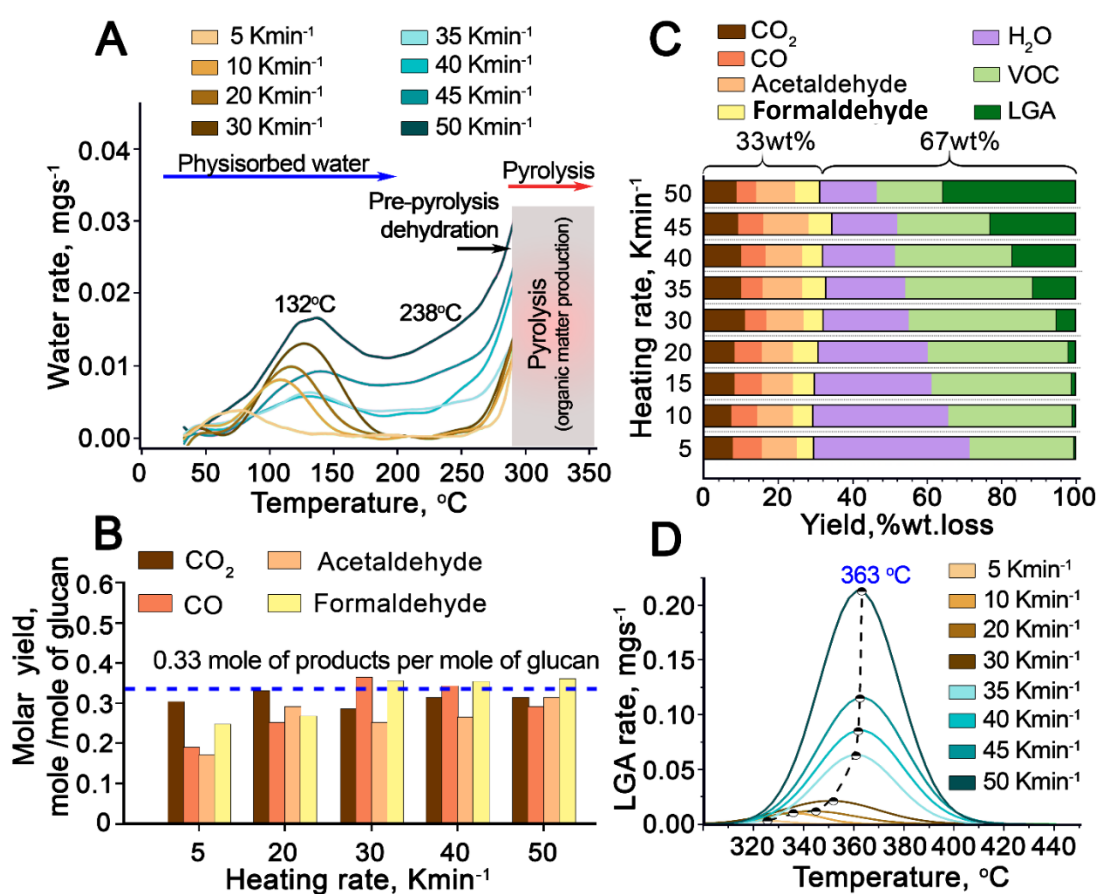
Figure 47. Experimental data: A – water kinetics, B – molar production of some compounds; C – weight production of some compounds; D – LGA kinetics

These observations are consistent with a cluster (elemental unit) of three glucans at the heart of cellulose pyrolysis. One glucan can decompose to produce the first group of compounds. The products of decomposition of the other two glucan molecules include levoglucosan (LGA), other volatile organic chemicals (VOC) and water (Figure 47C). The VOC composition is similar to

those previously reported for LGA decomposition.(*174*) It is reasonable to assume that LGA is the primary product of the decomposition of these two glucan molecules (within the cluster) which can then subsequently decompose to other organic compounds. The influence of heating rate on the LGA/VOC ratio could be explained by the existence of two different pathways for LGA release.(*219*) At low heating rates (<35 Kmin^{-1}) only a small fraction of LGA is removed from the cell by the gas flow. The major part of this compound likely decomposed to VOCs before its boiling point (~380 °C) (Figure 47C&D). The heating rate-raising increases the temperature of cellulose decomposition, allowing LGA to survive until it boils off. Therefore at fast heating rates, the LGA yield is considerably increased (Figure 47D, heating rate > 35 Kmin^{-1}).

2.7. The discussion of cluster cellulose pyrolysis mechanism

The first step in the proposed cluster transformation involves cleavage of a glycoside bond (Figure 48) to create a new $C^{(4)}$-O-$C^{(6)}$ intermolecular linkage and free cellulose chain-end (Figure 48, step 1a). This event causes irregularity of the crystal structure, damaging the hydrogen bonds of neighbouring molecules. Typically, point defects involve surrounding units, and we have considered the potential behaviour of 6 neighbouring glucan molecules (from **G-3 to G+3)** (Figure 48).
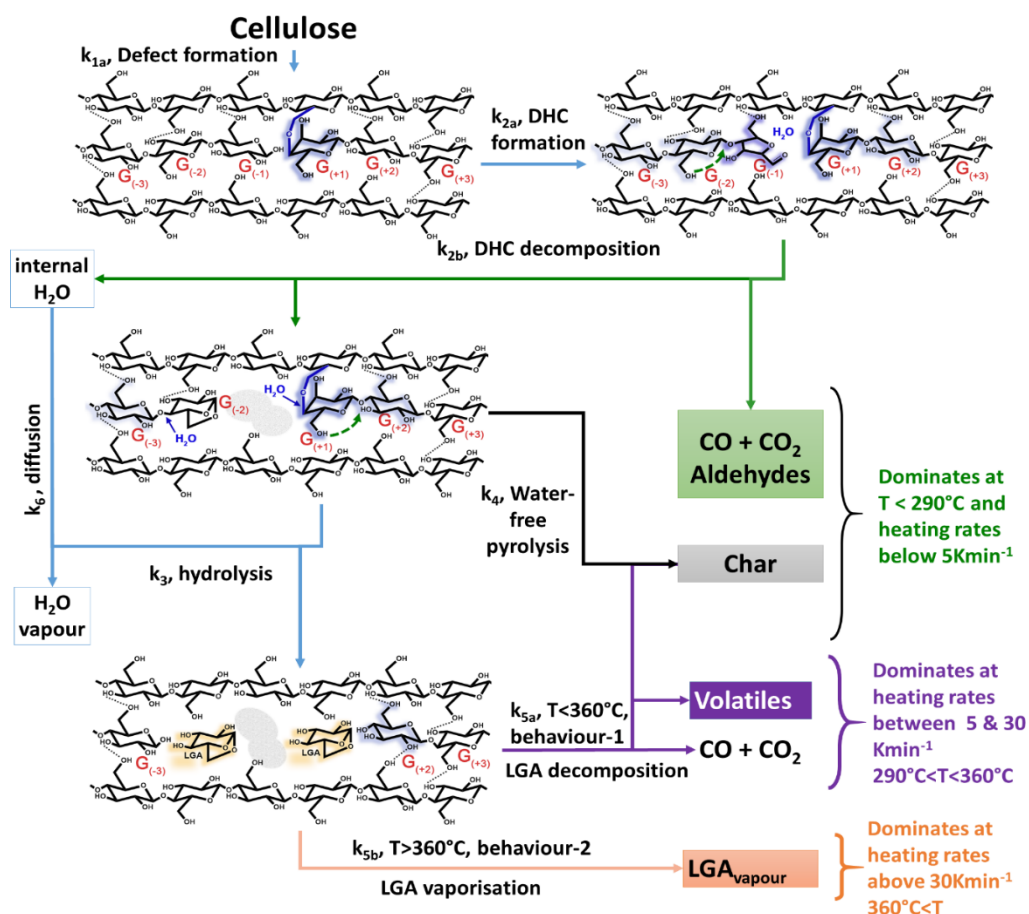
Figure 48. The suggested scheme for cellulose pyrolysis (where **G(-3)** is the glucan on the left of the chain and **G(+3)** is on the right)

After the formation of this new inter-molecular bond, the reaction can proceed via dehydration of **G(-1)** giving a 5-membered ring unit (Figure 48, step 2a and **G(-1)**) followed by conversion to the first group of compounds along with the production of an LGA-like structure from **G(-2)** (Figure 48, step 2b). Water molecules interact with **G(+1)** and G(**–2**) (Figure 48, step 3). The **G(-2)** is directly converted to LGA, while the **G(+1)** requires further glycosylation to produce another molecule of LGA (Figure 48, step 3). This mechanism could be repeated, but the H-bond to the $C^{(6)}H_2$-OH group of **G(+2)** orientated to the top cellulose chain is not damaged by the defect and blocks the cellulose unzipping in this direction. The self-developing depolymerisation on the left side of the cluster (**G-3**) is blocked due to both the H-bonding network and the lack of water available for hydrolysis.

The cluster mechanism explains the simultaneous production of up to 67wt% of the LGA/VOC fraction and 33wt % of the gases/aldehydes mixture during fast cellulose pyrolysis and is consistent with the reported practical maximum of 60-70% LGA.(*206*, *220*, *221*) Furthermore, it was observed that dried cellulose pyrolysis gives a 15% lower yield of LGA and a 15% increase in char.(*206*, *222*) Our scheme could likely explain this phenomenon showing that in the absence

of water, **G(-2)** and **G(+1)** cannot be hydrolysed to LGA and will instead be dehydrated to char (Figure 48, step 3a).

2.8. Chemical kinetics

The cluster mechanism (Figure 48) was described as a scheme (Figure 49A) representing a system of non-linear differential equations (Figure 49B). Notably, it was not considered the way of LGA release from the system to reduce the complexity (k_{5a} and k_{5b} from Figure 48 in the main body were not calculated). Furthermore, to reduce the number of parameters influencing the kinetic constants, it was decided to find them for isothermal pyrolysis conditions (T = const, then k_i are constants) and then to expand the solution for non-isothermal pyrolysis (250 °C<T<300 °C)

The isothermal pyrolysis of cellulose was done on the Bruker TGA furnace conducted at the temperature range between 255-300 °C. The thermal regime included the heating to 15 degrees below the targeting temperature with 10 Kmin^{-1}. Then the heating rate was reduced to 3 Kmin^{-1} to carefully reach the targeting isothermal pyrolysis temperature (255, 270, 280, 290 and 300 °C). The mass-loss curves are displayed in Figure 50.

A

$$\text{Cellulose} \xrightarrow{k_1,\ fluctuation} G(-2) + G(-1) + G(+1)$$

$$G(-1) \xrightarrow{k_2,\ decomposition} \text{Gases + aldehydes } (P_I)$$
$$\downarrow H_2O$$

Locally available H_2O:

$$G(-2) + H_2O \xrightarrow[\text{hydrolysis/rearrengment of sugar-end}]{k_3\ G(-2)} \text{LGA } (P_{II})$$

$$G(+1) + H_2O \xrightarrow[\text{hydrolysis/rearrengment of LGA-end}]{k_3\ (G+1)} \text{LGA } (P_{III})$$

No locally available H_2O:

$$G(-2) \xrightarrow{k_4\ G(-2),\ decomposition} \text{Organic fraction with M < 144 g/mol } (P_{IV})$$
$$\downarrow H_2O$$

$$G(+1) \xrightarrow{k_4\ G(+1),\ charring} \text{Char}$$

Weight loss function = $P_I + P_{II} + P_{III} + P_{IV} + H_2O$

B

$$\frac{dC}{dt} = -k_1C$$

$$\frac{dG(-1)}{dt} = \frac{k_1C}{3} - k_2G(-1)$$

$$\frac{dG(-2)}{dt} = \frac{k_1C}{3} - k_{4\ G(-2)} \cdot G(-2) - k_{3\ G(-2)}\ G(-2) \cdot H_2O$$

$$\frac{dG(+1)}{dt} = \frac{k_1C}{3} - k_{4\ G(+1)} \cdot G(+1) - k_{3\ G(+1)}\ G(+1) \cdot H_2O$$

$$\frac{dP_I}{dt} = k_2G(-1)$$

$$\frac{dP_{II}}{dt} = k_{3\ G(-2)}\ G(-2) \cdot H_2O$$

$$\frac{dP_{III}}{dt} = k_{3\ G(+1)}\ G(+1) \cdot H_2O$$

$$\frac{dP_{IV}}{dt} = k_{4\ G(-2)} \cdot G(-2)$$

$$\frac{dchar}{dt} = k_{4\ G(+1)} \cdot G(+1)$$

$$\frac{dH_2O}{dt} = k_2G(-1) + k_{4\ G(-2)} \cdot G(-2) - k_{3\ G(-2)}\ G(-2) \cdot H_2O - k_{3\ G(+1)}\ G(+1) \cdot H_2O - k_{DIFFUSION}$$

Figure 49. Scheme for the kinetics modelling and related system of non-linear differential equations
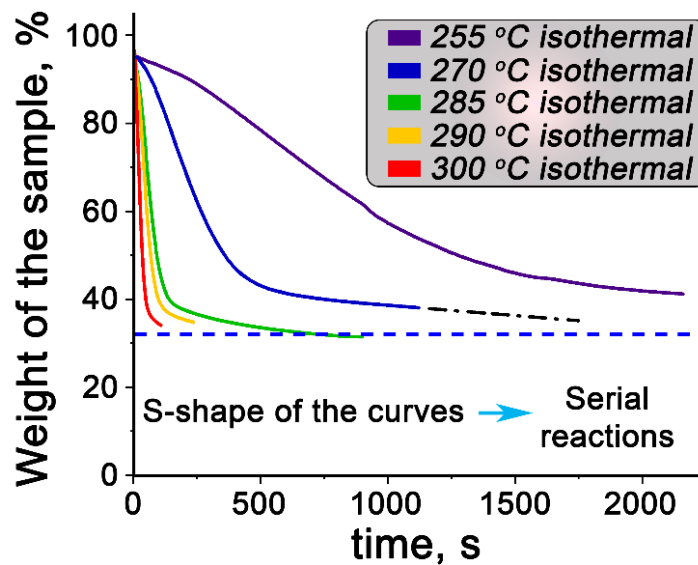
Figure 50. The mass-loss curves for isothermal pyrolysis of cellulose at different temperatures

The k_{1-4} and $k_{diffusion}$ are free parameters to be determined further in this section. The initial conditions (Figure 49B) are Dirichlet: $C|_{t=0} = 97$ (considering physisorbed water loss), $G(-2)|_{t=0} = 0$, $G(-1)|_{t=0} = 0$, $G(+1)|_{t=0} = 0$, $H_2O|_{t=0} = 0$. Solving a set of the first, second, third, fourth and ninth equations, we obtain C, $G_{1,2,3}$ and H_2O as functions of time. Then using the Barrow theorem, it is possible to calculate $P_{1,2,3,4}$ e.g. $P_1 = k_2 \int_0^t G_1 dt$, etc. Once the solutions are found, it was marked $P_1 + P_2 + P_3 + P_4 = P$ vs. t against the experimental data, C = C(t), varying the coefficients, k_{1-4} and $k_{diffusoin}$, until P and C match. This is to be solved numerically.

The results, including all the intermediates and fitting to the experimental mass-loss, are shown in Figure 51A (for 300 °C). One of the products resulted in cellulose pyrolysis is char (grey line, Figure 51A), and our model can predict its formation in time. It was decided to follow the grey char prediction line and stop cellulose pyrolysis at the time when the amount of char is not significant (below ATR-FTIR detection threshold, **point 1** in Figure 51A) and at the time, when the amount of char is significant following to the model prediction (**point 2** in Figure 51A). The ATR-FTIR spectra for these solids are shown in Figure 51B. The char characteristic bands (between 1550 and 1800 cm^{-1}) are absent for **point 1** and present for **point 2** as predicted. The same procedure was repeated for all samples of isothermally degraded cellulose, verifying the model. Natural logarithm of the found k_{1-4} and $k_{diffusoin}$ constants were plotted vs isothermal pyrolysis temperature Figure 51A. The found k_i dependency on the temperature was used to enhance the model to non-isothermal pyrolysis providing Figure 51A.
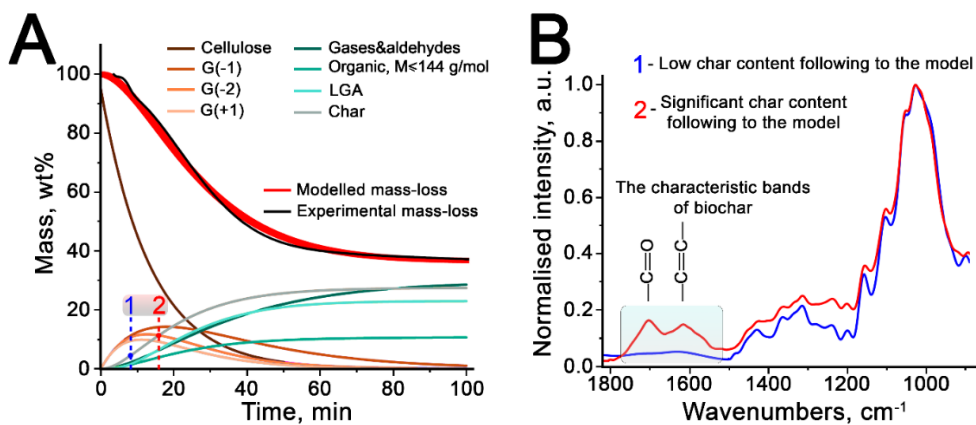
Figure 51. Modelling kinetics: A-formation of the intermediates in time; B-FTIR-verification of the modelling results (original in colours)

The determined kinetic constants follow the Arrhenius equation, demonstrating the robustness of the model and allows us to determine activation energies which are in the range of 100-215 kJmol^{-1} for most steps (Figure 52A).

Interception points for lines plotted in Arrhenius coordinate indicates a Kinetic Compensation Effect (KCE). KCE implies that the set of the chemical processes have the same rate-determining step but the parameters governing the process vary.(*223*) In the case of solid-state cellulose decomposition reactions, KCE could be associated with a combination of localised rate-determining step such as bond creation/breakage and a micro-phase rearrangement of the surrounding polysaccharide chains.(*224*) There are two isokinetic temperature points around 330 °C and 360 °C indicating the separation of all pyrolysis kinetic steps into two groups according to their rate-limiting step. The first, low-temperature point, could be associated with glucan transformation while the second is associated with hydrolysis.

The kinetic constants were also verified with the non-isothermal pyrolysis kinetic data and used to predict the influence of heating rates on cellulose pyrolysis (Figure 52B).
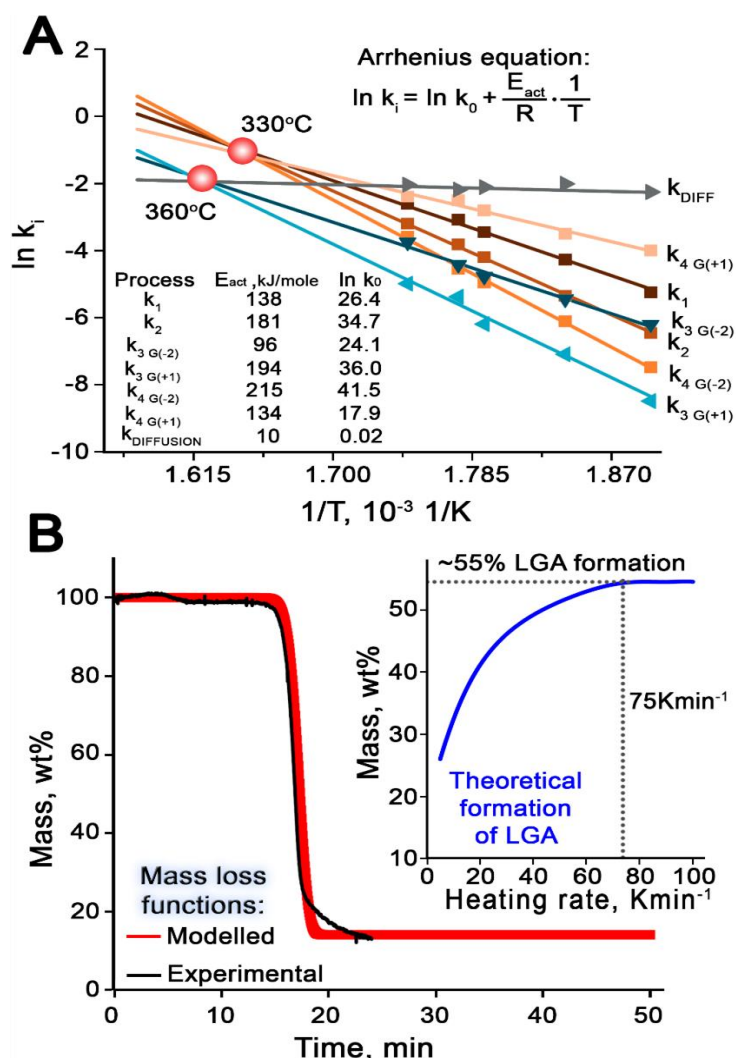
Figure 52. Modelling kinetic results: A – dependency of kinetic constants on the temperature; B – verification of model and LGA prediction (insertion)

The excellent correlation between modelled and experimental mass-loss curves is evidence for the predictive ability of the cluster model. Furthermore, the levoglucosan maximum yield of 55wt% predicted at a heating rate of 70 Kmin^{-1} is in good agreement with the literature (78 Kmin^{-1}, (*225*)) and quite close to the experimental value of 66wt %.

Conclusions

In conclusion, a quantitative FTIR analysis of pyrolysis gases in real-time has been developed and successfully applied to the investigation of the cellulose decomposition process. This allowed to achieve the following results:

- LGA was confirmed as a primary product of this process, and here it was shown how best to maximise its yield. This conclusion is crucial for the development of an efficient and selective LGA-centred biorefinery as well as the potential for the production of other compounds that are formed from LGA (e.g. the increasingly commercially important levoglucosenone).

- An updated mechanism of cellulose pyrolysis based on the quantitative FTIR analysis of pyro-gas was proposed. The model comprises defect formation (active centre) affecting a cluster of a minimum of three glucans. One glucan is decomposed to H_2O, CO_2, CO, formaldehyde and acetaldehyde, while the other two glucan can be converted to LGA at the presence of internal water. The suggested pathway of cellulose decomposition explains the maximum experimental yield of LGA of 66%. This conclusion is novel and substantially contribute to the development of state-of-the-art of pyrolysis science.

- Kinetic constants of the proposed mechanism of cellulose pyrolysis were determined based on the on the obtained kinetic data. The estimation of the kinetic constants was done solving the relevant system of non-linear differential equiations. The derived kinetic constants indicated on the presence of kinetic compensation effect, meaning there is a combination of localised rate-determining step such as bond creation/breakage and a micro-phase rearrangement of the surrounding polysaccharide chains. This conclusion reveal a crucial role of cellulose supramolecular structure and water-bonds in the thermal rearrengment of the polysaccharide.

- The obtained kinetic constants were used to predict the best conditions on the LGA yield. The suggested model predicts the production of LGA in a yield of ca 66wt% (practical maximum) at heating rates around 65-70 Kmin^{-1} and temperature of ca. 360 °C.

- Apart from the LGA pathway of cellulose decomposition, the suggested model predicts optimum conditions for the formation of bio-char and bio-tar. Both of these pathways are in good agreement with the concepts of Shafizadeh, Broido, and Antal.(*169*, *190*, *201*)

These conclusions facilitate the development of the state-of-the-art of pyrolysis science as well as industrial technology to produce LGA in multi-million tonnes.

CHAPTER 3. CONVENTIONAL PYROLYSIS OF CELLULOSE IN THE PRESENCE OF CATALYSTS

3.1. Introduction

Catalytic conventional pyrolysis of cellulose is one of the most popular routes to drive the pathway towards more valuable chemicals or high-value char.(*226*) Catalytic upgrading of cellulose pyrolysis volatiles plays a crucial role in the transformation of high-complex organic mixture towards valuable chemicals facilivating the development of large-scale biorefinery.(*135*, *137*, *227–229*) The catalysts for future sustainable biorefinery should be cheap and available. The approach developed in the chapter 2 can be extended towards catalytic pyrolysis of cellulose.

The aim of the current chapter is a thorough analysis of conventional cellulose decomposition in the presence of acidic catalysts. This study was performed based on the TG-FTIR experiment. Sulfuric acid was chosen as a strong acid, known for driving cellulose pyrolysis pathway towards levoglucosenone. Bentonite and ZSM-5 were chosen as aluminosilicate catalysts. These catalysts were mixed with cellulose at a set of different ratios from 5wt% to 99.5%.

3.2. Strong acids

The composition of bio-oil resulted in the pyrolysis of cellulose doped with phosphoric and sulfuric acids was reported between 1960-1980.(*72*, *101*, *103*)

The impregnation of cellulose with strong acids was carried out via soaking the cellulose in the aqueous solution containing the necessary amount of acid. The water was evaporated under vacuum. Such impregnation process is standard; however, it can result in partial hydrolysis of cellulose.

Huber group studied that sulfuric acid is a better catalyst for cellulose conversion to LGO compared to phosphoric acid.(*97*, *230*)

The amount of acid loading was 1, 3 and 7wt%. The TG-FTIR spectra were recorded at $10Kmin^{-1}$ heating rate. Processing of the collected data was done following the developed procedure developed in chapter 2, checking the data by the cold-trap experiments.

The yields of some valuable chemicals are represented in Table 14.

Table 14. Yields of some valuable chemicals resulted from H_2SO_4-doped cellulose pyrolysis

Chemical	Yield, wt%		
	1wt% H_2SO_4	3wt% H_2SO_4	7wt% H_2SO_4
HMF	4.3	4.1	3.7
LGO	3.1	7.7	5.2

LGA	1.8	1.1	0.4
Solid residue (at 500 °C)	14.1	15.2	18.5

As it is seen from Table 15, the yield of solid residue was increasing at higher acid content. The pyrolysis of biomass is related with the removal of oxygen, producing high-value char. The reduction in oxygen content can proceed in two different ways via the production of carbon-containing oxygenated species (CO_2, CO, oxygen-containing organic molecules) or H_2O. Sulfuric acid is a dehydration agent; therefore, it may result in deoxygenation via removal of water, keeping more carbon at the char. This would lead to a higher char yield.

The trends for HMF and LGA are similar (Table 14). Their yields are slightly decreasing at higher acid loading. Reduction of HMF yield can be associated with its further acid transformation, for example, to levulinic acid, which is a well-known product of 5-HMF decomposition. A decrease of LGA yield can be associated with its conversion to LGO.

The yield of LGO is passing via maximum, which is in line with other studies.(*101*, *103*) At low acid content, it helps to dehydrate the cellulose, while high acid loadings lead to the decomposition of LGO.

All in all, a direct mixing of cellulose with a strong acid is a well-known method for levoglucosenone production. The maximum LGO yield (7.7wt%) was achieved in the case of 3wt% loading of H_2SO_4, while higher acid loading caused the decreasing of the LGO yield. Therefore, the amount of acid catalyst should be optimal to prevent LGO decomposition.

3.3. Aluminosilicates

3.3.1. Bentonite

The conventional pyrolysis of cellulose in the presence of clays was reported to improve yields of valuable molecules, including LGO.(*231*) So a systematic investigation of the bentonite-cellulose system is necessary to find optimal pyrolysis parameters, targeting production of valuable chemicals.

The cellulose was mixed with bentonite in a set of different ratios from 2wt% to 99.5wt% of the clay. The solids were thoroughly mixed in an agate mortar over 15 mins prior to pyrolysis. The conventional pyrolysis of the clay/cellulose mixtures at the set of different ratios was studied via TG-FTIR method. The heating rate was 10 Kmin^{-1}. The mass of the cellulose in each sample was fixed at 50 mg.

It was found that the initiation of pyrolysis is independent of the amount of clay. It happens around 300 °C. In contrast, the temperature of the maximum of cellulose decomposition is sensitive to the clay content (Figure 53). Mixing cellulose with 40% of clay leads to an increase in the temperature of the decomposition rate maximum to ~360 °C. The further mixing does not crucially change the position of the maximum but significantly reduces its intensity. The shift of the maximum temperature of the decomposition is likely due to thermal lag.(*232*).
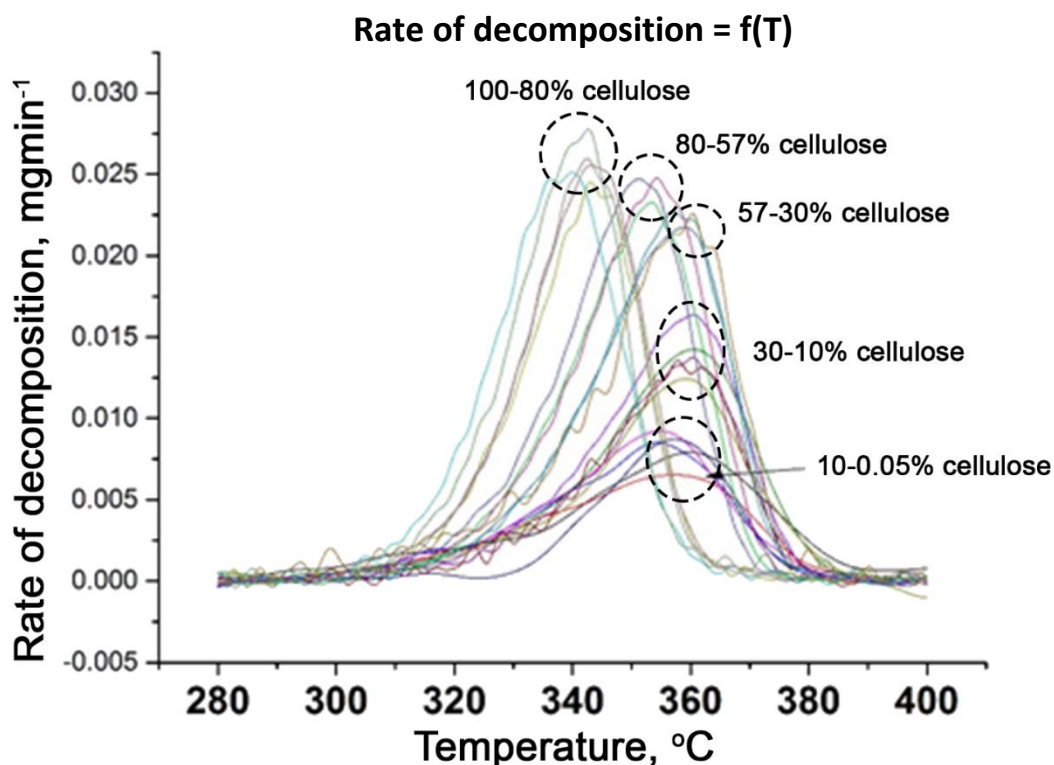
Figure 53. The decomposition rate of cellulose-bentonite mixtures

The processing of FTIR data included a spectrum extraction at the maximum of cellulose decomposition for each sample. Then, the extracted spectra were normalised from 0 to 1 and displayed at the graph showing the spectrum dependency on the cellulose/clay ratio (Figure 54). This approach helps to qualitatively identify the influence of clay on the composition of the produced volatiles. According to Figure 50, the FTIR spectra of this volatiles could be separated onto five zones. Switching between these zones happens suddenly. It is logical to match these zones to the five cellulose/clay systems with different properties.
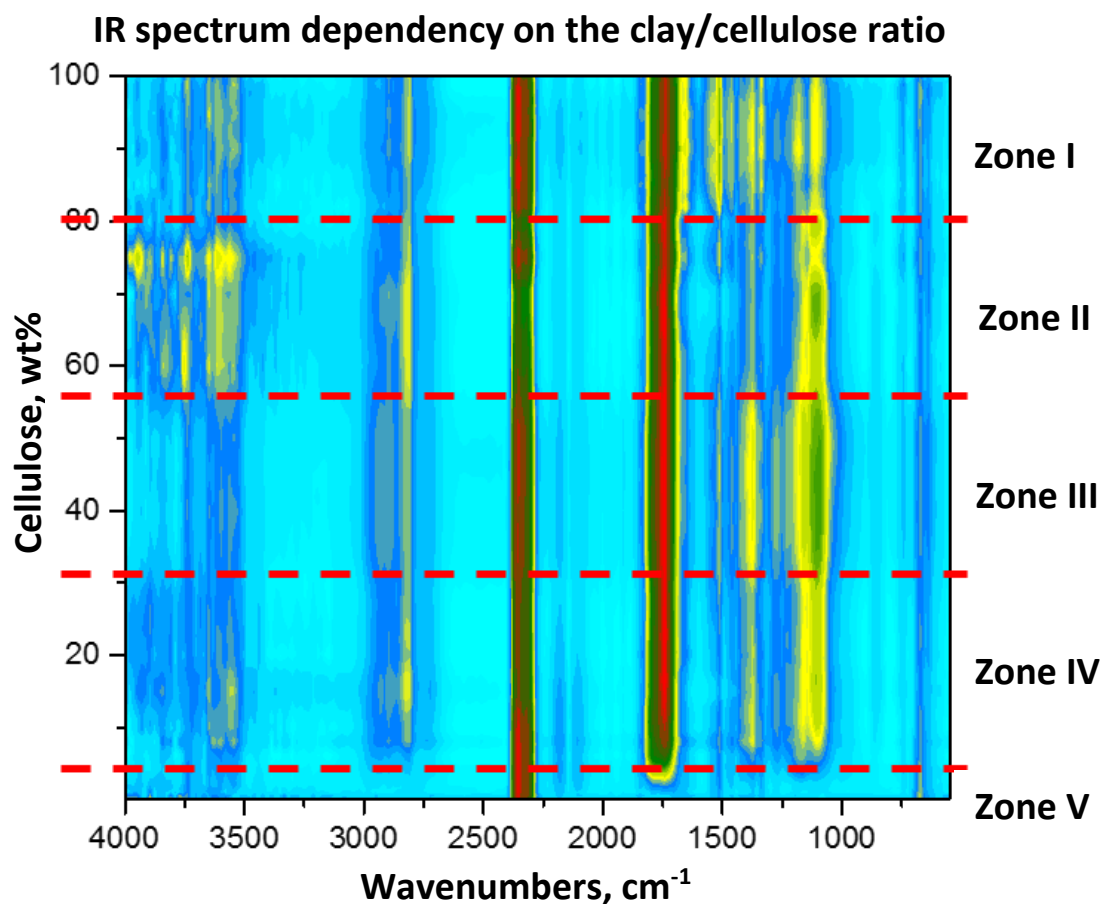
Figure 54. TG-FTIR of the cellulose/clay system: mapping of spectra at the maximum decomposition rate for each cellulose/clay ratio

Each of the zones has distinctive features (Figure 54):

1) The first zone (100% of cellulose up to 80% of cellulose/20% of clay) includes relatively complicated spectra which are close to the gas pahse spectrum obtained on heating (pyrolyzing) neat cellulose. The highest intensity is observed for carbonyls (HC=O, C=O groups, 1650-1900c m^{-1}) and CO_2 (2250-2400 cm^{-1}).

2) The second zone is characterised by the increased contribution of the water bands (3500-4000 cm^{-1}) and the reduction of CO_2.

3) The third zone showed increased impact and broadness of the C-O bands at the region 1000-1250 cm^{-1}.

4) The pattern of the fourth zone is similar to the second one, although less water

5) The fifth region represents the full decomposition of cellulose to CO_2, CO, H_2O.

The existence of these zones can be explained based on a combination of two effects: a catalytic transformation of gases over catalytically active solid and "dissolution/separation" of cellulose particles by the particles of clay.

To better understand the role of these two factors in the formation of the zonal performance of cellulose/call mixture, similar experiments have been done for cellulose mixture with catalytically inert material. Such materials should not possess any catalytic active centrs and it was decided to use a glass as such inert material. Ordinary borosilicate glass has been crushed over ball milling and mixed with cellulose at a set of different ratios. The borosilicate glass is considered to be chemically inert and does not contain porous media, making it an ideal candidate to study the effect of "dissolution".

Similarly to the bentonite samples, the spectra at the maximum rate of decomposition has been extracted for all glass/cellulose mixtures. The resulted graph is displayed in Figure 55.
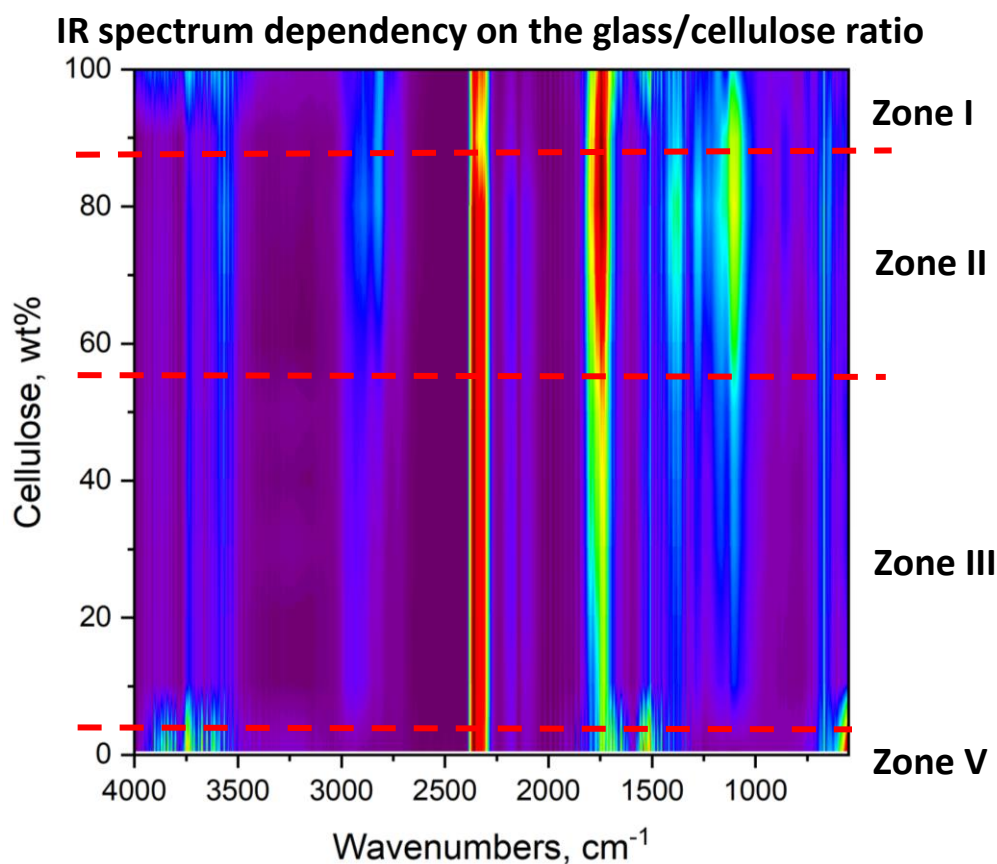
Figure 55. TG-FTIR of the cellulose/glass system: mapping of spectra at the maximum decomposition rate for each cellulose/glass ratio

The FTIR spectra obtained from the glass/cellulose system can be separated only into four zones, showing the absence of the 4th zone (Figure 54). The 5th zone is present because a complete decomposition to CO_2, CO and H_2O is observed. The absence of the 4th zone indicates that bentonite possesses catalytic effect, creating an additional zone and influencing on the distribution of the products.

The positions labelled with lines 1st, 2nd, and 5th of the glass/cellulose zones are close to theboundaries of bentonite/cellulose zones. This implies that one of the possible explanations of zonal behaviour is the effect of "dilution" of cellulose particles with the other particles of solid. Under the "dilution" it is needed to understand a distance between the cellulose particles or local concentration of the products of their (cellulose particles) decomposition.

As was shown in chapter 1 of this thesis, pyrolysis is a natural autocatalytic process, having an initiation stage. This initiation stage is complex and is related to the partial decomposition of the cellulose polymer.(*168*, *221*) The decomposition includes the production of water and acids, which have a strong influence on the pyrolysis pathway and may be partially responsible for the zonal behaviour.
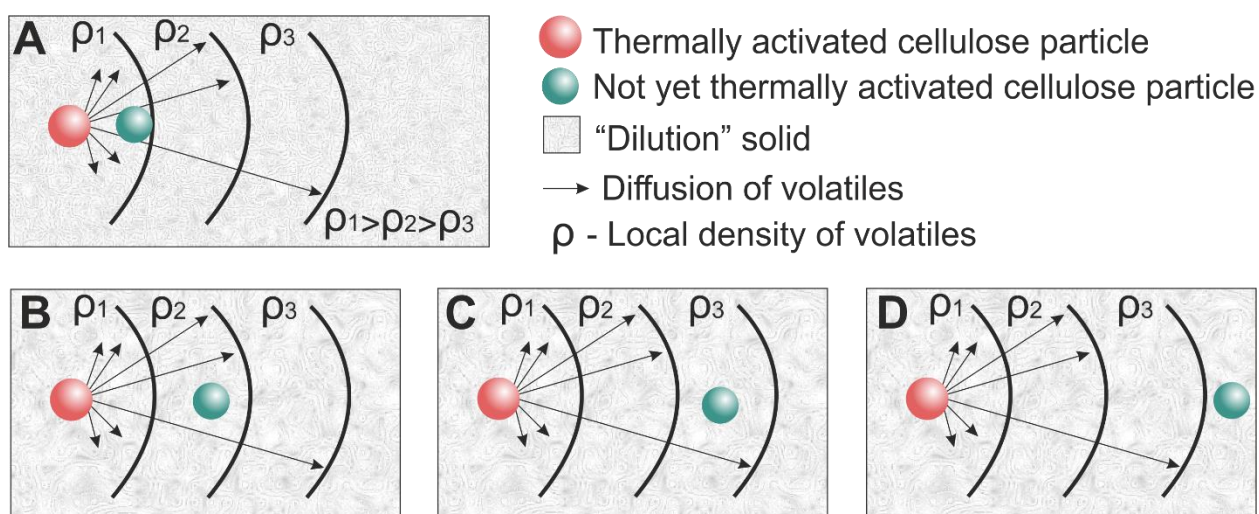
Figure 56. The scheme suggested explaining stepwise changes (zonal behaviour) of volatiles composition for cellulose-any solid pyrolysis

Figure 56 shows an imaginary experiment of cellulose pyrolysis at the initiation stage. Let us imagine that the small thermally-activated cellulose particle (red sphere, Figure 56) is decomposing, producing volatiles. The density (ρ) of these volatiles will be reduced inversely proportional to the square of the distance from the particle centre. Therefore, the catalytic effect of these active volatiles on the another nearest non-activated particle (blue sphere, Figure 52) will be reduced with a distance between the cellulose particles. At the specific degree of cellulose dilution, the autocatalytic pathway of pyrolysis will be inhibited. Accordingly, the cluster mechanism proposed in Chapter 2, the composition of the products, in this case, will be changed closer to the volatiles mixture produced from the self-decomposition of the first glucan (CO_2, CO, formaldehyde and acetaldehyde). Figure 50 shows the more substantial impact of FTIR spectra of these compounds into the 2nd and 4th zones while the contribution of products of LGA decomposition to these zones is reduced. This is in a good agreement with both cluster mechanism

and the hypothesis on the inhibition of autocatalytic pathway with cellulose dilution with another solid.

Introduction of self-oxidation processes is necessary to explain complete decomposition of active volatiles to CO_2, CO and H_2O, corresponding to the 5th zone at 10wt% of cellulose (Figure 54, Figure 55). The representative spectrum of the 5th zone is displayed on Figure 56. This decomposition happens even in the case of chemically inert glass because of increasing of the residence time of the active pyrolysis products within solid materials. Interaction between the pyrolysis volatiles with surface promotes charring reactions, giving CO_2, CO and H_2O in a gas phase.
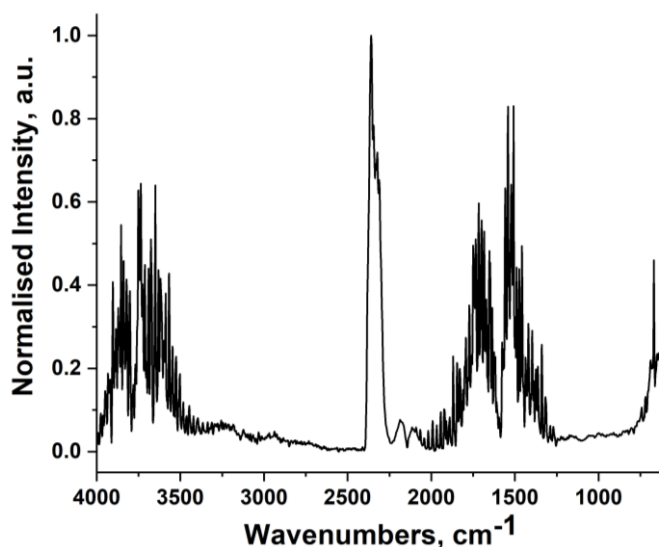
Figure 57. A spectrum extracted at the maximum decomposition rate of the cellulose-glass mixture (0.5:99.5), indicating the presence of only H_2O, CO_2 and CO

The existence of a larger number of zones can be due to the catalytic effect of the solid as it happens with the bentonite/cellulose system, which has a very complex character requiring a special investigation for an explanation.

It was shown that dilution of cellulose by other solid should be considered as an additional pyrolysis parameter. The presence of char influence on the diffusing volatiles, making them oxygen-rich. The occurrence of a larger number of zones in the case of bentonite is related to the catalytic effect of the clay mineral.

3.3.2. Zeolite

Conventional catalytic pyrolysis of cellulose over zeolites are intensively studied over the last decade.(*135*, *233*, *234*)

ZSM-5 was mixed with cellulose at the set of different ratios. Preparation of the samples was done via intensive mixing of cellulose with the necessary amount of ZSM-5 in an agate mortar

for over 15 mins. The obtained samples were studied using the TG-FTIR methodology developed in Chapter 2. The heating rate was $10°Cmin^{-1}$. The mass of the cellulose in each sample was fixed at 50 mg. The ZSM-5/cellulose system was accurately investigated with a step of 5wt%.

At the first stage, the data processing was done in the same way described for the bentonite-catalysed pyrolysis. The graph showing the dependency of the spectrum extracted at the maximum rate of decomposition on the cellulose/ZSM-5 ratio is shown in Figure 58. This gives an idea of the system evolution over the amount of the zeolite added.
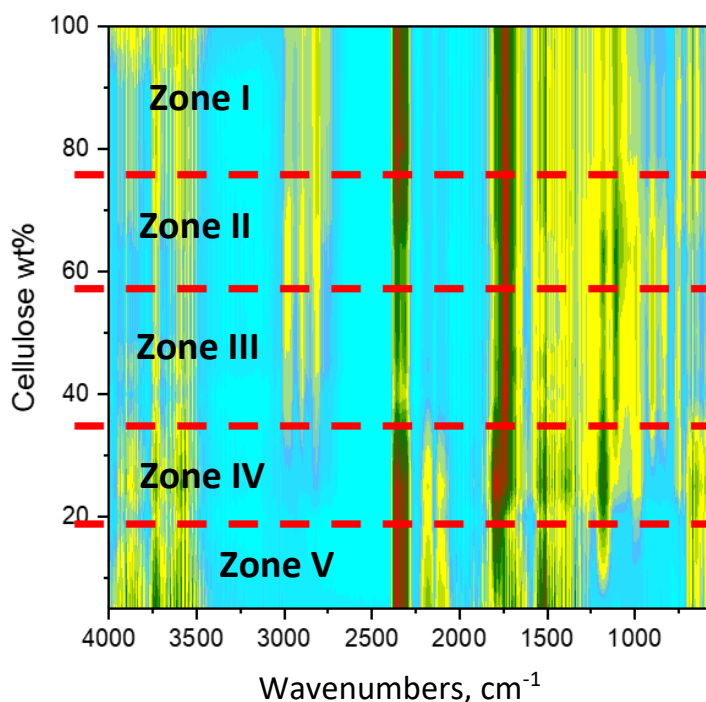
Figure 58. TG-FTIR of the cellulose/ZSM-5 system: mapping of spectra at maximum decomposition rate for each cellulose/ZSM-5 ratio

ZSM-5/cellulose mixtures revealed the same zonal behaviour as bentonite and glass. This phenomenon additionally evidencing the complex pyrolysis nature. The positions of zones are approximately the same of that one received for the bentonite.

The first zone (100% of cellulose up to 80% of cellulose/20% of ZSM-5) includes complicated spectrum looks like that one of pure cellulose with a small increase of the impact of compounds with carbonyl groups. The second zone is characterised by decreased intensity for hydroxyl groups region (OH groups). The third zone showed significantly decreased intensity for CO_2 production and appearance of levoglucosenone corresponding bands. The fourth zone includes the decreasing on the levoglucosenone production, but the increase of acids. The fifth region represents the full decomposition of cellulose to CO_2, CO, H_2O and char.

The programming software makes it enable to recognise and quantify chemicals on the FTIR set of spectra. The analysis of the ZSM-5/cellulose system has been started from the

determination of minimal references set to describe it. The set was including furfural (FFA), acetic acid (AA), LGO, CO_2, CO and H_2O (Figure 59). An introduction of additional aromatics references may result in better fitting coefficients over time because a catalytic upgrading of the volatiles fraction over ZSM-5 typically results in the formation of aromatic compounds.(*135*, *233*)
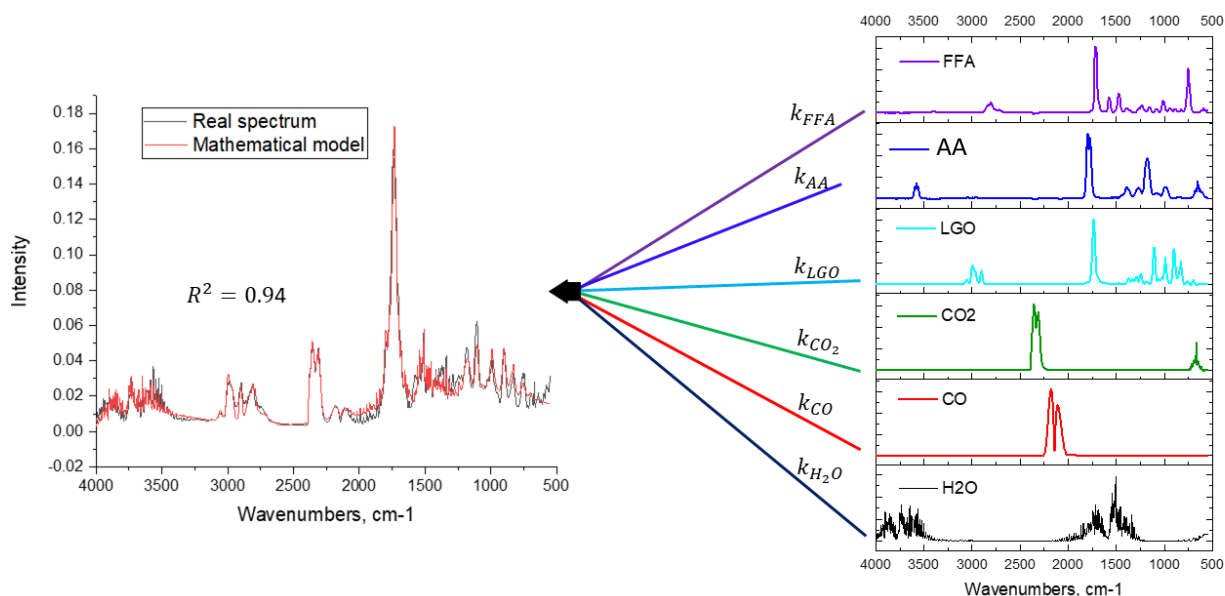
Figure 59. The list of the references (right) was including furfural (FFA), acetic acid (AA), LGO, CO_2, CO and H_2O. A comparison between the model and experimental spectra is given on the left.

Processing of the TG-FTIR data makes it possible to get yields and kinetics of the valuable chemicals.

Interestingly, a direct relation between yields of chemicals with zonal behaviour is observed. A decreasing/increasing of the chemicals yields has a strong correlation with the discussed zones, indicating of dilution factor partially influence on the distribution of the products.

It was found that the addition of ZSM-5 significantly influence on the composition of volatiles. Addition of the acid catalysts intensifies the production of some valuable chemicals. Adding ZSM-5 up to 50wt% increases the yield of LGO, giving maximum production of 9.0wt% maybe as a result of the larger number of available acid sites (Figure 60). A further catalyst loading leads to the reduction of LGO. This reduction could be related to the intensification of charring reactions. The trend of furfural production is following the LGO profile (Figure 61). The ratio between LGO and furfural is approximately between 3:1 and 2:1 (molar ratio), indicating that the formation mechanisms of these two molecules may be related. Simultaneous production of LGO and furfural has been known and previously reported.(*235*, *236*)
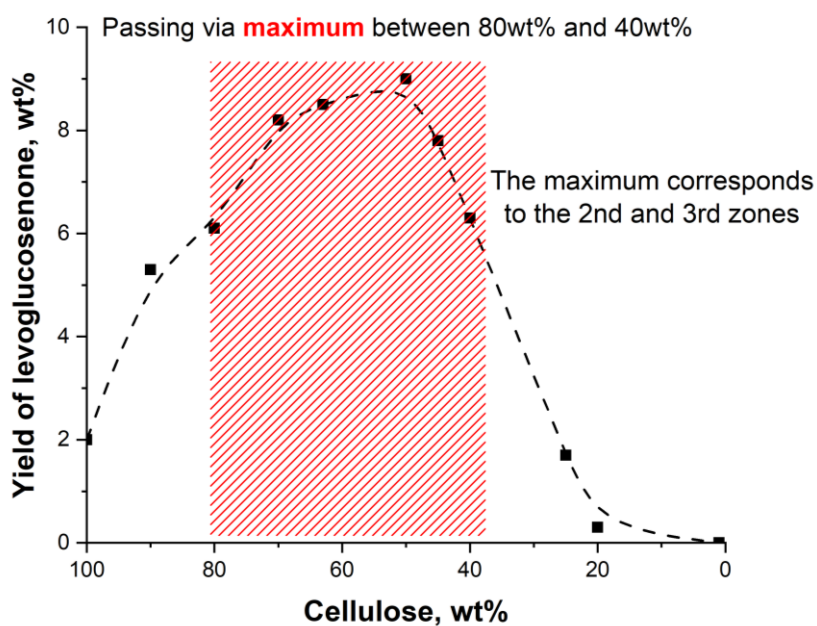
Figure 60. Yields of LGO depending on the ZSM-5 loading
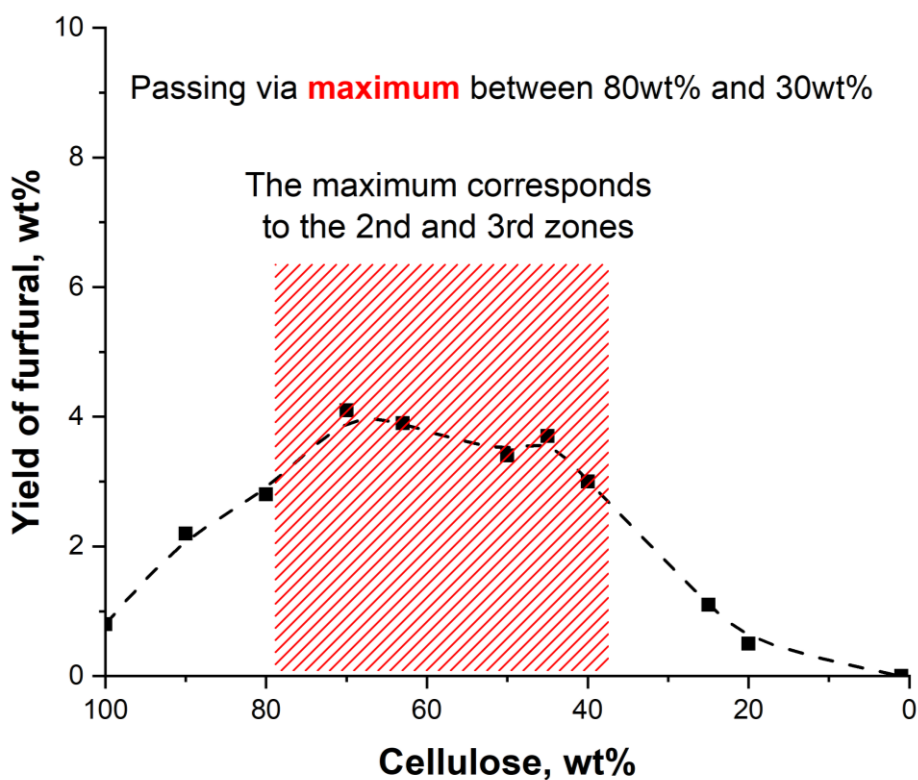
Figure 61. Yields of furfural depending on the ZSM-5 loading

A small addition of the catalyst slightly increases the yield of CO_2, while its further addition (up to 45wt%) gives a suppressed production of carbon dioxide (Figure 62). The decrease of carbon dioxide production is confirmed from the spectra extracted for samples with 50wt% and 90wt% of cellulose content (Figure 63). Notably, the zone of minimal CO_2 production is absolutely

the same for the zone of maximum LGO/furfural production. This implies these processes are controversy each other. In other words, if a generation of LGO/furfural does not happen, then its intermediate is partially decomposed to CO_2.
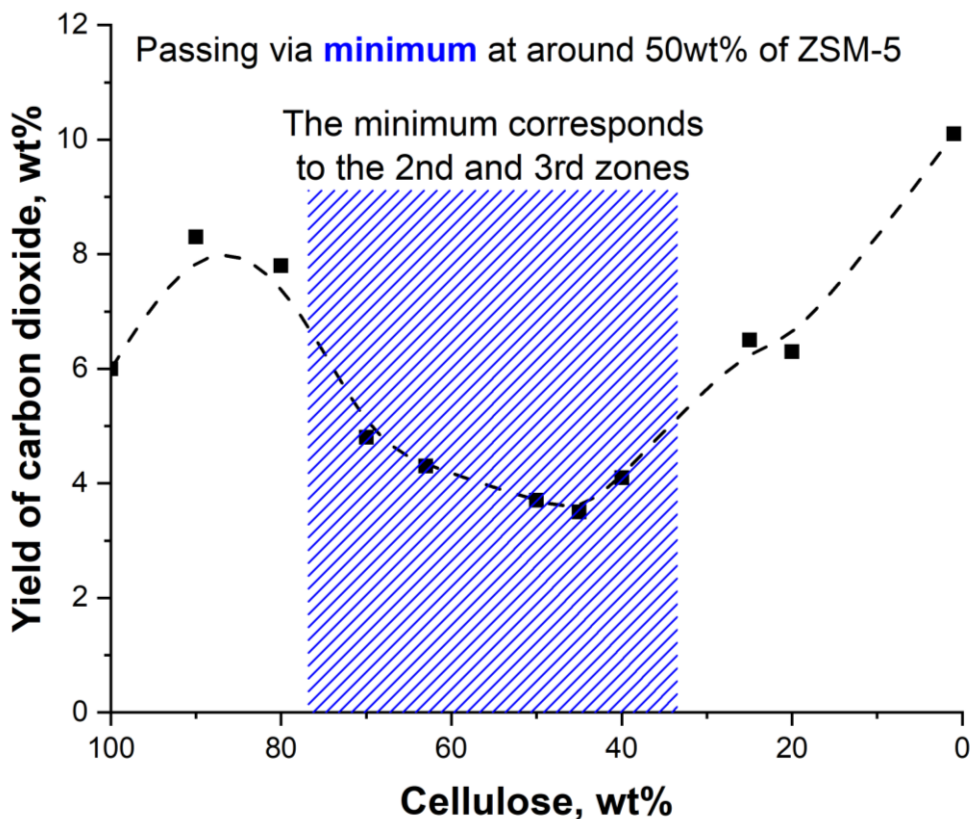
Figure 62. Yields of CO_2 depending on the ZSM-5 loading

The production of LGO is a result of dehydration reactions,(*230*) therefore it is logically to expect slightly increased generation of H_2O at the zone of LGO production. However, it was found, the amount of the escaped water is minimal at the zone (Figure 64) of LGO production (80-40wt%). This leads to an assumption that, if LGO/furfural are not produced/volitilised, then its intermediate is decomposed, giving a compound with a dehydration degree higher compared to LGO and furfural. Then at least three water molecules are removed from the intermediate of LGO, if LGO is not produced/volatilised.
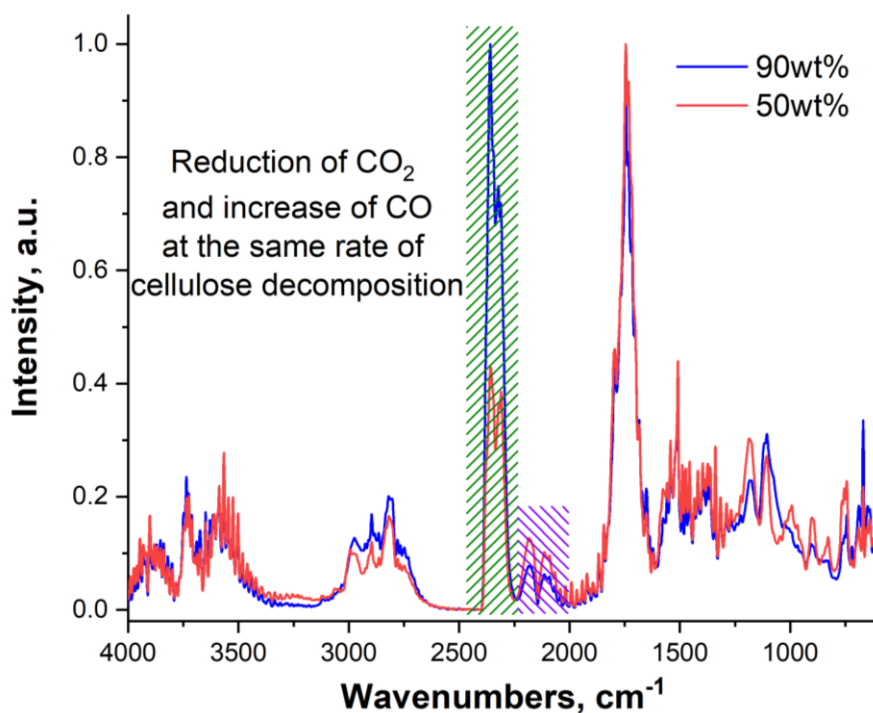
Figure 63. A comparison of TG-FTIR spectra extracted for 90wt% and 50wt%
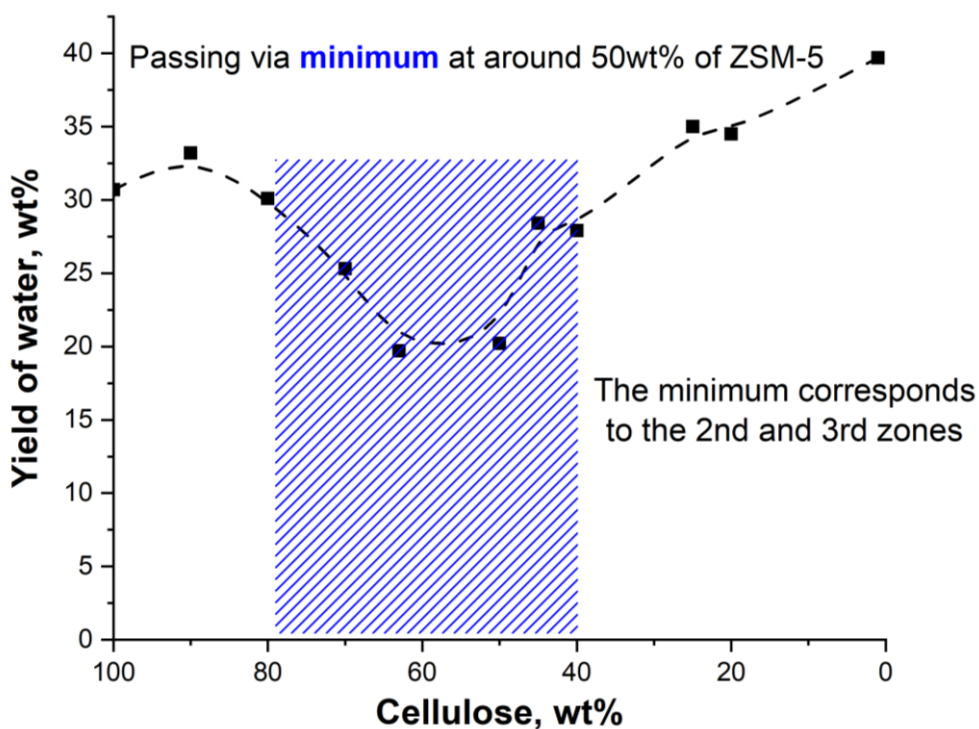
Figure 64. Yields of CO_2 depending on the ZSM-5 loading

The production of acetic acid was found to be almost independent on the catalyst loading (Figure 65), expect of its yields in the 5th zone, when complete decomposition of the volatiles happen towards CO_2, CO and water. The formation of acetic acid is not widely reported during cellulose pyrolysis because of the limitation of methods to get the yields of a low-volatile fraction.

Shafizadeh has reported a comparable amount of acetic acid received during levoglucosan pyrolysis,(*218*) through the mechanism of its formation is still under discussions. The formation of any CH_3- group containing molecules during cellulose pyrolysis should involve complicated transformations and proton exchanges.
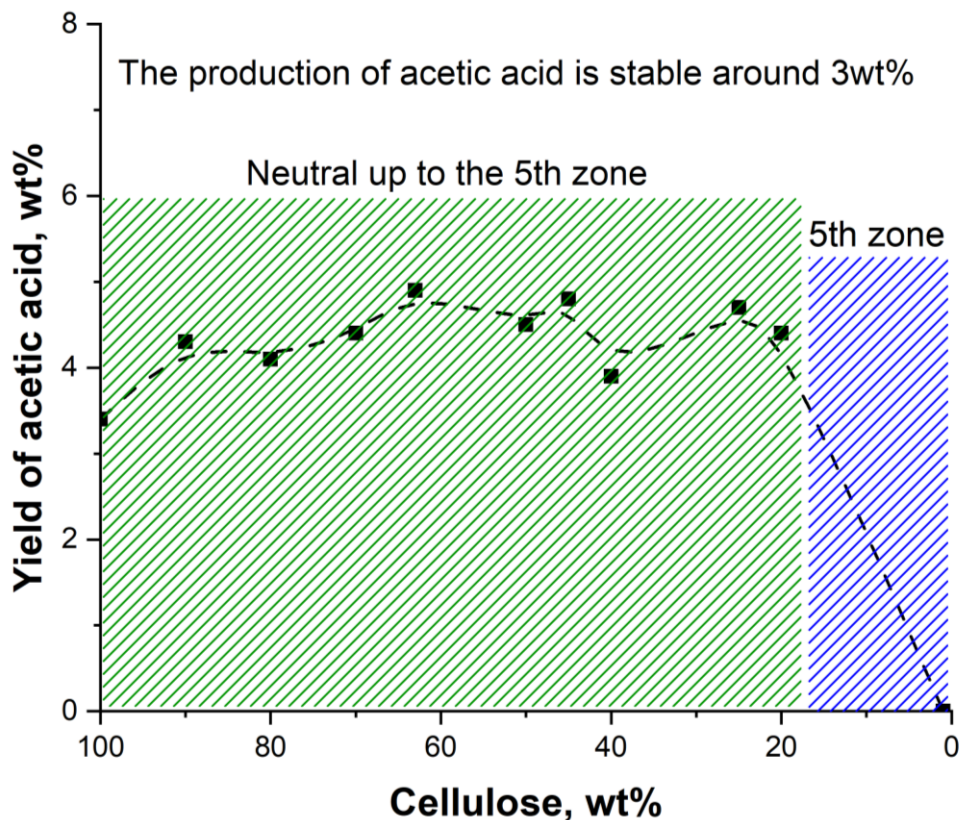
Figure 65. Yields of acetic acid depending on the ZSM-5 loading

Figure 66 represents the yields of CO depending on the catalyst loading. It is found that its yields is slightly increasing proportionally to the ZSM-5 amount. Following the vision of Shafizadeh, the formation of CO can proceed mainly via by decarbonylation of the various aldehydes and decomposition of formaldehyde, under the pyrolytic conditions.(*218*) Also, the increase in carbon monoxide can be related to the increase in char yield. It is known, that CO is a major product of charring reactions is CO.(*237*)
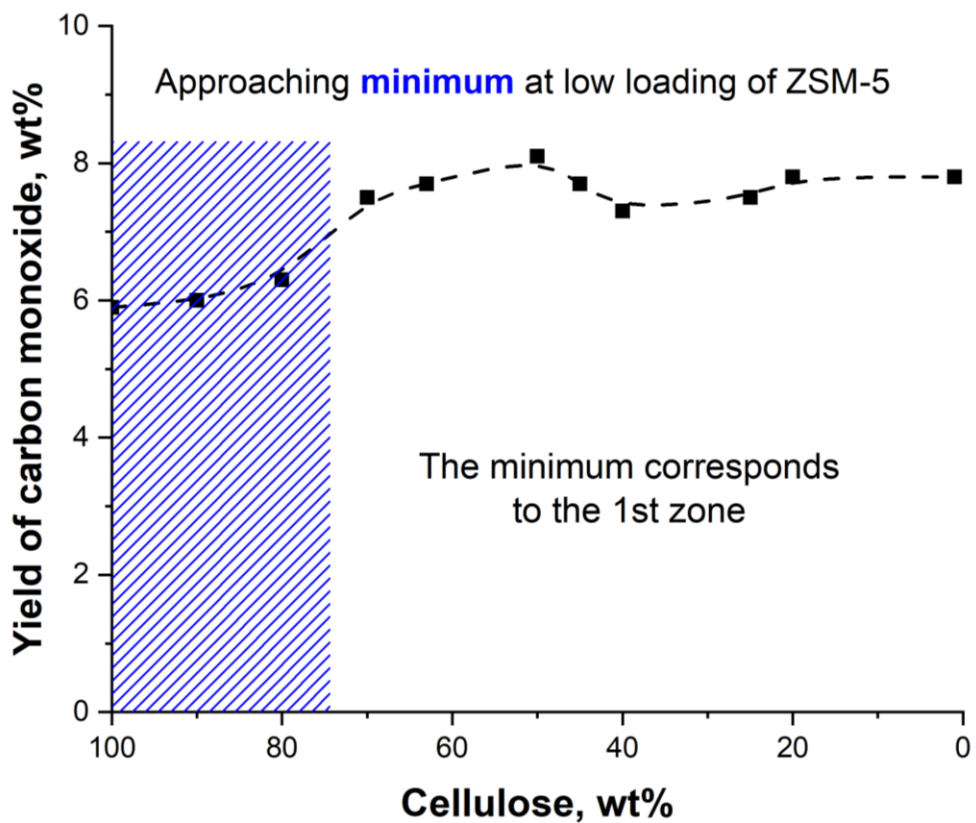
Figure 66. Yields of carbon monoxide depending on the ZSM-5 loading

The TG-FTIR processing procedure makes it possible to monitor kinetics of production of different volatiles.
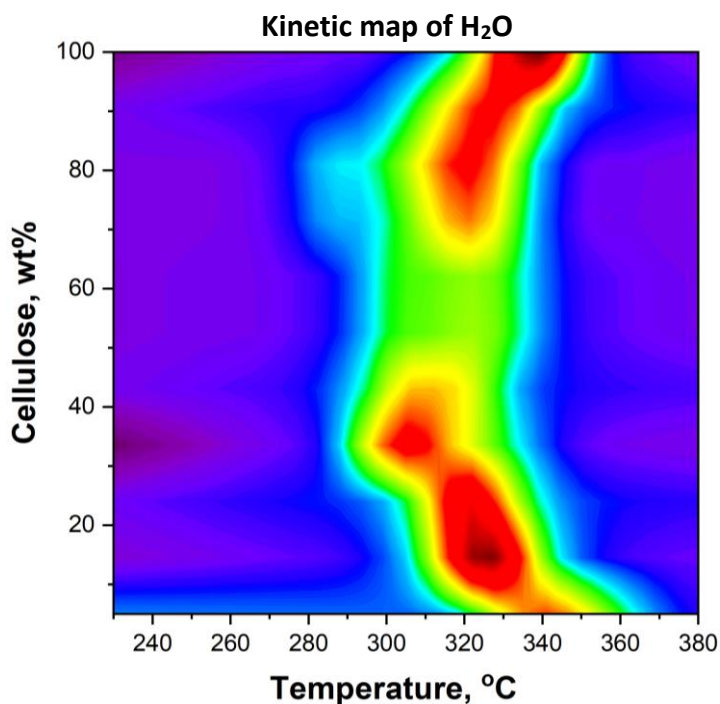
Figure 67. Kinetic map of H_2O during cellulose pyrolysis depending on the presence of ZSM-5

Mapping a chemical production rate over temperature (X-axis) and cellulose-ZSM-5 ratio (Y-axis) makes it possible to investigate its production during pyrolysis depending on the conditions. Such mapping can be used for kinetic separation of some chemicals.

The production of water indicates of initiation of pyrolysis (Figure 67), which usually begins between 220-240 °C. Addition of ZSM-5 in the amount of 20wt% decrease the maximum decomposition rate temperature of cellulose pyrolysis from ~335-340 °C to ~310-320 °C. In contrast, the catalyst loading over 80wt% shifts the pyrolysis temperature back to ~335-340 °C due to the diffusion phenomenon similarly to bentonite.
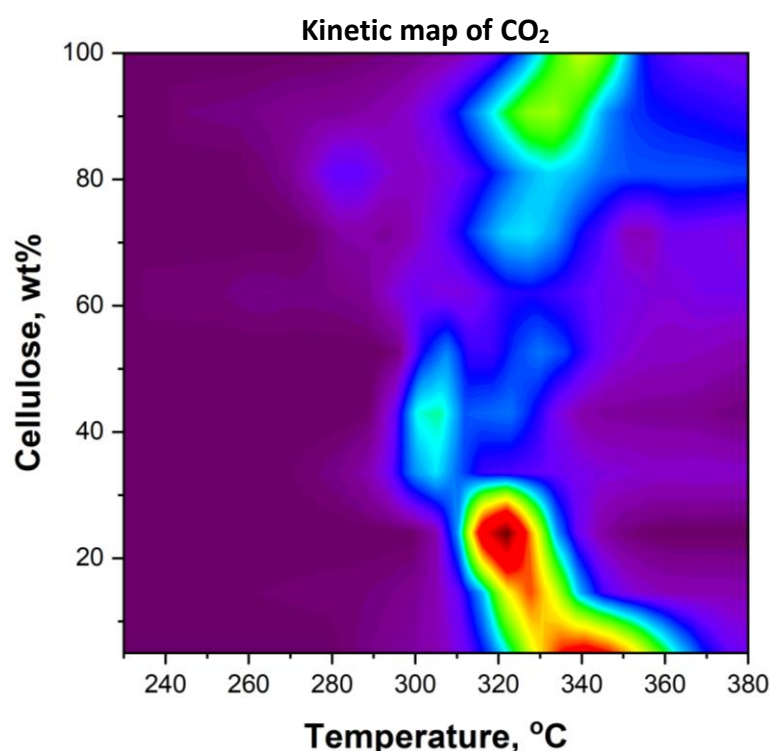
Figure 68. Kinetic map of CO_2 during cellulose pyrolysis depending on the presence of ZSM-5

The trend of CO_2 is following the shape of water (Figure 68). The production of CO_2 drops down between 80wt% and 30wt% of cellulose, emphasizing the decreasing of yield for carbon dioxide in this interval (Figure 62).

The maximum production of LGO was found to be around 310-315 °C (Figure 69). This implies the formation of its intermediate happens before this temperature interval. LGA seems to be the right candidate that satisfies this condition. Following to the kinetics of LGA production during native cellulose pyrolysis, studies in the relevant cellulose pyrolysis chapter, the formation of LGA may happen at around 300 °C. An interesting fact is that cellulose pyrolysis at T<300 °C is endothermic and apparently, the formation of LGA conjugated with its decomposition makes the pyrolysis exothermic at T>300 °C.(*213*, *238*)
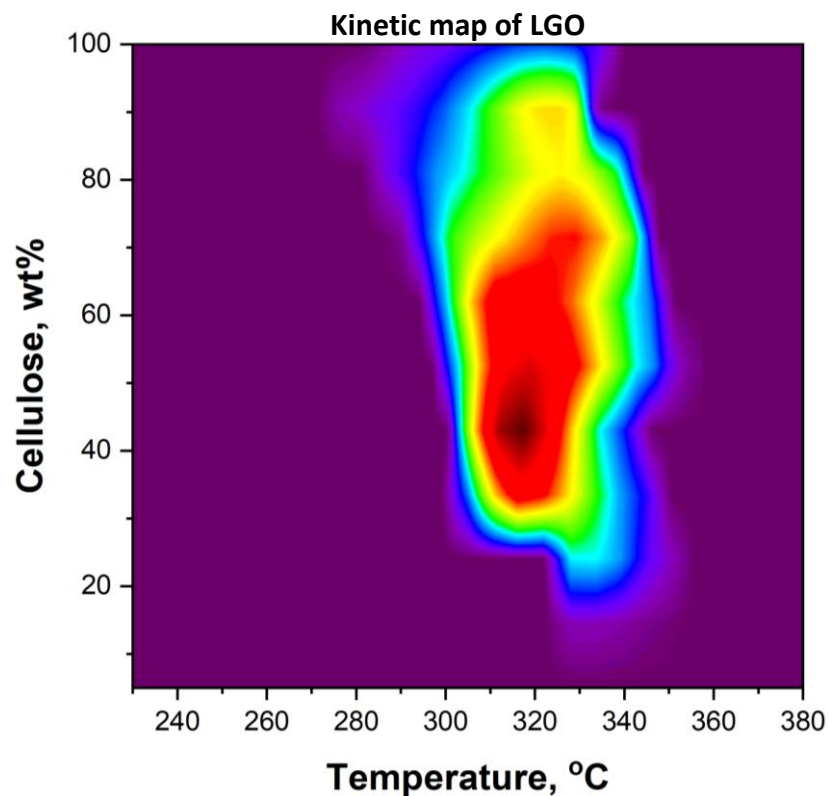
Figure 69. Kinetic map of LGO during cellulose pyrolysis depending on the presence of ZSM-5

The competitive nature of LGO and CO_2 production discussed above (see Figure 44, Chapter 2) in terms of yields is in a full agreement with kinetics data. Figure 70 shows scaled maps for CO_2 (left), LGO (right) and their overlay (middle).
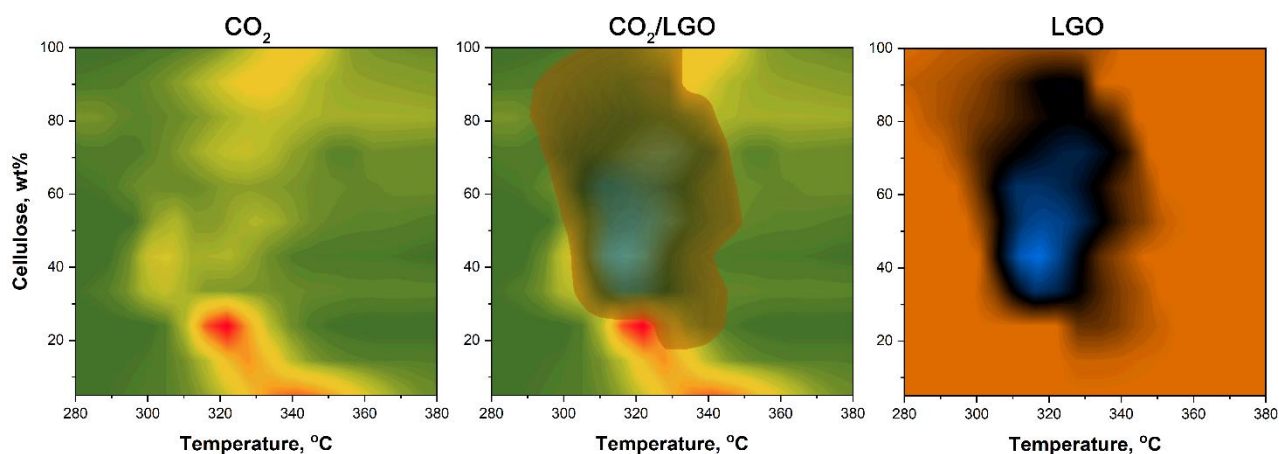
Figure 70. Kinetic mapping of CO_2 (left) and LGO (right) during cellulose pyrolysis in the presence of ZSM-5. The overlay of the maps is displayed in the middle

The figure demonstrates that the generation of LGO and CO_2 are competetive processes and kinetically separated from each other, evidencing their common origin from the same compound. This is in a line with the Chapter 2 of this thesis, the LGA could be the possible intermediate giving CO_2 and water or LGO and furfural depending on the environment.

91

Kinetics of furfural production is following the LGO trend (Figure 71). Furfural ($C_5H_4O_2$) is often reported, but not proved yet, being a by-product of LGO ($C_6H_6O_3$) production following the reaction $C_6H_6O_3 \rightarrow C_5H_4O_2 + CH_2O$.(*236*) Therefore, it is possible to conclude that during the pyrolysis furfural and formaldehyde are products of decomposition of LGO.
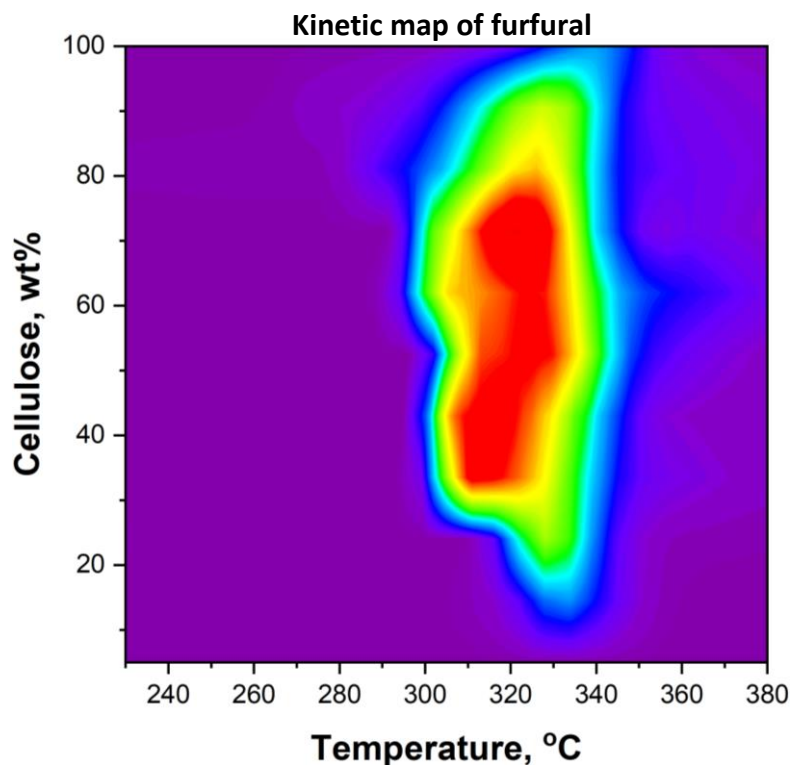
Figure 71. Kinetic map of furfural during cellulose pyrolysis in the presence of ZSM-5

In addition, the kinetics of CO is portrayed in Figure 72. As it is seen, the production of carbon monoxide covers the high-temperature map side, which is associated with charring reactions. Low production of CO occurs at 70wt% of cellulose, corresponding to the found maximum for furfural production. Probably, furfural can be partially decomposed to furan and CO, contribution to the production of carbon monoxide. Similar deoxygenation has been reported.(*239*)
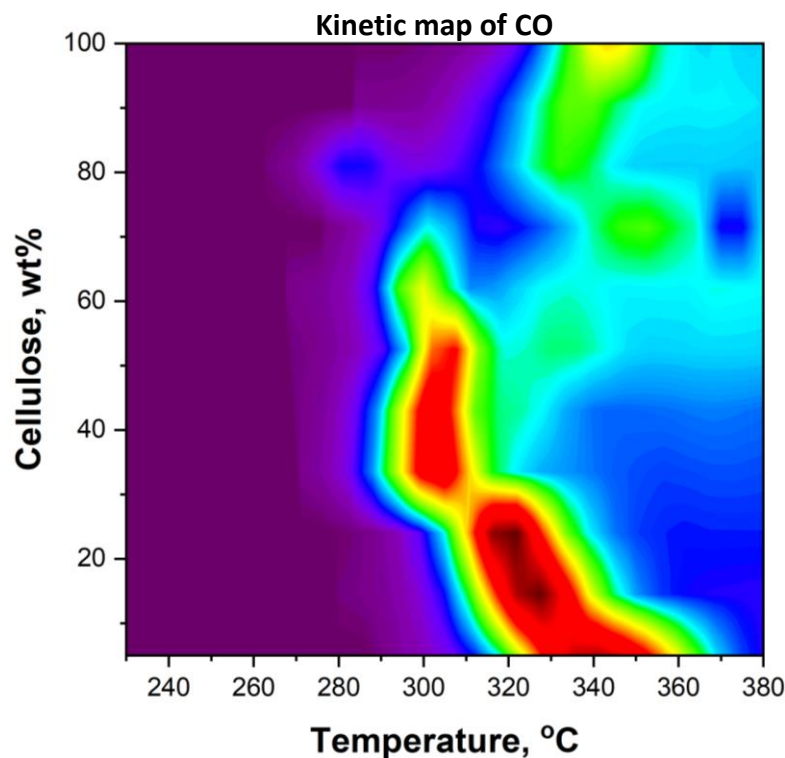
Figure 72. Kinetic map of CO during cellulose pyrolysis in the presence of ZSM-5

Conclusions

There are reported data on conventional cellulose pyrolysis in the presence of both liquid acids and heterogeneous catalysts.

Sulfuric acid was used as a liquid catalyst at various loading of 1, 3 and 7wt% (at the 10 Kmin^{-1} heating rate). It was confirmed that the amount of solid residue was increasing proportionally to the amount of the added acid. Impregnation of sulfuric acid has a substantial influence on the composition of volatiles. The highest yield of LGO was achieved at 3wt% of acid loading. This could happen at the expense of LGA, which yield was decreased by the factor of two compared to 1wt% acid loading. The higher loading of sulfuric acid (7wt%) resulted in the reduction of LGO yields, indicating an optimal acidity to produce LGO. This optium indicates that high acid loading facilitates LGO transformation to other chemicals.

A quantitative FTIR analysis of pyrolysis gases in real-time has been successfully applied to the investigation of catalytic thermal decomposition of cellulose in the presence of bentonite and ZSM-5. This allowed to achieve the following results:

- A direct mixing of cellulose with other solid can be considered as a "dilution" the polysaccharide. This was observed from the qualitative changes of the gas-FTIR spectra of cellulose-bentonite, cellulose-ZSM-5 and cellulose-borosilicate glass pyrolysis products. A rapid stepwise changes of volatiles composition was identified and five different zones were found. The first zone gives cellulose-like products, while the fifth

93

one results in the production of CO_2, CO and H_2O only. A scheme explaining the phenomenon of "dilution" with solids is suggested for the first time. In such a way, "dilution" of cellulose in another solid is one more important parameter to take into account during pyrolysis. This conclusion is critical for controlled pyrolysis of biomass.

- ZSM-5 is an efficient catalyst in the transformation of cellulose pyro-gas towards LGO. The process was optimised in terms of catalyst loading. The maximum yield of LGO (9.1wt%) was achieved in the case of 50wt% loading of the catalyst.

- Kinetic maps on the production of cellulose pyrolysis volatiles in time (temperature) were developed for the first time. The similar profiles and kinetics for LGO and furfural with almost constant ratio (~2:1) between these two molecules indicate of possibly the same origin for their production. This result is crucial for the development of efficient production of high-value chemicals from biomass.

- The found kinetic maps indicated that the productions of CO_2 and LGO are competitive processes. It was assumed that if LGO is not formed, then LGA is partially decomposed to CO_2 and H_2O. This observation could be a key to design a technology on the efficient production of levoglucosenone.

These results substantially contribute the understanding of catalytic conventional pyrolysis of cellulose in the presence in clays and zeolites. An extra parameter of "dilution" should be considered during cellulose pyrolysis control. Also kinetic maps on the production of volatiles during cellulose pyrolysis were presented for the first time. All presented kinetic maps were in a full agreement with the mechanism proposed in Chapter 2. The zonal behaviour together with kinetic maps make it possible to identify conditions (time, catalyst loading) giving high-purity LGO. The developed approaches should be further extended to achieve selective production of high-value chemicals form biomass.

CHAPTER 4. MICROWAVE-ASSISTED CELLULOSE PYROLYSIS IN THE PRESENCE OF CATALYSTS

4.1. Introduction

Microwave (MW) irradiation is a green alternative way to heating material.(*240*) Conventional heating is based on the heat from the surface to the middle of the material. The intensification of such flow is proportional to the temperature gradient between the surface and the sample centre, and it could be time-efficient only in the case of significant surface overheating. The electromagnetic field directly interacts with dipolar molecules or functional groups within the sample. It does not need to create a temperature gradient for fast heating. Therefore, MW has a real advantage above conventional heating in the case of materials with low thermal conductivity and sensitivity. So, MW heating is a known tool for biomass thermal activation.(*241–243*) It has been proven that MW can activate a different type of biomass at a temperature much lower than conventional heating, typically the MW activation takes place in the range between 150 °C and 250 °C. The process of pyrolysis benefits from a low temperature due to the substantial reduction of energy consumption and equipment cost. It has been shown in the second chapter of the thesis that at a temperature below 360-380 °C the primary product of the cellulose pyrolysis (LGA) stays within the sample and slowly decompose on the uncontrollable mixture of volatiles. Therefore, it was decided to combine the MW activation of biomass with an application of catalyst promoting decomposition of LGA to specific commercially valuable chemicals.

In this chapter, the biomass microwave-assisted pyrolysis of different types of biomass and catalysts influence on this process will be discussed.

4.2. Microwave-assisted pyrolysis of cellulose

There are four main parameters which control the MW-assisted pyrolysis: MW power, pyrolysis temperature, sample density and sample mass.(*240*)

It was decided to use the maximum available power to reach the maximum sample heating rate. The runs were carried out using CEM "Discover", applying the fixed power of 300 W at the closed vessel achieving maximum temperature. The samples were not densified to eliminate package density parameter. Therefore, initial research was limited only to the investigation of the sample mass influence on the efficiency of the pyrolysis.

To do that the MW-assisted pyrolysis of cellulose at different masses was tested. The temperature profiles of the reaction were almost independent of sample mass (Figure 73). While around the sample mass of 0.8-0.85 g, the final pressure was nearly doubled from 150 to 300 PSI (Figure 74). The pressure of the system (closed vessel) can be used as a marker for the degree of

cellulose decomposition. Therefore, the obtained data demonstrate that under chosen experimental conditions, a sample mass higher than 0.85 g provides the consistent efficiency of cellulose MW-assisted valorisation, and this sample mass was applied for the rest of catalytic experiments.
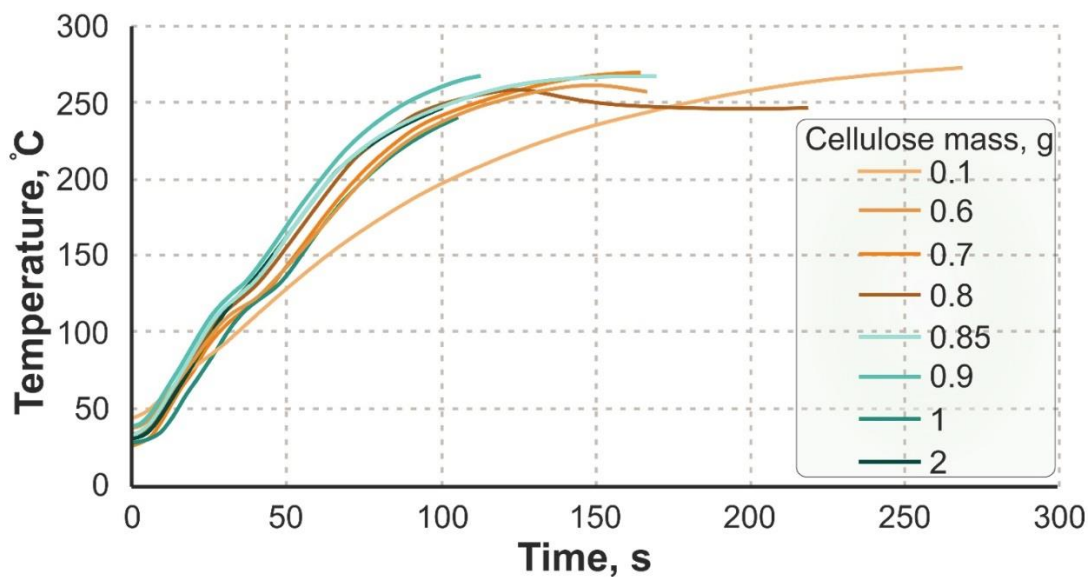
Figure 73. Temperature MW-traces of cellulose at different masses
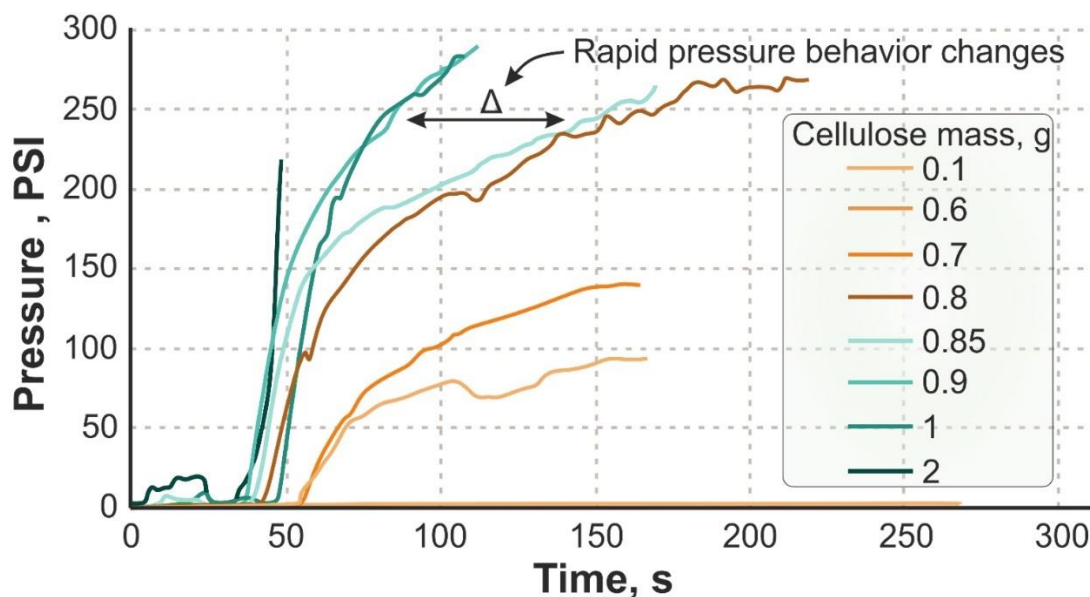
Figure 74. Pressure MW- traces of cellulose at different masses

4.3. Sulfuric and phosphoric acids

The preparation of the cellulose samples mixed with strong acids is reported in the relevant experimental section of the thesis.

Two types of experiments were conducted with sulfuric and phosphoric acids – closed and opened vessels. At both types of experiments, the power of the microwave reactor was set to 300W, and the working regime was established at fixed power.

The pressure MW-traces of cellulose doped with 3wt% of sulfuric and phosphoric acids are displayed in Figure 75. As it is seen from Figure 75, there is a fast-rising of the pressure over the MW Discover reactor limits of 300 PSI. This rapid increase of the system pressure indicates a high extend of gasification reactions, typically producing CO_2, CO and other gases.

This explosive-type of behaviour prevents the further heating of the samples, and the maximum temperature reached was ~150 °C, which is lower than microcrystalline cellulose pyrolysis point in MW (~180 °C). This is supported with the yield of bio-oil, that was lower than 3wt% of cellulose weight.
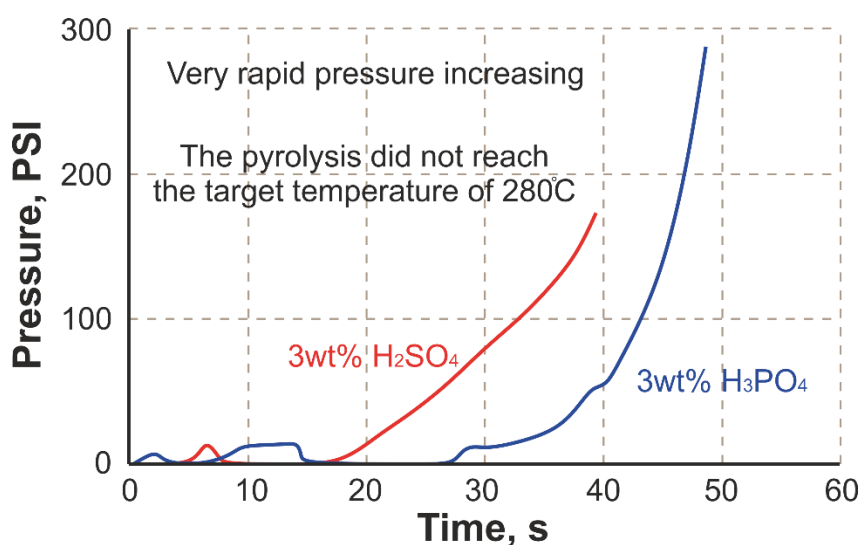
Figure 75. Pressure MW-traces of cellulose impregnated with 3wt% of sulfuric and phosphoric acids

The problem of increasing pressure can be solved in two ways. The first one is to work with the MW reactor, suitable for high-pressure reactions. The second one – make pyrolysis in an open vessel.

Open vessel

Open vessel experiment makes it possible to avoid the pressure limitations associated with MW Discovery reactor.

The MW-assisted pyrolysis of cellulose doped with 3wt% of sulfuric and phosphoric acids was successfully conducted at 300 W (fixed power) and 4 g of the total sample (35ml MW vessel). The collected bio-oil (18.9% and 19.1% for H_2SO_4 and H_3PO_4, respectively) and was carefully analysed using GC-MS and GC-FID techniques and the yields of the identified chemicals are presented in Table 15. Yields of valuable chemicals from MW-assisted pyrolysis of cellulose doped with strong acids at 3wt%.

Table 15. Yields of valuable chemicals from MW-assisted pyrolysis of cellulose doped with strong acids at 3wt%

Acid	Chemical	Yield, wt% bio-oil	Yield, wt% cellulose
Sulfuric acid	LGO	29.9	5.68
	DGP	5.7	1.08
	HMF	3.2	0.61
	LGA	8.4	1.60
	Rest, including H_2O	52.8	10.03
Phosphoric Acid	LGO	35.2	6.69
	DGP	3.2	0.61
	HMF	1.2	0.23
	LGA	7.6	1.44
	Rest, including H_2O	52.8	10.03

*The equal amounts of the rest fraction for both acids are a coincidence.

Following Table 15, there is no significant difference between the phosphoric and sulfuric acids. The observed small difference in LGO yields can be explained by a better distribution of acid within the cellulose sample. Interestingly, a slightly increased yield of LGO in the case of H_3PO_4 is associated with the reduction of yields of LGA and DGP. This supports the theory of LGA and DGP being intermediates for LGA production.

The yield of levoglucosenone of 6%, that is comparable to those one reported in MW-assisted pyrolysis of native cellulose. (*244*) Furthermore, such a yield is close to the yields resulted in conventional pyrolysis.

The main complexity associated with MW-assisted pyrolysis of the acid-doped samples is their partial escape of the MW-heating zone. It was found that during the pyrolysis, the cellulose particles are taken outside the reaction zone by the water and gases flow. This phenomenon can cause some difficulties at a larger scale and would require an additional filtration step.

4.4. Clays

It is well-known that water efficiently interact with microwaves. Usually, natural clays are hydrophilic, containing a large amount of water. The exact mechanisms of clays interaction with microwaves are still under discussion; however, it is proven that clays are great MW-adsorbers. This fact, together with clay's availability and cost-efficiency, make clays very promising catalysts for any MW-related processes.

In the current work, the investigation of MW interreaction with bentonite, kaolinite and Al-pillared bentonite (Al-PILC) has been carried out.

A set of preliminary experiments were done to check the activity of the native minerals in the MW reactor. The samples were expected to behave similarly; however, kaolinite was found to be completely different. As it can be seen from the temperature MW-traces of bentonite and kaolinite, the second one is not that active during MW heating (Figure 76).
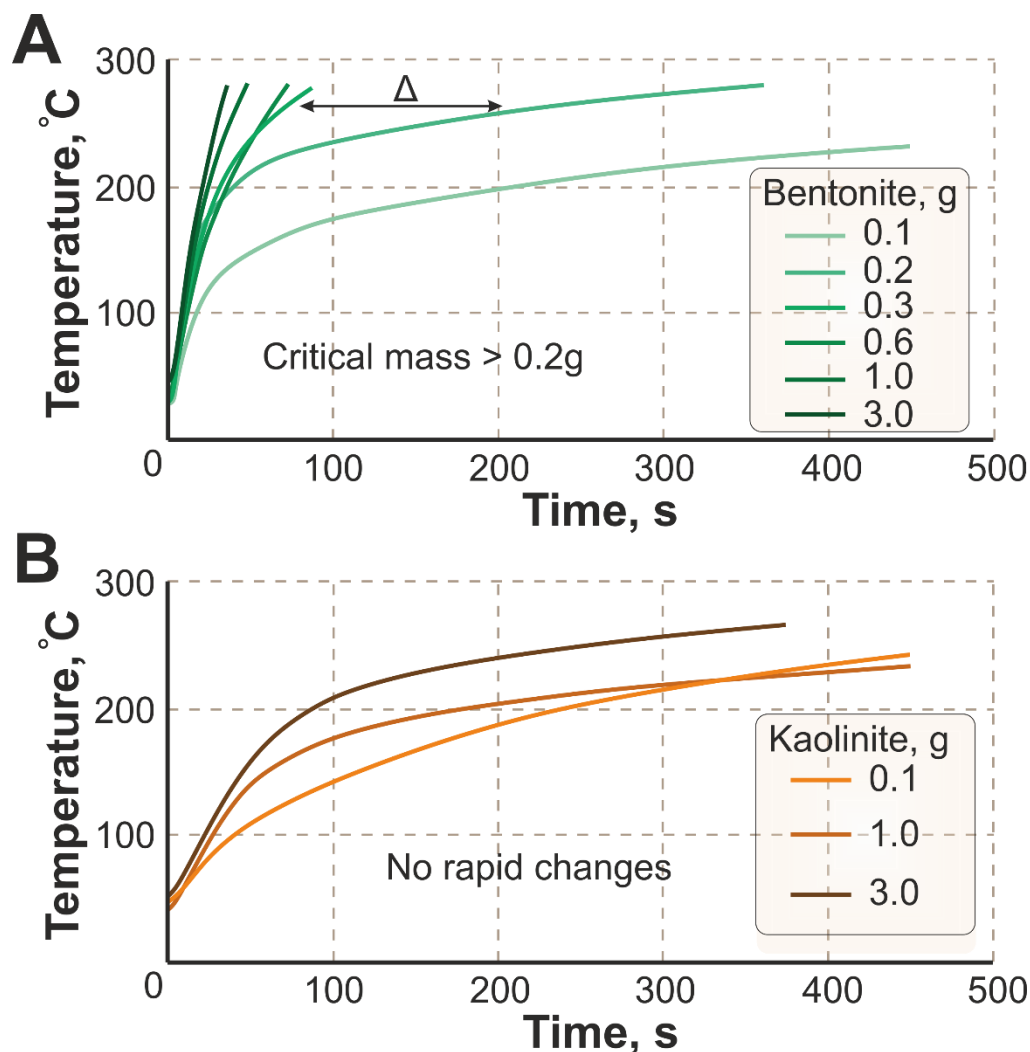
Figure 76. Temperature MW-traces of A) bentonite and B) kaolinite

The demonstrated dependencies show that bentonite takes active participation in interaction with microwaves, while kaolinite heating rate does not change a lot with mass increasing.

The phenomenon is linked probably to water content in clays and their ability to adsorb water molecules (to swell). Kaolinite is more hydrophobic clay mineral compared to bentonite (Figure 77A) because of its siloxane surface (Figure 77B). Thus, the amount of polar hydroxyl surface groups that can interact with microwaves is significantly reduced. Therefore, it was decided to eliminate kaolinite from the list of the catalysts investigated in the current work.
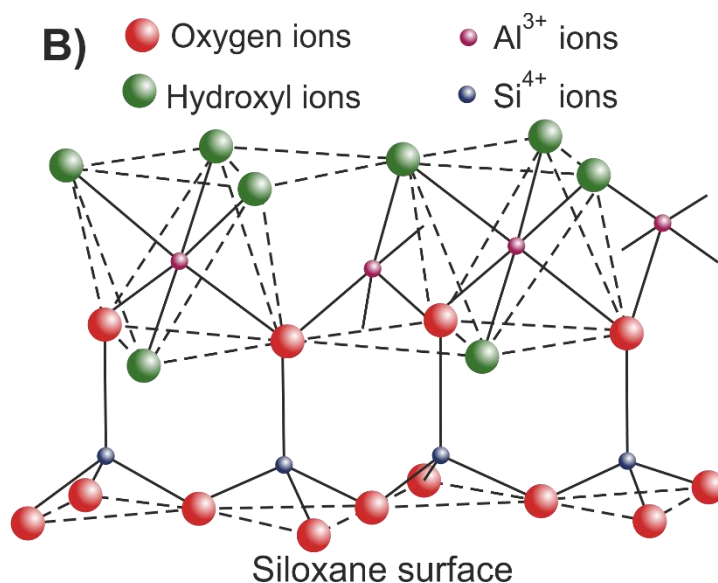
Figure 77. A) The ability of clays for swelling: the equal weight of kaolinite (left) and bentonite (right) were placed into cylinders. The initial levels of the samples are marked with red lines. The water was added to check the expansion and swelling properties; B) Siloxane surface of kaolinite

4.4.1. Closed vessel experiments

It is possible to monitor pressure during closed vessel microwave experiments. From the chemical point of view, the differences between closed and open vessels microwave experiment are:

-pressure influences the equilibrium;

-volatiles do not leave the reaction zone and shift the equilibrium;

As a result of joint work between the University of York and the National Technical University of Ukraine, it was possible to publish an article in ChemSusChem about closed vessel MW experiment.

4.4.2. ChemSusChem paper: Selective Microwave-assisted Pyrolysis of Cellulose towards Levoglucosenone using Clay Catalysts

Aim

This work was aimed at a detailed analysis of the MW-assisted pyrolysis of cellulose in the presence of clays and pillared clay (Al-pillared clay), which is a substantial part of the thesis because it covers the catalytic transformation of biomass towards valuable chemicals (levoglucosenone). Notably, the MW-assisted pyrolysis of cellulose in the presence of Al-pillared clays was not previously reported. Therefore, this integrated chapter aims to highlight this

phenomenon in detail, suggesting a scheme of cellulose MW-activation in the presence of clay catalysts.

Objectives

The main objective of this study was to investigate the mechanism of MW-assisted pyrolysis of cellulose in the presence of clay-based catalysts. The other objective was to study how the bentonite and Al-pillared bentonite influence the distribution of the chemicals in bio-oil.

Methodology

The synthesis of Al-pillared bentonite was carried out and proven with various techniques, including SAXS, N_2 adsorption analysis, thermal analysis, DRIFT, TPD of ammonia. Bentonite and Al-pillared bentonite were mixed with cellulose at a set of different ratios. The MW-assisted pyrolysis of the samples was achieved using an MW Discover reactor at 300W. The measurements on the yield of biochar, bio-oil and gas were done following the procedure described in the supplementary material section. The analysis of the bio-oil was carried out using GC-FID, GC-MS and HPLC equipment.

Results

Both catalysts were charaterised, and it was found that Al-pillared bentonite incorporates a large number of Bronsted acid sites. It was found that Al-pillared bentonite works well in the MW-assisted conversion of cellulose towards levoglucosenone (6.3wt% at 50wt% loading of the catalyst). The addition of bentonite, which produces a substantial amount of water, located below the cellulose, leads to increased amounts of bio-oil. This effect was used to increase the amount of LGO (12.3wt%) produced during MW-pyrolysis of cellulose mixed with Al-pillared bentonite. A key role of Bronsted acid sites is discussed.

ChemSusChem paper

Alisa Doroshenko,[a] Ihor Pylypenko,[b] Karl Heaton,[c] Stephen Cowling,[d] James Clark,*[a] and Vitaliy Budarin*[a]

[a]   Alisa Doroshenko, Prof. James Clark, Dr. Vitaliy Budarin Green Chemistry Centre of Excellence Department of Chemistry University of York Heslington, York, UK, YO10 5DD

[b]   Dr. Ihor Pylypenko Department of Chemical Technology of Ceramic and Glass The National Technical University of Ukraine "Igor Sikorsky Kyiv Polytechnic Institute" Peremohy Ave, 37, Kyiv, Ukraine, 03056

[c]   Karl Heaton MS Service Department of Chemistry University of York Heslington, York, UK, YO10 5DD

[d]   Dr. Stephen Cowling Liquid Crystals and Materials Chemistry Group Department of Chemistry University of York Heslington, York, UK, YO10 5DD

*Corresponding authors: vitaliy.budarin@york.ac.uk, james.clark@york.ac.uk

Homepage: www.vitaliybudarin.com

4.4.2.1. Abstract

Levoglucosenone (anhydrosugar) is one of the most promising chemical platforms derived from the pyrolysis of biomass. It is a chiral building block for pharmaceuticals as well as an intermediate in the production of solvents and polymers. Therefore, the development of cost-efficient, low-energy production methods are vital for a future sustainable biorefinery. Here we report a novel, green approach to the production of levoglucosenone using a microwave (MW) assisted pyrolysis of cellulose in the presence of readily available clays. We showed that natural and pillared clays in the presence of MW irradiation significantly increase the yield of levoglucosenone from cellulose. Both the water content and the presence of acid centers are critical characteristics which influence the yield and distribution of catalyzed products. A unique experiment was designed using a synergetic effect between different types of catalysts which enhanced the levoglucosenone yield to 12.3wt% with 63% purity.

4.4.2.2. Introduction

Bio-oil is a complex organic mixture resulting from thermal processing (pyrolysis) of biomass and bio-waste and represents an alternative renewable source for chemicals and fuels. The majority of individual compounds in bio-oil are multi-functional oxygen-containing chemicals. Some of them are attractive platform molecules ready for industrial use without any pre-functionalization.(10) These platform molecules could form the core of a sustainable and efficient biorefinery.

Currently, one of the biggest challenges for such a biorefinery is separation of the complex bio-oil to individual compounds. The direct distillation of the oxygen-containing compounds is

impossible, while the application of chromatography columns is an expensive decision for the large-scale chemical industry.

A possible solution is selective in-situ targeting of the desired compounds during pyrolysis of biomass (which typically contains hemicellulose, cellulose and lignin). At present, most of the problems associated with refining hemicellulose have been addressed,(*245*) while refining cross-linked lignin requires significant further developments. Hence our focus on cellulose. Pyrolysis of cellulose to a complex mixture of chemicals is already developed but a controllable and sustainable production of the platform molecules levoglucosenone (LGO) and 5-hydroxymethylfurfural (5-HMF) is not. Conventional pyrolysis of cellulose proceeds at high temperatures (T>360 °C), inducing secondary reactions and therefore producing a complex mixture of products.

One of the ways to increase selectivity during pyrolysis is catalysis.(*246*) Natural aluminosilicates such as zeolites are widely reported to preferentially catalyze the conversion of biomass to aromatics.(*247, 248*) However, although cost-efficient and readily-available, clays have not attracted significant attention. Pillared clays (a class of swollen clays modified with a variety of large polynuclear hydroxo-complexes) are of particular interest.(*249*)

Another way to improve the pyrolysis selectivity is the application of MW-assisted heating, which proceeds at lower temperatures (~165-220 °C) than conventional pyrolysis.

In this paper we investigated the synergy between MW-assisted cellulose pyrolysis in the presence of natural bentonite and pillared bentonite. We chose Al-pillared bentonite (Al-PILC) as pillared clay because of its commercial availability, simple synthesis and high acidity, caused by the intercalated Al_{13} hydroxo-complexes $(AlO_4Al_{12}(OH)_{24}(H_2O)_{12})^{7+}$, acting as a heteropoly acid.

4.4.2.3. Experiment and methodology

Successful intercalation of the Al_{13} hydroxo-complexes into native bentonite (Na-form) increases the basal spacing (d_{001}) from 15.20 Å to 18.11 Å (Figure 1a-b). Furthermore, thermally-resolved Small-Angle X-ray Scattering (SAXS) (Figure 1a-b, insertion graphs) shows the difference in water behaviour between the pillared and native bentonite. The step-wise changes (w_2, w_1, w_0) of the basal spacing for the bentonite are related to a serial removal of discrete water sheets in the interlamellar space of this catalyst.(*250*) The absence of such a phenomenon for an Al-PILC (Figure 1b, insertion graph) indicates that Al_{13}-complexes are acting as supportive pillars between the clay sheets, preventing their collapse. Additionally, the N_2 adsorption results indicate the formation of a larger number of micro- and meso-pores for Al-PILC in comparison to the non-pillared clay leading to ca. a six-fold increase in BET surface area (Figure 1c and S6).
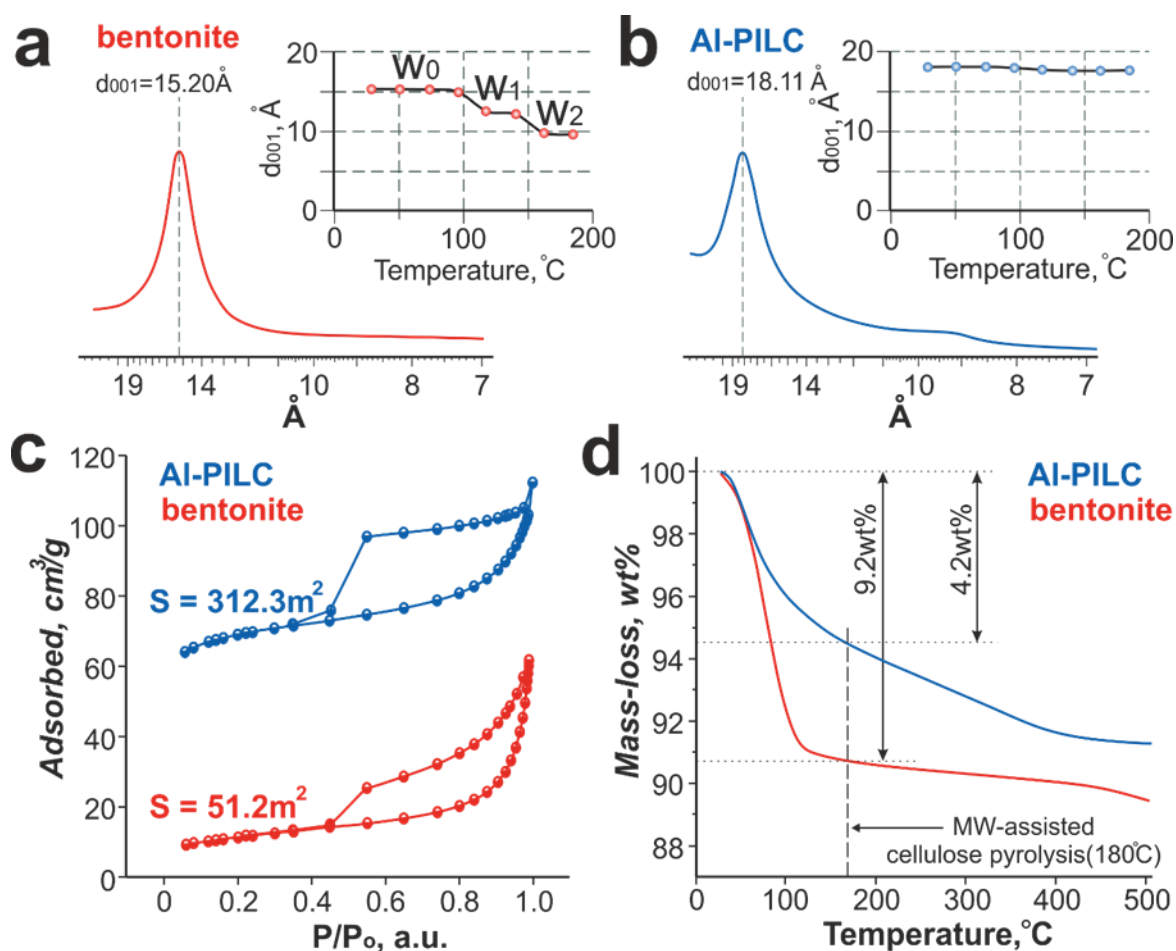
Figure 1. Characterisation of the catalysts: a), b) SAXS analysis and thermally-resolved SAXS data; c) N_2 adsorption data; d) thermal analysis

The different environment for water within the samples is shown by thermal gravimetric analysis. The bentonite desorbs twice as much water as Al-PILC (4.2wt%) below 180 °C, (the temperature of cellulose pyrolysis in an MW-reactor, Figure 1d). Mass-loss of the Al-PILC is stretched out in time and temperature because of a slower water diffusion compared to the original macro-porous bentonite (Figure 1d).(*251, 252*)

The acid properties of materials were confirmed to be different through pyridine titration and temperature-programed desorption of ammonia (Figure S8-9). The original bentonite contains mainly Lewis species while Al-PILC has both Lewis and Bronsted acid centres.

The influence of the clay catalysts on the MW-assisted cellulose pyrolysis has been systematically investigated. The catalysts were intensively mixed together with cellulose at different loads and subjected to microwave-assisted pyrolysis (Figure S10).

4.4.2.4. Results and discussion

The results obtained clearly show that the Al_{13} pillaring procedure significantly changes the catalytic performance of the bentonite (Figure 2a-b). Low bentonite loading (<20wt%) increases bio-oil production (Figure 2a), which is in good agreement with previous studies.(*253, 254*) However, we found that at higher loading, the bio-oil yield is decreased. This effect can be attributed to competition between the cellulose hydrolysis process and the bio-oils interaction with clay (charring and adsorption). The moisture produced below 180 °C from macropore bentonite promotes cellulose hydrolysis and increases yields of sugars and bio-oil (Figure 2a). In contrast to the bentonite, the Al-PILC (which releases low amounts of water 4.2wt%, Figure 1d), leads to a gradual decrease in the bio-oil yield (Figure 2a).

Interestingly, we found that levoglucosan yields are proportional to bio-oil yields independent of the nature and quantity of the catalyst (Figure 2a-b). This observation confirms levoglucosan as being a primary intermediate for low molecular weight organic volatiles (M<162 $gmol^{-1}$) through its decomposition in cellulose pyrolysis.(*175, 255*) Moreover, levoglucosan is an intermediate for the production of sugars via interaction with internally produced water.(*256*)

The production of sugars in the presence of bentonite slows down at >20wt% of the catalyst, while the yield of 5-HMF starts to increase up to 4wt% (Figure 2a). It is reasonable to assume that 5-HMF is a product of sugars conversion.(*257, 258*) In contrast, the use of Al-PILC gives a maximum yield of 5-HMF at 20wt% of the catalyst (Figure 2b). This pronounced difference in HMF yields could be due to differences in both the water content and nature of acid centres of these catalysts. Recently Lewis acid species were reported to play a significant role in glucose transformation to 5-HMF,(*256, 259*) and bentonite, incorporating Lewis sites, could be a promising candidate for this reaction. In contrast, Al-PILC contains many more Bronsted centres. Moreover, additional acid centres are produced during the thermal decomposition of the Al_{13}-complex towards Al_2O_3 (Figure 3). We did not find any evidence of Al_2O_3 having a catalytic effect, while the Al_{13}-complex produced acid sites could promote reactions typical for Bronsted species such as LGO production – a well-known product of cellulose pyrolysis in the presence of Bronsted acids.(*251, 252*) This explains a nearly negligible LGO yield with bentonite (Figure 2a) and its substantial growth to 6.3wt% (40% purity) at 50wt% of Al-PILC (Figure 2b). Conventional pyrolysis of cellulose mixed with the same Al-PILC loading resulted in higher LGO yield (10.1%),

but much lower selectivity of ~26% (Figure S15). Thus, our experiments show that MW irradiation improves pyrolysis selectivity and that the
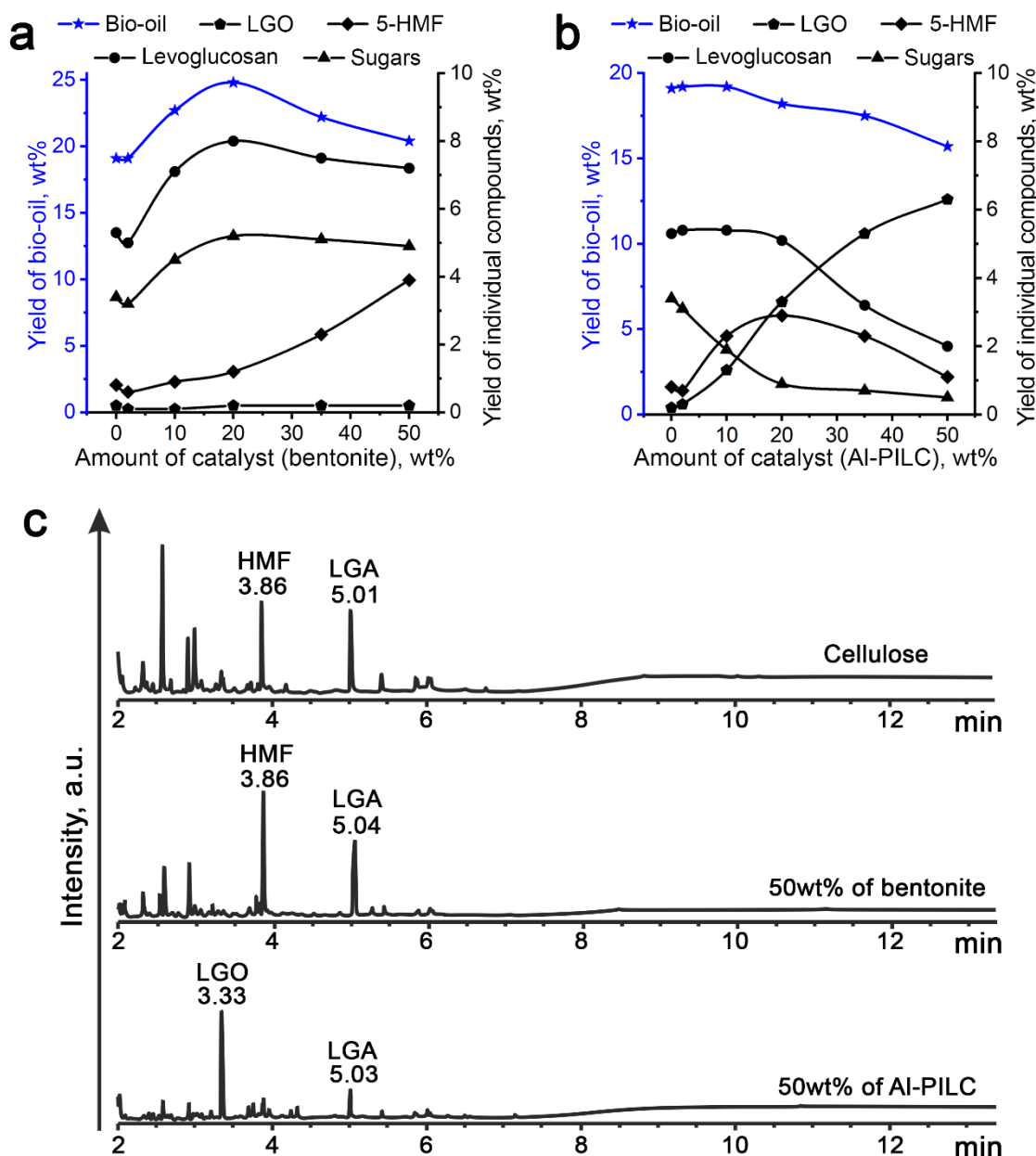
Figure 2. Experimental data: a), b) – composition of the bio-oils resulted from the MW-assisted pyrolysis of cellulose mixed with bentonite and Al-PILC respectively (all yields are calculated with respect to the cellulose weight); c) GC-FID data of the extracted bio-oil for cellulose (top), 50wt% of bentonite (middle) and 50wt% of Al-PILC (bottom)

production of 5-HMF and LGO are competitive (Figure 2c) and depend on the amount of locally available water and type of acid centers.(*230*)

Stoichiometrically the formation of levoglucosan ($C_6H_{10}O_5$) from cellulose ($C_6H_{10}O_5$)$_n$ does not require H_2O, but surprisingly its production needs a catalytic amount of water, while an excess

of H_2O promotes cellulose hydrolysis to sugars (Figure 3). Final yield of the pyrolysis of dry cellulose favors charring reactions.(*206*) We believe that the ratio between levoglucosan and sugars determines the possible yields of LGO and 5-HMF and is controlled by the amount of available water. The final yield of LGO is controlled by the presence of Bronsted acid sites, such as those present in Al-PILC (Figure 3). The catalytic formation of LGO can occur directly from levoglucosan, or indirectly via 1,4:3,6-dianhydro-α-D-glycopyranose (DGP) intermediate.(*260*)

Cellulose

+ H_2O, hydrolysis
water donator at ~100 °C

H_2O cat.

Oligosugars

Glucose $\xrightleftharpoons[-H_2O]{+H_2O}$ **LGA**

Lewis centers cat.

Al$_{13}$ - *pillared clay reaction:*

$$[Al_{13}O_4(OH)_{24}(H_2O)_{12}]^{7+}$$

$$[Al_{13}O_4(OH)_{24+x}(H_2O)_{12-x}]^{7-x} + x \cdot H^+$$

$$6.5Al_2O_3 + 7 \cdot H^+ + 20.5H_2O$$

Fructose

[DGP]

Acid cat., -H_2O

$+H^+, -H_2O$

Products of decomposition   **HMF**   **LGO**   **Products of decomposition**
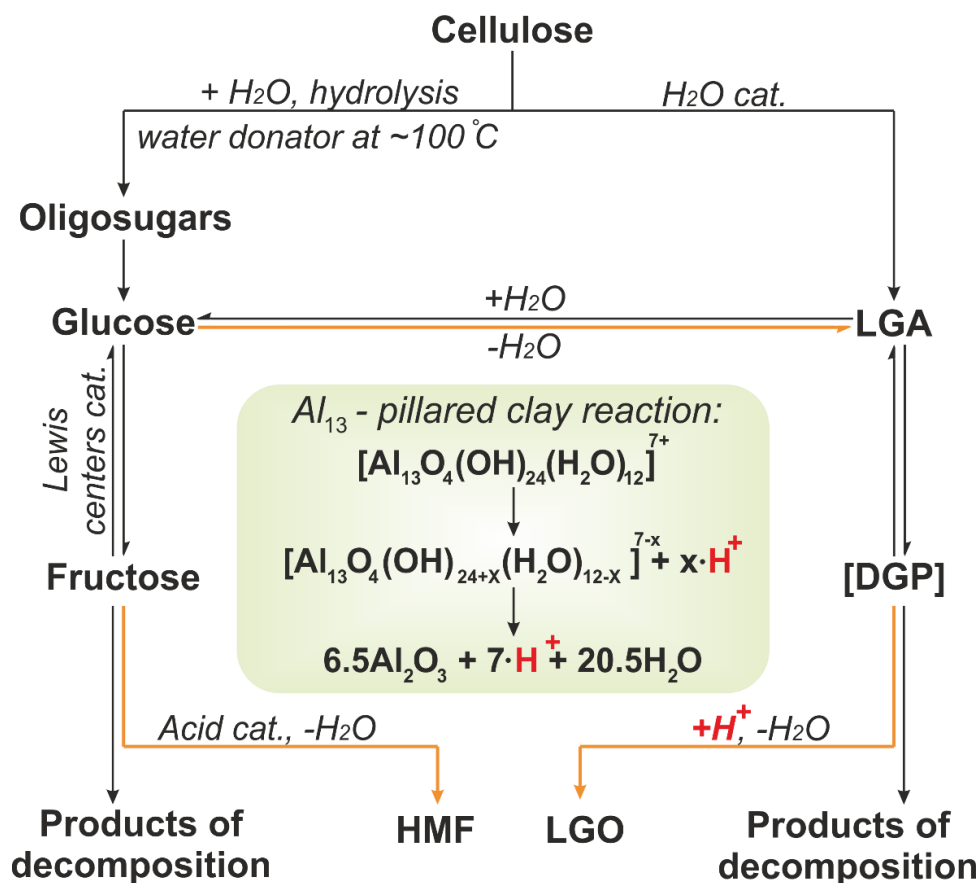
Figure 3. The suggested scheme of MW-assisted pyrolysis of cellulose

Therefore, based on these observations, we designed a "layer" experiment to enhance the yield of LGO (Figure 4a) emphasizing a synergetic effect between both catalysts. The vessel was packed with of bentonite at the bottom to generate water, enhancing the bio-oil yield during MW-assisted pyrolysis (Figure 4a). The bentonite loading (20wt%) was chosen based on the highest yield of bio-oil obtained in the previous experiments (Figure 2a). Cellulose was mixed with Al-PILC, and a layer of pure Al-PILC catalyst was placed on the top (Figure 4a). The yield of the bio-oil increased, and the composition analysis showed the presence of 12.3wt% of LGO of ~60% purity in the bio-oil mixture (Figure 4b).
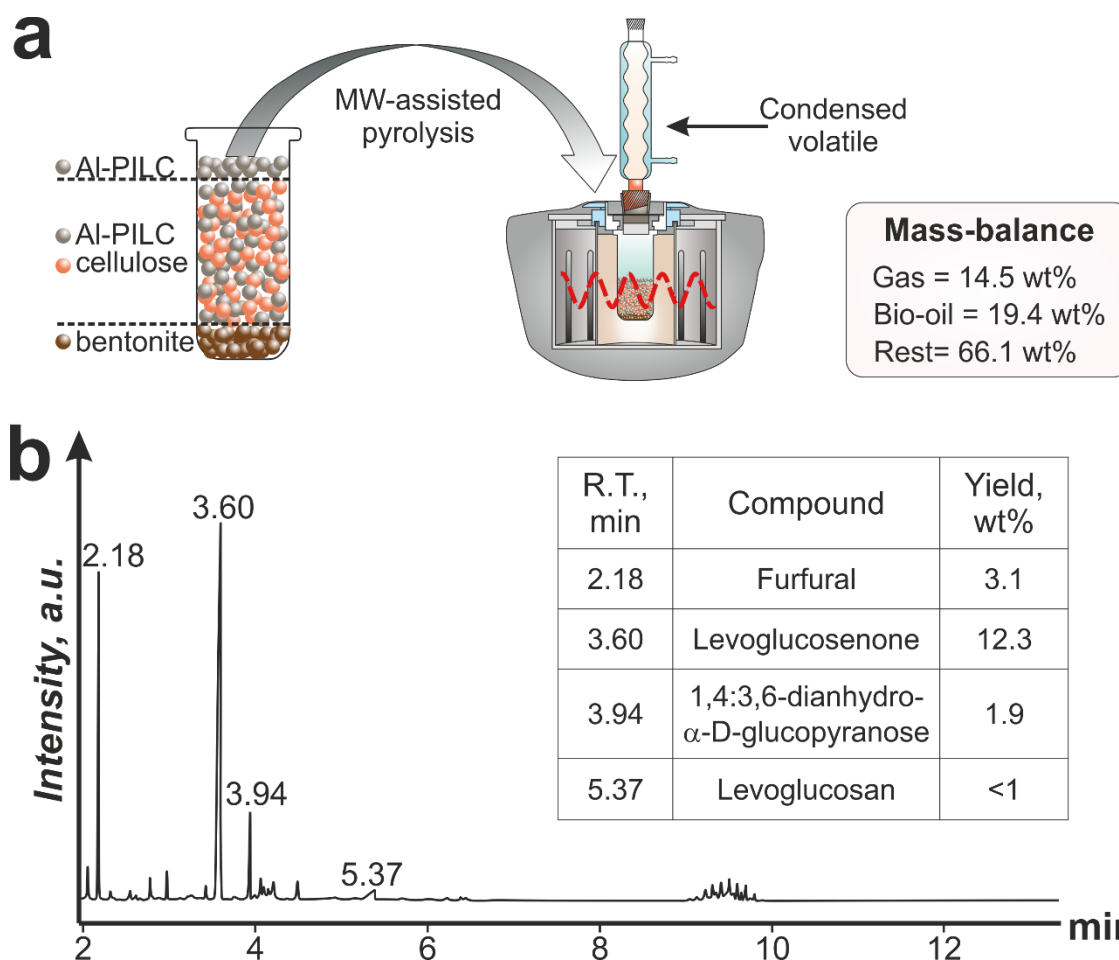
Figure 4. Synergetic effect of bentonite and Al-PILC to enhance the yield of LGO (notably, the retention time of the LGO is longer compared to that one on Figure 2c, because the spectra were collected at different times)

To demonstrate a significant biorefinery potential, we successfully performed MW-assisted pyrolysis of paper waste simply mixed with 50wt% of the Al-PILC, giving 4.8wt% of LGO (Figure S16). To reactivate the catalyst, we followed a two-step process: acidic MW-hydrolysis followed by oxidation with hydrogen peroxide. The MW-hydrolysis resulted in the production of glucose, 5-HMF, levulinic and lactic acids (Figure S18). The Al-PILC was successfully regenerated three times, losing a total of ~34% of its activity.

4.4.2.5. Conclusion

In conclusion, through MW-assisted pyrolysis of cellulose in the presence of bentonite and Al-PILC, we have identified a competitive nature between the production of 5-HMF and LGO. We believe the majority of LGO and 5-HMF comes from levoglucosan and sugars, respectively. The ratio between sugars and levoglucosan is controlled mainly by the amount of water produced during the pyrolysis stage. This water favours hydrolysis reactions, increasing the yields of sugars,

which are partially converted to 5-HMF on the Lewis acid sites. The Bronsted acid sites of Al-PILC promote the production of 40% pure LGO at 6.3wt% yield at 50wt% of the catalyst loading. We also found a synergetic effect between both catalysts to enhance the yield of LGO to 12.3wt%, which is comparable with our conventional pyrolysis experiment, but the selectivity towards LGO is three times higher. The Al-PILC catalysts are considered a good candidate for LGO production, and in the MW-assisted pyrolysis of the paper waste was regenerated three times.

4.4.2.6. Experimental section

All experimental details are available in the Supplementary Materials.

The Supplementary Materials to this paper is available at Appendix 1 of the thesis

4.4.2.7. Contributions

Alisa Doroshenko has conducted and analyzed the majority of the experiments with the help of Karl Heaton and Stephen Cowling. Vitaliy Budarin, Ihor Pylypenko, Alisa Doroshenko and James Clark have developed the mechanistic understanding of the MW-pyrolysis process in the presence of clays. All authors have discussed the manuscript and were involved in the writing process.

4.4.2.8. A coherent body of the work

The presented article describes an original contribution to the pyrolysis science, particularly on the MW-assisted pyrolysis of cellulose in the presence of catalysts (e.g. bentonite and Al-pillared bentonite). The MW-thermal activation of cellulose in the presence of pillared clays was not previously investigated. Detailed analysis of the role of Lewis and Bronsted acid sites and a role of water was studied using various techniques, showing its influence on the distribution of chemicals in the bio-oil. Therefore, the presented article and this integrated chapter are complementing the title of the thesis: "Catalytic Thermal Conversion of Biomass Towards Valuable Chemicals".

4.4.3. Open vessel and MW-FTIR

As it was discussed in the previous section, the conventional pyrolysis of the clay/cellulose mixtures at the set of different ratios was studied via TG-FTIR method. The combination of the FTIR gas detector with MW reactor makes it possible to study the kinetic of MW-related processes. Permanent N_2 flow at 100 ml/min guarantees the delivery of the released chemicals to the IR detector with the constant delay time.

The MW-power was established at 300W at fixed power mode. The mass of the cellulose in each sample was fixed at 50 mg. It has been investigated the whole clay/cellulose system with a step of 5wt%.

The data processing included a spectrum extraction at the maximum of IR-trace for each sample. Then, the extracted spectra were normalised from 0 to 1 and displayed at the graph showing the spectrum dependency on the cellulose/clay ratio (Figure 78). This gives an idea of the system evolution over the amount of the clay added.
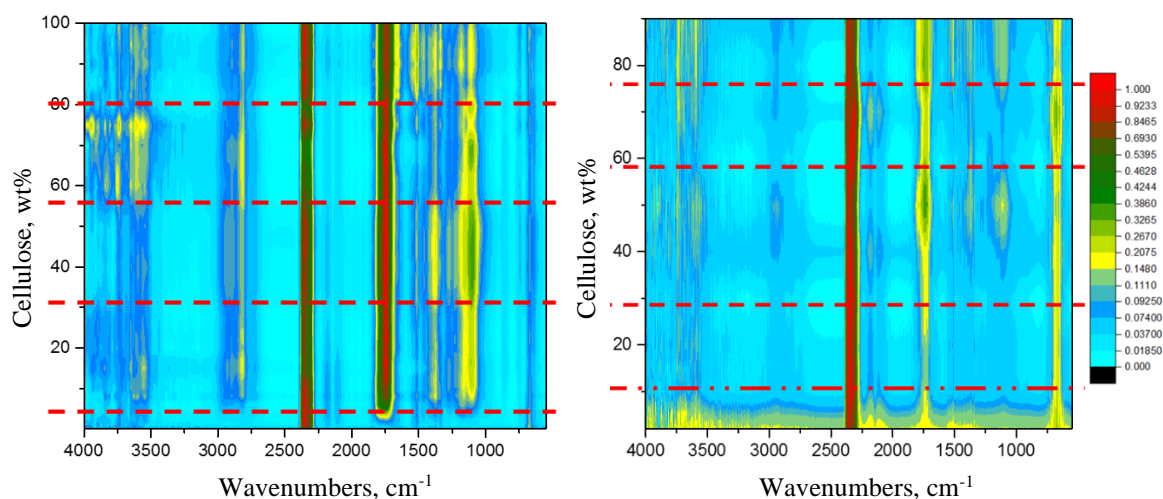
Figure 78. (left) TG-IR of the cellulose/clay system; (right) MW-IR of the cellulose/clay system

It is clearly seen zonal behaviour, which was discussed at the conventional pyrolysis section, indicating that this phenomenon is independent on the type of heating.
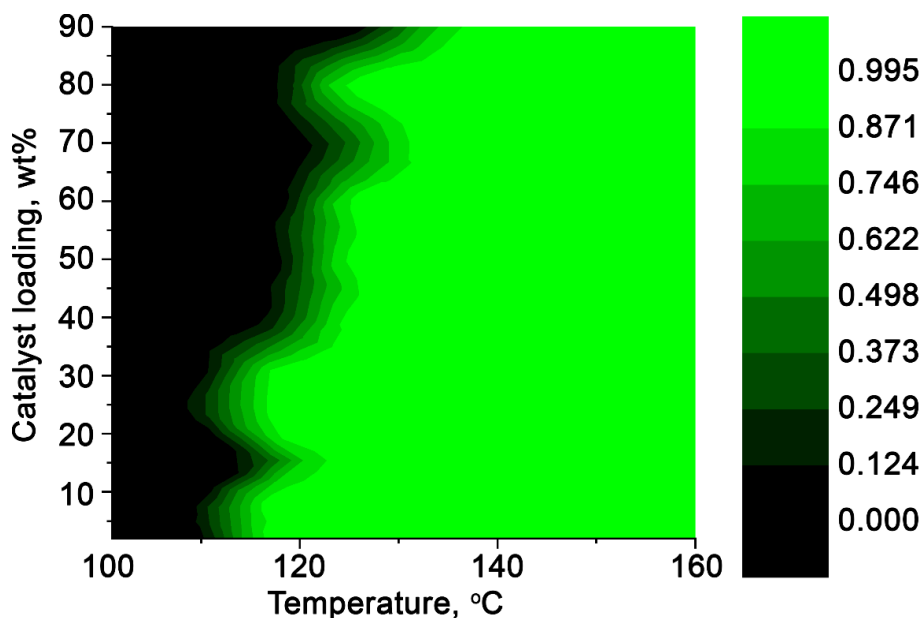
Figure 79. Map for the presence of CO_2 during cellulose MW-pyrolysis

MW-FTIR data can be processed in various ways, including correlation analysis between the references and spectra of the samples. Such analysis was done between CO_2-reference and the

collected MW-FTIR data. If the correlation coefficient is higher than 0.5, then CO_2 is detected. Higher correlation coefficient indicates improving confidence on the presence of CO_2. Production of CO_2 is an indicator of pyrolysis initiation.

Higher clay loading increases the temperature of cellulose decomposition in MW (Figure 79). The similar phenomenon was observed during conventional pyrolysis when the temperature of maximum cellulose decomposition was shifted in the right of the diagram. However, the initial degradation point was the same (Figure 53). Probably, the difficulties with diffusion are also observed in the case of MW-assisted pyrolysis similarly to the conventional.

The composition of the volatiles is mainly consisted of CO_2, with a low impact of organic products, which can be observed from weak alcohol and carbonyl bands in Figure 78-right. Low yields of volatiles are related to the low cellulose mass loading to the MW reactor, which was limited to 50mg due to gas-FTIR cell capacity.

The kinetic map on the distribution of CO_2 is given on Figure 80. Interestingly, similarly to the conventional pyrolysis the production of CO_2 is slowing down at around 50wt% of the catalysts.
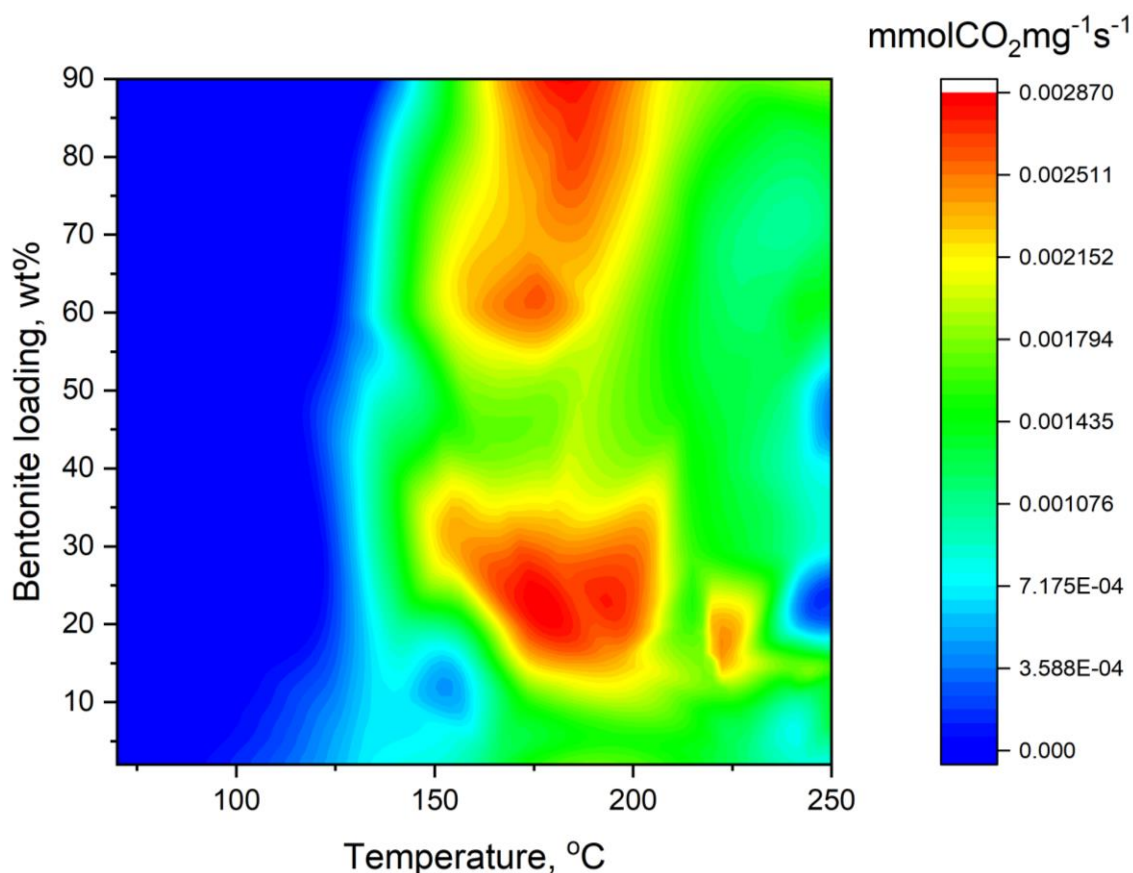
Figure 80. Kinetic map of CO_2 production during MW-assisted pyrolysis of cellulose in the presence of bentonite

A great selectivity of MW-assisted pyrolysis, probably, happen because of two phenomena. In the first turn, the lower temperature of biomass activation. These temperatures make it possible to gain better control on polysaccharide depolymerization. At the second turn, MW-radiation seems to initiate a large number of self-oxidation reactions (at 50 mg mass loading), improving selectivity via the inducing the decomposition of other non-stable volatiles.

4.5. Zeolite

The samples were prepared via intensive mixing between cellulose and ZSM-5 at different loadings of 2, 10, 20 and 50wt%.

The temperature MW- traces resulted from the pyrolysis of the prepare mixtures are shown on Figure 81.
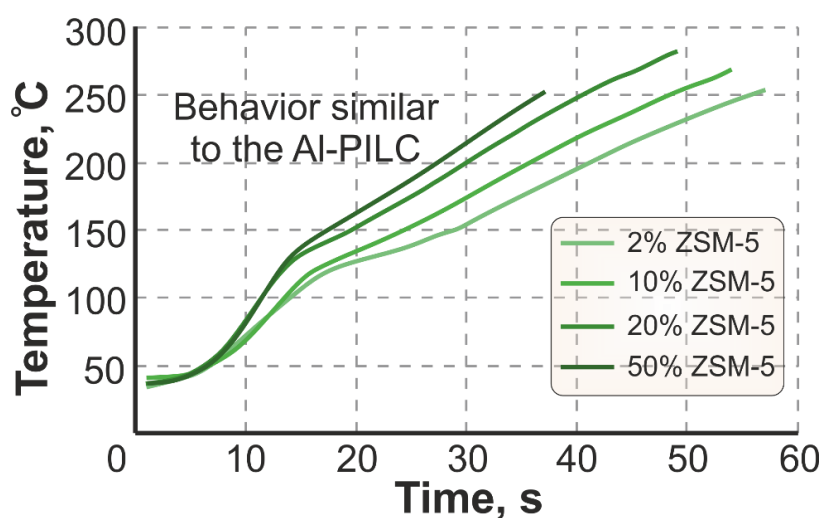
Figure 81. Temperature MW traces for zeolite/cellulose system

The type of temperature behaviour is very similar to that one of Al-PILC, rather than bentonite. Two factors could cause this. The first one is the presence of a stable porous structure that is not changed with temperature. Al-PILC and ZSM-5 have a stable porous structure, while the bentonite fragmentation pattern is changing during heating. The second factor can be the amount of physisorbed water. The bentonite has a higher amount of physically-bonded water, compared to the Al-PILC and ZSM-5.

Increasing the loading of ZSM-5 results on the faster heating rates. There is a switching of the heating rate around 120-150 °C, which is associated with complete evaporation of physisorbed water. The desorption of this water happens slightly higher than typical free water (100 °C). This temperature delay is caused by complicated diffusion because of the developed porous structure of the catalyst.

The composition of the bio-oil was thoroughly investigated by GC-MS and GC-FID. The GC-MS spectra of the sample mixed at 50wt% is displayed on Figure 82.
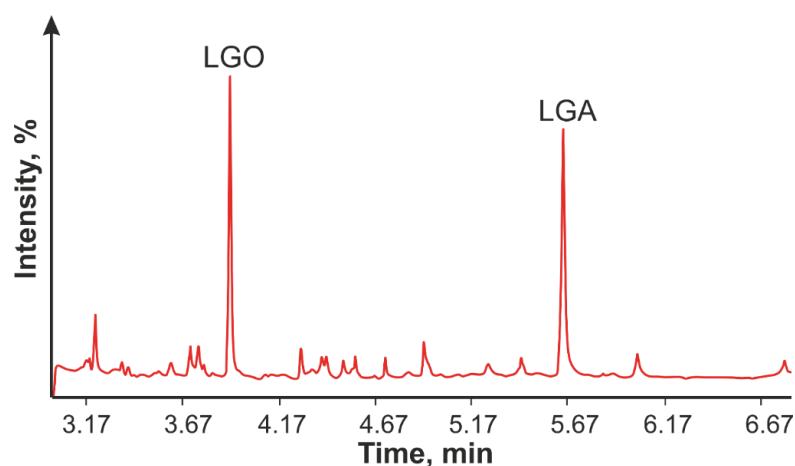
Figure 82. GC spectrum of the bio-oil collected during pyrolysis of cellulose-ZSM-5 mixtire (50wt%)

The yield of LGO was increasing at increasing the part of zeolite in the mixture. This can be associated with increasing the amount of available Bronsted acid sites. Moreover, ZSM-5 zeolite has a developed microporous structure, which could help it to act as molecular sieves. This process would favour the production of levoglucosenone, acting as a water adsorber, shifting the equilibrium toward the reagent side. The overall yields of some valuable chemicals are presented in the table.

Table 16. Yields of some valuable chemicals during cellulose pyrolysis in the presence of ZSM-5

Zeolite loading, wt%	Yield of valuable chemical, wt%		
	LGO	HMF	LGA
2	0.8	1.3	4.8
10	1.3	1.7	4.4
20	2.8	0.8	3.9
50	5.1	0.1	1.7

The catalytic effect of ZSM-5 on cellulose pyrolysis is similar to that one of Al-pillared clay. This can be explained with the stable mesoporous structure of both catalysts and similar surface properties, including high acidity. The microporous zeolite could partially favour the process of LGO formation via trapping of the excess of water. It is predicted that the ratio between microporosity and mesoporosity should have an optimum in terms of maximizing the yield of LGO.

Conclusions

113

In the current chapter, there are reported data on MW-assisted cellulose pyrolysis in the presence of both liquid acids and heterogeneous catalysts. The following conclusions were achieved:

- Sulfuric and phosphoric acids were confirmed to be an efficient liquid catalysts in the production of LGO during cellulose pyrolysis. It was found that in the presence of these catalysts, the MW-assisted pyrolysis of cellulose released a significant volume of gases, which was not reported previously. In the closed vessel, the volume of gases released was so large that pressure was rising higher than the limits of the equipment and the run was cut off, limiting the amount of produced bio-oil. The pressure limitation was overcome in the opened vessel experiment. It has been obtained 19% bio-oil with significantly improved (up to 30-35%) yield of LGO. These findings are important for the establishment of efficient MW-technology for biorefinery.

- It was found that clay hydrophobicity plays a substantial role in their MW activity. Even a low quantity of hydrophilic bentonite intensively interact with microwave radiation while the activity of hydrophobic kaolinite is much lower. These results are crucial in choosing the catalyst for a MW-related process.

- MW-assisted pyrolysis of cellulose in the presence of clays and zeolite was done for the first time. It has been found that the clay water capacity substantially influences on cellulose pyrolysis products distribution. In the closed vessel experiments Al-pillared bentonite favouring the formation of LGO (~6wt%) rather than HMF and LGA. While water-rich bentonite, at loadings less than 20wt%, was found to increase the yield of bio-oil probably because of the higher degree of hydrolysis reactions in the presence of water. This assumption is supported by HPLC data on the sugars content of the bio-oils. The addition of Al-PILC results on a gradual decrease of bio-oil yields due to the intensification of charring reactions. These findings is a key on the impoertment of bio-oil yield during MW-assisted pyrolysis, which is an important task for profitable value-added biorefinery.

- A scheme on MW-assisted pyrolysis of cellulose in the presence of clays is suggested. To prove this scheme a unique experiment has been designed. In this experiment, the sample was prepared as three layers: bentonite is underneath, cellulose/Al-PILC mixture in the middle and Al-PILC on the top. Such a design improved the yield of LGO to 12.13wt% and evidenced the suggested mechanism.

Such a scheme predicts the paramenets driving the pyrolysis processes and therefore substantially contributes to the state-of-art of pyrolysis science.

- Open vessel MW-assisted pyrolysis of cellulose (50 mg) in the presence of bentonite has been recorded using specifically developed MW-FTIR setup (which was done for the first time). It was found MW-pyrolysis results in a higher degree of gasification compared to conventional pyrolysis. This phenomenon can be used to get better quality char, but not suitable for the production of valuable chemicals.

- Based on the collected MW-FTIR data, a spectrum at the maximum rate of the cellulose decomposition has been extracted for each cellulose-bentonite ratio. These spectra have been combined together on the same graph depending on the catalyst loading. Such graph revealed a zonal behaviour of cellulose in the presence of bentonite. This effect could be important for kinetics separation of the volatile component.

All in all, MW-assisted pyrolysis of cellulose in the presence of clays and zeolite was reported for the first time in terms of the volatile compositions. The suggested scheme and the monitoring approach are useful to identify an appropriate atmosphere and catalyst during MW-assisted pyrolysis of cellulose. Therefore, these findings are substantially contribute to starte-of-art of the pyrolysis science.

CHAPTER 5. CONVENTIONAL PYROLYSIS OF STARCH IN THE PRESENCE OF ACID CATALYST

5.1. Introduction

The amount of global food waste is estimated at around 1.6 billion tonnes annually, massively impacting on the dissipation of resources and high carbon footprint.(*261*) The most important reason for effective waste utilization is to protect the environment and for the health and safety of the population.

The food waste has a high content of organic matter, consisting of fat, starch, protein and other compounds.(*262*) Existed technology can create recycling values from fat and proteins. Fat is a cheap feedstock for the production of biodiesel, while proteins are used for animals feed.(*263*) As it was noted in the literature overview, starch is a native polysaccharide represented with a formula $(C_6H_{10}O_5)_n$. It gives LGA in the amount of 50wt% under pyrolysis, which can be extended at high heating rates under vacuum. Surprisingly, the pyrolysis of cellulose (polysaccharide with the same stichometrical formula as cellulose) has been studying for the last few decades, while the pyrolysis of starch, surprisingly, did not attract significant attention. At the same time, starch, having LGA as an intermediate, could represent a valuable source of chemicals typically received from cellulose pyrolysis, but in easier way. For example, the energy inputs on the decomposition of starch (~200 °C) are much lower compared to cellulose (~330 °C). Moreover, the yield of levoglucosan (LGA – considered to be a primary intermediate in pyrolysis of cellulose and starch) is reported to be higher from starch compared to cellulose at similar conditions. An efficient conversion of starch towards valuable chemicals could forward a wastes utilization technology and biorefinery to another level.

Therefore, here is reported acid-catalytic pyrolysis of starch towards valuable chemicals at different heating rates. This chapter is an effort to fill the gap in the mechanistic insights of starch pyrolysis doped with acids. A detailed composition of the produced volatiles and their kinetics are given for the first time.

The loading process of the chosen acid should be energy-efficient and straightforward. It was decided to test *p*-toluenesulfonic acid (PTSA) as a catalyst and compare results with sulfuric acid (H_2SO_4) and zeolite (ZSM-5). The market price for PTSA is ~8 times higher than H_2SO_4, but its impregnation process is low-energy and allows to achieve high-degree of homogenous distribution of the acid in the feedstock. Considering the high importance of starch utilization in large-scale, the loading of catalysts was only 0.5wt%.

The impregnation was done in the expanded material following to the methods described in the relevant chapter, achieving a homogenous distribution of acids in starch.(*264*) The addition of heterogeneous ZSM-5 was performed by mechanical mixing of the solid catalyst with expanded starch and evaporation of the residual solvent under vacuum. Detailed preparation of the samples is given in the relevant section.

The cold trap experiment has been carried out in to choose adapted reference set for the quantitative spectra processing. The bio-oil was extracted with acetone and submitted for GC-MS, following to the procedure described in Materials and Methods.

The samples were investigated using TG-FTIR method, described in the Methods. The starch/PTSA samples were heated at different heating rates (2, 10, 20, 30, 40 and 50 Kmin^{-1}) from T_{start}= 23 °C to T_{final}= 600 °C. The H_2SO_4 and ZSM-5 doped samples were heated at 10, 30 and 50 Kmin^{-1} heating rates within the same temperature range. The received data were processed following to the developed TG-FTIR quantitative processing procedure, that is described in details at the relevant section.

5.2. Yields of chemicals during acid-doped starch pyrolysis

The results of the cold-trap experiment collected for the PTSA-doped sample at 50 Kmin^{-1} are displayed on the Figure 83.
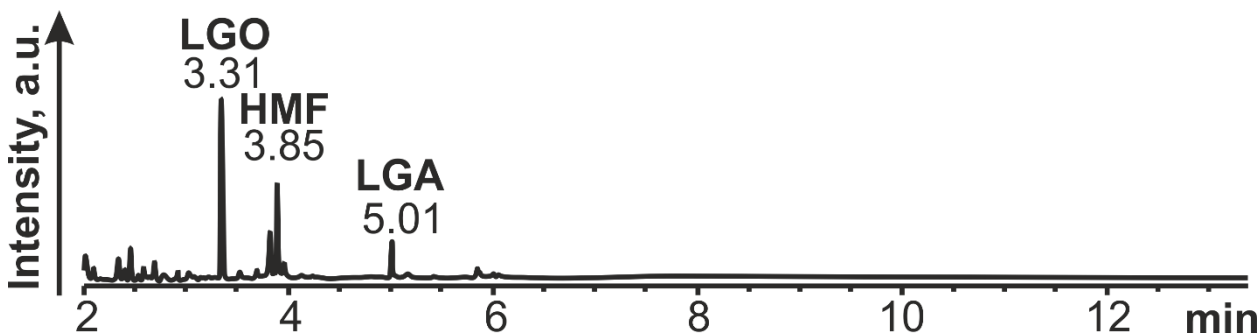
Figure 83. GC-FID data of the bio-oil resulted in the PTSA-doped starch at 50Kmin^{-1}

As it is seen from Figure 83, the volatile fraction was mainly consisting of LGO, HMF, DGP and LGA. Levulinic acid was also found, which is going to be discussed further down.

Therefore, a set consisting of 15 chemical compounds (standards) was chosen to describe the FTIR spectra for the samples. The volatiles produced at different heating rates during acid-catalysed pyrolysis of starch were characterized using the TG-FTIR technique. This method allows in-situ monitoring the FTIR composition of the produced pyro-gas in real-time and assigns the recorded spectra to the pyrolysis temperature for a deep kinetics investigation Figure 84A-C.

117
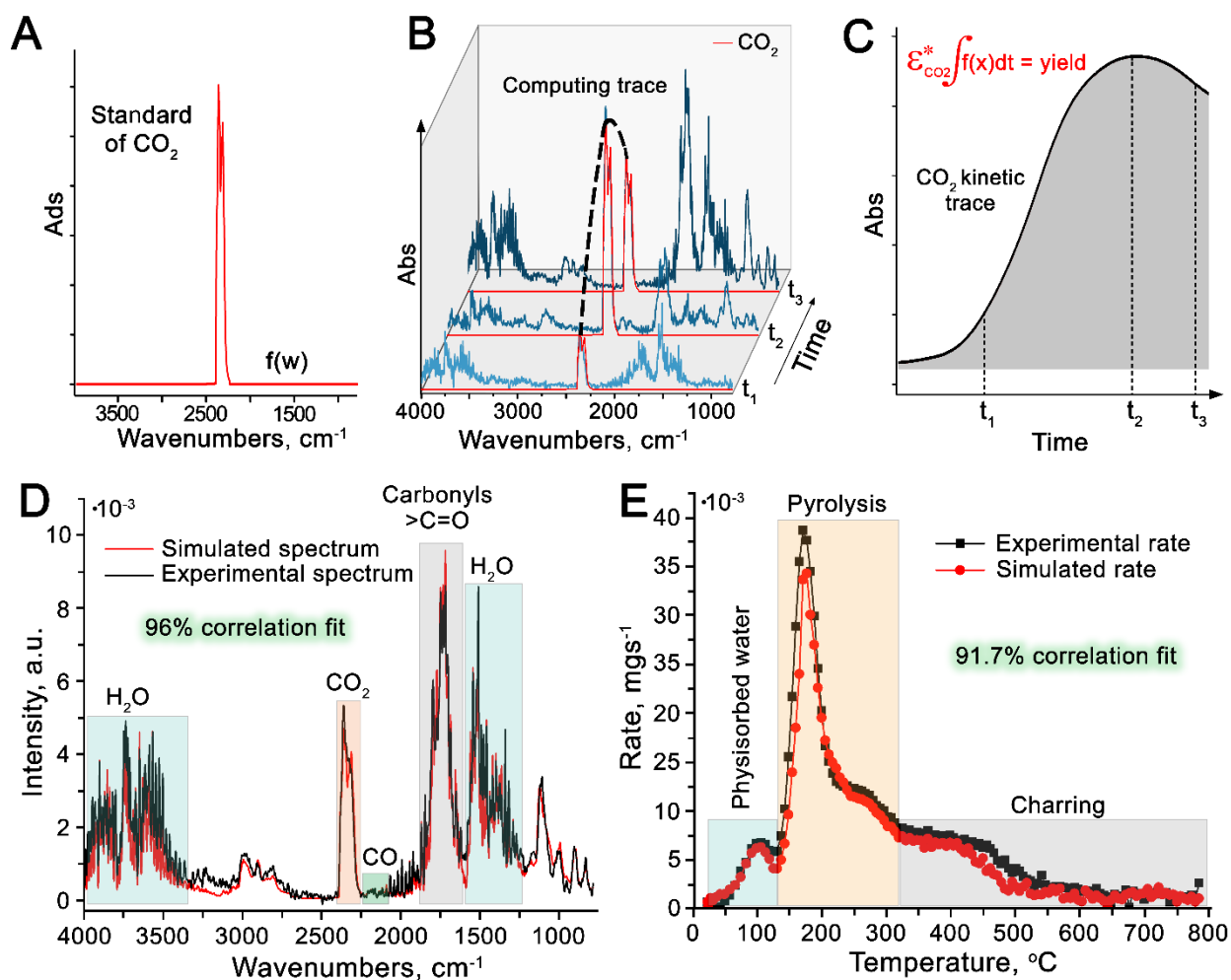
Figure 84. Processing of the TG-FTIR data and the verification procedures for the proposed algorithm

TG-FTIR simulated spectra can be done by adding the standards in the determined proportion and can be used for verification of the results (Figure 84D). Furthermore, the fitting between the calculated FTIR-rate and the experimental TG-measured rate can be used as another evidence verifying the data processing approach (Figure 84E).

Table 17. Yields of chemicals at different heating rate during pyrolysis of starch doped with PTSA

Chemical	Heating rate, Kmin⁻¹					
	2	10	20	30	40	50
H_2O	56.96	46.34	43.07	37.81	37.02	38.45
CO	6.17	8.54	11.15	11.41	12.24	13.00
CO_2	19.87	18.60	16.72	16.75	16.27	17.06
Formaldehyde	0.93	1.23	1.32	1.63	1.84	2.01
Formic Acid	8.58	5.71	1.77	1.50	1.28	1.26

Acetaldehyde	3.07	3.41	3.93	4.25	4.35	4.09
Acetic Acid	1.11	0.98	0.85	0.78	0.75	0.78
Hydroxyacetone	0.88	1.21	2.02	2.71	2.94	3.43
Furfural	1.28	1.70	1.26	1.54	1.41	1.45
Levulinic Acid	0.12	1.69	1.83	0.49	0.21	0.14
LGO	1.70	2.54	4.94	7.99	4.82	4.75
HMF	0	0.56	2.76	4.29	2.82	1.51
DGP	0.03	0.34	0.79	1.14	1.38	0.81
LGA	0.24	0.40	0.67	1.10	2.31	2.95

The heating rates significantly influence the distribution of chemical products in the result of pyrolysis of PTSA-doped starch (Table 17). The yield of LGA, a primary intermediate in pyrolysis of non-doped starch,(*179*, *265*) is increasing with heating rates. As it was reported by Kawamoto, fast heating rates shift the temperature of starch decomposition to the higher range, presumably favouring both LGA formation and vaporization.(*219*) Also, it can cause partial volatilization of PTSA from the reaction zone, reducing the acidity. Generally, the amount of the produced LGA is influenced by heating rate, reaction temperature and residence time.(*266*) The maximum yield of LGA from acid-doped starch was only ~3% (50 Kmin^{-1}), that is low compared to the pure starch yielding between 30-60wt%.(*179*, *265*, *267*) The presence of acid can provoke decomposition of the formed LGA towards secondary pyrolysis products such as LGO,(*104*) HMF,(*268*) DGP and other lighter molecules. Interestingly, these chemicals are passing via maximum yields depending on the heating rate: DGP (40 Kmin^{-1}), HMF and LGO (30 Kmin^{-1}). These maximums are probably corresponding to the different degree of dehydration of the primary intermediate depending on its residence time. Longer residence time leads to deeper dehydration of LGA (max at 50 Kmin^{-1}) via DGP (max at 40 Kmin^{-1}) towards LGO (max at 30 Kmin^{-1}). In the case of PTSA, the maximum yield of LGO can be explained by partial volatilisation of PTSA, reducing the total acidity and dehydration degree. Such scheme of dehydration is completely in line with Shafizadeh assumption of DGP being a precursor for LGO. This transfer of yields is clearly displayed on Figure 85.
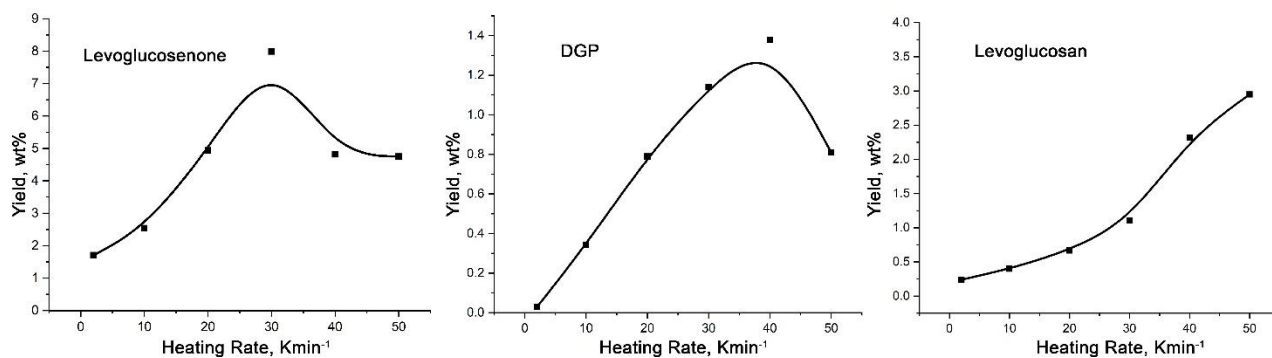
Figure 85. Chemical yields of LGO, DGP and LGA depending on heating rates

Surprisingly, the yield of LGO is relatively high for such a small amount of acid loading. There is no data available on the production of LGO from starch, but this amount is relatively high in comparison with acid-doped cellulose at 0.5wt% concentration. The results on the yields of LGO for H_2SO_4 and ZSM-5 are displayed in Table 18.

Notably, in the case of non-volatile acid catalysts, such as sulfuric acid and ZSM-5, there is no optimum condition found and logically to assume that higher loading non-volatile acid can cause even higher yield of platform molecules including LGO.

Table 18. Yields of LGO during pyrolysis of acid-doped starch with sulfuric acid and ZSM-5

Heating rate	Yield of LGO, wt%	
	H_2SO_4	ZSM-5
10	2.7	0.7
30	4.1	1.6
50	5.3	1.7

5.3. Kinetic analysis of chemicals during acid-doped starch pyrolysis

The heating rates lower 30 $Kmin^{-1}$ cause the higher yield of smaller molecules such as water, CO_2 and acid. Special attention was given to the production of formic acid, the yield of which has substantially arisen at low heating rates (2 and 10 $Kmin^{-1}$, Table 17). The phenomenon of the remarkable yield increase of formic acid at slow heating rates was investigated via kinetic traces (Figure 86A-B). It was found that pyrolysis of PTSA-doped starch is initiated with the production of CO_2 followed by the appearance of LGA (Figure 86 A-B) for all heating rates. The chemicals produced next are CO and formaldehyde. In the case of slow pyrolysis, these two chemicals are coming together with formic acid (peak at ~160 °C, Figure 86 A), which also gives a shoulder around 225-240 °C. In contrast, at moderate heating rates (>10 $Kmin^{-1}$), the formic acid trace has only one band at ~225-240 °C.
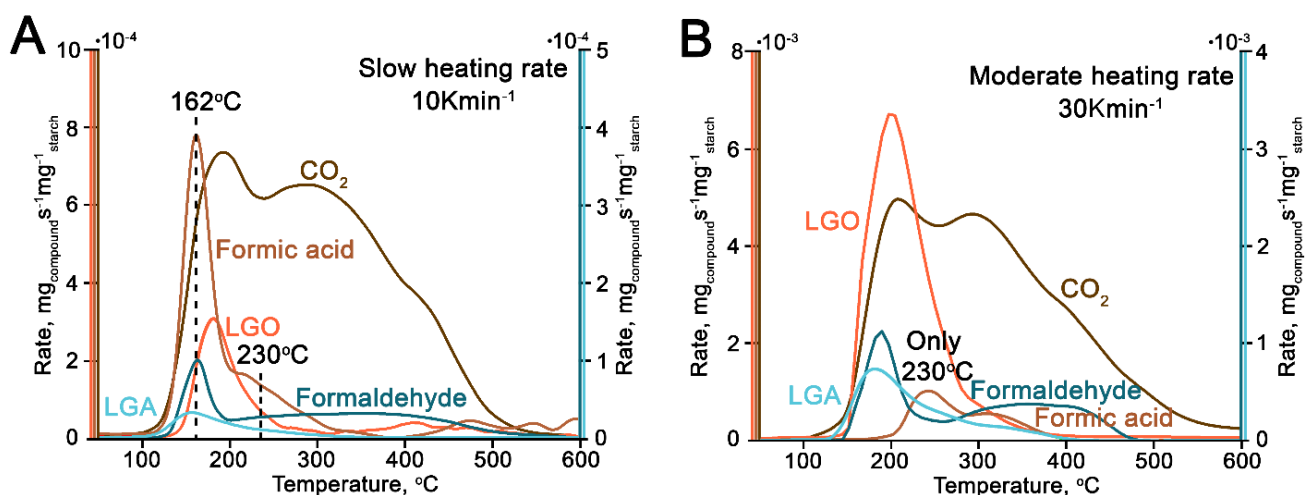
Figure 86. A, B – kinetic traces of a few chemicals at 10 Kmin^{-1} and 30 Kmin^{-1};

This substantial difference in the formic acid kinetics has a significant influence on its yield (Figure 87). Presumably, the retention time of chemicals in the reaction zone at slow heating rates is high enough to be decomposed to formic acid at ~160 °C, while at faster heating rates these chemicals can be boiled off or follow another transformation pathway. The amount of the formic acid produced at ~225-240 °C (20-50 Kmin^{-1}) is almost constant, indicating some degradation process happening at exactly this temperature and being almost independent on the heating rates. Thermal degradation of sugars could be a potential candidate for this reaction, and if so, then the yield of the sugars during pyrolysis are almost independent on heating rates.
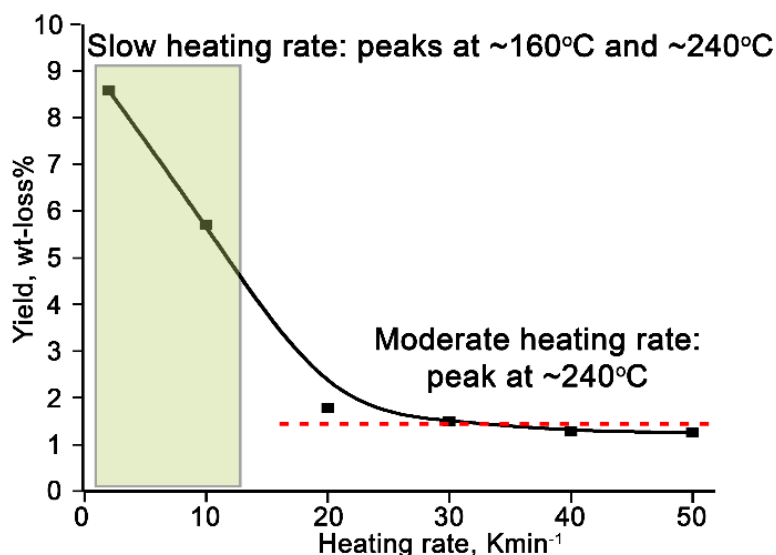
Figure 87. The yield of formic acid depending on the heating rates

Relatively high yields of oxygenated species such as formic acid and CO_2 at low heating rates (Table 17 and Figure 87) imply of less oxygenated solid residue left after pyrolysis. Considering the initial formula of starch ($[C_6H_{10}O_5]_n$) and the evolution of $C_xH_yO_z$ composition of

the evolved pyro-gas (combined kinetic traces) during pyrolysis, it is possible to calculate the formula of solid residue changing continuously over temperature. A plot reflecting the properties of solid carbon-based materials is called van Krevelen diagram. Usually to place a point on van Krevelen diagram require CHO analysis of the left solid residue, implying termination of the experiment. The continues van Krevelen diagrams of the solid residue are reported for the first time. Such diagrams for the solid residue left after PTSA-doped starch pyrolysis are displayed in Figure 88.

Furthermore, such diagrams completely fit the expected H:C and O:C ratio using original the van Krevelen diagram obtained for solid fuels, that is another evidence of accurate TG-FTIR data processing.
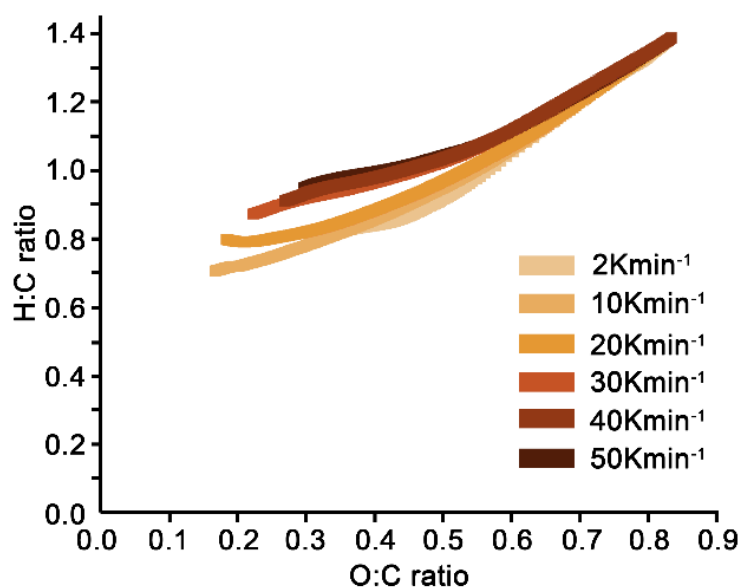
Figure 88. Continues van Krevelen diagrams of the solid residue during PTSA-starch pyrolysis.

The processing of kinetic traces of the produced pyro-chemicals allowed us to map their distribution depending on temperature and heating rates. Such maps make it possible to reveal the processes; those are depending on each other. For example, we found an interesting dependency between HMF and levulinic acid (Figure 89 A, left – HMF, right – levulinic acid, middle – combined). The longer residence time of HMF in the acidic reaction zone leads to its conversion to levulinic acid. This concept is in agreement with studies on the synthesis of levulinic acid using HMF as a precursor.(*269*) Following to the distributions of CO_2 and LGO (Figure 89B, CO_2 – left, LGO – right, combined – middle), these processes could be related. The zone of the maximum LGO rate corresponds to the minimal CO_2 production in the temperature range.
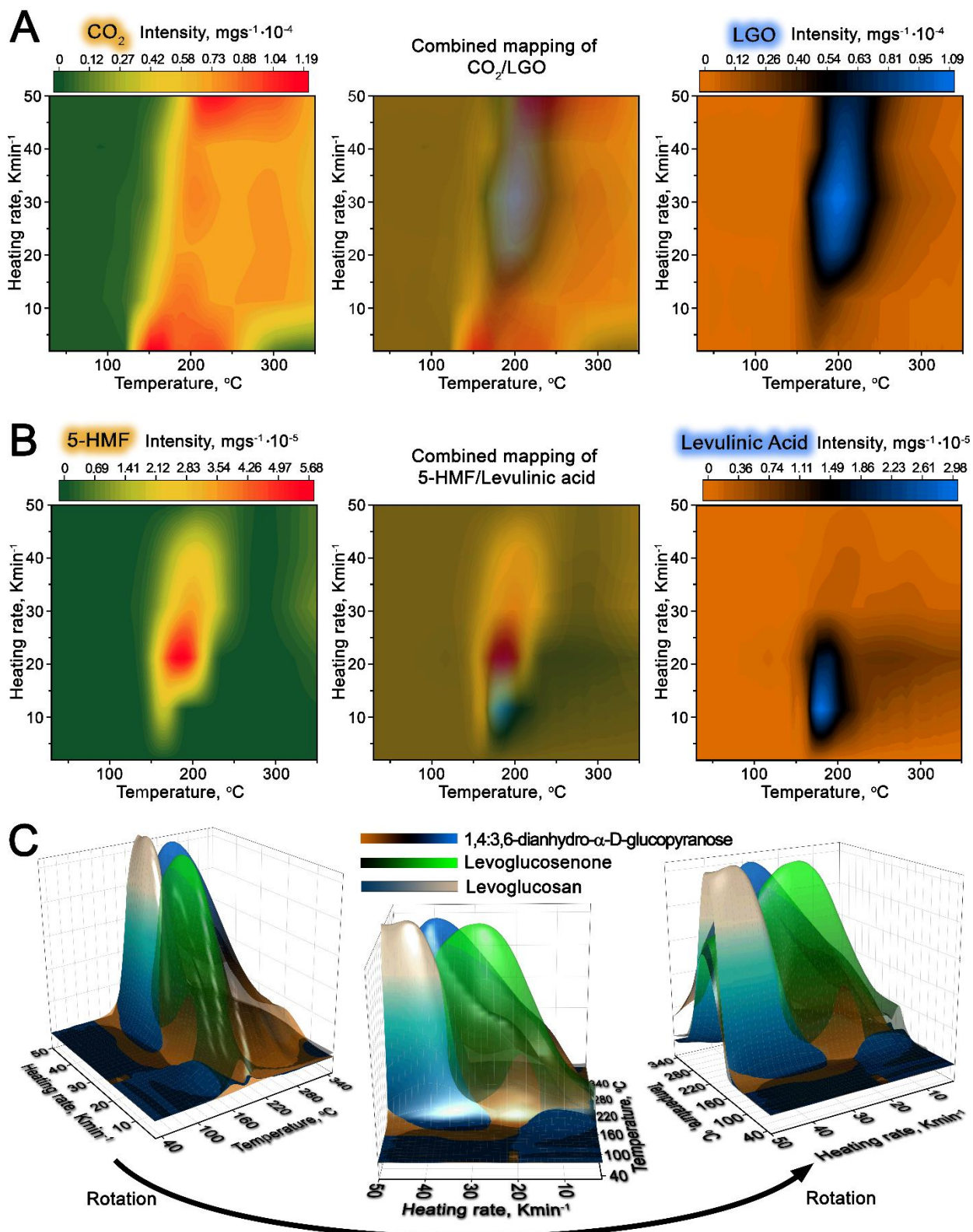
Figure 89. A – distribution maps for CO_2 and LGO; B – distribution maps for HMF and levulinic acid; C – normalized 3D distribution map for LGA, DGP and LGO

It was decided to review the assumption made by Shafizadeh on the LGA ($C_6H_{10}O_5$) dehydration via DGP intermediate ($C_6H_8O_4$) towards LGO ($C_6H_6O_3$).(*191*) Considering the low yields of DGP and LGA compared to the LGO, a normalized 3D map for these chemicals is displayed on Figure 89C. The middle graph (Figure 89C) reveals two separate peaks for DGP at moderate heating rates (20-30 Kmin^{-1}) produced straight after the initiation of pyrolysis and at 222 °C independently on heating rates. These peaks are merged at faster pyrolysis (40 Kmin^{-1}), presumably because of the shift in temperature of starch decomposition. Based on the kinetic traces of DGP, it starts to be produced just a few degrees earlier than LGO (20-30 Kmin^{-1}), supporting the assumption of being a potential precursor. Interestingly, the DGP produced at 222 °C is not converted to LGO, which could happen because of both blocked acid sites and partial evaporation of PTSA at this temperature.

Conclusions

At the current chapter, it was offered a methodology on the sustainable and efficient valorisation of starch-related wastes towards simultaneous production of multifunctional mesoporous materials (Starbon) and valuable chemicals. The following results were achieved:

- For the first of the time, it was found that levoglucosenone is a value-added product during Starbon preparation process. Even at small acid loading (0.5wt%) the yield of levoglucosenone was 1.7wt% at 2 Kmin^{-1}. This heating rate is essential for the development of mesoporosity. However, various heating rates were tested to maximise LGO production. The yield of LGO is passing via maximum depending on the heating rate, giving the highest amount of 7.99wt% at 30 Kmin^{-1}. The existence of the maximum can be explained by partial volatilisation of PTSA at higher heating rates, reducing the number of acid sites. This result can be crucial in for making Starbon production process more profitable.

- A detailed analysis of kinetic data for starch pyrolysis in the presence of PTSA is reported for the first time. It was found that there is a chemical compound which is partially decomposed to formic acid at 162 °C at relatively low heating rates (2-10 Kmin^{-1}). The yield of formic acid at heating rates between 10-50 Kmin^{-1} is almost constant. It is around 1.5wt%, and the maximum production is happening at around 230 °C. Potentially this temperature can be associated with decomposition of sugars. If sugars are intermediates of formic acid at 230 °C, then considering constant (1.5wt%) yield, it is possible to assume that amount of generated sugars is

independent on heating rates. These findings are important in the development of understanding of starch pyrolysis mechanism.

- The kinetic analysis showed that the production of CO_2 and LGO are competitive processes, supporting the data obtained in conventional pyrolysis of cellulose-zeolite mixtures. This indicates that the mechanism of LGO production seems to be the same for thermal degradation of starch and cellulose. Indeed, these two polymers have an identical chemical formula, but different structures.

- The hypothesis of Shafizadeh on the production of LGO via DGP intermediate was investigated. Analysis of the volatile's kinetics shows that DGP production happens a few degrees earlier than LGO. Furthermore, interesting LGA-DGP-LGO transformations were highlighted depending on the heating rates. These results are crucial for the efficient production of valuable chemicals from biomass.

- A comparison of the nature of catalysts such as PTSA-, H_2SO_4- and ZSM-5 on LGO yield was investigated. The experiments were carried out at different heating rates. ZSM-5 have no influence at such small loading, and a slight increase of LGO at high heating rates is a result of the intensified evaporation process. Starch pyrolysis in the presence of sulfuric acid results on levoglucosenone production. Its yield was constantly increasing at higher heating rates because H_2SO_4 is not volatile acid.

These conclusions facilitate the development of the state-of-the-art of pyrolysis science as well as industrial technology on the efficient valorisation of starch-related wastes.

CHAPTER 6. REAL-BIOMASS: MW-ASSISTED PYROLYSIS OF NI-HYPERACCUMULATORS

6.1. Introduction

Transition metals are widely known as efficient catalysts in many processes, including biomass transformations.(*270*) Due to various collaborations of the GCCE at the University of York, there was a chance to study utilization and valorization of Ni-hyperaccumulator plants. These plants are used for phytoremediation of Ni-contaminated land.(*271*) By collecting a large amount of nickel, the plant is becoming toxic for the environment, including birds and bees.(*272*) Therefore, it is essential to offer a sustainable solution to the utilization of Ni-hyperaccumulators.

Currently, these plants are burned to recover the metal. However, naturally incorporated nickel can cause substantially different pyrolysis pathways, potentially leading to valuable chemicals. As was discussed at the literature overview, nickel is considered to be one of the most promising catalytic metals among others because of its complex oxidation states chemistry that involves the accessibility of Ni(0) /Ni(I) /Ni(II) /Ni (III) oxidation states and facile activation of unsaturated molecules. (*146*, *147*)

It was decided to study MW-assisted pyrolysis of Ni-hyperaccumulating plants, which was never studied before. The aim was to investigate any value-added products during the pyrolysis process and to get insights about the role of nickel during this process.

This work was done in collaboration with the Biology Department at the University of York as well as partners from Massey University (New Zealand).

6.2. Green Chemistry paper: Using in vivo nickel to direct pyrolysis of hyperaccumulator plant biomass

As a result of joint work together with the Biology Department at the University of York as well as partners from Massey University, it was possible to publish an article in the leading journal Green Chemistry.

<u>Aim</u>

This work was aimed at a detailed analysis of MW-assisted pyrolysis of various Ni-hyperaccumulators, which is a substantial part of the thesis because it covers pyrolysis of the real biomass in the presence of transition metals as a catalyst. Notably, the MW-assisted pyrolysis of Ni-hyperaccumulators was not previously reported. Therefore, this integrated chapter aims to highlight this phenomenon in detail, suggesting a mechanism of Ni-hyperaccumulators behaviour during MW-assisted thermal activation.

Objectives

The main objective of this study was to investigate the mechanism of MW-assisted pyrolysis of Ni-hyperaccumulators. The other objective was to study how the naturally occurring nickel influences the distribution of the chemicals in bio-oil.

Methodology

There were used different Ni-hyperaccumulators, containing different metals loading (0, 0.35 and 0.93wt%). Furthermore, a cross-experiment methodology was applied, and the Ni-free plant was artificially doped with appropriate nickel amounts (0.93wt% and 0.35wt%) to get a full comparison. The MW-assisted pyrolysis of the samples was done using MW Discover reactor at 300W. The measurements on the yield of biochar, bio-oil and gas were done following the developed procedure described in the supplementary material section. The analysis of the bio-oil was carried out using GC-FID.

Results

It was found that nickel in hyperaccumulator plant acts as a binder, changing the decomposition of hemicellulose during MW-assisted pyrolysis. This effect was detected from the mass-balance, which showed a low gas yield in the case of MW-assisted pyrolysis of all Ni-hyperaccumulation plants. This phenomenon substantially influences the distribution of the products in the bio-oil. The chemical composition of the bio-oil resulting from MW-pyrolysis of Ni-hyperaccumulators is more similar to the cellulose pattern compared to the control and artificially Ni-impregnated samples.

Conclusions

In conclusion, we have studied the MW-assisted pyrolysis of Ni-hyperaccumulating plants, revealing the role of nickel in this process. The effect of nickel as a binder for hemicellulose can be used for selective MW-activation of cellulose in hyperaccumulator plants, keeping the hemicellulose intact. The use of the Ni-hyperaccumulating plants to make chemicals and energy can add a significant attractiveness for the wider application of such plants for land remediation.

Green Chemistry paper

Doroshenko Alisa,[a] Vitaliy Budarin,[a] Robert McElroy,[a] Andrew J. Hunt, [b] Elizabeth Rylott,[c] Christopher Anderson,[d] Mark Waterland,[e] James Clark [a]*

a. Department of Chemistry, The University of York, Heslington, York, YO10 5DD, United Kingdom

b. Materials Chemistry Research Center, Department of Chemistry and Center of Excellence for Innovation in Chemistry, Faculty of Science, Khon Kaen University, Khon Kaen, 40002, Thailand

c. Department of Biology, The University of York, Heslington, York, YO10 5DD, United Kingdom

d. School of Agriculture and Environment, Massey University,Auckland, New Zealand

e. Institute of Fundamental Science, Massey University, Auckland, New Zealand Electronic

*Corresponding author: james.clark@york.ac.uk

6.2.1. Abstract

The effects of naturally occurring nickel in hyperaccumulator plants used for phytoremediation of contaminated soils on the microwave (MW) biomass pyrolysis is described for the first time. The presence of natural nickel appears to protect the hemicellulose component of the plant leading to 3 times lower yields of bio-gas and increased quantities of bio-char. The composition of the bio-oil is also affected.

6.2.2. Introduction

Large areas of land in many parts of the world are unavailable for agriculture due to the presence of the high levels of metals within the soils. Although these areas are unsuitable for growing food crops, they are rarely considered for non-food applications, and this represents a missed opportunity for biorefineries which requires increasing land area to be dedicated to non-food energy or chemical crops.(*273, 274*) While some soils naturally contain high levels of potentially toxic elements, including heavy metals, significant contamination has occurred from anthropogenic activities, such industrial land use, mine tailings, wastes disposal, pesticides, irrigation of wastewater, spillage of petrochemicals, and others.(*274*) Heavy metals represent an ill-defined group of hazardous inorganic chemicals, and those most commonly found include lead, chromium, arsenic, nickel. Land pollution with heavy metals is a long-term problem because the majority of these elements do not undergo microbial or chemical degradation unlike organics.(*275*)

One of a number of ways to clean-up contaminated land is phytoremediation, the use of plants to detoxify the environment. This method is relatively simple, can be cost-effective, and presents the opportunity to restore the local ecology.(*276*) Moreover, the use of plants to remediate polluted land presents an aesthetically pleasing approach with high public acceptance. One facet of this technique is the use of hyperaccumulator plants to take

up heavy metals. These species naturally accumulate specific metals to concentrations in their tissues that can be many thousand-role higher than the surrounding soil.(*277*, *278*) When the biomass of these plants is harvested to recover the metals, this process is called phytomining.(*276*)

Phytomining by hyperaccumulators has the potential to allow economic exploitation of low-grade surface ores or metal-contaminated soils. The final product could be both recovered metal and remediated land suitable for agriculture. A number of publications have highlighted the economic potential of phytomining,(*111*, *279*) with this technology mainly developed for nickel-contaminated soils.(*280*) Nickel has a relatively high market price compared to many other metals. Moreover, there are many countries, such as Australia, Canada, Italy, Russia, Brazil, and Turkey that contain large areas of low-grade, surface Ni ore. Currently, these nickel-contaminated lands are mostly left unused.(*280*)

An essential step in phytomining is the use of Ni – hyperaccumulators for metal recovery, but this metal-containing biomass can itself be converted to valuable products as part of a holistic biorefinery.(*281*) One pathway to recover the metal from such plants involves their thermal treatment to produce catalysts for use in organic chemistry,(*282*, *283*) metal or its salts.(*284*, *285*)

Several reported studies have focused on the catalytic effect of different transition metals on the thermal conversion of plant biomass to platform chemicals.(*109*, *110*) Nickel is considered to be one of the more promising metals for this because of its complex oxidation chemistry that involves the accessibility of different oxidation states and its ability to activate unsaturated organic molecules.(*112*) Impregnated nickel has been reported to reduce the coke deposition on the surface of some catalysts and increase the yields of syngas and aromatic hydrocarbons in some reductive conversions of biomass.(*113*, *286*) The Ni-impregnated catalysts demonstrated good thermal stability and reduced oxygenate breakthrough.(*286*) Extrapolating from this result, it is likely that the catalytic activity of naturally accrued nickel in plant hyperaccumulators could improve biomass valorisation processes (see Figure 1A). To our knowledge, the production of value-added products in the further processing of Ni-hyperaccumulators has not yet been studied.

Use of microwave-assisted pyrolysis as an energy-efficient, and more controlled, way of converting biomass to chemicals has recently been reported(*287*, *288*). Microwave (MW) heating has a number of advantages over conventional types of heating, including the selective activation of the principal components of the biomass.(*289*, *290*) Herein, the

initial results studying the effect of hyperaccumulated nickel on biomass pyrolysis using microwave activation have been reported.

Sample	Nickel contrent, wt%	Water contrent, wt%	Ash residue, wt%
Stackhousia tryonii	0.93	5.3	4.2
Alyssum bertolonii	0.35	6.1	4.6
Stackhousia Control	0	5.0	3.8
Alyssum Control	0	5.1	3.7
Ni-modified *Stackhousia* Control	0.93	6.5	4.4
Ni-modified *Alyssum* Control	0.35	6.8	4.6
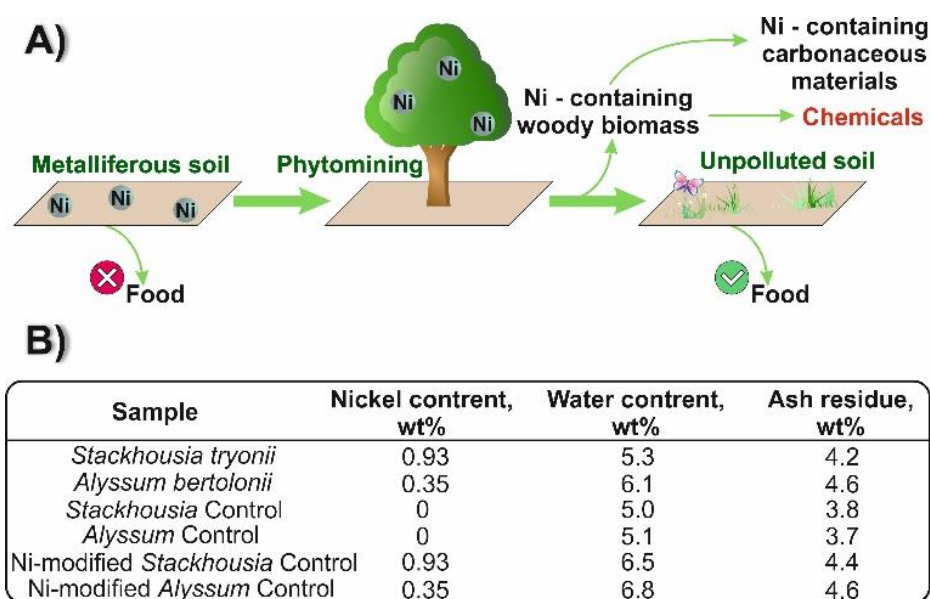
Fig. 1. The concept of the work and characterisation of the ground leaf materials used in this study

6.2.3. Experiment and methodology

The role of nickel in the MW-assisted pyrolysis of biomass, including its structural components both using classically impregnated and naturally accrued metal has been investigated. Samples of the Ni- hyperaccumulator plant species, *Stackhousia tryonii* were field collected from natural populations growing on nickel-rich soils in Queensland, Australia, while samples of the hyperaccumulator *Alyssum bertolonii*, were provided from plants growing on nickel-rich soil under controlled growth conditions by the University of Queensland in Brisbane, Australia. These hyperaccumulator species have evolved to grow on nickel-rich soils, and are difficult to cultivate in nickel-poor soils. All land plants require trace quantities of nickel as an essential element for growth, so providing nickel-free plant biomass is not possible, therefore, as controls, non-hyperaccumlator species sweet alyssum (*Alyssum maritimum*) and *Lobelia sp.* purchased from a commercial garden centre in New Zealand were chosen for this study. In the current work, *Alyssum maritimum* and *Lobelia sp.* are coded as *Alyssum* Control and *Stackhousia* Control respectively.

Firstly, the MW pyrolysis on ground leaf tissues from the hyperaccumulator species was compared with the control plants. Ground leaf materials from these control samples were then impregnated with Ni, using 0.1 M $NiCl_2 \cdot 6H_2O$ aqueous solution to achieve final nickel concentrations equivalent to the those in the hyperaccumulator species - 0.93 and 0.35wt% for

Stackhousia and *Alyssum* respectively. Water and ash residue contents were measured using STA-625 under nitrogen and oxygen atmospheres, respectively (10 Kmin^{-1}). Nickel content determined using Microwave Plasma Atomic Emission Spectroscopy (see Figure 1B). The nickel content between the two hyperaccumulators was significantly different. The higher ash contents of the two Ni-hyperaccumulators could be due to the presence of nickel oxide and increased level of the charring reactions. Nickel may catalyse the condensation of organic products of biomass depolymerisation to produce graphitic species that survive the STA-heating (to 625 °C).

Microwave-assisted pyrolysis was conducted at dynamic power mode, on a CEM Discover, equipped with 10 ml closed vial. The target temperature was 280 °C. The extraction of bio-oil was carried out using acetone; centrifuged, decanted, filtrated. GC-MS and GC-FID analysis was performed (see ESI).

6.2.4. Results and discussion

The mass balances from the microwave-assisted pyrolysis experiments are shown in Figure 2A. To better understand the nickel role in the MW pyrolysis, we extended the range of the natural Ni-containing plants including two tropical hyperaccumulator tree species *Phyllanthus balgooyi* collected from field populations growing on nickel laterite soils in Sulawesi, Indonesia, and *Rinorea bengalensis* collected from field populations growing on nickel laterite soils in Malaysia (leaf tissues contained 3.19 and 0.81wt% of nickel respectively). The MW-assisted pyrolysis of ground leaf material from these hyperaccumulator species resulted in substantially lower yields of biogas than control samples (including artificially impregnated). Furthermore, samples from all four of the hyperaccumulator species showed the same product distribution pattern (different from control) clearly demonstrating that naturally accumulated nickel has a fundamentally different effect on biomass pyrolysis to artificially impregnated. It is also interesting to note that artificially impregnated samples gave significantly increased yields of bio-oils, which is not observed with samples from the hyperaccumlators.

The influence of nickel on MW-pyrolysis of the plant materials can also be observed in the different temperature profiles of the microwave experiments (Figure 2B). For the samples from the hyperaccumulator plants, the heating rate at around 160 °C was significantly reduced in comparison with the control plants. It has been recently shown that this temperature corresponds to the activation of hemicellulose.[291] Remarkable, the amount of hemicellulose for the Ni-hyperaccumulators and their controls before the MW-assisted pyrolysis were similar (see ESI) and the heating rate intensities at 160 °C were expected to be similar as well (figure 2B). It is possible that the presence of nickel inhibits

131

the decomposition of hemicellulose. The presence of substantial amounts of hemicellulose in the leaf material from the hyperaccumulator species after microwave-assisted pyrolysis was confirmed by ATR-FTIR (evident from the strong carboxyl stretching bands). This inhibition could also explain the reduction of gas production (Figure 2A) since it is well-known that the main gas production in biomass pyrolysis is as a result of decomposition of glucuronic/galactonic acid present in hemicellulose.[292] Nickel has a high affinity for oxygen and nitrogen centres as ligands.[293, 294] Moreover, the Ni-like metals tend to be accumulated in the hemicellulose part of the plant.[295] Thus nickel could be acting as a stabiliser in hemicellulose, preventing its decomposition. This stabilisation effect is not seen with the artificially impregnated control plants and could be due to the accumulation of the metal on the biomass surface, rather than its incorporation within the plant biomass. Thus the artificial addition of nickel to plant biomass does not affect the temperature profiles on microwave heating and gives the yields of biogas same to the control samples. There was no evidence of any significant amounts of residual hemicellulose in artificially modified Ni materials (Figure 2C).
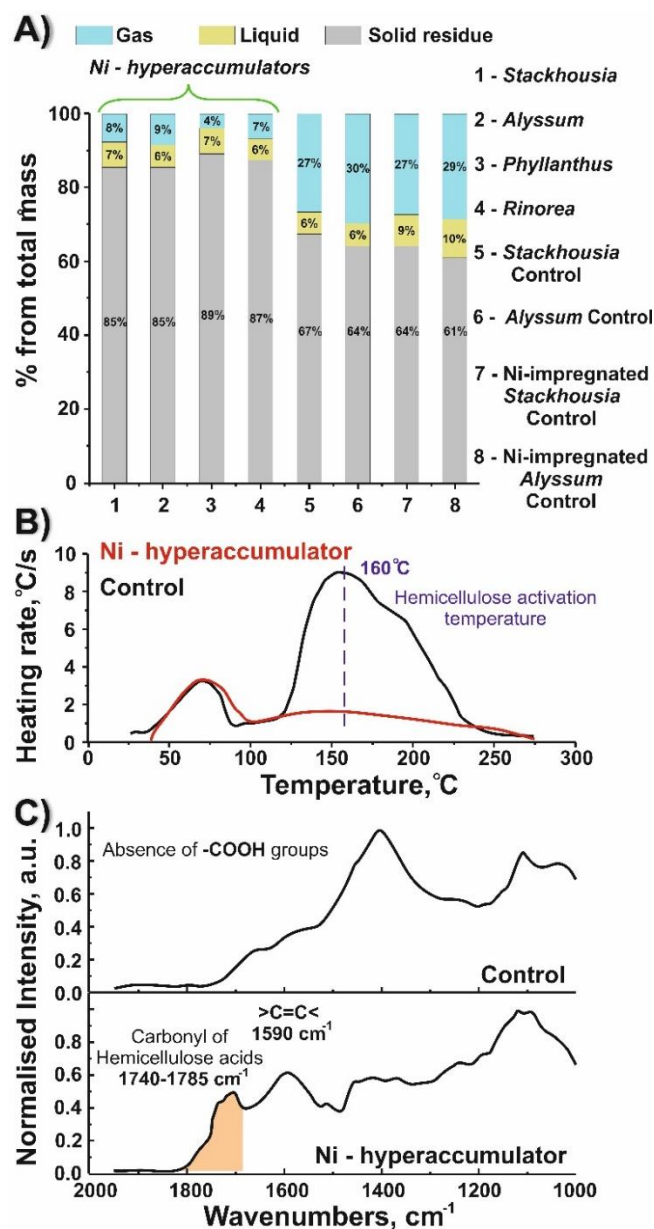
Fig. 2. A) Mass balance for all the samples; B) MW traces; C) ATR-FTIR spectra of the Ni-hyperaccumulator and its control

Interestingly, the presence of nickel in the hyperaccumulator species does not influence the pyrolysis of plants using conventional heating. The deconvolution of the DTGs shows no changes in the decomposition order, giving a natural one(*296*): hemicellulose → cellulose → lignin (see ESI). This suggests that the inhibition effect of the metal on hemicellulose decomposition is related to the dielectric properties of materials. It is recognised that the efficiency of the interaction of microwaves with matter depends on both the polarity of the molecule or functional groups and their ability to rotate. Typically, molecules involved in intense physical and chemical interactions do not interact with microwave as they are not free to rotate. This unique selectivity interaction of nickel with

hemicellulose makes it stable in the presence of MW and can be used to activate the cellulose before the hemicellulose – the opposite of what is expected (see Figure 3).
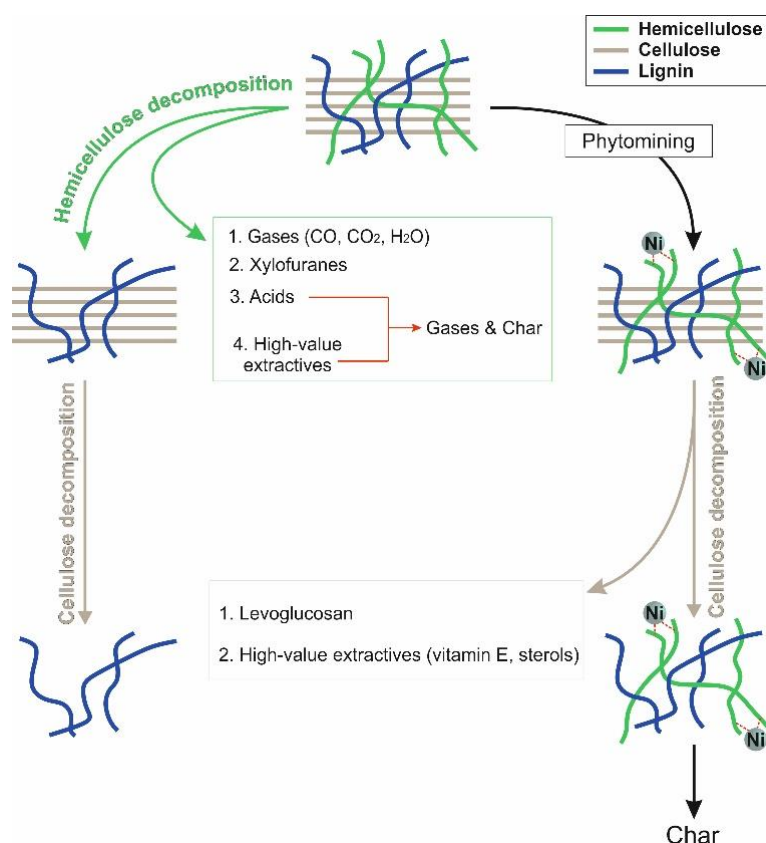
Fig. 3. Proposed role of naturally accrued nickel found in hyperaccumulator species during microwave-assisted pyrolysis

The nickel in hyperaccumulator plants also affected the bio-oils composition significantly increasing production of nitrogen-containing compounds such as triacetoamine (see Figure 4) which are known products of biomass pyrolysis.(*297*) The CHN analysis of the bio-oil has also demonstrated that nitrogen is present showing an overall composition profile of 49.3% of carbon, 8.8% of hydrogen and 8.3% of nitrogen. The bio-oil from the microwave-assisted pyrolysis of the Ni- hyperaccumulator-derived samples showed significant quantities of levoglucosan resulting from the cellulose in the plants**.** Alternatively, the quantities of extractives such as sterols and vitamins were significantly reduced in the samples from the Ni-hyperaccumulators, possibly as a result of the catalytic effect of acids produced from hemicellulose on the pyrolysis chemistry.
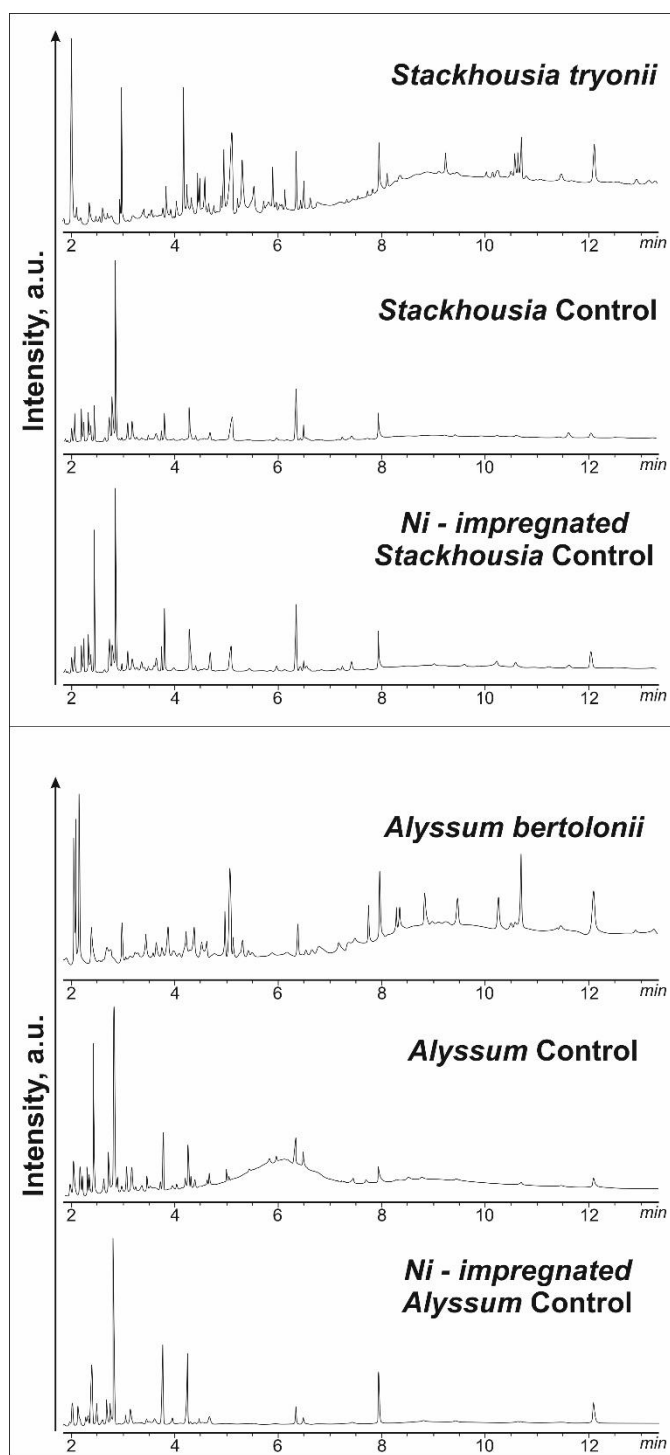
Fig. 4. GC-FID spectra of all the investigated samples

6.3.5. Conclusions

By studying the effects of naturally accumulated nickel on the pyrolysis behaviour of the host plants, we have demonstrated both an interesting inhibitory effect of the metal on parts of the plant biomass decomposition and a surprising microwave-specific effect. Compared to leaf material from low nickel, non-hyperaccumulator species and artificially impregnated plant biomass, the naturally accumulated Ni-rich biomass from hyperaccumulator species offer very

different product distributions with unusually high bio-char yields and different, more cellulose-derived chemical products. Thus the phenomenon may be exploitable in both maximising the energy value of biomass (by co-firing with coal) and the more selective production of cellulose-derived essential platform chemical products. The use of hyperaccumulator plants to make chemicals and energy can significantly add to the economic attractiveness of using these species to remediate nickel contaminated land, or in the alternative land use of metalliferous soil that is poorly suited to food crop production. We believe our research also opens the door to further application of metals-doped plant to control thermochemical biomass valorisation.

6.3.6. Conflict of interest

There are no conflicts to declare.

6.3.7. Acknowledgements

6.3.8. Contributions

The contributions of the authors:

Alisa Doroshenko has conducted and analyzed all of the experiments. Elizabeth Rylott has prepared the Ni-free control samples. Alisa Doroshenko, Vitaliy Budarin and James Clark have developed the mechanistic understanding of the MW-pyrolysis of Ni-hyperaccumulators. All authors have discussed the manuscript during the supervision meetings. Alisa Doroshenko has prepared all the figures. Alisa Doroshenko, Vitaliy Budarin were involved in a draft manuscript preparation, and all authors were involved in the further development of the final version of the article.

The supplementary to this paper is available at appendix 2 of the thesis.

6.3.9. A coherent body of the work

The presented article describes an original contribution to the pyrolysis science, particularly on the MW-assisted pyrolysis of Ni-hyperaccumulating plants, which was not previously investigated. Detailed analysis of the role of naturally incorporated nickel was studied using various techniques, showing its influence on the yield of valuable chemicals. Therefore, the presented article and this integrated chapter are complementing the title of the thesis: "Catalytic Thermal Conversion of Biomass Towards Valuable Chemicals".

CHAPTER 7. MATERIALS AND METHODS

7.1. Materials

The majority of the materials were purchased from various chemical suppliers (Table 19).

Given that 1,4:3,6-dianhydro-α-D-glucopyranose (DGP) is not commercially available, its synthesis and isolation of was carried out following the Shafizadeh procedure.(*18*) The relevant GC-MS spectrum is displayed in Figure 90 (with the corresponding fragmentation patterns for the sample (top) and library reference (bottom) being inset therein).

Table 19. Chemicals (and their respective suppliers) used in the present work

Chemical	Supplier
MC Cellulose	Sigma-Aldrich
Calcium oxalate	Sigma-Aldrich
Formaldehyde	Merck
Formic acid	Fisher Scientific
Acetaldehyde	Sigma-Aldrich
Glyoxal	Sigma-Aldrich
Acetic acid	Honeywell Fluka
Acrolein	Restek
Hydroxyacetone	Sigma-Aldrich
Furan	Sigma-Aldrich
Crotonaldehyde	Sigma-Aldrich
2,3-butanedione	Sigma-Aldrich
Furfural	Sigma-Aldrich
5-hydroxymethylfurfural	Sigma-Aldrich
Levoglucosenone	Circa LTD
Levoglucosan	Carbosynth
Methanol	Sigma-Aldrich
Ethanol	Sigma-Aldrich
Acetone	Sigma-Aldrich
$AlCl_3$	Sigma-Aldrich
NaCl	Sigma-Aldrich
KCl	Sigma-Aldrich
LiCl	Sigma-Aldrich
$MgCl_2$	Sigma-Aldrich
$CaCl_2$	Sigma-Aldrich
$BaCl_2$	Sigma-Aldrich
Pyridide	Fisher Scientific
Bentonite	Alfa Aesar
ZSM-5	Fisher Scientific

Kaolinite	Alfa Aesar
NaOH	Fisher Scientific
H_2SO_4	Honeywell Fluka
H_3PO_4	Honeywell Fluka
HCl	Honeywell Fluka
$Ca(OH)_2$	Fisher Scientific
Glucose	Sigma-Aldrich
Fructose	Sigma-Aldrich
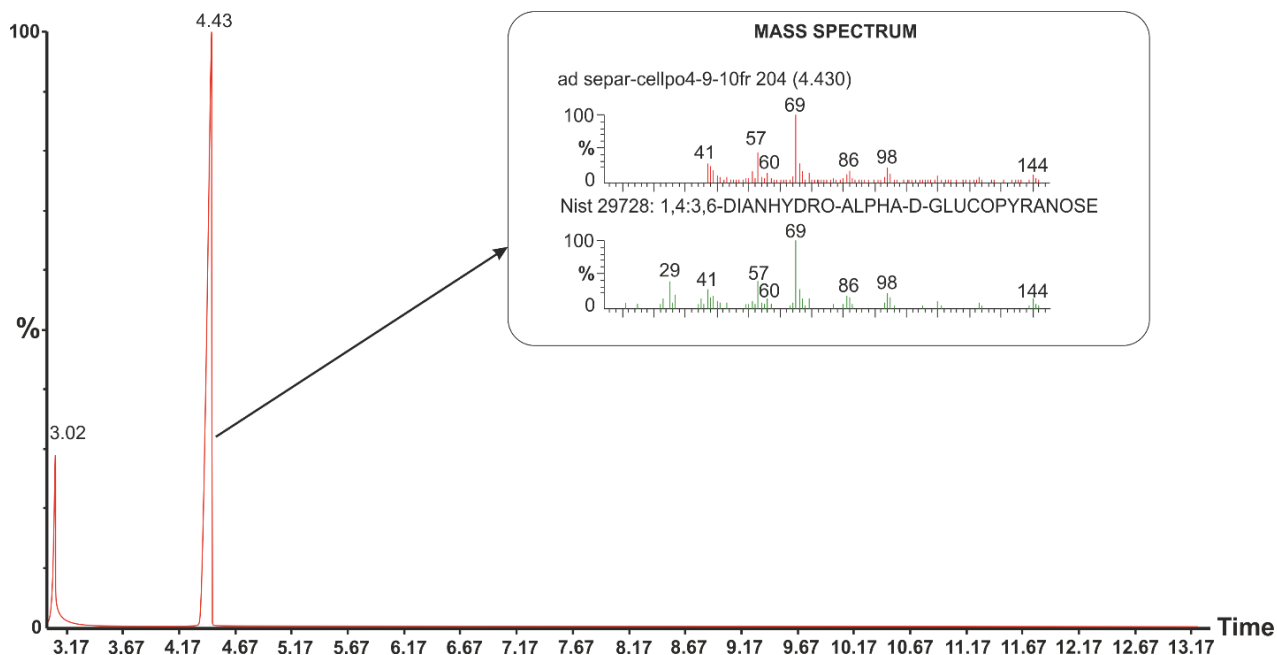
Figure 90. GC-MS spectrum of DGP synthesized and isolated via the Shafizadeh procedure

7.2. Equipment & Methods

TG-FTIR setup

The TG-FTIR scheme is displayed in Figure 91. The equipment consists of a Netzsch STA 409 linked to a Bruker Equinox 55 via a heated transfer-pipe. The products evolved during pyrolysis in the STA are carried over to the FTIR gas cell in a flow of nitrogen. The FTIR detector records the spectra of the evolved gas in real time from the start of the reaction to its end. To prevent the condensation of the evolved gas, the temperatures of the adapter, transfer-pipe and FTIR cell are maintained at 160 °C, 180 °C and 200 °C respectively. The FTIR cell is 'double glazed' with KBr and ZnSe windows, again to prevent condensation. A liquid nitrogen was used for cooling MCT detector for the speed of data collection giving enhanced time resolution.
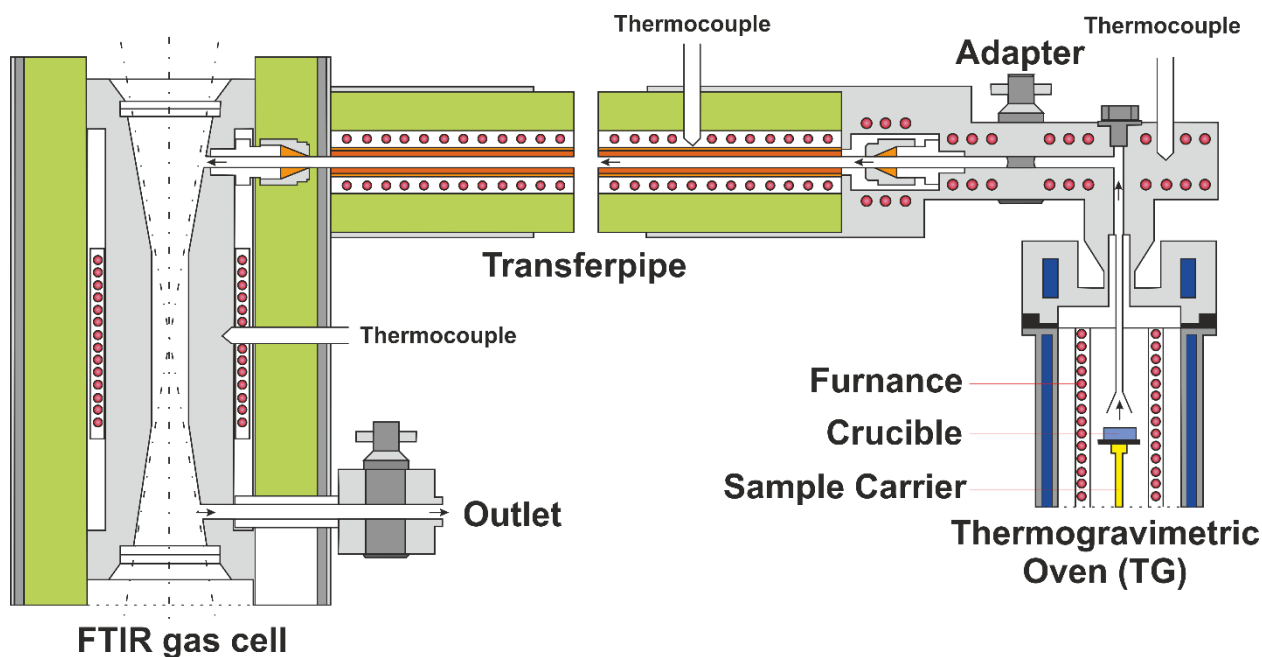
Figure 91. Scheme of the TG-FTIR setup

TG-FTIR experiment

The sample in the amount of 50±2 mg was placed into the thermostable and chemically inert ceramic crucible. The crucible was located on the sample carrier (stand) connected to balances. When the sample is placed into the oven, the vacuum pump was making the pressure about 5 mbar in the system. In the current experiment, it was used nitrogen as a carrier gas. The oven is filled with nitrogen gas to get atmospheric pressure. The vacuum procedure is repeated three times to remove all oxygen from the system. At the last run, the oven filled with nitrogen gas was opened by means of adapter switcher. The flux of nitrogen at 300ml/min rate was passed via the transfer-pipe and FTIR cell for 40 mins to remove oxygen molecules from the system. Meanwhile, the FTIR detector is cooled with liquid nitrogen. Then the nitrogen gas flow was established at 100ml/min, and the background is recorded. The background was collected on 128 scans at a 4 cm^{-1} resolution for a 550-4000 cm^{-1} range. The temperature intervals were from $T_{start}=$ 23 °C to $T_{final}=$ 500 °C. The MCT detector records the evolved pyro-gas spectra in real-time averaging 32 scans for heating rates below 35Kmin^{-1} or 16 scans for heating rates above 35 Kmin^{-1} at the resolution of 4 cm^{-1} and 550-4000 cm^{-1} range of wavenumbers. Each spectrum was automatically associated with the spectra collection starting and finishing times. These times are matching to the thermal regime to understand what an average sample temperature should be assigned with the relevant spectrum.

TG-FTIR quantification procedure

The TG-FTIR run of each standard sample was carried out in order to calculate the absorption coefficient using the correlation between the integrated FTIR signal and the dTG data. Deconvolution of the cellulose-evolved gas spectrum using the spectra of the standards provides quantitative data on the evolved product composition generated at a certain time or temperature. Application of this analytical method to all the FTIR spectra obtained during the TG-FTIR experiment gives a kinetic trace (product concentration vs. time) of each volatile component. The kinetic traces were integrated giving the yield of the products. The sum of all identified products is close to 97% showing the high-quality of the applied analysis.

Moreover, the developed approach was further verified by two independent procedures. Firstly, the sum of the obtained kinetic curves was compared with the experimental dTG trace. Finally, the C:H:O balance for the pyrolysis system which includes the solid residue and all the volatiles was calculated for different cellulose decomposition temperatures. The elemental C:H:O composition of the evolved gas mixture at any temperature can be calculated from the mole fraction of each volatile ($C_xH_yO_z$) and the x,y,z index for the relevant C, H, O element.

Bio-oil collection and analysis

A) Conventional reaction

The collection of bio-oil was happened by the means of Netzsch STA 409 (TG part of the TG-FTIR), which was slightly modified whereby an adapter was used to connect it to a liquid nitrogen cooled trap (Figure 92). The hot pyro-gas is rapidly cooled down and condensed inside the trap. The carrier gas (nitrogen) can pass via the trap to prevent overpressure in the system. After pyrolysis, the trap is rapidly washed with acetone and the washings collected and subsequently stored within a tightly sealed vial.

B) Microwave reactor

The Microwave reactor was connected with a modified adapter to connect it to a liquid nitrogen cooled trap. The hot pyro-gas is rapidly cooled down and condensed inside the trap. After pyrolysis, the trap is rapidly washed with acetone and the washings collected and subsequently stored within a tightly sealed vial.

Mass-balance

The mass-balance measurments were done following knowing procedures.

The amount of gas in the case of MW-assisted pyrolysis was done by measuring masses of the sample together with the vial before and after pyrolysis The procedure for the measuring of bio-

oil was: 1) extraction of the bio-oil with known voluemt of acetone; 2) an aliquot of 10 ml was placed on a Petri plate (weighted in advance); 3) evaporation; 4) Petri plate was weighted together with the organic residue. The amount of solid residue was calculated as 100wt% minus amount of gas and bio-oil.

In the case of conventional heating, the amount of char was measured using real-time TG estimation.
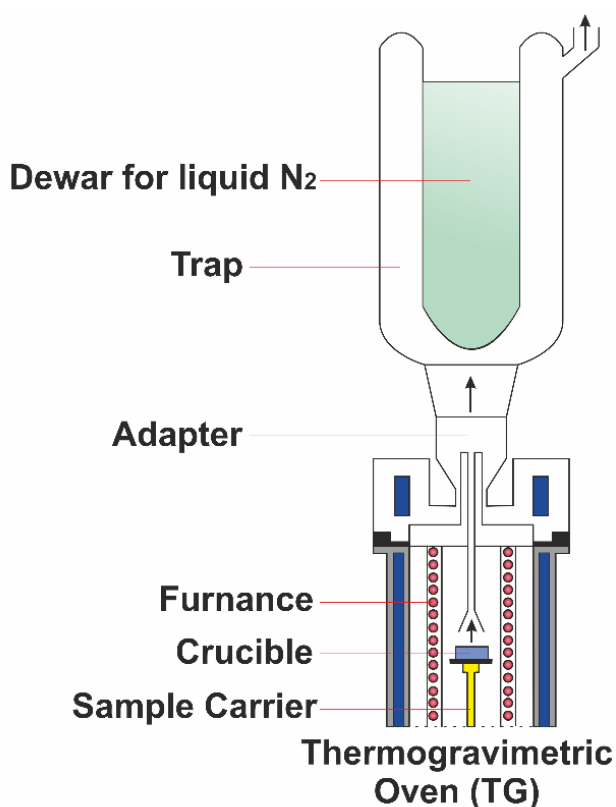
Figure 92. Cold-trap experimental setup (adjusted to the TG part of the TG-FTIR)

Gas Chromatography – Mass Spectrometry (GC-MS)

The GC-MS analysis was carried out on a Perkin Elmer Clarus 500 GC with a Perkin Elmer Clarus 560S Mass Spectrometer using a Rxi-5HT column (30 m, 0.25 mm, 0.25 µm). The gas chromatography program ramps from 50 °C to 300 °C at 30 Kmin^{-1} followed by a hold at 300 °C for 5 mins and uses a split ratio of 5:1. The GC-MS was used only for qualitative analysis of the bio-oil components.

Gas Chromatography-Flame Ionisation Detector (GF-FID)

The GC-FID analysis was done on an Agilent equipment using a Rxi-5HT column (30 m, 0.25 mm, 0.25 µm). The gas chromatography program ramps from 50 °C to 300 °C at 30 Kmin^{-1} followed

by a hold at 300 °C for 5 mins and uses a split ratio of 5:1. The GC-FID analysis was used for the quantitative analysis of furfural, LGO, 5-HMF and LGA components based on the method of internal standards.

Thermogravimetric analysis

The thermal analysis was performed in N_2 (or air) flow conditions ($60 ml min^{-1}$) using Stanton Redcroft STA625 Thermal Analysis at the temperature range between ambient and 500°C and heating rate of $10°C min^{-1}$. The mass of the samples for the analysis was 10mg accurately.

SAXS and thermally-resolved SAXS analysis

Small angle X-ray diffraction was performed using a Bruker D8 Discover equipped with a temperature controlled, bored graphite rod furnace, custom built at the University of York. Samples were filled into 1 mm o/d glass capillaries. The radiation source was microfocus source using CuKα radiation λ = 1.5406 Å which was trimmed using a 1 mm circular slot and 0.5 mm collimator. Diffraction patterns were collected between 110 and 3.9 Å. The calibration of the instrument was done using Silver Behenate.

N_2 adsorption analysis

Nitrogen physisorption was carried out using an ASAP 2020 equipment, with measurements performed at 77 K. The catalysts (20mg) were degassed under vacuum at 40 °C and 130 °C respectively for 6 h prior to analysis. The Brunauer–Emmett–Teller (BET) methodology was used to determine the surface area, with a minimum of 5 data points used over a relative pressure range of (P/P_0) 0.05–0.30, maintaining a linear relationship and an $R^2 \geq 0.995$.

Synthesis of Al-pillared bentonite

Following the diagram of Al^{3+} forms distribution depending on the pH, the necessary volume of 0.1M NaOH was slowly added to $AlCl_3$ by drops until the ratio of 2.5 between OH- and Al^{3+} at intensive magnetic stirring. The final pH of the solution was 4.8, indicating of acceptable region for existence of Al_{13} heteropoly acid polynuclear hydroxo-complexes.

The bentonite was swollen in water at intensive stirring for 24 hours. The intercalation process involved by-drops adding of the synthesized Al_{13} complex solution to the swollen bentonite at magnetic stirring. The agglomeration of the colloidal particles proceeded in 1 hour. The deposited sample was filtrated and washed from the excess of Cl^- anions, that was checked by adding Ag^+ solution to the filtrate. The catalyst was thermally treated at 250°C for 5 hours.

The repeatability and reproducibility of the Al_{13}-pillared clays were studied by many authors. The main problem is that any materials obtained on the basis of natural minerals (which very often have different chemical composition and structure) will have different chemical and physical features. However, if the pillaring process is repeated using the same clay, then repeatability depends only on accuracy of the synthesis. Therefore, we have accurately performed the synthesis of Al-pillared clays for three times and studied them using SAXS analysis.

Temperature-resolved DRIFT (Diffuse Reflectance Infrared Fourier Transform) spectroscopy for pyridine titration

The catalysts were taken in the amount of 100 mg and soaked in pyridine at petri dish for 24 hours followed by drying at 120 °C during 30 mins. Then each sample was mixed with KBr (fresh grinded, optical purity) in an agate mortar for 20 mins at a ratio of 1:50.

The FTIR spectra were recorded using Bruker Equinox 55 FT-IR.

Pure KBr was recorded as a background at a set of different temperatures (120 °C, 250 °C and 400 °C) in a special heating cell quipped with a vacuum pump and water flow (at the frame) to prevent the overheating (Figure 93). The KBr was vacuumed and the background was recorded at 2 cm^{-1} resolution in 550-4000 cm^{-1} and 128 scans for each temperature. The same procedure was repeated for each sample.
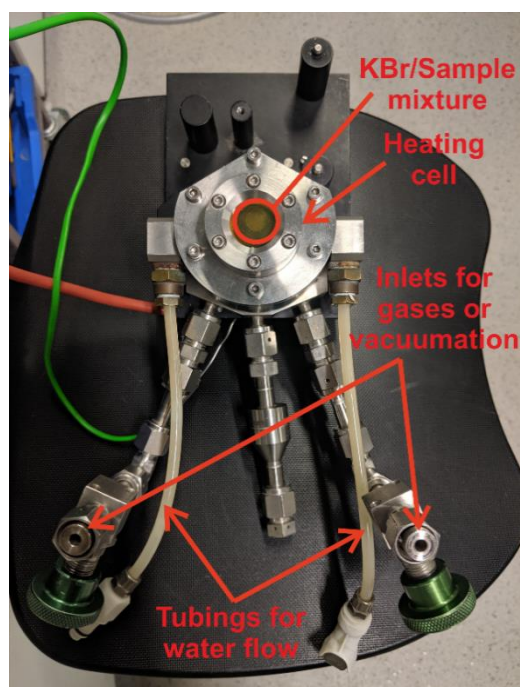
Figure 93. The Diffuse Reflectance Infrared Fourier Transform cell used for pyridine titration

Temperature-Programmed Desorption of ammonia (TPD of ammonia)

The quantification of the acid sites was done using ammonia TPD technique.

The samples were treated under vacuum for 24h at 150 °C. Afterwards, the ammonia gas was injected (Figure 94) to keep the reactor overpressure for 3 hours. Then, the temperature was slowly decreased to the ambient conditions.

The TPD of ammonia were using thermogravimetry coupled with Fourier Transformed Infrared spectrometer (TG-FTIR).

 The background is collected in advance in N_2 flow at 100 mlmin^{-1}, 128 scans at 4 cm^{-1} resolution in the range 550-4000 cm^{-1}. The samples (501.3 mg of Al-PILC and 594.1 mg of bentonite) were placed into a thermally and chemically inert ceramic crucible which is positioned on a sample carrier linked to a microbalance. The system is then sealed before blowing with nitrogen (300 mlmin^{-1}) at 50 °C for 30 mins to remove an excess of physiosorbed ammonia. The nitrogen gas flow is then established at 100ml/min. The catalysts samples were heated at 10 Kmin^{-1} heating rate from Tstart= 23 °C to Tfinal= 800 °C. The MCT detector records the evolved gas spectra in real-time averaging 32 scans. After taking into account both the start and end time in addition to the heating and data collection rates, an average temperature can then be assigned to each collected spectrum.

Figure 94. The set-up for ammonia adsorption on the catalysts surface

MW-assisted pyrolysis

The microwave assisted pyrolysis was carried out in CEM Discover MW reactor (Figure 95). The experiments were done in a fixed power mode (300W) to reach the target temperature of 280 °C. The pressure limitations were set up to 300 PSI. The vessel volume was 35ml.

An infrared temperature detector at the bottom of the vessel allows us to monitor MW pyrolysis temperature in time.
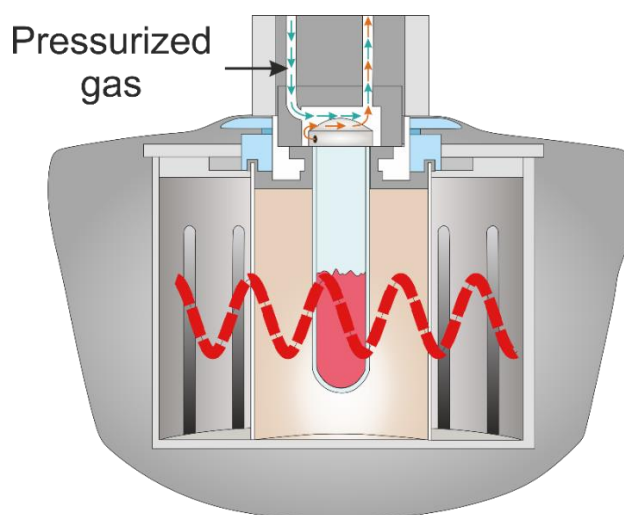
Figure 95. The scheme of the MW reactor (CEM Discover)

MW-assisted hydrolysis

The microwave assisted hydrolysis was carried out in CEM Discover MW reactor. The experiments were done in a dynamic power mode with the established MW power limit of 300 W. The target temperature was 170 °C, which was maintained for 15 mins. The pressure limitations were set up to 300 PSI. The vessel volume was 35 ml. The sample (3 g) was mixed with 20 ml of water, containing H_2SO_4 to reach the pH of 4.8.

High-performance Liquid-Chromatography (HPLC)

The Agilent Technologies 1260 Infinity II was used for HPLC analysis, using Hi PLEX H Column at 60 °C. The mobile phase was consisting of 0.005M H_2SO_4 and the flow rate was established at 0.4 mlmin^{-1}. Low- and high-pressure limits were 0 and 40 bars. The draw and eject speeds were set up to 200.0 µLmin^{-1} and 400.0 µLmin^{-1} respectively. The wait time after draw was 1.2 s. The injection volume was 5.00 µL. The quantification of the acetic acid, lactic acid, glucose, xylose, levoglucosan, levulinic acid and 5-HMF was done using the method of internal standards.

Attenuated Total Reflectance-FTIR (ATR-FTIR)

145

The FTIR spectra were recorded at Perkin Elmer Spectrum 400. The measured wavenumbers range was 650-4000 cm^{-1} with a step of 4 cm^{-1}. The number of collected scans was 32 in an adsorption mode for all experiments.

CHAPTER 8. CONCLUSIONS AND PERSPECTIVES

8.1 Conclusions

This research aimed to identify sustainable and practical strategies for selective biomass pyrolysis towards valuable chemicals. Based on a detailed kinetic analysis of cellulose and starch thermal decomposition at the different experimental conditions, it could be concluded that lignocellulosic materials can be selectively and with substantial yield transformed to such platform molecules as LGO and 5-HMF. It was found that the best strategy of such pyrolysis-based biorefinery is to generate LGA vapour conducting conventional pyrolysis at a temperature higher than 360°C and in the presence of water. The heterogeneous acid catalyst should be designed to interact with LGA in the vapour phase. It was also found that the application of MW radiation reduces the optimum temperature of pyrolysis and increases the yield of LGO and its purity.

The main dissertation goal was accomplished based on the following achievements:

1. The analysis of research publications was carried out in the field of structure and chemical properties of biomass. The dissertation systematically analysed the number of mechanical models of cellulose pyrolysis discussed in the literature. Particular attention was paid to levoglucosan (anhydrosugar), which was identified as a possible primary cellulose pyrolysis product. The physical-chemical properties of levoglucosan, including its phase transition temperatures and possible chemical transformation, were considered. Levoglucosenone (product of catalytic decomposition of levoglucosan) due to its low-temperature boiling point and potential applications in the production of solvents and polymers was identified as a possible target chemical. It has been demonstrated that novel green technologies such as microwave and catalysis could play a significant role in pyrolysis increasing bio-oil yield and process selectivity.

2. The dissertation's significant outcome is developing a novel TG-FTIR approach for continuous quantitative measurement of off-gas concentration and pyrolysis kinetic. This analysis was based on the identification of 18 significant pyrolysis products and calibration of their FTIR spectra.

3. Based on obtained kinetic data, an improved "cluster" model of cellulose pyrolysis was proposed. The model predicts that strong intermolecular hydrogen bonding restricts cellulose polymers rearrangement needed for LGA production. The activation happens only when the one monomer cellulose unit from three is decomposed onto small molecules generating water and allowing the other two unites to rearrange to LGA. Therefore, the "cluster" model, predicts a maximum LGA yield as 66% and a temperature of cellulose activation higher than 360 °C.

4. The dissertation considered conventional *in-situ* catalytic LGA transformation to LGO in the presence of sulfuric acid. The direct mixing of acid and cellulose increases solid residue yield and, at the low loading, enhancing, the yield of LGO up to 7.7wt% at 3wt% of loading.

5. ZSM-5 were tested as a heterogeneous catalyst. A systematic study of the influence of the loading of aluminosilicates indicates sharp stepwise changes in the composition of volatile compounds. These step changes in the pyrolysis products are divided into five clear zones caused by different catalyst loadings. Changes in the catalyst concentration within each of these zones little affect the product mixture's composition. This phenomenon allows us to predict the chemical composition, obtained by a specific catalyst loading.

6. The thesis proves that a combination of MW-assisted cellulose pyrolysis with an acid catalyst (both liquid acids and heterogeneous) significantly improved (up to 30-35%) LGO content in the bio-oil. Clay hydrophobicity plays a substantial role in the MW pyrolysis controlling the content of HMF and LGO in the bio-oil. The water in the clay favours hydrolysis reactions and produces sugars converted on Lewis acid sites to 5-HMF. The Bronsted acid sites of Al-PILC promote the formation of 40% pure LGO at 6.3wt% yield at 50wt% of the catalyst loading. It was found that a combination of hydrophilic bentonite and hydrophobic kaolinite enhances the yield of LGO to 12.3wt%, with selectivity towards LGO three times higher than in conventional experiment.

7. The approaches developed for activation of cellulose pyrolysis were tested using another polysaccharide- starch. Starch was pyrolysed in the presence of *p*-toluenesulfonic acid (PTSA) which is the standard acid catalyst for the production of mesoporous materials Starbons®. The composition of off-gas produced during the acid-doped starch pyrolysis was investigated using a developed TG-FTIR technology to improve valorisation of starch-related wastes through Starbon® technology. It was shown that LGA is the primary product of starch non-catalytic pyrolysis. In the presence of an acid catalyst, starch produces a gas mixture which contains LGA as the primary compound. The yield of LGO passes a maximum depending on the heating rate, giving the highest amount of 7.99wt% at 30 Kmin^{-1}.

8. The dissertation also considered transition metals as catalysts for the pyrolysis of biomass investigating the effects of naturally accumulated nickel on the host plants' pyrolysis behaviour. The presence of nickel in biomass substantially changes the pyrolysis product distribution with unusually high bio-char yields and different, more cellulose-derived chemical products. Such an influence maximizes both the energy value of biomass and the production of cellulose-derived platform chemical products.

8.2   Relevance

The development of novel pyrolysis technology of biomass for controllable chemical production is a significant part of sustainable chemistry. Biomass-based pyrolysis is a source of carbon-neutral energy produced in biochar (it could substitute coal in power stations) and bio-oil (it could partly substitute diesel). The substantial increase of pyrolysis industry is essential for potentially reducing fossil fuel use and associated greenhouse gas (GHG) emissions which are in a good agreement with targets of such international treaties as the Kyoto Protocol and the Paris Agreement. These targets are well-represented in the national regulations. For example, in September 2020, the European Commission proposed to set the 2030 greenhouse gas emission reduction target to at least 55% compared to 1990. While, in June 2019, the British parliament passed legislation requiring the government to reduce the UK's net emissions of greenhouse gases by 100% relative to 1990 levels by 2050.

One of the critical challenges of current pyrolysis technology is low profitability due to competition with relatively low-price fossil fuels.   The methodology developed during the dissertation project shows that the novel pyrolysis concept opens an opportunity to produce valuable chemicals such as LGO, HMF and levulinic acid. The production of these chemicals could make the pyrolysis more profitable, increasing its robustness and independence from fossil fuel prices.

It is important to note that both LGO and HMF, are precursors of synthesis of 1,6-hexanediamine, caprolactone and caprolactam, which are used in multi-million tonne per year manufacturing processes for polyester, polyamide, and polyurethanes. The application of pyrolysis products in the production of bio-based plastics will significantly impact the circular economy. More than 95% of the world's plastic today is made from crude oil or natural gas, and therefore the plastics industry has been keen to get sustainable solutions. The most widely claimed benefit of bio-based plastic is to reduce a final product's carbon footprint, due to the sequestration of CO_2 during the life of the plant.

LGO could also make an impact in the circular economy as a precursor of biobased solvent Cyrene^{TM}. Cyrene^{TM} is a biobased dipolar, aprotic alternative for many solvents classified by REACH (regulation of the European Union, adopted to improve the protection of human health and the environment from the risks that can be posed by chemicals) and an increasing number of other national policies as Substances of Very High Concern (SVHC), such as N-

Methylpyrorrolidone (NMP) and Dimethylformamide (DMF). The renewable nature of the Cyrene^{TM} makes it particularly attractive, especially as regions such as the EU encourage a bio-based economy, including the production and use of chemicals from biomass.

8.3   Recommendations

Based on the obtained results and conclusion I think possible directions for further investigation could include:

• The clarification of the nature of cellulose nature (molecular weight, density, number of the defects) and how it influences pyrolysis kinetics. This study could shed more light on the first stage of pyrolysis and therefore raise the yield of LGA above the current 67%.

• The estimation of the role which volatiles play in the activation of cellulose pyrolysis. Primary data shows the possibility that acidic pyrolysis products play an essential role in the activation of cellulose along with water. The pyrolysis experiment in the presence of acetic and formic acids vapour would be interesting to carry out.

• The investigation of a possibility to produce LGA during cellulose pyrolysis in water-saturated atmosphere. The isolation of pure LGA could open an opportunity to develop LGA transformation to LGO using "wet" organic chemistry

• The development of a procedure to isolate hemicellulose applying MW heating for metal-hypeaccumulator plants.

• The scaling-up the catalytic thermal decomposition of cellulose. This experiment helps to estimate heat- and mass-balance of the process.

8.4   Perspectives

The in-depth study of the cellulose pyrolysis mechanism and the proposed new approaches to control secondary reactions of this process open up an avenues for promising research agenda across the biorefinery concept, specifically its thermochemical direction. Our proposed vision onto the cellulose thermal decomposition has perspectives in application to areas including:

• Cellulose activation. The cluster hypothesis can stimulate extensive research related to the influence of cellulose's nature on its thermal properties, specifically on its high temperature of pyrolysis. It can be primarily related to the study of the pyrolysis of cellulose with varying degrees of its amorphous nature and exploring the possibility of reducing the strength of the hydrogen bond between polymers using chemical and genetic methods.

• *In-situ* conversion of LGA. It has been shown that the LGA obtained as a primary product could be converted to valuable chemicals or platform molecules such as LGO, HMF and levulinic acid. The high catalytic activity of the clays in this conversion, their low-price and wide

available, as well as simplicity of regeneration, could attract researchers and industrialists. The strong dependency of catalysis efficiency on the cellulose/clay composition could guide the optimisation of catalytic systems.

• MW-assisted catalytic cellulose pyrolysis. The promising synergy between MW irradiation and the nature of the clay catalyst in cellulose pyrolysis needs detailed investigation. This could stimulate the study of MW interactions both with the inorganic clay framework and overheated water adsorbed in the clay pore, as well as the influence of water polarisation caused by cations on the MW clay activity.

• Industrial applications of the proposed approach. Exemplary effectivity and controllability of the proposed technology based on the use of a clay catalyst in conditions much milder than fast pyrolysis open an opportunity for industrial applications notably in the production of LGO as it moves to larger scale production over the next few years

Appendix 1. Supplementary of the ChemSusChem paper: Selective Microwave-assisted Pyrolysis of Cellulose towards Levoglucosenone using Clay Catalysts

<u>Experimental Procedures</u>

Materials

The sodium form of bentonite was purchased from Alfa Aesar. The base (NaOH), aluminum salt AlCl3•6H2O and microcrystalline cellulose were purchased from Sigma Aldrich.

Synthesis of Al-pillared bentonite

Following the diagram of Al^{3+} forms distribution depending on the pH (Figure S1), the necessary volume of 0.1M NaOH was slowly added to $AlCl_3$ by drops until the ratio of 2.5 between OH- and Al^{3+} at intensive magnetic stirring. The final pH of the solution was 4.8, indicating of acceptable region for existence of Al_{13} heteropoly acid polynuclear hydroxo-complexes (Figure S2).

The bentonite was swollen in water at intensive stirring for 24 hours. The intercalation process (Figure S3) involved by-drops adding of the synthesized Al_{13} complex solution to the swollen bentonite at magnetic stirring. The agglomeration of the colloidal particles proceeded in 1 hour. The deposited sample was filtrated and washed from the excess of Cl^- anions, that was checked by adding Ag^+ solution to the filtrate. The catalyst was thermally treated at 250 °C for 5 hours.

The repeatability and reproducibility of the Al_{13}-pillared clays were studied by many authors. The main problem is that any materials obtained on the basis of natural minerals (which very often have different chemical composition and structure) will have different chemical and physical features. However, if the pillaring process is repeated using the same clay, then repeatability depends only on accuracy of the synthesis. Therefore, we have accurately performed the synthesis of Al-pillared clays for three times and studied them using SAXS analysis.

SAXS and thermally-resolved SAXS analysis

Small angle X-ray diffraction was performed using a Bruker D8 Discover equipped with a temperature controlled, bored graphite rod furnace, custom built at the University of York. Samples were filled into 1 mm o/d glass capillaries. The radiation source was microfocus source using CuKα radiation λ = 1.5406 Å which was trimmed using a 1 mm circular slot and 0.5 mm collimator. Diffraction patterns were collected as a function of temperature using a Bruker Vantec 500 detector positioned on the goniometer to allow data to be collected between 110 and 3.9 Å. The instrument was calibrated using Silver Behenate. The data was processed using Bruker DIFFRAC.SUITE EVA software. Samples were acquired for 900 s per scan and equilibrated for 20 s at each temperature interval.

N₂ adsorption analysis

Nitrogen physisorption was carried out using an ASAP 2020 from Micrometrics, with measurements performed at 77 K. The catalysts (20mg) were degassed under vacuum at 40 °C and 130 °C respectively for 6 h prior to analysis. The Brunauer–Emmett–Teller (BET) methodology was used to determine the surface area, with a minimum of 5 data points used over a relative pressure range of (P/P₀) 0.05–0.30, maintaining a linear relationship and an $R^2 \geq 0.995$.

Thermal analysis

The thermal analysis was performed in N₂ flow conditions (60 mlmin⁻¹) using Stanton Redcroft STA625 Thermal Analysis at the temperature range between ambient and 500 °C and heating rate of 10 Kmin⁻¹. The mass of the samples for the analysis was 10 mg accurately.

Temperature-resolved DRIFT (Diffuse Reflectance Infrared Fourier Transform) spectroscopy for pyridine titration

The catalysts were taken in the amount of 100mg and soaked in pyridine at petri dish for 24 hours followed by drying at 120 °C during 30 mins. Then each sample was mixed with KBr (fresh grinded, optical purity) in an agate mortar for 20 mins at a ratio of 1:50.

The FTIR spectra were recorded using Bruker Equinox 55 FTIR equipped with a special cell (Figure 4S).

Pure KBr was recorded as a background at a set of different temperatures (120 °C, 250 °C and 400 °C) in a special heating cell quipped with a vacuum pump and water flow (at the frame) to prevent the overheating (Figure S4). The KBr was vacuumed and the background was recorded at 2 cm⁻¹ resolution in 550-4000 cm⁻¹ and 128 scans for each temperature. The same procedure was repeated for each sample.

Temperature-Programmed Desorption of ammonia (TPD of ammonia)

The quantification of the acid sites was done using ammonia TPD technique.

The samples were treated under deep vacuum for 24 h at 150 °C. Afterwards, the ammonia gas was injected (figure S5) to keep the reactor overpressure for 3 hours. Then, the temperature was slowly decreased to the ambient conditions.

The TPD of ammonia were using thermogravimetry coupled with Fourier Transformed Infrared spectrometer (TG-FTIR). The TG-FTIR scheme is displayed in figure S6. The equipment consists of a Netzsch STA 409 linked to a Bruker Equinox 55 via a heated transfer-pipe. The products evolved during pyrolysis in the STA are carried over to the FTIR gas cell in a flow of nitrogen. The FTIR detector records the spectra of the evolved gas in real time from the start of the reaction to its end. To prevent the condensation of the evolved gas, the temperatures of the adapter, transfer-pipe and FTIR cell are maintained at 160 °C, 180 °C and 200 °C respectively.

The FTIR cell is 'double glazed' with KBr and ZnSe windows, again to prevent condensation. We use a liquid nitrogen cooled MCT detector for the speed of data collection giving enhanced time resolution.

The background is collected in advance in N_2 flow at 100 mlmin^{-1}, 128 scans at 4 cm^{-1} resolution in the range 550-4000 cm^{-1}. The samples (501.3mg of Al-PILC and 594.1mg of bentonite) were placed into a thermally and chemically inert ceramic crucible which is positioned on a sample carrier linked to a microbalance. The system is then sealed before blowing with nitrogen (300 mlmin^{-1}) at 50 °C for 30 mins to remove an excess of physiosorbed ammonia. The nitrogen gas flow is then established at 100 mlmin^{-1}. The catalysts samples were heated at 10 Kmin^{-1} heating rate from Tstart= 23 °C to Tfinal= 800 °C. The MCT detector records the evolved gas spectra in real-time averaging 32 scans. After taking into account both the start and end time in addition to the heating and data collection rates, an average temperature can then be assigned to each collected spectrum.

The results in terms of temperature and time are present at the figure S9 and table S1 respectively.

MW-assisted pyrolysis

The microwave assisted pyrolysis was carried out in CEM Discover MW reactor (Figure S10). The experiments were done in a fixed power mode (300 W) to reach the target temperature of 280 °C. The pressure limitations were set up to 300 PSI. The vessel volume was 35 ml.

An infrared temperature detector at the bottom of the vessel allows us to monitor MW pyrolysis temperature in time.

MW-assisted pyrolysis

The microwave assisted hydrolysis was carried out in CEM Discover MW reactor (Figure S10). The experiments were done in a dynamic power mode with the established MW power limit of 300 W. The target temperature was 170 °C, which was maintained for 15 mins. The pressure limitations were set up to 300PSI. The vessel volume was 35 ml. The sample (3 g) was mixed with 20 ml of water, containing H_2SO_4 to reach the pH of 4.8.

Gas Chromatography – Mass Spectrometry (GC-MS)

The bio-oil obtained in acetone was submitted for GC-MS analysis on a Perkin Elmer Clarus 500 GC with a Perkin Elmer Clarus 560S Mass Spectrometer using a Rxi-5HT column. The gas chromatography program ramps from 50 °C to 300 °C at 30 Kmin^{-1} followed by a hold at 300 °C for 5 mins and uses a split ratio of 5:1. The GC-MS was used only for qualitative analysis of the bio-oil components.

Gas Chromatography – Flame Ionisation Detector (GC-FID)

The bio-oil obtained in acetone was submitted for GC-FID analysis on a Perkin Elmer Clarus 500 GC with a Perkin Elmer Clarus 560S Mass Spectrometer using a Rxi-5HT column. The gas chromatography program ramps from 50 °C to 300 °C at 30 Kmin^{-1} followed by a hold at 300 °C for 5 mins and uses a split ratio of 5:1. The GC-FID analysis was used for the quantitative analysis of furfural, LGO, 5-HMF and LGA components based on the method of internal standards.

High-performance Liquid-Chromatography (HPLC)

The Agilent Technologies 1260 Infinity II was used for HPLC analysis, using Hi PLEX H Column at 60 °C. The mobile phase was consisting of 0.005M H_2SO_4 and the flow rate was established at 0.4 mlmin^{-1}. Low- and high-pressure limits were 0 and 40 bars. The draw and eject speeds were set up to 200.0 µLmin^{-1} and 400.0 µLmin^{-1} respectively. The wait time after draw was 1.2 s. The injection volume was 5.00 µL. The quantification of the acetic acid, lactic acid, glucose, xylose, levoglucosan, levulinic acid and 5-HMF was done using the method of internal standards.

Attenuated Total Reflectance-FTIR (ATR-FTIR)

The FTIR spectra were recorded at Perkin Elmer Spectrum 400. The measured wavenumbers range was 650-4000 cm^{-1} with a step of 4 cm^{-1}. The number of collected scans was 32 in an adsorption mode for all experiments.

Supplementary Text

Catalyst characterization

Nitrogen adsorption showed that the both samples can be attributed to mesoporous solids. However, the Na-bentonite has larger impact of macro-porosity, while Al-pillared bentonite incorporates a significant amount of micropores.

Original bentonite was found to have mainly the Lewis sites (1452, 1491, 1575, 1626 and 1621 cm^{-1}) and a small number of Bronsted acid sites following to a shoulder at 1540 cm^{-1} (Figure S8A). The amount of Bronsted sites (1540 cm^{-1}) was higher for Al-pillared bentonite than that one Na-bentonite (Figure S8B). This band, however, was decreasing upon heating. The thermal processing of Al-pillared sample at 400 °C has followed by Lewis sites rearrangements, indicating the presence of new bands (Figure S8B, 400 °C). A similar process has been reported for aluminas and associated with the reaction of Lewis coordinated pyridine molecule with a nearby hydroxyl, forming α-pyridone and hydrogen.(*298*)

MW-traces

The MW traces are used to estimate strength of the interaction between microwaves and sample in the MW reactor. Figure S11A-B demonstrates such traces for a few investigated samples.

The interaction between MW and bentonite is relatively strong with maximum heating rates below 100 °C (Figure S11A, points 1-3). The higher clay loading causes faster heating rate, that is in a full agreement with previously published data.(*144*) This is probably due to high content of physisorbed water in Na-bentonite. Al-pillared bentonite does not exhibit the similar behavior (Figure S11B). We found a linear correlation between the maximums of heating rates and the catalysts loadings (Figure S11C). An addition of bentonite to cellulose even in the amount of 2wt% is followed by two times increasing of the heating rate maximum.

The "layer" experiment results and LGO identification

The packaging of the samples is displayed on Figure S12. The presence of LGO was confirmed by GC-MS analysis, portrayed on Figure S13.

Conventional pyrolysis

The conventional pyrolysis was done in Netzsch STA 409 equipped with liquid N_2 trap to collect the volatiles (Figure S14). The heating rate was 30 $Kmin^{-1}$ and the carrier gas was N_2 at 1 $lmin^{-1}$ flow. The sample preparation involved intensive mixing of the Al-pillared clay with cellulose in 1:1 ratio. The sample loading was 0.5 g. Then it was accurately washed with acetone and submitted for GC-FID analysis, giving 10.1wt% yield of LGO.

The amount of produced bio-oil was calculated as a result of organic residue left after acetone evaporation at a rotary evaporator under vacuum. The purity of the LGO was ~26% and this was estimated as a ratio between the yield of LGO and the amount of organic residue (Figure S15).

The pyrolysis of paper waste

The paper waste was mixed with the Al-pillared clay in the 1:1 ratio. The MW-assisted pyrolysis and analysis of the bio-oil were conducted following to the procedures described above. The GC-FID spectra of the collected bio-oil is shown on Figure S16.

The catalyst recovery

The Al-pillared clay was recovered for three times losing 15%, 26% and 34% of its activity towards LGO yield at the first, second and third cycles respectively (Figure S17). The catalyst, containing solid carbonaceous material after the pyrolysis, was hydrolyzed. The solid was carefully washed with water and this water fraction together with the hydrolysate was consisting of additional high-value chemicals. The rest of the char was oxidized with 30wt% H_2O_2 in water with pH of 4.7 (HCl).

Analysis of the hydrolysate

The HPLC spectra and the related table of the chemicals quantified are given on Figure S18 and table S1.

Repeatability and reproducibility of Al-pillared clay synthesis

The SAXS analysis for two additional Al-pillared samples are displayed on Figure S19. There parallel samples were synthesized to show the reproducibility of the catalyst.

Supporting Figures and Tables
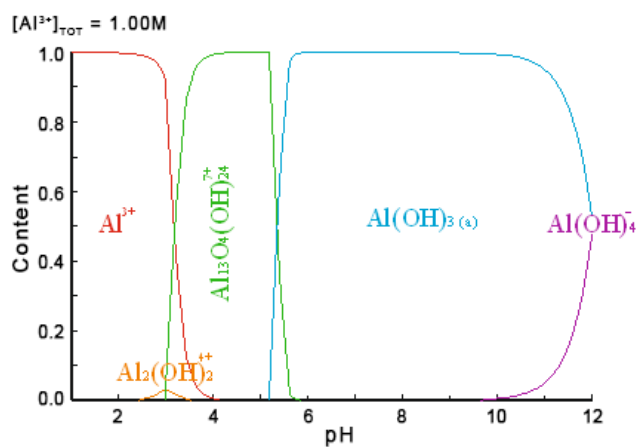
FigureS1. Diagram of Al^{3+} forms distribution depending on the cation content and pH (Medusa programming data)
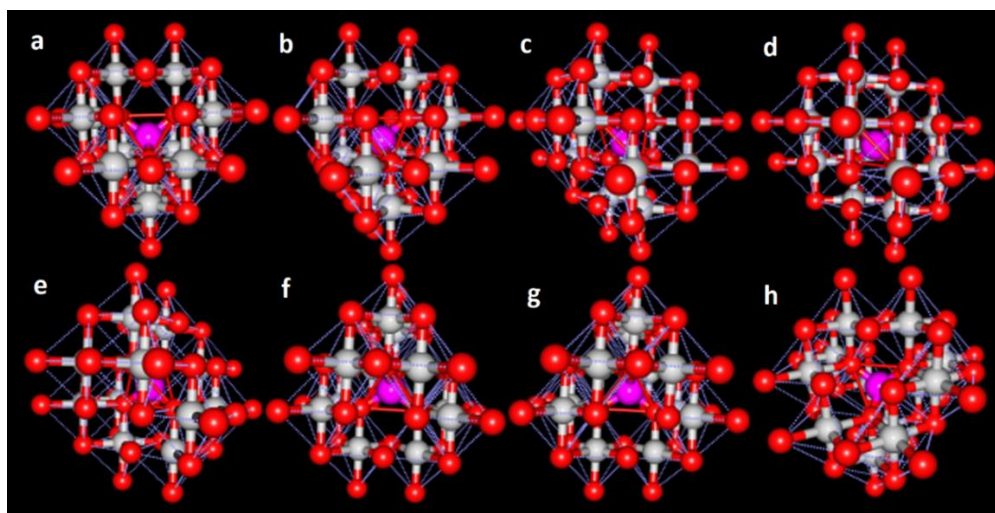
FigureS2. Structure of the polynuclear hydroxo-complexe Al_{13}; a) "frontal" view; b), c), d), e), f), g) – slow rotation of the complex; h) – free view
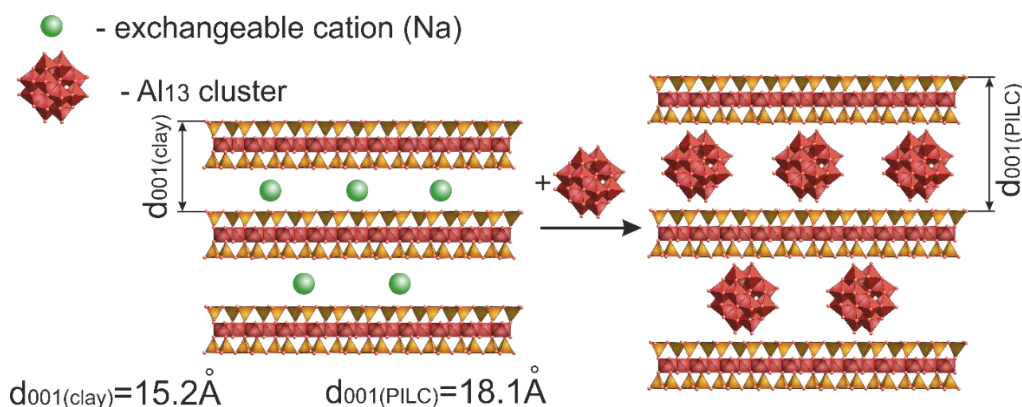
FigureS3. The intercalation process and the resulted expanded distance between the layers
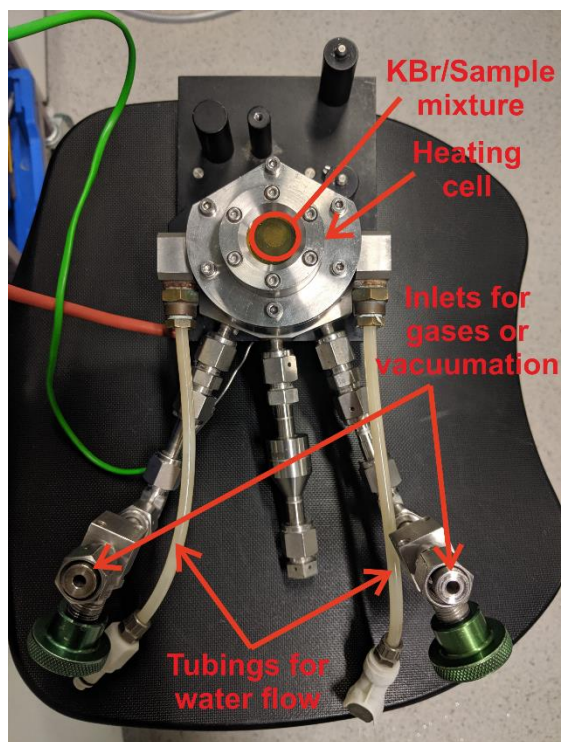
FigureS4. The Diffuse Reflectance Infrared Fourier Transform cell used for pyridine titration

FigureS5. The set-up for ammonia adsorption on the catalysts surface
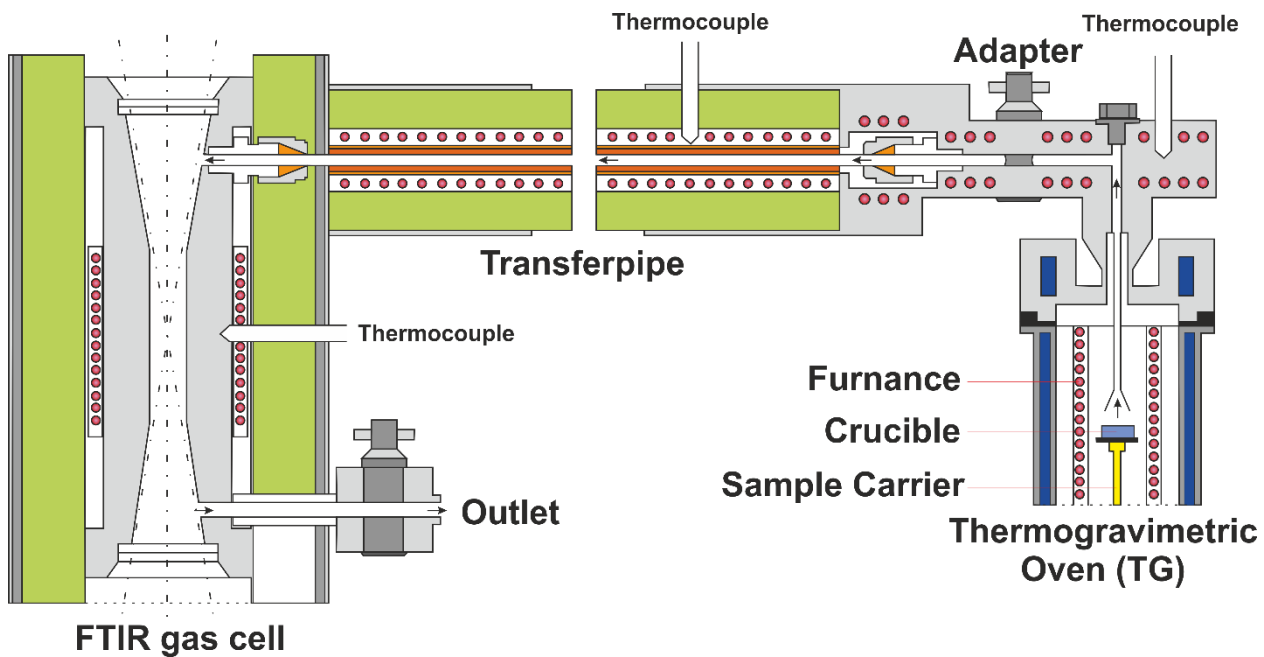
FigureS6. Schematic of the TG-FTIR setup
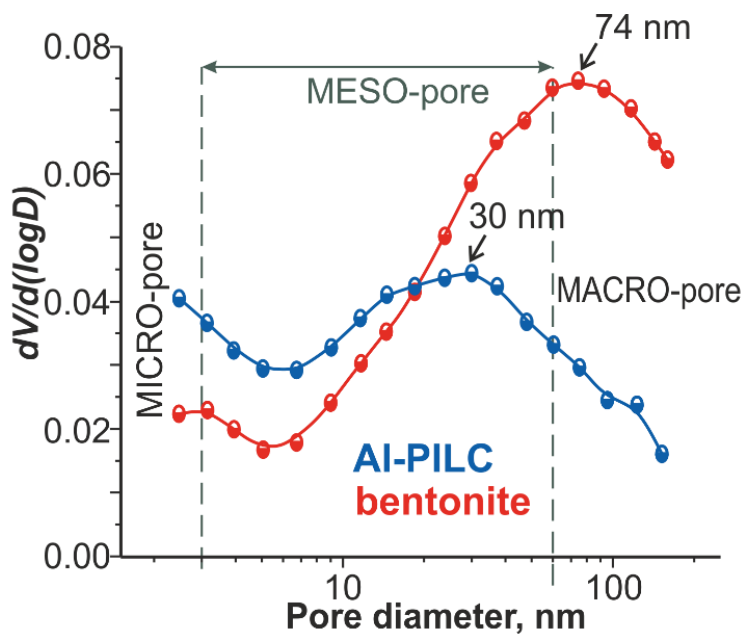
FigureS7. The BJH distribution of pore diameter
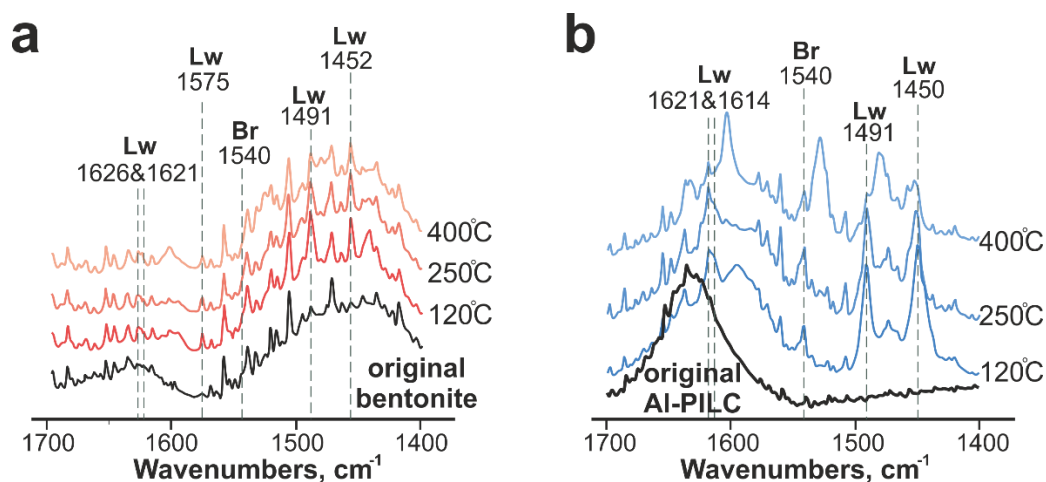
FigureS8. Experimental data of pyridine titration: A – original Na-bentonite (black) and pyridine adsorbed Na-bentonite treated at different temperatures (120-400°C); B – original Al-pillared bentonite and pyridine adsorbed Al-pillared bentonite treated at different temperatures (120-400°C)

Table S1. The TPD of ammonia quantification results

Sample	Acid concentration, μmol/g			
	100-250°C	250-500°C	500-800°C	Total
Na-bentonite	126.5	67.1	60.9	254.5
Al-pillared bentonite	244.6	343.4	62.6	650.6
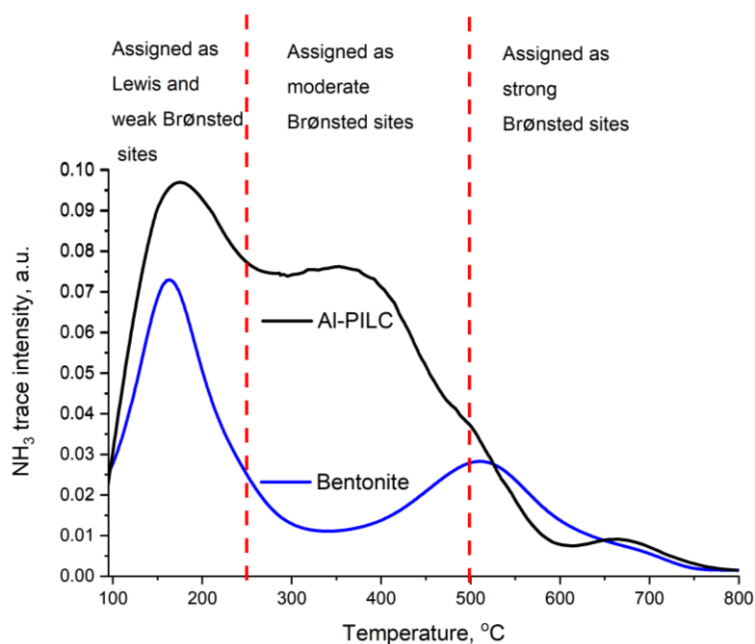
FigureS9. Experimental results of TPD of ammonia: original Na-bentonite (blue) and Al-pillared bentonite (black)
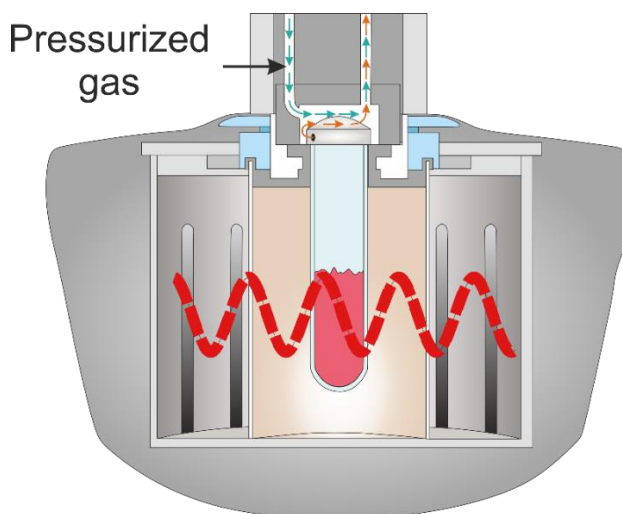
FigureS10. The scheme of the MW reactor (CEM Discover)
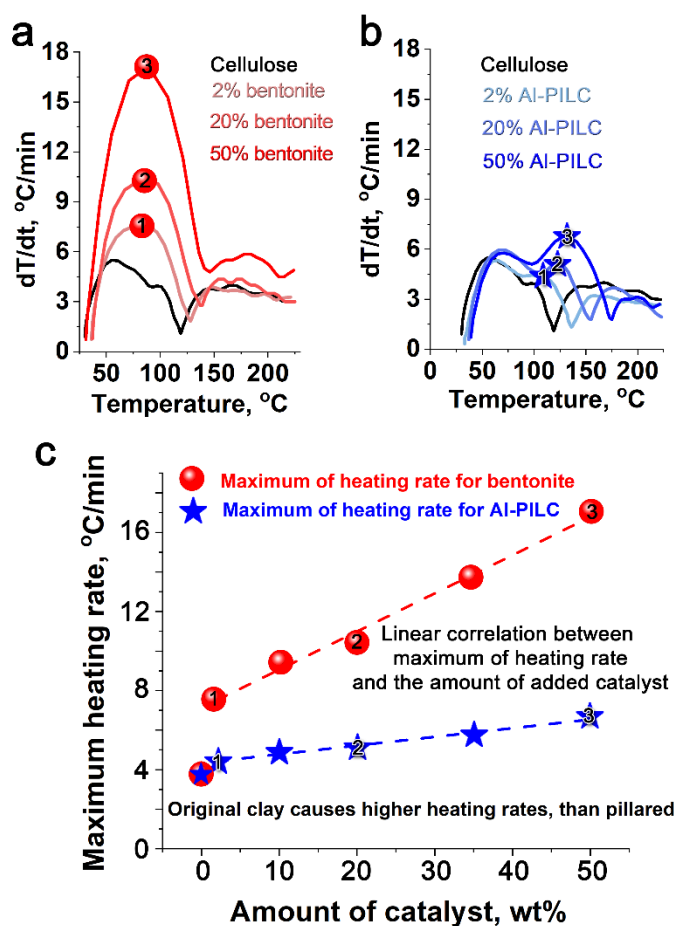
FigureS11. The MW traces: A – mixtures between cellulose and bentonite; B – mixtures between cellulose and Al-pillared bentonite
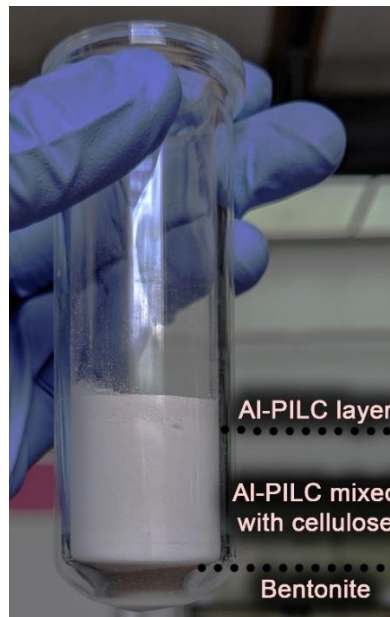
FigureS12. Sample packaging for the designer "layer" experiment
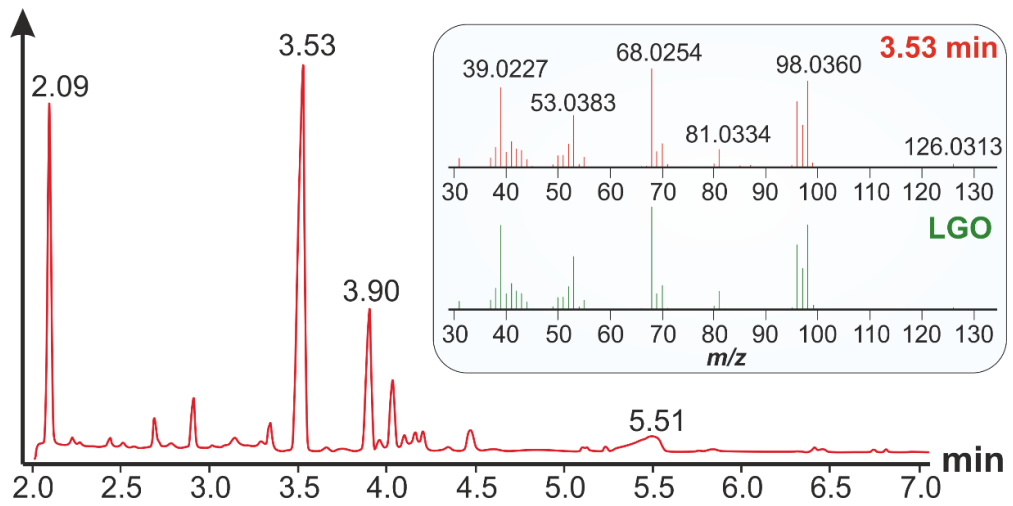
FigureS13. GC-MS of the bio-oil collected in the layer experiment
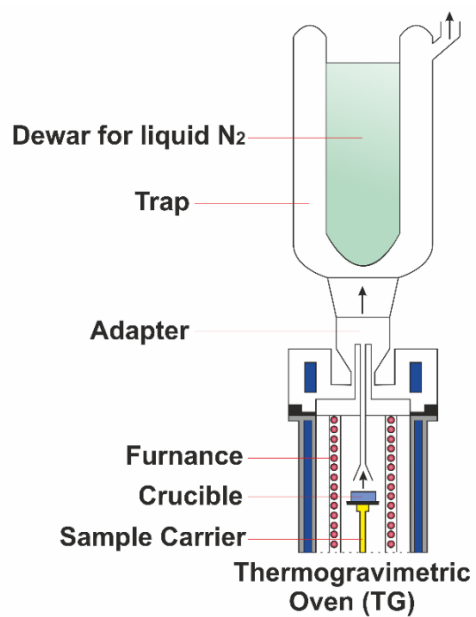
FigureS14. Cold-trap experiment with conventional heating
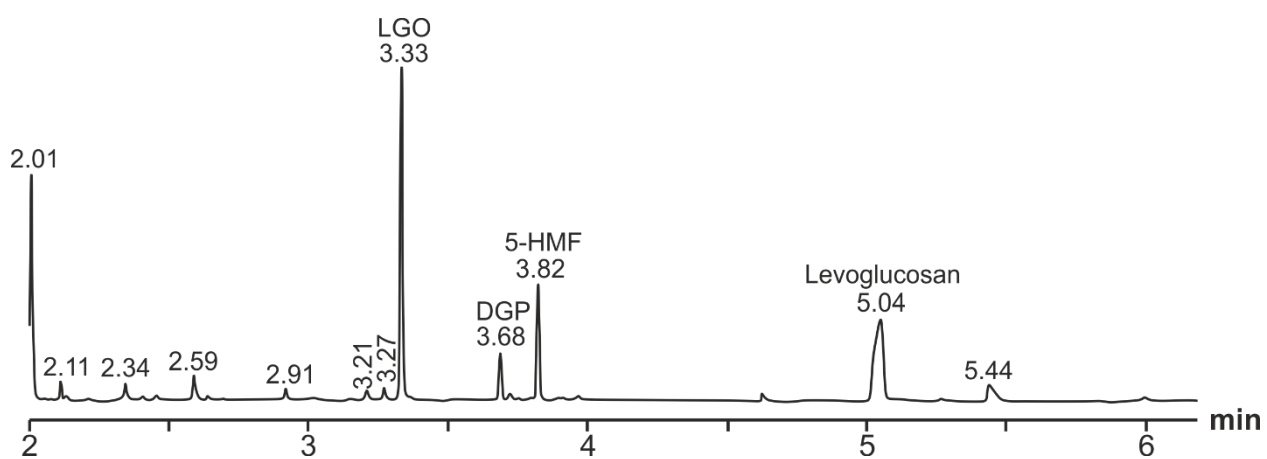
FigureS15. GC-FID analysis of the volatiles collected from conventional pyrolysis of cellulose mixed with the Al-pillared clay in the ratio of 1:1
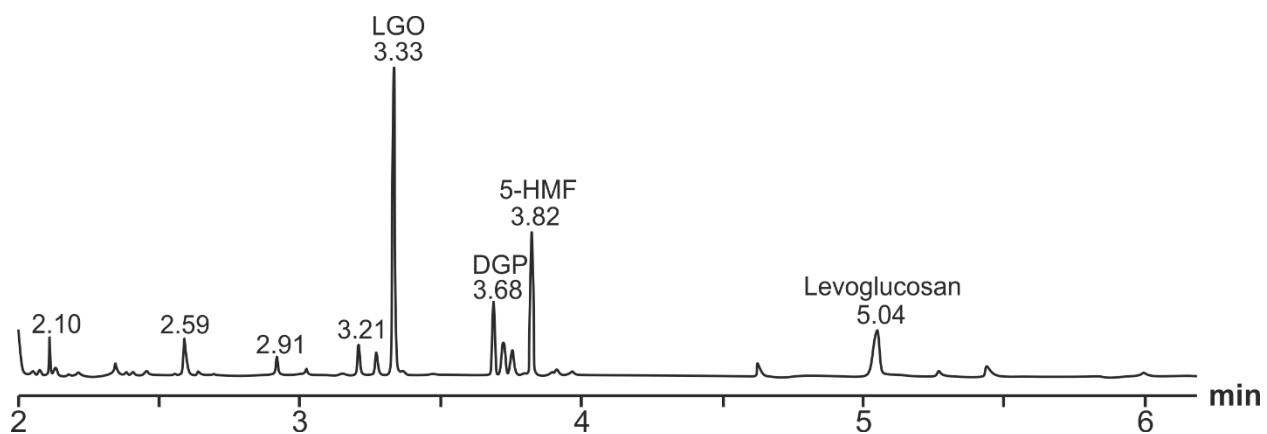
FigureS16. GC-FID of the bio-oil collected for MW-assisted pyrolysis of the paper waste loaded with 50wt% of Al-pillared catalyst
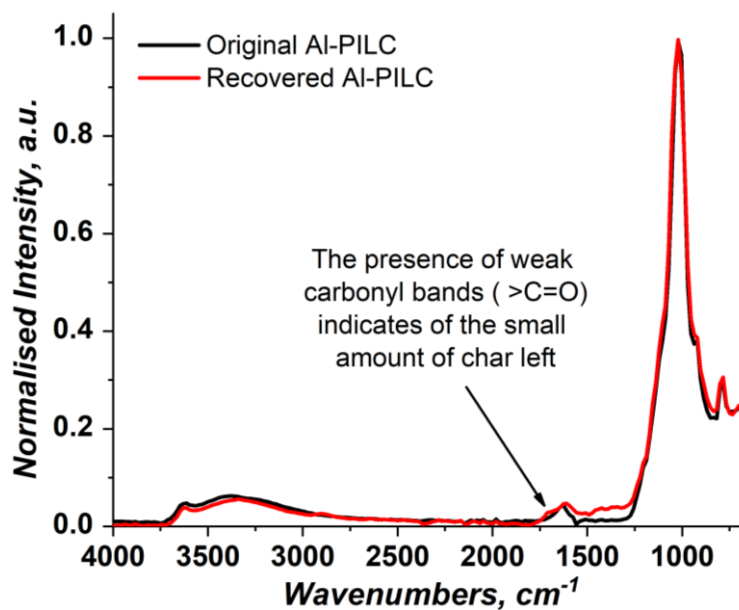
FigureS17. ATR-FTIR of the original Al-PILC and Al-PILC recovered after pyrolysis for the first time
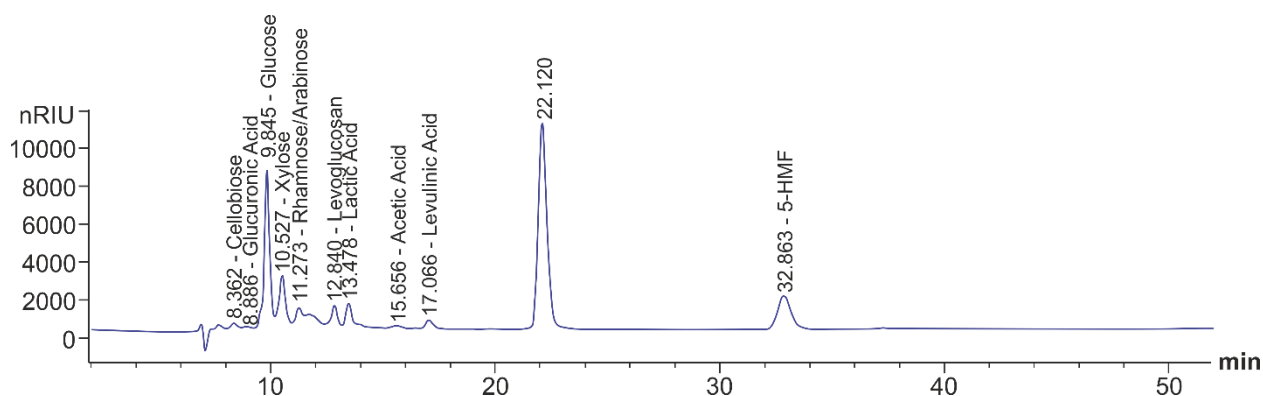
FigureS18. HPLC spectra of the hydrolysate

Table S2. The HPLC quantification of the hydrolysate

Compound	Yield, wt% from char
Glucose	4.90
Xylose	1.89
Levoglucosan	0.74
Lactic Acid	1.23

164

Acetic Acid	0.49
Levulinic Acid	0.42
5-HMF	2.59
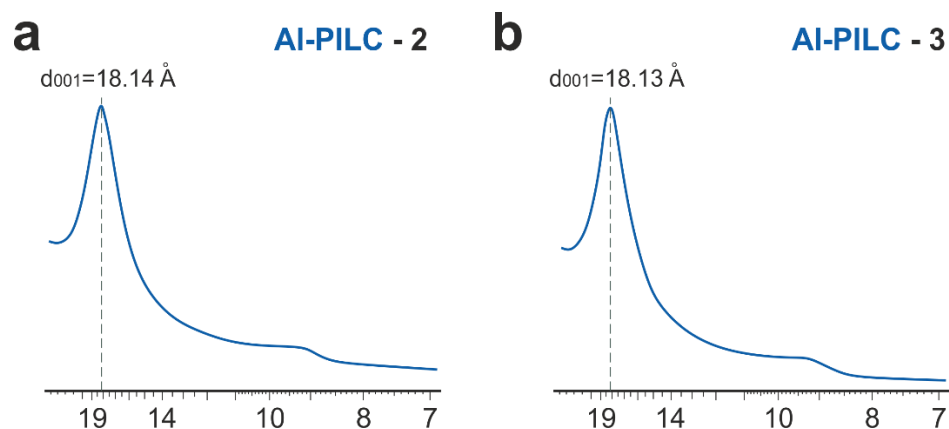
FigureS19. SAXS of the Al-pillared bentonite samples, which were synthesised in parallel to show the reproducibility of the catalyst

References

Author Contributions

Alisa Doroshenko has conducted and analyzed the majority of the experiments with the help of Karl Heaton and Stephen Cowling. Vitaliy Budarin, Ihor Pylypenko, Alisa Doroshenko and James Clark have developed the mechanistic understanding of the MW-pyrolysis process in the presence of clays. All authors have discussed the manuscript and were involved in a writing process.

Appendix 2. Supplementary of the Green Chemistry paper: Using in vivo nickel to direct the pyrolysis of hyperaccumulator plant biomass

The impregnation of nickel in the Control samples.

Ground leaf material from these control samples were then impregnated with Ni, using 0.1 M NiCl$_2$·6H$_2$O aqueous solution to achieve final nickel concentrations equivalent to the those in the hyperaccumulator species - 0.93 and 0.35 wt% for *Stackhousia* and *Alyssum* respectively. The water was removed on a rotary evaporator at 40°C and 50 mbar. The samples were placed on a glass filter and carefully washed with distilled water (figure 1S) several times until the negative reaction on the chloride anions with AgNO$_3$ solution (figure 2S). The possible leaching of the metal during washing step was checked by NaHS solution. The precipitation of NiS was not observed (figure 3S).

Fig. 1S. Washing on a glass filter from the excess of chloride anions
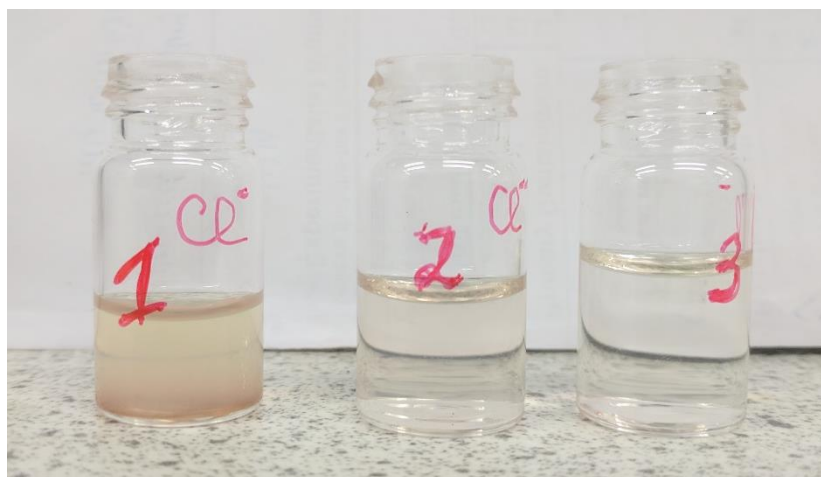
Fig. 2S. Analysis for the presence of chloride anions by Ag$^+$. The partial occurrence of the red colour happened because of the partial oxidation of the silver
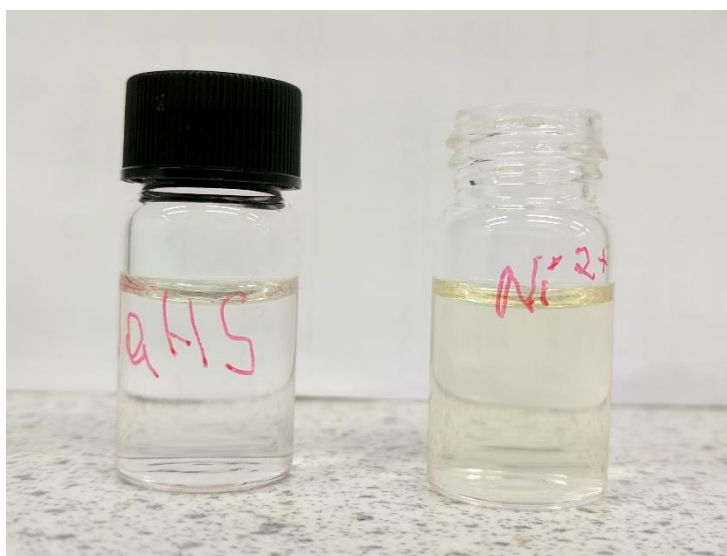
Fig. 3S. The test for the leaching of nickel with NaHS solution

MW-assisted pyrolysis

Microwave assisted pyrolysis was conducted at dynamic power mode, on a CEM Discover, equipped with 10 ml closed vial. The target temperature was 280 °C (figure 4S). The extraction of bio-oil was carried out using acetone; centrifuged, decanted, filtrated on a glass filter.

Fig. 4S. The microwave reactor – CEM Discover

GC-MS and GC-FID procedures

GC-MS and GC-FID analysis was performed using a premier TOF mass spectrometer coupled to an Agilent Technologies 6890A gas chromatograph equipped with a 30 m x 0.25 x 0.25 ZB-5HT inferno column. The MS acquisition mass range was between m/z 50 and 750, electron energy 70 eV, trap current 200 uA. The GC method used was isothermal for 2min at 50 °C, then increased to 280 °C at 10 Kmin^{-1}, held for 15 mins at maximum temperature, with a total runtime of 40 mins. The GC-FID analysis was performed on a Hewlett Packard HP 6890 with a 30 m x 0.25 x 0.25 Rxi-5HT column. The GC method held a starting temperature of 50 °C and then an increase to 300 °C at 30 °C/min, held for 5 mins, with a total runtime of 13.33 mins. The GC-MS spectra for all the samples are portrayed on figure 5S and 6S.

ATR-FTIR

Attenuated total reflection is a sampling technique used in conjunction with infrared spectroscopy makes it enable t record the infrared spectra of the samples. The analysis was carried out on the Perkin Elmer FTIR/FTNIR Spectrum 400 in the range of 600-4000 cm^{-1}. The amount of scans was 32 with 4 cm^{-1} recording step.

The spectra for the *Alyssum bertolonii* hyperaccumulator and its control are displayed on the figure 7S. The Control sample revealed increased amount of lignin in comparison to the hyperaccumulator. The similar adsorbance of the carbonyl bands (figure 7S), which can be attributed to the acid constituents of the hemicellulose, makes it possible to assume that amount of hemicellulose is similar for the samples.

<u>Thermal analysis</u>

The thermal analysis was conducted on the Netzsch STA 409 using linear heating with ramping rate 10 Kmin^{-1}. The experiment was performed in inert atmosphere of N$_2$ with a gas-flow of 100 mlmin^{-1}. The processing of the received data (including the deconvolution procedure) was done in OriginPro 2018 (figure 8S). The integrated signal of the lignin for the *Alyssum* Control was larger than that of the *Alyssum bertolonii*, that is in a line with the ATR-FTIR analysis.
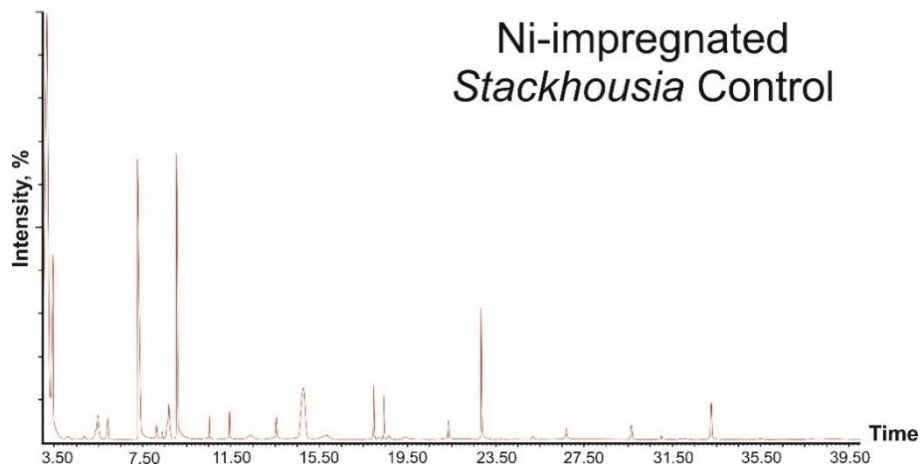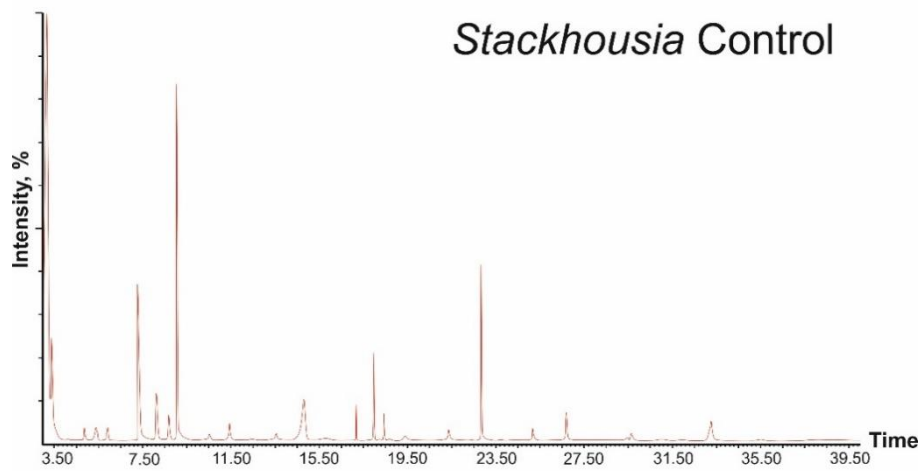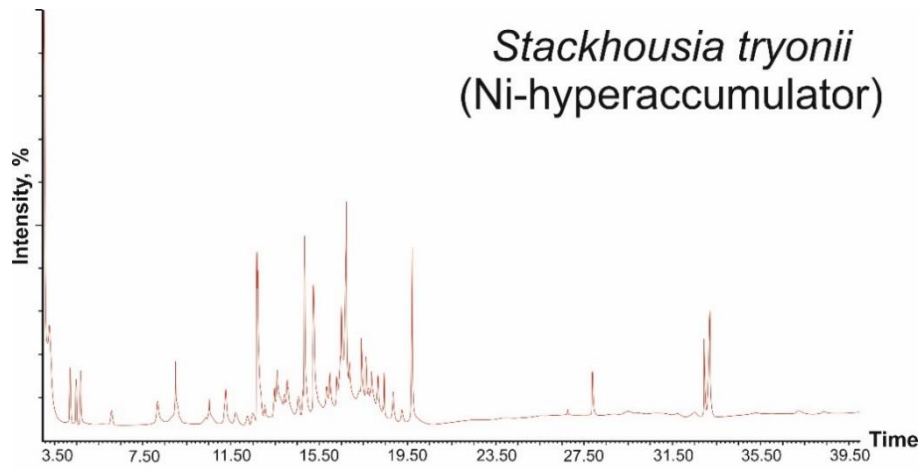
Fig. 5S. GC-MS of the *Stackhousia* related samples
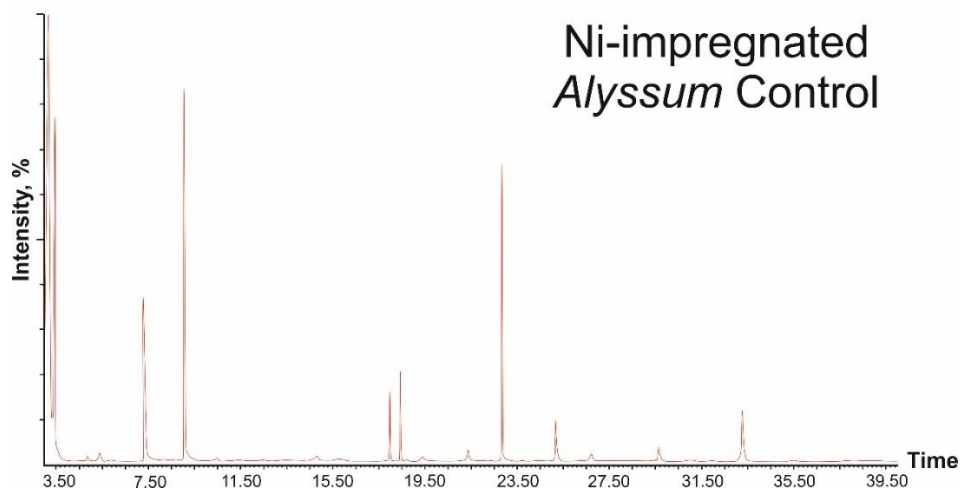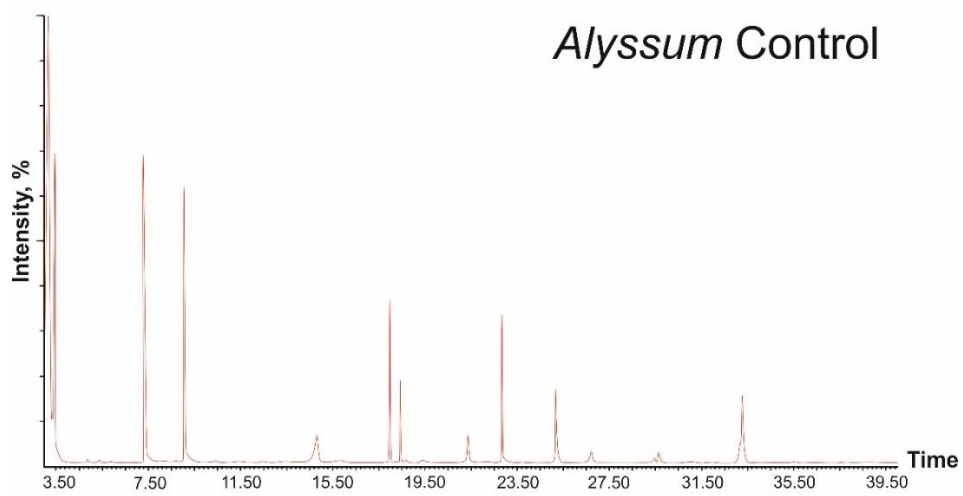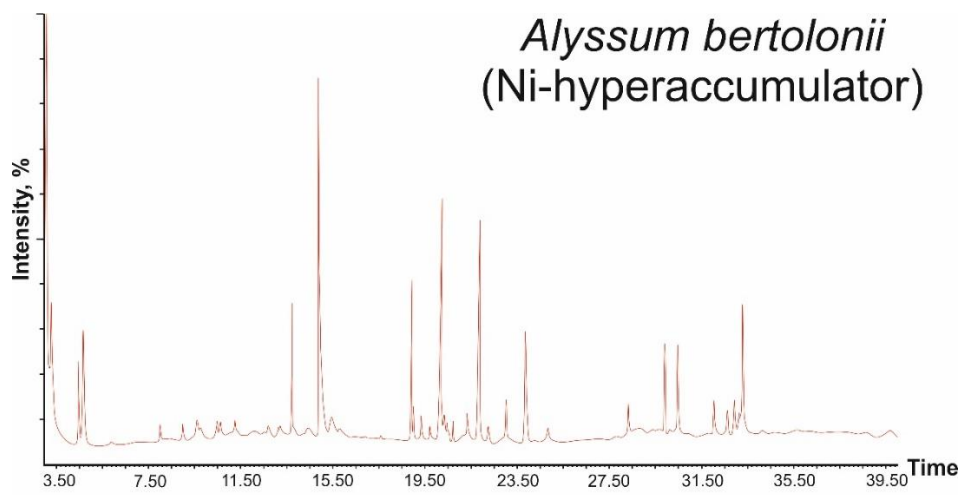
Fig. 6S. GC-MS of the *Alyssum* related samples
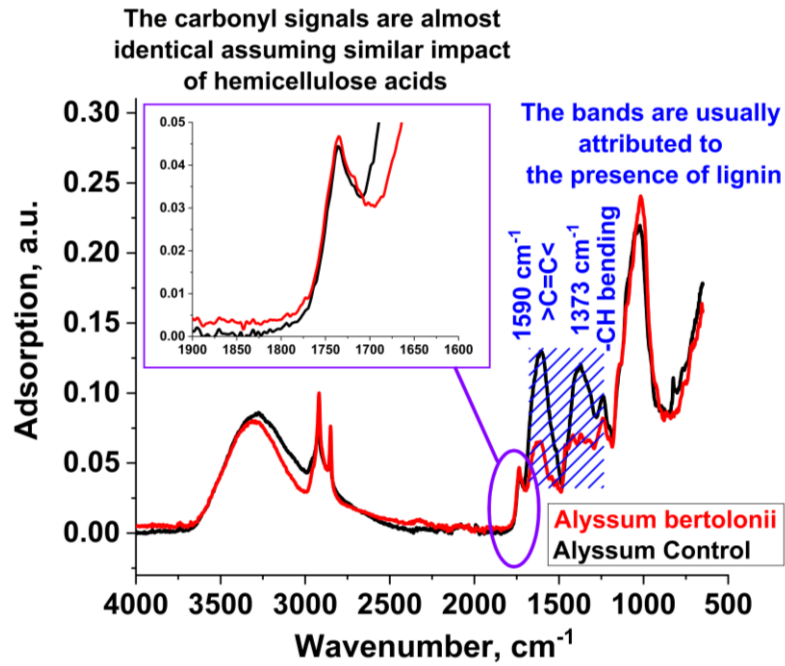
Fig. 7S. ATR-FTIR of the samples before MW-assisted pyrolysis
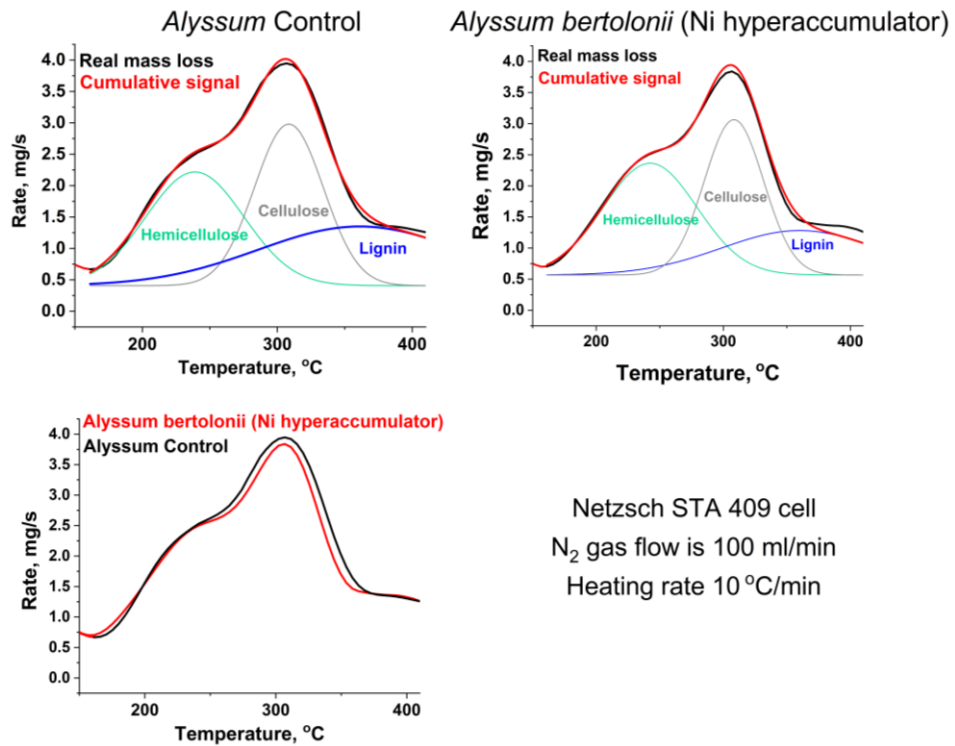
Fig. 8S. Mass-loss curves resulted from the conventional heating

ABBREVIATIONS

TG-FTIR - thermogravimetry coupled with Fourier Transformed Infrared spectrometer

TPD - Temperature-Programmed Desorption

SAXS - Small angle X-ray

GC-FID – Gas Chromatography – Flame Ionization Detector

GC-MS – Gas Chromatography – Mass Spectrometry

DRIFT - Diffuse Reflectance Infrared Fourier Transform

FTIR - Fourier Transformed Infrared

HPLC - High-performance Liquid-Chromatography

MCT (detector) - Mercury(M), Cadmium(Cd) & Lead(Pb) detector

MW – Microwave

ATR-FTIR - Attenuated Total Reflectance- Fourier Transformed Infrared spectrometer

PILC – Pillared (clay)

LGO - Levoglucosenone

LGA - Levoglucosan

DGP – 1,4:3,6-dianhydro-α-D-glucopyranose

5-HMF – 5-hydroxymethylfurfural

BJH – Barrett-Joyner-Halenda

BET – Brunauer-Emmett-Teller

FTNIR - Fourier Transformed Near-Infrared

ZSM-5 – Zeolite Socony Mobil–5

IPCC – Intergovernmental Panel on Climate Change

NMP – *N*-Methyl-2-pyrrolidone

DMF – Dimethylformamide

NMR – Nuclear Magnetic Resonance

CHN (analyser) – Carbon Hydrogen and Nitrogen (analyser)

IR – Infrared

kJ – Kilojoule

GHz – Gigahertz

MHz – Megahertz

DTA – Differential Thermal Analysis

TGA – Thermogravimetric analysis

TG-MS – Thermogravimetry - Mass Spectrometry

K – Kelvin Degree

$Kmin^{-1}$ – Kelvin per minute

TG – Thermogravimetry

VOC - Volatile Organic Compounds

KCE - Kinetic Compensation Effect

FFA – Furfural

AA – Acetic Acid

MW-IR – Microwave – Infrared

PTSA – *para*-Toluenesulforic acid

STA – Simultaneous Thermal Analysis

References

1. M. H. Bender, Potential conservation of biomass in the production of synthetic organics. *Resources, Conservation and Recycling*. **30**, 49–58 (2000).
2. A. Carroll, C. Somerville, Cellulosic biofuels. *Annu Rev Plant Biol*. **60**, 165–182 (2009).
3. IEA Bioenergy, "Biorefineries: adding value to the sustainable utilisation of biomass" (T42:2009:01, 2009), (available at https://www.ieabioenergy.com/wp-content/uploads/2013/10/Task-42-Booklet.pdf).
4. G. Mulhern, The future of bio-based chemicals in the EU Bioeconomy. *EU Science Hub - European Commission* (2019), (available at https://ec.europa.eu/jrc/en/science-update/future-bio-based-chemicals-eu-bioeconomy).
5. F. Cherubini, The biorefinery concept: Using biomass instead of oil for producing energy and chemicals. *Energy Conversion and Management*. **51**, 1412–1421 (2010).
6. Z. Miao, T. E. Grift, A. C. Hansen, K. C. Ting, An overview of lignocellulosic biomass feedstock harvest, processing and supply for biofuel production. *Biofuels*. **4**, 5–8 (2013).
7. F. E. I. Deswarte, J. H. Clark, A. J. Wilson, J. J. E. Hardy, R. Marriott, S. P. Chahal, C. Jackson, G. Heslop, M. Birkett, T. J. Bruce, G. Whiteley, Toward an integrated straw-based biorefinery. *Biofuels, Bioproducts and Biorefining*. **1**, 245–254 (2007).
8. M. Londo, E. Deurwaarder, Developments in EU biofuels policy related to sustainability issues: overview and outlook. *Biofuels, Bioproducts and Biorefining*. **1**, 292–302 (2007).
9. B. Kamm, M. Kamm, P. R. Gruber, S. Kromus, in *Biorefineries-Industrial Processes and Products*, B. Kamm, P. R. Gruber, M. Kamm, Eds. (Wiley-VCH Verlag GmbH, Weinheim, Germany, 2005; http://doi.wiley.com/10.1002/9783527619849.ch1), pp. 1–40.
10. M. De bruyn, J. Fan, V. L. Budarin, D. J. Macquarrie, L. D. Gomez, R. Simister, T. J. Farmer, W. D. Raverty, S. J. McQueen-Mason, J. H. Clark, A new perspective in bio-refining: levoglucosenone and cleaner lignin from waste biorefinery hydrolysis lignin by selective conversion of residual saccharides. *Energy & Environmental Science*. **9**, 2571–2574 (2016).
11. F. net GmbH, Ethanol PRICE Today | Ethanol Spot Price Chart | Live Price of Ethanol per Ounce | Markets Insider. *markets.businessinsider.com*, (available at https://markets.businessinsider.com/commodities/ethanol-price).
12. Ethanol price information, (available at https://markets.ft.com/data/commodities/tearsheet/summary?c=Ethanol).
13. T. Buntara, S. Noel, P. H. Phua, I. Melián-Cabrera, J. G. de Vries, H. J. Heeres, Caprolactam from Renewable Resources: Catalytic Conversion of 5-Hydroxymethylfurfural into Caprolactone. *Angewandte Chemie International Edition*. **50**, 7083–7087 (2011).
14. M. B. Comba, Y. Tsai, A. M. Sarotti, M. I. Mangione, A. G. Suárez, R. A. Spanevello, Levoglucosenone and Its New Applications: Valorization of Cellulose Residues. *European Journal of Organic Chemistry*. **2018**, 590–604 (2018).
15. S. V. Vassilev, D. Baxter, L. K. Andersen, C. G. Vassileva, An overview of the chemical composition of biomass. *Fuel*. **89**, 913–933 (2010).
16. A. Torano Caicoya, F. Kugler, I. Hajnsek, K. P. Papathanassiou, Large-Scale Biomass Classification in Boreal Forests With TanDEM-X Data. *IEEE Trans. Geosci. Remote Sensing*. **54**, 5935–5951 (2016).
17. J. F. Robyt, in *Glycoscience: Chemistry and Chemical Biology*, B. O. Fraser-Reid, K. Tatsuta, J. Thiem, Eds. (Springer, Berlin, Heidelberg, 2008; https://doi.org/10.1007/978-3-540-30429-6_35), pp. 1437–1472.
18. A. Cano, A. Jiménez, M. Cháfer, C. Gónzalez, A. Chiralt, Effect of amylose:amylopectin ratio and rice bran addition on starch films properties. *Carbohydrate Polymers*. **111**, 543–555 (2014).
19. D. Schwartz, R. L. Whistler, in *Starch (Third Edition)*, J. BeMiller, R. Whistler, Eds. (Academic Press, San Diego, 2009; http://www.sciencedirect.com/science/article/pii/B978012746275200001X), *Food Science and Technology*, pp. 1–10.
20. H. V. Scheller, P. Ulvskov, Hemicelluloses. *Annu Rev Plant Biol*. **61**, 263–289 (2010).
21. R. L. Whistler, in *Industrial Gums (Third Edition)*, R. L. Whistler, J. N. Bemiller, Eds. (Academic Press, London, 1993; http://www.sciencedirect.com/science/article/pii/B9780080926544500152), pp. 295–308.

22. L. Mišurcová, S. Škrovánková, D. Samek, J. Ambrožová, L. Machů, in *Advances in Food and Nutrition Research*, J. Henry, Ed. (Academic Press, 2012; http://www.sciencedirect.com/science/article/pii/B9780123945976000033), vol. 66, pp. 75–145.

23. J. Huang, S. Fu, L. Gan, Eds., in *Lignin Chemistry and Applications* (Elsevier, 2019; http://www.sciencedirect.com/science/article/pii/B9780128139417000023), pp. 25–50.

24. Y. Lu, Y.-C. Lu, H.-Q. Hu, F.-J. Xie, X.-Y. Wei, X. Fan, Structural Characterization of Lignin and Its Degradation Products with Spectroscopic Methods. *Journal of Spectroscopy* (2017).

25. M. Abhilash, D. Thomas, in *Biopolymer Composites in Electronics*, K. K. Sadasivuni, D. Ponnamma, J. Kim, J.-J. Cabibihan, M. A. AlMaadeed, Eds. (Elsevier, 2017; http://www.sciencedirect.com/science/article/pii/B9780128092613000152), pp. 405–435.

26. Solubility of lignin and acetylated lignin in organic solvents :: BioResources, (available at https://bioresources.cnr.ncsu.edu/).

27. V. K. Thakur, M. K. Thakur, P. Raghavan, M. R. Kessler, Progress in Green Polymer Composites from Lignin for Multifunctional Applications: A Review. *ACS Sustainable Chem. Eng.* **2**, 1072–1092 (2014).

28. A. Vishtal, A. Kraslawski, Challenges in industrial applications of technical lignins. *BioResources*. **6**, 3547–3568 (2011).

29. E. Windeisen, G. Wegener, in *Polymer Science: A Comprehensive Reference*, K. Matyjaszewski, M. Möller, Eds. (Elsevier, Amsterdam, 2012; http://www.sciencedirect.com/science/article/pii/B9780444533494002636), pp. 255–265.

30. A. O'Sullivan, Cellulose: the structure slowly unravels. *Cellulose*. **4**, 173–207 (1997).

31. R. Ergun, J. Guo, B. Huebner-Keese, in *Encyclopedia of Food and Health*, B. Caballero, P. M. Finglas, F. Toldrá, Eds. (Academic Press, Oxford, 2016; http://www.sciencedirect.com/science/article/pii/B9780123849472001276), pp. 694–702.

32. A. Chami Khazraji, S. Robert, Interaction Effects between Cellulose and Water in Nanocrystalline and Amorphous Regions: A Novel Approach Using Molecular Modeling. *Journal of Nanomaterials*. **2013** (2013), p. e409676.

33. FAO Forest Paper Report, "Global Forest Resources Assessment 2000" (ISSN 0258-6150, 2001), (available at http://www.fao.org/tempref/docrep/fao/003/Y1997E/FRA%202000%20Main%20report.pdf).

34. R. Liguori, V. Faraco, Biological processes for advancing lignocellulosic waste biorefinery by advocating circular economy. *Bioresour Technol*. **215**, 13–20 (2016).

35. J. Zhao, X. Ge, J. Vasco-Correa, Y. Li, Fungal pretreatment of unsterilized yard trimmings for enhanced methane production by solid-state anaerobic digestion. *Bioresource technology*. **158**, 248–252 (2014).

36. D. Salvachúa, A. Prieto, M. López-Abelairas, T. Lu-Chau, A. T. Martínez, M. J. Martínez, Fungal pretreatment: An alternative in second-generation ethanol from wheat straw. *Bioresource Technology*. **102**, 7500–7506 (2011).

37. G. Kumar, P. Bakonyi, P. Sivagurunathan, N. Nemestóthy, K. Bélafi-Bakó, C.-Y. Lin, Improved microbial conversion of de-oiled Jatropha waste into biohydrogen via inoculum pretreatment: process optimization by experimental design approach. *Biofuel Research Journal*. **2**, 209–2014 (2015).

38. E. U. Kiran, A. P. Trzcinski, Y. Liu, Enhancing the hydrolysis and methane production potential of mixed food waste by an effective enzymatic pretreatment. *Bioresour. Technol.* **183**, 47–52 (2015).

39. G. Kumar, B. Sen, C.-Y. Lin, Pretreatment and hydrolysis methods for recovery of fermentable sugars from de-oiled Jatropha waste. *Bioresour. Technol.* **145**, 275–279 (2013).

40. K. Amulya, S. Jukuri, S. Venkata Mohan, Sustainable multistage process for enhanced productivity of bioplastics from waste remediation through aerobic dynamic feeding strategy: Process integration for up-scaling. *Bioresource Technology*. **188**, 231–239 (2015).

41. J. M. Naranjo, C. A. Cardona, J. C. Higuita, Use of residual banana for polyhydroxybutyrate (PHB) production: case of study in an integrated biorefinery. *Waste Manag*. **34**, 2634–2640 (2014).

42. R. E. Quiroz-Castañeda, J. L. Folch-Mallol, Hydrolysis of Biomass Mediated by Cellulases for the Production of Sugars. Sustainable Degradation of Lignocellulosic Biomass. *Techniques, Applications and Commercialization* (2013).

43. J. B. Binder, R. T. Raines, Fermentable sugars by chemical hydrolysis of biomass. *PNAS*. **107**, 4516–4521 (2010).

44. S. Caillat, E. Vakkilainen, in *Biomass Combustion Science, Technology and Engineering*, L. Rosendahl, Ed. (Woodhead Publishing, 2013), *Woodhead Publishing Series in Energy*, pp. 189–224.

45. P. L. Spath, D. C. Dayton, "Preliminary Screening – Technical and Economic Assessment of Synthesis Gas to Fuels and Chemicals with Emphasis on the Potential for Biomass-Derived Syngas," *510-34929* (NREL/TP-510-34929, National Renewable Energy Lab., Golden, CO. (US), 2003), p. 160.

46. A. Molino, S. Chianese, D. Musmarra, Biomass gasification technology: The state of the art overview. *Journal of Energy Chemistry*. **25**, 10–25 (2016).

47. "Industrial charcoal making," *63* (FAO Mechanical Wood Products Branch Forest Industries Division FAO Foresty Department, Rome, 1985).

48. D. Mohan, C. U. Pittman, P. H. Steele, Pyrolysis of wood/biomass for bio-oil: A critical review. *Energy Fuels*. **20**, 848–889 (2006).

49. A. Bridgwater, Fast pyrolysis processes for biomass. *Renewable and Sustainable Energy Reviews*. **4**, 1–73 (2000).

50. M. I. Jahirul, M. G. Rasul, A. A. Chowdhury, N. Ashwath, Biofuels Production through Biomass Pyrolysis —A Technological Review. *Energies*. **5**, 4952–5001 (2012).

51. A. Raab, A. Bonhage, A. Schneider, T. Raab, H. Rösler, K.-U. Heußner, F. Hirsch, Spatial distribution of relict charcoal hearths in the former royal forest district Tauer (SE Brandenburg, Germany). *Quaternary International*. **511**, 153–165 (2019).

52. A. Raab, M. Takla, T. Raab, A. Nicolay, A. Schneider, H. Rösler, K.-U. Heußner, E. Bönisch, Pre-industrial charcoal production in Lower Lusatia (Brandenburg, Germany): Detection and evaluation of a large charcoal-burning field by combining archaeological studies, GIS-based analyses of shaded-relief maps and dendrochronological age determination. *Quaternary International*. **367**, 111–122 (2015).

53. Continuous charcoal kiln BIO-KILN. *GreenPower*, (available at https://greenpower.equipment/produkciya/continuous-charcoal-kiln-bio-kiln/).

54. A. Doroshenko, I. Pylypenko, K. Heaton, S. Cowling, J. Clark, V. Budarin, Selective Microwave-Assisted Pyrolysis of Cellulose towards Levoglucosenone with Clay Catalysts. *ChemSusChem*. **12**, 5224–5227 (2019).

55. P. L. Spargo, Microwave Assisted Organic Synthesis. *Org. Process Res. Dev.* **9**, 697–697 (2005).

56. K. Wendler, J. Thar, S. Zahn, B. Kirchner, Estimating the Hydrogen Bond Energy. *J. Phys. Chem. A*. **114**, 9529–9536 (2010).

57. D. E. Clark, W. H. Sutton, Microwave Processing of Materials. *Annual Review of Materials Science*. **26**, 299–331 (1996).

58. A. de la Hoz, Á. Díaz-Ortiz, A. Moreno, Microwaves in organic synthesis. Thermal and non-thermal microwave effects. *Chem. Soc. Rev.* **34**, 164–178 (2005).

59. M. J. Gronnow, R. J. White, J. H. Clark, D. J. Macquarrie, Energy efficiency in chemical reactions: A comparative study of different reaction techniques. *Org. Process Res. Dev.* **9**, 516–518 (2005).

60. R. Ruan, P. Chen, R. Hemmingsen, R. Morey, D. Tiffany, Size matters: Small distributed biomass energy production systems for economic viability. *International Journal of Agricultural and Biological Engineering*. **1**, 64–68 (2008).

61. D. Beneroso, T. Monti, E. T. Kostas, J. Robinson, Microwave pyrolysis of biomass for bio-oil production: Scalable processing concepts. *Chemical Engineering Journal*. **316**, 481–498 (2017).

62. R. Luque, J. A. Menéndez, A. Arenillas, J. Cot, Microwave-assisted pyrolysis of biomass feedstocks: the way forward? *Energy Environ. Sci.* **5**, 5481–5488 (2012).

63. V. Sukumar, M. V, S. Shanmugam, Bio oil Production from Biomass using Pyrolysis and Upgrading - A Review. *International Journal of ChemTech Research*. **8**, 196–206 (2015).

64. T. P. Vispute, H. Zhang, A. Sanna, R. Xiao, G. W. Huber, Renewable Chemical Commodity Feedstocks from Integrated Catalytic Processing of Pyrolysis Oils. *Science*. **330**, 1222–1227 (2010).

65. Y. Wang, C. A. Brown, R. Chen, Industrial production, application, microbial biosynthesis and degradation of furanic compound, hydroxymethylfurfural (HMF). *AIMS Microbiol*. **4**, 261–273 (2018).

66. J. B. Heo, Y.-S. Lee, C.-H. Chung, Raw plant-based biorefinery: A new paradigm shift towards biotechnological approach to sustainable manufacturing of HMF. *Biotechnology Advances.* **37**, 107422 (2019).

67. V. M. Chernyshev, O. A. Kravchenko, V. P. Ananikov, Conversion of plant biomass to furan derivatives and sustainable access to the new generation of polymers, functional materials and fuels. *Russ. Chem. Rev.* **86**, 357 (2017).

68. R.-J. van Putten, J. C. van der Waal, E. de Jong, C. B. Rasrendra, H. J. Heeres, J. G. de Vries, Hydroxymethylfurfural, A Versatile Platform Chemical Made from Renewable Resources. *Chem. Rev.* **113**, 1499–1597 (2013).

69. B. F. M. Kuster, 5-Hydroxymethylfurfural (HMF). A Review Focussing on its Manufacture. *Starch - Stärke.* **42**, 314–321 (1990).

70. R. Vinu, L. J. Broadbelt, A mechanistic model of fast pyrolysis of glucose-based carbohydrates to predict bio-oil composition. *Energy Environ. Sci.* **5**, 9808–9826 (2012).

71. H. B. Mayes, M. W. Nolte, G. T. Beckham, B. H. Shanks, L. J. Broadbelt, The Alpha–Bet(a) of Glucose Pyrolysis: Computational and Experimental Investigations of 5-Hydroxymethylfurfural and Levoglucosan Formation Reveal Implications for Cellulose Pyrolysis. *ACS Sustainable Chem. Eng.* **2**, 1461–1473 (2014).

72. Y. Halpern, R. Riffer, A. Broido, Levoglucosenone (1,6-anhydro-3,4-dideoxy-delta-3-beta-D-pyranosen-2-one). Major product of the acid-catalyzed pyrolysis of cellulose and related carbohydrates. *J. Org. Chem.* **38**, 204–209 (1973).

73. D. Urabe, T. Nishikawa, M. Isobe, An efficient total synthesis of optically active tetrodotoxin from levoglucosenone. *Chem Asian J.* **1**, 125–135 (2006).

74. F. A. Valeev, E. V. Gorobets, I. P. Tsypysheva, G. Sh. Singizova, L. Kh. Kalimullina, M. G. Safarov, O. V. Shitikova, M. S. Miftakhov, Stereochemical Aspects of the Beckman Rearrangement of Oximes of Levoglucosenone and Its Dihydro Derivative. Enantioselective Synthesis of (+)-γ-Pelargonolactone. *Chemistry of Natural Compounds.* **39**, 563–568 (2003).

75. A. M. Sarotti, R. A. Spanevello, A. G. Suárez, A chiral auxiliary derived from levoglucosenone in asymmetric Diels–Alder transformations. *Tetrahedron Letters.* **46**, 6987–6990 (2005).

76. A. M. Sarotti, R. A. Spanevello, C. Duhayon, J.-P. Tuchagues, A. G. Suárez, Exploring structural effects of levoglucosenone derived chiral auxiliaries in asymmetric Diels–Alder cycloadditions. *Tetrahedron.* **63**, 241–251 (2007).

77. A. V. Samet, D. N. Lutov, S. I. Firgang, Y. V. Nelyubina, V. V. Semenov, Synthesis of chiral chromenes from levoglucosenone. *Russian Chemical Bulletin.* **62**, 2196–2201 (2013).

78. K. P. Stockton, C. J. Merritt, C. J. Sumby, B. W. Greatrex, Palladium-Catalyzed Suzuki–Miyaura, Heck and Hydroarylation Reactions on (−)-Levoglucosenone and Application to the Synthesis of Chiral γ-Butyrolactones. *European Journal of Organic Chemistry.* **2015**, 6999–7008 (2015).

79. M. Miftakhov, F. Valeev, I. Gaisina, Levoglucosenone: the properties, reactions, and use in fine organic synthesis. *Usp. Khim.* **63**, 922–936 (1994).

80. A. M. Sarotti, M. M. Zanardi, R. A. Spanevello, A. G. Suarez, Recent Applications of Levoglucosenone as Chiral Synthon. *Curr. Org. Synth.* **9**, 439–459 (2012).

81. R. Demange, C. Buhlmann, P. Vogel, Syntheses of beta-C(1 -> 3)-Glucopyranosides of 2-and 4-deoxy-D-hexoses. *Helvetica Chimica Acta.* **86**, 361–376 (2003).

82. I. Navarro, P. Vogel, Synthesis of a new C(1 -> 2)-linked iminodisaccharide starting from levoglucosenone. *Helv. Chim. Acta.* **85**, 152–160 (2002).

83. L. Awad, R. Demange, Y.-H. Zhu, P. Vogel, The use of levoglucosenone and isolevoglucosenone as templates for the construction of C-linked disaccharides. *Carbohydr. Res.* **341**, 1235–1252 (2006).

84. Z. J. Witczak, R. Chhabra, J. Chojnacki, C-disaccharides .1. Stereoselective approach to beta-(1-4)-3-deoxy-C-disaccharides from levoglucosenone. *Tetrahedron Lett.* **38**, 2215–2218 (1997).

85. Z. J. Witczak, P. Kaplon, P. M. Dey, Thio sugars VII. Effect of 3-deoxy-4-S-(beta-D-gluco- and beta-D-galactopyranosyl)-4-thiodisaccharides and their sulfoxides and sulfones on the viability and growth of selected murine and human tumor cell lines. *Carbohydr. Res.* **338**, 11–18 (2003).

86. Z. J. Witczak, P. Kaplon, M. Kolodziej, Thiosugars VI: A simple stereoselective approach to (1 -> 3)-3-S-thiodisaccharides from levoglucosenone. *Mon. Chem.* **133**, 521–530 (2002).

87. L. K. Faizullina, M. G. Safarov, L. V. Spirikhin, V. S. Kolosnitsyn, Y. A. Kondrova, F. A. Valeev, Reaction of nitroalkanes with levoglucosenone and its alpha-bromo and alpha-iodo derivatives. Cyclopentaannulation of alpha-halocyclenones. *Russ. J. Organ. Chem.* **47**, 914–919 (2011).

88. A. V. Samet, D. N. Lutov, L. D. Konyushkin, Y. A. Strelenko, V. V. Semenov, Preparation of chiral cyclopropanecarboxylic acids and 3-oxabicyclo[3.1.0]hexane-2-ones from levoglucosenone. *Tetrahedron-Asymmetry*. **19**, 691–694 (2008).

89. A. V. Samet, A. M. Shestopalov, D. N. Lutov, L. A. Rodinovskaya, A. A. Shestopalov, V. V. Semenov, Preparation of chiral cyclopropanes with a carbohydrate fragment from levoglucosenone. *Tetrahedron-Asymmetry*. **18**, 1986–1989 (2007).

90. K. Kadota, K. Ogasawara, A carbohydrate synthesis employing a photochemical decarbonylation. *Tetrahedron Lett.* **42**, 8661–8664 (2001).

91. A. M. Allgeier, J. C. Ritter, S. K. Sengupta, Process for preparing 1,6-hexanediol (2013), (available at https://patents.google.com/patent/US20130231505A1/en?q=levoglucosenone&assignee=du+pont&oq=du+pont+levoglucosenone).

92. A. M. Allgeier, D. R. Corbin, W. I. N. D. Silva, E. Korovessi, C. A. Menning, J. C. Ritter, S. K. Sengupta, Process for preparing 1, 6-hexanediol (2014), (available at https://patents.google.com/patent/US8889922B2/ja).

93. J. Sherwood, M. De Bruyn, A. Constantinou, L. Moity, C. R. McElroy, T. J. Farmer, T. Duncan, W. Raverty, A. J. Hunt, J. H. Clark, Dihydrolevoglucosenone (Cyrene) as a bio-based alternative for dipolar aprotic solvents. *Chem. Commun.* **50**, 9650–9652 (2014).

94. Circa'S new e-commerce store brings green chemicals directly to researchers. *Circa Group*, (available at https://www.circagroup.com.au/news/2020/11/5/circas-new-e-commerce-store-brings-green-chemicals-directly-to-researchers-nbsp-nbsp).

95. T. R. Carlson, R. G. Durbal, J. C. Ritter, C. S. Stauffer, S. K. Sengupta, Production of Levoglucosenone (2016), (available at https://worldwide.espacenet.com/publicationDetails/biblio?FT=D&date=20160317&DB=&locale=en_EP&CC=WO&NR=2016039996A1&KC=A1&ND=1).

96. M. C. Botta, H. D. Biava, R. A. Spanevello, E. G. Mata, A. G. Suárez, Development of polymer-supported chiral aminoalcohols derived from biomass and their application to asymmetric alkylation. *Tetrahedron Letters*. **57**, 2186–2189 (2016).

97. J. He, M. Liu, K. Huang, T. W. Walker, C. T. Maravelias, J. A. Dumesic, G. W. Huber, Production of levoglucosenone and 5-hydroxymethylfurfural from cellulose in polar aprotic solvent–water mixtures. *Green Chemistry.* **19**, 3642–3653 (2017).

98. P. Zhao, H. Cui, Y. Zhang, Y. Zhang, Y. Wang, Y. Zhang, Y. Xie, W. Yi, Synergetic Effect of Brønsted/Lewis Acid Sites and Water on the Catalytic Dehydration of Glucose to 5-Hydroxymethylfurfural by Heteropolyacid-Based Ionic Hybrids. *ChemistryOpen*. **7**, 824–832 (2018).

99. Z. Wang, Q. Lu, X.-F. Zhu, Y. Zhang, Catalytic Fast Pyrolysis of Cellulose to Prepare Levoglucosenone Using Sulfated Zirconia. *ChemSusChem*. **4**, 79–84 (2011).

100. A. M. Sarotti, R. A. Spanevello, A. G. Suarez, An efficient microwave-assisted green transformation of cellulose into levoglucosenone. Advantages of the use of an experimental design approach. *Green Chemistry*. **9**, 1137–1140 (2007).

101. G. Dobele, G. Rossinskaja, G. Telysheva, D. Meier, O. Faix, Cellulose dehydration and depolymerization reactions during pyrolysis in the presence of phosphoric acid. *Journal of Analytical and Applied Pyrolysis*. **49**, 307–317 (1999).

102. Y. Long, Y. Yu, Y. W. Chua, H. Wu, Acid-catalysed cellulose pyrolysis at low temperatures. *Fuel*. **193**, 460–466 (2017).

103. G. Dobele, T. Dizhbite, G. Rossinskaja, G. Telysheva, D. Meier, S. Radtke, O. Faix, Pre-treatment of biomass with phosphoric acid prior to fast pyrolysis. *Journal of Analytical and Applied Pyrolysis*. **68–69**, 197–211 (2003).

104. O. Oyola-Rivera, J. He, G. W. Huber, J. A. Dumesic, N. Cardona-Martínez, Catalytic dehydration of levoglucosan to levoglucosenone using Brønsted solid acid catalysts in tetrahydrofuran. *Green Chemistry*. **21**, 4988–4999 (2019).

105. Z. Wang, S. Zhou, B. Pecha, R. J. M. Westerhof, M. Garcia-Perez, Effect of Pyrolysis Temperature and Sulfuric Acid During the Fast Pyrolysis of Cellulose and Douglas Fir in an Atmospheric Pressure Wire Mesh Reactor. *Energy Fuels*. **28**, 5167–5177 (2014).

106. Z. Zhang, C. Zhang, L. Zhang, C. Li, S. Zhang, Q. Liu, Y. Wang, M. Gholizadeh, X. Hu, Pyrolysis of cellulose with co-feeding of formic or acetic acid. *Cellulose* (2020).

107. C. Zhu, S. Maduskar, A. D. Paulsen, P. J. Dauenhauer, Alkaline-Earth-Metal-Catalyzed Thin-Film Pyrolysis of Cellulose. *ChemCatChem*. **8**, 818–829 (2016).

108. M. Zabeti, K. B. Sai Sankar Gupta, G. Raman, L. Lefferts, S. Schallmoser, J. A. Lercher, K. Seshan, Aliphatic Hydrocarbons from Lignocellulose by Pyrolysis over Cesium-Modified Amorphous Silica Alumina Catalysts. *ChemCatChem*. **7**, 3386–3396 (2015).

109. Z. Xiang, J. Liang, H. M. Morgan, Y. Liu, H. Mao, Q. Bu, Thermal behavior and kinetic study for co-pyrolysis of lignocellulosic biomass with polyethylene over Cobalt modified ZSM-5 catalyst by thermogravimetric analysis. *Bioresource Technology*. **247**, 804–811 (2018).

110. P. H. Mouda, E. Kantarelis, K. J. Andersson, K. Engvall, Biomass pyrolysis gas conditioning over an iron-based catalyst for mild deoxygenation and hydrogen production. *Fuel*. **211**, 149–158 (2018).

111. A. van der Ent, A. J. M. Baker, R. D. Reeves, R. L. Chaney, C. W. N. Anderson, J. A. Meech, P. D. Erskine, M.-O. Simonnot, J. Vaughan, J. L. Morel, G. Echevarria, B. Fogliani, Q. Rongliang, D. R. Mulligan, Agromining: Farming for Metals in the Future? *Environ. Sci. Technol.* **49**, 4773–4780 (2015).

112. V. P. Ananikov, Nickel: The "Spirited Horse" of Transition Metal Catalysis. *ACS Catalysis*. **5**, 1964–1971 (2015).

113. S. Kumagai, J. Alvarez, P. H. Blanco, C. Wu, T. Yoshioka, M. Olazar, P. T. Williams, Novel Ni–Mg–Al–Ca catalyst for enhanced hydrogen production for the pyrolysis–gasification of a biomass/plastic mixture. *Journal of Analytical and Applied Pyrolysis*. **113**, 15–21 (2015).

114. Y. Liu, F. Guo, X. Li, T. Li, K. Peng, C. Guo, J. Chang, Catalytic Effect of Iron and Nickel on Gas Formation from Fast Biomass Pyrolysis in a Microfluidized Bed Reactor: A Kinetic Study. *Energy Fuels*. **31**, 12278–12287 (2017).

115. H. Yu, T. Ma, Y. Shen, D. Chen, Experimental study on catalytic effect of biomass pyrolysis volatile over nickel catalyst supported by waste iron slag. *Int. J. Energy Res.* **41**, 2063–2073 (2017).

116. M. M. Yung, A. K. Starace, C. Mukarakate, A. M. Crow, M. A. Leshnov, K. A. Magrini, Biomass Catalytic Pyrolysis on Ni/ZSM-5: Effects of Nickel Pretreatment and Loading. *Energy Fuels*. **30**, 5259–5268 (2016).

117. Phytocat website, (available at www.phytocat.org).

118. K. Tanabe, W. F. Holderich, Industrial application of solid acid-base catalysts. *Appl. Catal. A-Gen.* **181**, 399–434 (1999).

119. M. Occelli, Catalytic Cracking with an Interlayered Clay - a Two-Dimensional Molecular-Sieve. *Industrial & Engineering Chemistry Product Research and Development*. **22**, 553–559 (1983).

120. E. A. Emam, *Clays as Catalysts in Petroleum Refining Industry* (2013), *Materials Science*.

121. P. Hopkins, Cracking Activity of Some Synthetic Zeolites and Nature of Active Sites. *J. Catal.* **12**, 325–331 (1968).

122. N. Chen, S. Lucki, E. Mower, Cage Effect on Product Distribution from Cracking Over Crystalline Aluminosilicate Zeolites. *J. Catal.* **13**, 329–333 (1969).

123. L. Bonetto, M. Camblor, A. Corma, J. Perezpariente, Optimization of Zeolite-Beta in Cracking Catalysts - Influence of Crystallite Size. *Appl. Catal. A-Gen.* **82**, 37–50 (1992).

124. M. Guisnet, N. Gnep, F. Alario, Aromatization of Short Chain Alkanes on Zeolite Catalysts. *Appl. Catal. A-Gen.* **89**, 1–30 (1992).

125. W. Xu, Y. Yao, X. Xie, S. Liu, T. Zhang, Catalytic Cracking Properties of Al-Zr-B Composite Pillared Clays. *Applied Catalysis*. **75**, 33–40 (1991).

126. J. Harris, Effect of Aging of Pillaring Reagent on the Microstructure and Cracking Activity of Pillared Clay. *Acs Symposium Series*. **375**, 253–265 (1988).

127. H. Sakurai, K. Urabe, Y. Izumi, Pillared Tetrasilicic Mica Catalysts Having Fixed Interlayer Ca Ions - Comparison with Other Clays. *Bull. Chem. Soc. Jpn.* **64**, 227–235 (1991).

128. Y. Shi, E. Xing, K. Wu, J. Wang, M. Yang, Y. Wu, Recent progress on upgrading of bio-oil to hydrocarbons over metal/zeolite bifunctional catalysts. *Catal. Sci. Technol.* **7**, 2385–2415 (2017).

129. M. Shemfe, S. Gu, B. Fidalgo, Techno-economic analysis of biofuel production via bio-oil zeolite upgrading: An evaluation of two catalyst regeneration systems. *Biomass Bioenerg.* **98**, 182–193 (2017).

130. S. Vitolo, B. Bresci, M. Seggiani, M. G. Gallo, Catalytic upgrading of pyrolytic oils over HZSM-5 zeolite: behaviour of the catalyst when used in repeated upgrading-regenerating cycles. *Fuel*. **80**, 17–26 (2001).

131. H. Chen, Y. Dai, X. Jia, H. Yu, Y. Yang, Highly selective gas-phase oxidation of ethanol to ethyl acetate over bi-functional Pd/zeolite catalysts. *Green Chemistry*. **18**, 3048–3056 (2016).

132. T. C. Keller, E. G. Rodrigues, J. Perez-Ramirez, Generation of Basic Centers in High-Silica Zeolites and their Application in Gas-Phase Upgrading of Bio-Oil. *ChemSusChem*. **7**, 1729–1738 (2014).

133. A. Martinez, G. Prieto, The Application of Zeolites and Periodic Mesoporous Silicas in the Catalytic Conversion of Synthesis Gas. *Top. Catal.* **52**, 75–90 (2009).

134. A. Veses, B. Puertolas, M. S. Callen, T. Garcia, Catalytic upgrading of biomass derived pyrolysis vapors over metal-loaded ZSM-5 zeolites: Effect of different metal cations on the bio-oil final properties. *Microporous Mesoporous Mat.* **209**, 189–196 (2015).

135. T. R. Carlson, G. A. Tompsett, W. C. Conner, G. W. Huber, Aromatic Production from Catalytic Fast Pyrolysis of Biomass-Derived Feedstocks. *Top Catal*. **52**, 241–252 (2009).

136. H. Zhang, Y.-T. Cheng, T. P. Vispute, R. Xiao, G. W. Huber, Catalytic conversion of biomass-derived feedstocks into olefins and aromatics with ZSM-5: the hydrogen to carbon effective ratio. *Energy Environ. Sci.* **4**, 2297–2307 (2011).

137. T. R. Carlson, T. P. Vispute, G. W. Huber, Green Gasoline by Catalytic Fast Pyrolysis of Solid Biomass Derived Compounds. *ChemSusChem*. **1**, 397–400 (2008).

138. Y.-T. Cheng, J. Jae, J. Shi, W. Fan, G. W. Huber, Production of Renewable Aromatic Compounds by Catalytic Fast Pyrolysis of Lignocellulosic Biomass with Bifunctional Ga/ZSM-5 Catalysts. *Angew. Chem.-Int. Edit.* **51**, 1387–1390 (2012).

139. S. Katikaneni, J. Adjaye, N. Bakhshi, Catalytic Conversion of Canola Oil to Fuels and Chemicals Over Various Cracking Catalysts. *Can. J. Chem. Eng.* **73**, 484–497 (1995).

140. M. E. Gyftopoulou, M. Millan, A. V. Bridgwater, D. Dugwell, R. Kandiyoti, J. A. Hriljac, Pillared clays as catalysts for hydrocracking of heavy liquid fuels. *Appl. Catal. A-Gen.* **282**, 205–214 (2005).

141. A. Suseno, in *13th Joint Conference on Chemistry (13th Jcc)* (Iop Publishing Ltd, Bristol, 2019), vol. 509, p. 012005.

142. H. Mao, B. Li, L. Yue, L. Wang, J. Yang, X. Gao, Aluminated mesoporous silica-pillared montmorillonite as acidic catalyst for catalytic cracking. *Appl. Clay Sci.* **53**, 676–683 (2011).

143. V. V. Bokade, G. D. Yadav, Synthesis of Bio-diesel and Bio-lubricant by transesterification of vegetable oil with lower and higher alcohols over heteropolyacids supported by clay (K-10). *Process Saf. Environ. Protect.* **85**, 372–377 (2007).

144. B. A. Mohamed, C. S. Kim, N. Ellis, X. Bi, Microwave-assisted catalytic pyrolysis of switchgrass for improving bio-oil and biochar properties. *Bioresource Technology*. **201**, 121–132 (2016).

145. S. M. Hick, C. Griebel, D. T. Restrepo, J. H. Truitt, E. J. Buker, C. Bylda, R. G. Blair, Mechanocatalysis for biomass-derived chemicals and fuels. *Green Chemistry*. **12**, 468–474 (2010).

146. F. Gonzalez, C. Pesquera, I. Benito, E. Herrero, C. Poncio, S. Casuscelli, Pillared clays: catalytic evaluation in heavy oil cracking using a microactivity test. *Appl. Catal. A-Gen.* **181**, 71–76 (1999).

147. B. Jiang, C. Zhang, K. Wang, B. Dou, Y. Song, H. Chen, Y. Xu, Highly dispersed Ni/montmorillonite catalyst for glycerol steam reforming: Effect of Ni loading and calcination temperature. *Appl. Therm. Eng.* **109**, 99–108 (2016).

148. H. Mao, B. Li, X. Li, Z. Liu, W. Ma, Mesoporous nickel containing silica-pillared clays (Ni-SPC): Synthesis, characterization and catalytic behavior for cracking of plant asphalt. *Catal. Commun.* **10**, 975–980 (2009).

149. S. Jeenpadiphat, D. N. Tungasmita, Acid-activated pillar bentonite as a novel catalyst for the esterification of high FFA oil. *Powder Technol.* **237**, 634–640 (2013).

150. M. A. Olutoye, S. W. Wong, L. H. Chin, H. Amani, M. Asif, B. H. Hameed, Synthesis of fatty acid methyl esters via the transesterification of waste cooking oil by methanol with a barium-modified montmorillonite K10 catalyst. *Renew. Energy*. **86**, 392–398 (2016).

151. H. J. Alves, A. M. da Rocha, M. R. Monteiro, C. Moretti, M. D. Cabrelon, C. A. Schwengber, M. C. Milinsk, Treatment of clay with KF: New solid catalyst for biodiesel production. *Appl. Clay Sci.* **91–92**, 98–104 (2014).

152. Y. Liu, K. Murata, K. Okabe, M. Inaba, I. Takahara, T. Hanaoka, K. Sakanishi, Selective Hydrocracking of Fischer-Tropsch Waxes to High-quality Diesel Fuel Over Pt-promoted Polyoxocation-pillared Montmorillonites. *Top. Catal.* **52**, 597–608 (2009).

153. J. Adjaye, N. Bakhshi, Production of Hydrocarbons by Catalytic Upgrading of a Fast Pyrolysis Bio-Oil .1. Conversion Over Various Catalysts. *Fuel Process. Technol.* **45**, 161–183 (1995).

154. A. G. Gayubo, B. Valle, A. T. Aguayo, M. Olazar, J. Bilbao, Pyrolytic lignin removal for the valorization of biomass pyrolysis crude bio-oil by catalytic transformation. *J. Chem. Technol. Biotechnol.* **85**, 132–144 (2010).

155. K. Wang, R. C. Brown, Catalytic Pyrolysis of Corn Dried Distillers Grains with Solubles to Produce Hydrocarbons. *ACS Sustain. Chem. Eng.* **2**, 2142–2148 (2014).

156. G. T. Neumann, J. C. Hicks, Novel Hierarchical Cerium-Incorporated MFI Zeolite Catalysts for the Catalytic Fast Pyrolysis of Lignocellulosic Biomass. *ACS Catal.* **2**, 642–646 (2012).

157. W. Huang, F. Gong, M. Fan, Q. Zhai, C. Hong, Q. Li, Production of light olefins by catalytic conversion of lignocellulosic biomass with HZSM-5 zeolite impregnated with 6 wt.% lanthanum. *Bioresour. Technol.* **121**, 248–255 (2012).

158. C. Hong, F. Gong, M. Fan, Q. Zhai, W. Huang, T. Wang, Q. Li, Selective production of green light olefins by catalytic conversion of bio-oil with Mg/HZSM-5 catalyst. *J. Chem. Technol. Biotechnol.* **88**, 109–118 (2013).

159. S. Zhang, M. Yang, J. Shao, H. Yang, K. Zeng, Y. Chen, J. Luo, F. A. Agblevor, H. Chen, The conversion of biomass to light olefins on Fe-modified ZSM-5 catalyst: Effect of pyrolysis parameters. *Sci. Total Environ.* **628–629**, 350–357 (2018).

160. A. Pictet, J. Sarasin, Sur la distillation de la cellulose et de l'amidon sous pression réduite. *Helvetica Chimica Acta*. **1**, 87–96 (1918).

161. P. Karrer, Glucoside VI. Beitrag zur Konstitution und Konfiguration der Glucoside. *Helvetica Chimica Acta*. **3**, 258–260 (1920).

162. B. K. Kandola, A. R. Horrocks, D. Price, G. V. Coleman, Flame-Retardant Treatments of Cellulose and Their Influence on the Mechanism of Cellulose Pyrolysis. *Journal of Macromolecular Science, Part C*. **36**, 721–794 (1996).

163. W. Parks, R. Esteve, M. Gollis, R. Guercia, A. Pertrarca, Mechanismus Der Thermischen Zersetzung Von Cellulose. *Angew. Chem.-Int. Edit.* **67**, 351–351 (1955).

164. S. L. Madorsky, V. E. Hart, S. Straus, Pyrolysis of cellulose in a vacuum. *J. Res. Natl. Bur. Stan.* **56**, 343–350 (1956).

165. O. P. Golova, Chemical Effects of Heat on Cellulose. *Russ. Chem. Rev.* **44**, 687–697 (1975).

166. E. Franck, W. A. Reeves, Some Effects of the Nature of Cross-Links on the Properties of Cotton Fabrics. *Journal of the Textile Institute Proceedings*. **53**, P22–P36 (1962).

167. D. Gardiner, The pyrolysis of some hexoses and derived di-, tri-, and poly-saccharides. *J. Chem. Soc. C*, 1473–1476 (1966).

168. F. Kilzer, A. Broido, Speculations on Nature of Cellulose Pyrolysis. *Pyrodynamic*. **2**, 151–172 (1965).

169. A. G. W. Bradbury, Y. Sakai, F. Shafizadeh, A kinetic model for pyrolysis of cellulose. *Journal of Applied Polymer Science*. **23**, 3271–3280 (1979).

170. V. Mamleev, S. Bourbigot, J. Yvon, Kinetic analysis of the thermal decomposition of cellulose: The change of the rate limitation. *Journal of Analytical and Applied Pyrolysis*. **80**, 141–150 (2007).

171. A. Pictet, J. Sarasin, Sur la distillation de la cellulose et de l'amidon sous pression reduite. *Helvetica Chimica Acta*. **1**, 87–96 (1918).

172. E. Lehnartz, B. Flaschenträger, *Physiologische Chemie. ein Lehr- und Handbuch für Ärzte, Biologen und Chemiker, Erster Band: Die Stoffe* (Berlin, Springer, 1951).

173. J. C. Irvine, J. W. H. Oldham, CXCVIII.—The constitution of polysaccharides. Part III. The relationship of l-glucosan to d-glucose and to cellulose. *J. Chem. Soc., Trans.* **119**, 1744–1759 (1921).

174. F. Shafizadeh, M. Wolfrom, S. Tipson, in *Advances in Carbohydrate Chemistry* (Academic Press, 1968), vol. 23, pp. 419–474.

175. S. Maduskar, V. Maliekkal, M. Neurock, P. J. Dauenhauer, On the Yield of Levoglucosan from Cellulose Pyrolysis. *ACS Sustainable Chemistry & Engineering*. **6**, 7017–7025 (2018).

176. J. Proano-Aviles, J. K. Lindstrom, P. A. Johnston, R. C. Brown, Heat and Mass Transfer Effects in a Furnace-Based Micropyrolyzer. *Energy Technology*. **5**, 189–195 (2017).

177. O. P. Golova, A. M. Pakhomov, E. A. Andrievskaya, R. G. Krylova, On the mechanism of the thermal breakdown of cellulose in vacuo and the formation of l,6-anhydro-l,5-glucopyranose, a levoglucosan. *Dokl. Acad. Nauk SSSR*. **115**, 5–12 (1957).

178. P. R. Patwardhan, J. A. Satrio, R. C. Brown, B. H. Shanks, Influence of inorganic salts on the primary pyrolysis products of cellulose. *Bioresource Technology*. **101**, 4646–4655 (2010).

179. G.-J. Kwon, D.-Y. Kim, S. Kimura, S. Kuga, Rapid-cooling, continuous-feed pyrolyzer for biomass processing. *Journal of Analytical and Applied Pyrolysis*. **80**, 1–5 (2007).

180. J. Zhang, M. W. Nolte, B. H. Shanks, Investigation of Primary Reactions and Secondary Effects from the Pyrolysis of Different Celluloses. *ACS Sustainable Chemistry & Engineering*. **2**, 2820–2830 (2014).

181. R. F. Schwenker, Eugene. Pacsu, Chemically Modifying Cellulose for Flame Resistance. *Ind. Eng. Chem.* **50**, 91–96 (1958).

182. C. M. McCloskey, G. H. Coleman, A proposed inversion mechanism for the formation of levoglucosan from phenyl beta-D-glucose and trimethylglucoselammonium compounds. *J. Org. Chem.* **10**, 184–193 (1945).

183. J. C. Arthur, O. Hinojosa, Thermal Initiation of Free Radicals in Cotton Cellulose. *Textile Research Journal*. **36**, 385–387 (1966).

184. Z. A. Rohovyn, *Chemistry of Cellulose* (Chimia, Moscow, Moscow., 1972), vol. 1 of *1*.

185. F. Shafizadeh, Y. Z. Lai, C. R. Nelson, Thermal degradation of 6-chloro carbohydrates. *Journal of Applied Polymer Science*. **20**, 139–152 (1976).

186. Role of inorganic additives in the smoldering combustion of cotton cellulose. *Industrial & Engineering Chemistry Product*, (available at https://pubs.acs.org/doi/abs/10.1021/i300005a021).

187. G. Byrne, D. Gardiner, F. Holmes, Pyrolysis of Cellulose and Action of Flame-Retardants .2. Further Analysis and Identification of Products. *Journal of Applied Chemistry*. **16**, 81–88 (1966).

188. D. Arseneau, Competitive Reactions in the Thermal Decomposition of Cellulose. *Canadian Journal of Chemistry*. **49**, 632–638 (1971).

189. A. Broido, M. A. Nelson, Char yield on pyrolysis of cellulose. *Combustion and Flame*. **24**, 263–268 (1975).

190. A. Broido, in *Thermal Uses and Properties of Carbohydrates and Lignins* (Elsevier, 1976), pp. 19–36.

191. F. Shafizadeh, Y. Z. Lai, Thermal degradation of 1,6-anhydro-.beta.-D-glucopyranose. *J. Org. Chem.* **37**, 278–284 (1972).

192. T. Stevenson, M. Essig, F. Shafizadeh, L. Jensen, R. Stenkamp, The Crystal-Structure of an Epoxide of a Levoglucosenone Cyclopentadiene Adduct. *Carbohydr. Res.* **118**, 261–268 (1983).

193. F. Shafizadeh, M. Essig, D. Ward, Additional Reactions of Levoglucosenone. *Carbohydr. Res.* **114**, 71–82 (1983).

194. F. Shafizadeh, D. Ward, D. Pang, Michael-Addition Reactions of Levoglucosenone. *Carbohydr. Res.* **102**, 217–230 (1982).

195. F. Shafizadeh, R. Furneaux, D. Pang, T. Stevenson, Base-Catalyzed Oligomerization of Levoglucosenone. *Carbohydr. Res.* **100**, 303–313 (1982).

196. I. A. Wolff, D. W. Olds, Levoglucosan production by pyrolysis of pretreated starches (1969), (available at https://patents.google.com/patent/US3478012/en?oq=Shafizadeh+F+levoglucosan).

197. F. Shafizadeh, R. H. Furneaux, T. G. Cochran, J. P. Scholl, Y. Sakai, Production of levoglucosan and glucose from pyrolysis of cellulosic materials. *Journal of Applied Polymer Science*. **23**, 3525–3539 (1979).

198. W. K. Tang, W. K. Neill, Effect of flame retardants on pyrolysis and combustion of α-cellulose. *Journal of Polymer Science Part C: Polymer Symposia*. **6**, 65–81 (1964).

199. A. E. Lipska, F. A. Wodley, Isothermal pyrolysis of cellulose: Kinetics and gas chromatographic mass spectrometric analysis of the degradation products. *J. Appl. Polym. Sci.* **13**, 851–865 (1969).

200. A. F. Roberts, The kinetic behavior of intermediate compounds during the pyrolysis of cellulose. *Journal of Applied Polymer Science*. **14**, 244–247 (1970).

201. G. Varhegyi, E. Jakab, M. J. Antal, Is the Broido-Shafizadeh Model for Cellulose Pyrolysis True? *Energy Fuels*. **8**, 1345–1352 (1994).

202. J. L. Banyasz, S. Li, J. H. Lyons-Hart, K. H. Shafer, Gas evolution and the mechanism of cellulose pyrolysis. *Fuel*. **80**, 1757–1763 (2001).

203. X. Zhou, M. W. Nolte, H. B. Mayes, B. H. Shanks, L. J. Broadbelt, Experimental and Mechanistic Modeling of Fast Pyrolysis of Neat Glucose-Based Carbohydrates. 1. Experiments and Development of a Detailed Mechanistic Model. *Ind. Eng. Chem. Res.* **53**, 13274–13289 (2014).

204. H. B. Mayes, L. J. Broadbelt, Unraveling the Reactions that Unravel Cellulose. *J. Phys. Chem. A*. **116**, 7098–7106 (2012).

205. V. Mamleev, S. Bourbigot, M. Le Bras, J. Yvon, The facts and hypotheses relating to the phenomenological model of cellulose pyrolysis. *Journal of Analytical and Applied Pyrolysis*. **84**, 1–17 (2009).

206. M. J. Antal, H. L. Friedman, F. E. Rogers, Kinetics of Cellulose Pyrolysis in Nitrogen and Steam. *Combustion Science and Technology*. **21**, 141–152 (1980).

207. M. Poliakoff, Green Chemistry: Science and Politics of Change. *Science*. **297**, 807–810 (2002).

208. C. O. Tuck, E. Perez, I. T. Horvath, R. A. Sheldon, M. Poliakoff, Valorization of Biomass: Deriving More Value from Waste. *Science*. **337**, 695–699 (2012).

209. A. J. Ragauskas, The Path Forward for Biofuels and Biomaterials. *Science*. **311**, 484–489 (2006).

210. J. N. Chheda, G. W. Huber, J. A. Dumesic, Liquid-Phase Catalytic Processing of Biomass-Derived Oxygenated Hydrocarbons to Fuels and Chemicals. *Angewandte Chemie International Edition*. **46**, 7164–7183 (2007).

211. S. Czernik, A. V. Bridgwater, Overview of Applications of Biomass Fast Pyrolysis Oil. *Energy & Fuels*. **18**, 590–598 (2004).

212. J. C. Ritter, C. S. Stauffer, Production of hydroxymethylfurfural from levoglucosenone (2013), (available at https://patents.google.com/patent/US20130172580A1/en?q=levoglucosenone&assignee=du+po nt&oq=du+pont+levoglucosenone).

213. G. Várhegyi, M. J. Antal, E. Jakab, P. Szabó, Kinetic modeling of biomass pyrolysis. *Journal of Analytical and Applied Pyrolysis*. **42**, 73–87 (1997).

214. Y.-C. Lin, J. Cho, G. A. Tompsett, P. R. Westmoreland, G. W. Huber, Kinetics and Mechanism of Cellulose Pyrolysis. *The Journal of Physical Chemistry C*. **113**, 20097–20107 (2009).

215. R. Bassilakis, R. M. Carangelo, M. A. Wojtowicz, TG-FTIR analysis of biomass pyrolysis. *Fuel*. **80**, 1765–1786 (2001).

216. A. V. Bridgwater, Principles and practice of biomass fast pyrolysis processes for liquids. *Journal of Applied Polymer Science*. **51**, 3–22 (1999).

217. A. D. Pouwels, G. B. Eijkel, J. J. Boon, Curie-Point Pyrolysis-Capillary Gas Chromatography —High-Resolution Mass Spectrometry of Microcrystalline Cellulose. *Journal of Analytical and Applied Pyrolysis*. **14**, 237–280 (1989).

218. F. Shafizadeh, Y. Z. Lai, Thermal degradation of 1,6-anhydro-.beta.-D-glucopyranose. *The Journal of Organic Chemistry*. **37**, 278–284 (1972).

219. T. Shoji, H. Kawamoto, S. Saka, Boiling point of levoglucosan and devolatilization temperatures in cellulose pyrolysis measured at different heating area temperatures. *Journal of Analytical and Applied Pyrolysis*. **109**, 185–195 (2014).

220. L.-Q. Jiang, Z. Fang, Z.-L. Zhao, A.-Q. Zheng, X.-B. Wang, H.-B. Li, Levoglucosan and its hydrolysates via fast pyrolysis of lignocellulose for microbial biofuels: A state-of-the-art review. *Renewable and Sustainable Energy Reviews*. **105**, 215–229 (2019).

221. J. K. Lindstrom, J. Proano-Aviles, P. A. Johnston, C. A. Peterson, J. S. Stansell, R. C. Brown, Competing reactions limit levoglucosan yield during fast pyrolysis of cellulose. *Green Chemistry*. **21**, 178–186 (2019).

222. J. Scheirs, G. Camino, W. Tumiatti, Overview of water evolution during the thermal degradation of cellulose. *European Polymer Journal*. **37**, 933–942 (2001).

223. T. B. Brill, P. E. Gongwer, G. K. Williams, Thermal Decomposition of Energetic Materials. 66. Kinetic Compensation Effects in HMX, RDX, and NTO. *The Journal of Physical Chemistry*. **98**, 12242–12247 (1994).

224. S. Vyazovkin, C. A. Wight, Kinetics in Solids. *Annual Review of Physical Chemistry*. **48**, 125–149 (1997).

225. Miura M., Tanaka S., Ando K., Effects of Heating rate on Yield of Levoglucosan in Wood Pyrolysis. *Kagaku Kogaku Ronbunshu*. **21**, 843–846 (1995).

226. E. F. Iliopoulou, K. S. Triantafyllidis, A. A. Lappas, Overview of catalytic upgrading of biomass pyrolysis vapors toward the production of fuels and high-value chemicals. *WIREs Energy and Environment*. **8**, e322 (2019).

227. J. Adam, M. Blazsó, E. Mészáros, M. Stöcker, M. H. Nilsen, A. Bouzga, J. E. Hustad, M. Grønli, G. Øye, Pyrolysis of biomass in the presence of Al-MCM-41 type catalysts. *Fuel*. **84**, 1494–1502 (2005).

228. E. Antonakou, A. Lappas, M. H. Nilsen, A. Bouzga, M. Stöcker, Evaluation of various types of Al-MCM-41 materials as catalysts in biomass pyrolysis for the production of bio-fuels and chemicals. *Fuel*. **85**, 2202–2212 (2006).

229. M. H. Nilsen, E. Antonakou, A. Bouzga, A. Lappas, K. Mathisen, M. Stöcker, Investigation of the effect of metal sites in Me–Al-MCM-41 (Me=Fe, Cu or Zn) on the catalytic behavior during the pyrolysis of wooden based biomass. *Microporous and Mesoporous Materials*. **105**, 189–203 (2007).

230. F. Cao, T. J. Schwartz, D. J. McClelland, S. H. Krishna, J. A. Dumesic, G. W. Huber, Dehydration of cellulose to levoglucosenone using polar aprotic solvents. *Energy Environ. Sci.* **8**, 1808–1815 (2015).

231. A. Solak, P. Rutkowski, The effect of clay catalyst on the chemical composition of bio-oil obtained by co-pyrolysis of cellulose and polyethylene. *Waste Management*. **34**, 504–512 (2014).

232. R. Narayan, M. J. Antal, Thermal Lag, Fusion, and the Compensation Effect during Biomass Pyrolysis. *Ind. Eng. Chem. Res.* **35**, 1711–1721 (1996).

233. S.-N. Liu, J.-P. Cao, X.-Y. Zhao, J.-X. Wang, X.-Y. Ren, Z.-S. Yuan, Z.-X. Guo, W.-Z. Shen, J. Bai, X.-Y. Wei, Effect of zeolite structure on light aromatics formation during upgrading of cellulose fast pyrolysis vapor. *Journal of the Energy Institute*. **92**, 1567–1576 (2019).

234. Y. Wu, S. Wu, H. Zhang, R. Xiao, Cellulose-lignin interactions during catalytic pyrolysis with different zeolite catalysts. *Fuel Processing Technology*. **179**, 436–442 (2018).

235. H. Kawamoto, S. Saito, W. Hatanaka, S. Saka, Catalytic pyrolysis of cellulose in sulfolane with some acidic catalysts. *J Wood Sci*. **53**, 127–133 (2007).

236. Z. Zhang, Q. Lu, X. Ye, T. Wang, X. Wang, C. Dong, Selective Production of Levoglucosenone from Catalytic Fast Pyrolysis of Biomass Mechanically Mixed with Solid Phosphoric Acid Catalysts. *Bioenerg. Res.* **8**, 1263–1274 (2015).

237. W. Li, H. Huang, Q. Wang, Z. Zhang, Protection of pyrolysis gases combustion against charring materials' surface ablation. *International Journal of Heat and Mass Transfer*. **102**, 10–17 (2016).

238. M. J. Antal, in *Advances in Solar Energy: An Annual Review of Research and Development*, K. W. Böer, J. A. Duffie, Eds. (Springer New York, Boston, MA, 1983), vol. 1, pp. 61–111.

239. J. R. McManus, J. M. Vohs, Deoxygenation of glycolaldehyde and furfural on Mo2C/Mo(100). *Surface Science*. **630**, 16–21 (2014).

240. J. Fan, P. S. Shuttleworth, M. Gronnow, S. W. Breeden, J. H. Clark, D. J. Macquarrie, V. L. Budarin, Influence of Density on Microwave Pyrolysis of Cellulose. *ACS Sustainable Chemistry and Engineering*. **6**, 2916–2920 (2018).

241. W. Ao, J. Fu, X. Mao, Q. Kang, C. Ran, Y. Liu, H. Zhang, Z. Gao, J. Li, G. Liu, J. Dai, Microwave assisted preparation of activated carbon from biomass: A review. *Renewable and Sustainable Energy Reviews*. **92**, 958–979 (2018).

242. S. Tsubaki, K. Oono, A. Onda, T. Ueda, T. Mitani, M. Hiraoka, Microwave-assisted hydrolysis of biomass over activated carbon supported polyoxometalates. *RSC Adv.* **7**, 12346–12350 (2017).

243. V. L. Budarin, J. H. Clark, B. A. Lanigan, P. Shuttleworth, S. W. Breeden, A. J. Wilson, D. J. Macquarrie, K. Milkowski, J. Jones, T. Bridgeman, A. Ross, The preparation of high-grade bio-oils through the controlled, low temperature microwave activation of wheat straw. *Bioresource Technology*. **100**, 6064–6068 (2009).

244. A. Corsaro, U. Chiacchio, V. Pistara, G. Romeo, Microwave-assisted Chemistry of Carbohydrates. *Current Organic Chemistry*. **8**, 511–538 (2004).

245. G. T. Mihiretu, M. Brodin, A. F. Chimphango, K. Øyaas, B. H. Hoff, J. F. Görgens, Single-step microwave-assisted hot water extraction of hemicelluloses from selected lignocellulosic materials – A biorefinery approach. *Bioresource Technology*. **241**, 669–680 (2017).

246. G. W. Huber, S. Iborra, A. Corma, Synthesis of Transportation Fuels from Biomass: Chemistry, Catalysts, and Engineering. *Chem. Rev.* **106**, 4044–4098 (2006).

247. Md. M. Rahman, R. Liu, J. Cai, Catalytic fast pyrolysis of biomass over zeolites for high quality bio-oil – A review. *Fuel Processing Technology*. **180**, 32–46 (2018).

248. T. R. Carlson, J. Jae, Y.-C. Lin, G. A. Tompsett, G. W. Huber, Catalytic fast pyrolysis of glucose with HZSM-5: The combined homogeneous and heterogeneous reactions. *Journal of Catalysis*. **270**, 110–124 (2010).

249. F. Bergaya, A. Aouad, T. Mandalia, in *Developments in Clay Science* (Elsevier, 2006; https://linkinghub.elsevier.com/retrieve/pii/S1572435205010123), vol. 1, pp. 393–421.

250. M. Ammar, W. Oueslati, H. Ben Rhaiem, A. Ben Haj Amara, Quantitative XRD analysis of the dehydration–hydration performance of (Na $^+$, Cs $^+$) exchanged smectite. *Desalination and Water Treatment*. **52**, 4314–4333 (2014).

251. F. Figueras, Pillared Clays as Catalysts. *Catalysis Reviews*. **30**, 457–499 (1988).

252. J. T. Kloprogge, E. Booy, J. B. H. Jansen, J. W. Geus, The Effect of Thermal Treatment on the Properties of Hydroxy-Al and Hydroxy-Ga Pillared Montmorillonite and Beidellite. *Clay miner.* **29**, 153–167 (1994).

253. B. A. Mohamed, N. Ellis, C. S. Kim, X. Bi, Microwave-assisted catalytic biomass pyrolysis: Effects of catalyst mixtures. *Applied Catalysis B: Environmental*. **253**, 226–234 (2019).

254. M. Sulman, Yu. Kosivtsov, E. Sulman, V. Alfyorov, Yu. Lugovoy, V. Molchanov, I. Tyamina, O. Misnikov, A. Afanasjev, N. Kumar, D. Murzin, Influence of aluminosilicate materials on the peat low-temperature pyrolysis and gas formation. *Chemical Engineering Journal*. **154**, 355–360 (2009).

255. X. Zhang, W. Yang, C. Dong, Levoglucosan formation mechanisms during cellulose pyrolysis. *Journal of Analytical and Applied Pyrolysis*. **104**, 19–27 (2013).

256. P. H. Blanco, J. B. Lad, A. V. Bridgwater, M. S. Holm, Production of Glucose from the Acid Hydrolysis of Anhydrosugars. *ACS Sustainable Chem. Eng.* **6**, 12872–12883 (2018).

257. P. Daorattanachai, S. Namuangruk, N. Viriya-empikul, N. Laosiripojana, K. Faungnawakij, 5-Hydroxymethylfurfural production from sugars and cellulose in acid- and base-catalyzed conditions under hot compressed water. *Journal of Industrial and Engineering Chemistry*. **18**, 1893–1901 (2012).

258. M. Ohara, A. Takagaki, S. Nishimura, K. Ebitani, Syntheses of 5-hydroxymethylfurfural and levoglucosan by selective dehydration of glucose using solid acid and base catalysts. *Applied Catalysis A: General*. **383**, 149–155 (2010).

259. A. A. Marianou, C. M. Michailof, A. Pineda, E. F. Iliopoulou, K. S. Triantafyllidis, A. A. Lappas, Effect of Lewis and Brønsted acidity on glucose conversion to 5-HMF and lactic acid in aqueous and organic media. *Applied Catalysis A: General*. **555**, 75–87 (2018).

260. F. Shafizadeh, R. H. Furneaux, T. T. Stevenson, Acid-catalyzed Pyrolytic Synthesis and Decomposition of 1,4:3,6-Dianhydro-Alpha-D-Glucopyranose. *Carbohydrate Research*. **61**, 519–528 (1978).

261. Tackling the 1.6-Billion-Ton Food Loss and Waste Crisis. *BCG Global* (2020), (available at https://www.bcg.com/publications/2018/tackling-1.6-billion-ton-food-loss-and-waste-crisis).

262. J. Jara-Samaniego, M. D. Pérez-Murcia, M. A. Bustamante, C. Paredes, A. Pérez-Espinosa, I. Gavilanes-Terán, M. López, F. C. Marhuenda-Egea, H. Brito, R. Moral, Development of organic fertilizers from food market waste and urban gardening by composting in Ecuador. *PLOS ONE*. **12**, e0181621 (2017).

263. P. Adewale, M.-J. Dumont, M. Ngadi, Recent trends of biodiesel production from animal fat wastes and associated production techniques. *Renewable and Sustainable Energy Reviews*. **45**, 574–588 (2015).

264. V. Budarin, J. H. Clark, J. J. E. Hardy, R. Luque, K. Milkowski, S. J. Tavener, A. J. Wilson, Starbons: New starch-derived mesoporous carbonaceous materials with tunable properties. *Angewandte Chemie - International Edition*. **45**, 3782–3786 (2006).

265. Z. Yang, X. Liu, Z. Yang, G. Zhuang, Z. Bai, H. Zhang, Y. Guo, Preparation and formation mechanism of levoglucosan from starch using a tubular furnace pyrolysis reactor. *Journal of Analytical and Applied Pyrolysis*. **102**, 83–88 (2013).

266. D. Radlein, J. Piskorz, D. S. Scott, Fast pyrolysis of natural polysaccharides as a potential industrial process. *Journal of Analytical and Applied Pyrolysis*. **19**, 41–63 (1991).

267. C. M. Lakshmanan, H. E. Hoelscher, Production of Levoglucosan by Pyrolysis of Carbohydrates. Pyrolysis in Hot Inert Gas Stream. *Ind. Eng. Chem. Prod. Res. Dev.* **9**, 57–59 (1970).

268. M. Käldström, N. Kumar, T. Heikkilä, D. Yu. Murzin, Pillared H-MCM-36 mesoporous and H-MCM-22 microporous materials for conversion of levoglucosan: Influence of varying acidity. *Applied Catalysis A: General*. **397**, 13–21 (2011).

269. B. Girisuta, L. P. B. M. Janssen, H. J. Heeres, A kinetic study on the decomposition of 5-hydroxymethylfurfural into levulinic acid. *Green Chemistry.* **8**, 701–709 (2006).

270. C. M. Bohn, Transformation of biomass carbohydrates by transition metal catalysts. *Theses and Dissertations Available from ProQuest*, 1–107 (2014).

271. X. Zhang, V. Houzelot, A. Bani, J.-L. Morel, G. Echevarria, M.-O. Simonnot, Selection and Combustion of Ni- Hyperaccumulators for the Phytomining Process. *International Journal of Phytoremediation*. **16**, 1058–1072 (2014).

272. M. N. V. Prasad, Nickelophilous plants and their significance in phytotechnologies. *Brazilian Journal of Plant Physiology*. **17**, 113–128 (2005).

273. S. Khan, Q. Cao, Y. M. Zheng, Y. Z. Huang, Y. G. Zhu, Health risks of heavy metals in contaminated soils and food crops irrigated with wastewater in Beijing, China. *Environ. Pollut.* **152**, 686–692 (2008).

274. R. A. Wuana, F. E. Okieimen, Heavy Metals in Contaminated Soils: A Review of Sources, Chemistry, Risks and Best Available Strategies for Remediation. *International Scholarly Research Notices.* **2011**, 1-20 (2011).

275. T. A. Kirpichtchikova, A. Manceau, L. Spadini, F. Panfili, M. A. Marcus, T. Jacquet, Speciation and solubility of heavy metals in contaminated soil using X-ray microfluorescence, EXAFS spectroscopy, chemical extraction, and thermodynamic modeling. *Geochimica et Cosmochimica Acta*. **70**, 2163–2190 (2006).

276. A. J. Hunt, C. W. N. Anderson, N. Bruce, A. M. Garcia, T. E. Graedel, M. Hodson, J. A. Meech, N. T. Nassar, H. L. Parker, E. L. Rylott, K. Sotiriou, Q. Zhang, J. H. Clark, Phytoextraction as a tool for green chemistry. *Green Process. Synth.* **3**, 3–22 (2014).

277. R. R. Brooks, M. F. Chambers, L. J. Nicks, B. H. Robinson, Phytomining. *Trends Plant Sci.* **3**, 359–362 (1998).

278. R. R. Brooks, B. H. Robinson, A. W. Howes, A. Chiarucci, An evaluation of Berkheya coddii Roessler and Alyssum bertolonii Desv. for phytoremediation and phytomining of nickel. *S. Afr. J. Sci.* **97**, 558–560 (2001).

279. C. W. N. Anderson, R. R. Brooks, A. Chiarucci, C. J. LaCoste, M. Leblanc, B. H. Robinson, R. Simcock, R. B. Stewart, Phytomining for nickel, thallium and gold. *J. Geochem. Explor.* **67**, 407–415 (1999).

280. R. Boominathan, N. M. Saha-Chaudhury, V. Sahajwalla, P. M. Doran, Production of nickel bio-ore from hyperaccumulator plant biomass: Applications in phytomining. *Biotechnology and Bioengineering*. **86**, 243–250 (2004).

281. V. Houzelot, B. Ranc, B. Laubie, M.-O. Simonnot, Agromining of hyperaccumulator biomass: Study of leaching kinetics of extraction of nickel, magnesium, potassium, phosphorus, iron, and manganese from Alyssum murale ashes by sulfuric acid. *Chem. Eng. Res. Des.* **129**, 1–11 (2018).

282. H. L. Parker, E. L. Rylott, A. J. Hunt, J. R. Dodson, A. F. Taylor, N. C. Bruce, J. H. Clark, Supported Palladium Nanoparticles Synthesized by Living Plants as a Catalyst for Suzuki-Miyaura Reactions. *PLoS One*. **9**, e87192 (2014).

283. Z. A. S. Harumain, H. L. Parker, A. Muñoz García, M. J. Austin, C. R. McElroy, A. J. Hunt, J. H. Clark, J. A. Meech, C. W. N. Anderson, L. Ciacci, T. E. Graedel, N. C. Bruce, E. L. Rylott, Toward Financially Viable Phytoextraction and Production of Plant-Based Palladium Catalysts. *Environ. Sci. Technol.* **51**, 2992–3000 (2017).

284. X. Zhang, V. Houzelot, A. Bani, J. L. Morel, G. Echevarria, M.-O. Simonnot, Selection and Combustion of Ni-Hyperaccumulators for the Phytomining Process. *International Journal of Phytoremediation*. **16**, 1058–1072 (2014).

285. R. L. Chaney, J. S. Angle, C. L. Broadhurst, C. A. Peters, R. V. Tappero, D. L. Sparks, Improved Understanding of Hyperaccumulation Yields Commercial Phytoextraction and Phytomining Technologies. *Journal of Environmental Quality*. **36**, 1429–1443 (2007).

286. M. M. Yung, A. K. Starace, C. Mukarakate, A. M. Crow, M. A. Leshnov, K. A. Magrini, Biomass Catalytic Pyrolysis on Ni/ZSM-5: Effects of Nickel Pretreatment and Loading. *Energy & Fuels*. **30**, 5259–5268 (2016).

287. B. De, J. Fan, V. L. Budarin, D. J. Macquarrie, L. D. Gomez, R. Simister, T. J. Farmer, W. D. Raverty, S. J. McQueen-Mason, J. H. Clark, A new perspective in bio-refining: Levoglucosenone and cleaner lignin from waste biorefinery hydrolysis lignin by selective conversion of residual saccharides. *Energy and Environmental Science*. **9**, 2571–2574 (2016).

288. L. Zhou, F. Santomauro, J. Fan, D. Macquarrie, J. Clark, C. J. Chuck, V. Budarin, Fast microwave-assisted acidolysis: A new biorefinery approach for the zero-waste utilisation of lignocellulosic biomass to produce high quality lignin and fermentable saccharides. *Faraday Discussions*. **202**, 351–370 (2017).

289. L. Zhou, V. Budarin, J. Fan, R. Sloan, D. Macquarrie, Efficient Method of Lignin Isolation Using Microwave-Assisted Acidolysis and Characterization of the Residual Lignin. *ACS Sustainable Chemistry and Engineering*. **5**, 3768–3774 (2017).

290. V. L. Budarin, P. S. Shuttleworth, B. De, T. J. Farmer, M. J. Gronnow, L. Pfaltzgraff, D. J. Macquarrie, J. H. Clark, The potential of microwave technology for the recovery, synthesis and manufacturing of chemicals from bio-wastes. *Catalysis Today*. **239**, 80–89 (2015).

291. T. Li, J. Remon, P. S. Shuttleworth, Z. Jiang, J. Fan, J. H. Clark, V. L. Budarin, Controllable production of liquid and solid biofuels by doping-free, microwave-assisted, pressurised pyrolysis of hemicellulose. *Energy Conv. Manag.* **144**, 104–113 (2017).

292. H. Kauss, Biosynthesis of the glucuronic acid unit of hemicellulose B from UDP-glucuronic acid. *Biochimica et Biophysica Acta (BBA)-General Subjects*. **148**, 572–574 (1967).

293. M. Gaber, S. S. Al-Shihry, Cobalt (II), nickel (II) and copper (II) complexes of carbohydrazide and its arylidene derivatives. *Scientific Journal of King Faisal University (Basic and Applied Sciences)*. **5**, 1425-1431 (2004).

294. X. Tian, R. K. Fu, L. Wang, P. K. Chu, Oxygen-induced nickel segregation in nitrogen plasma implanted AISI 304 stainless steel. *Materials Science and Engineering: A*. **316**, 200–204 (2001).

295. Y. A. Mørch, I. Sandvig, O. Olsen, I. Donati, M. Thuen, G. Skjåk-Braek, O. Haraldseth, C. Brekken, Mn-alginate gels as a novel system for controlled release of Mn2+ in manganese-enhanced MRI. *Contrast Media Mol Imaging*. **7**, 265–275 (2012).

296. R. S. Miller, J. Bellan, A Generalized Biomass Pyrolysis Model Based on Superimposed Cellulose, Hemicelluloseand Liqnin Kinetics. *Combustion Science and Technology*. **126**, 97–137 (1997).

297. O. Debono, A. Villot, Nitrogen products and reaction pathway of nitrogen compounds during the pyrolysis of various organic wastes. *Journal of Analytical and Applied Pyrolysis*. **114**, 222–234 (2015).

298. S. Bodoardo, F. Figueras, E. Garrone, IR Study of Bronsted Acidity of Al-Pillared Montmorillonite. *Journal of Catalysis*. **147**, 223–230 (1994).